Universität Ulm

Abteilung Oberflächenchemie & Katalyse

Mechanistic Insights into the Preferential CO Oxidation in H_2-rich Gas (PROX) over Supported Noble Metal Catalysts

Dissertation

vorgelegt von

Markus Matthias Schubert

2000

Karin

Abteilung Oberflächenchemie & Katalyse
Universität Ulm

Mechanistic Insights into the Preferential CO Oxidation in H_2-rich Gas (PROX) over Supported Noble Metal Catalysts

Dissertation
zur Erlangung des Doktorgrades Dr. rer. nat.
der Fakultät für Naturwissenschaften
der Universität Ulm

vorgelegt von
Markus Matthias Schubert
aus München

Ulm 2000

Der experimentelle Teil dieser Arbeit wurde in der Zeit von Oktober 1996 bis September 1999 in der Abteilung Oberflächenchemie und Katalyse der Universität Ulm angefertigt.

Wissenschaftlicher Betreuer: Prof. Dr. R. J. Behm
(Leiter der Abteilung Oberflächenchemie & Katalyse)

Amtierender Dekan: Prof. Dr. O. Marti

1. Gutachter: Prof. Dr. R. J. Behm
2. Gutachter: Prof. Dr. J. Garche

Tag der Promotion: 11. Mai 2000

CONTENTS

I. Introduction

1. The selective CO oxidation - reactions..........1

2. Technical application: PROX..........3

3. Intention of this work..........5

II. Experimental

1. Setup..........6

1.1 Reaction gases & mixture facility..........6

1.2 The plug-flow reactor..........9

1.3 Infrared spectroscopy - DRIFTS..........12

1.3.1 DRIFTS-theory..........13
1.3.2 DRIFTS-setup..........15
1.3.3 Processing of DRIFTS spectra..........17

1.4 On-line GC analysis..........20

1.5 Other methods used..........22

1.5.1 XPS..........22
1.5.2 On-line IMR-MS analysis..........22
1.5.3 Isotope studies / pulse experiments..........23
1.5.4 XRD..........23

2. Catalyst characterization..........24

2.1 Platinum catalysts..........24

2.2 Pt_3Sn catalyst..........24

2.3 Gold catalysts..........25

III. Results & discussion

1. The standard catalyst - Pt/γ-Al_2O_3....................26

1.1 The influence of the CO coverage on the activity / selectivity....................27

1.1.1 Selectivity & hydrogen induced rate enhancement....................27

1.1.2 Experimental limitations - neglecting the reaction rate....................29

1.1.3 Adsorption of CO in pure N_2....................32

1.1.4 Adsorption of CO in H_2 / N_2....................36

1.1.5 Coadsorption behaviour of CO and H_2....................39

1.2 From idealized to more realistic conditions....................46

1.2.1 Self-poisoning by CO_{ad}....................46

1.2.2 Influence of water....................48

1.2.3 Performance in CO_2-rich gas....................56

1.3 Other support materials....................63

1.3.1. Comparison of activity / selectivity....................63

1.3.2. The water-gas shift - limiting the CO conversion....................66

1.4 Summary on platinum catalysts....................71

2. Improved performance on bimetallic systems - Pt_3Sn/Vulcan....................73

2.1 Low-temperature CO oxidation over Pt_3Sn/Vulcan....................75

2.1.1 Superior performance on Pt_3Sn/Vulcan vs Pt/γ-Al_2O_3....................75

2.1.2 Alloying effects....................78

2.1.3 Coverage dependence of the selectivity....................82

2.1.4 Catalyst state during conditioning & reaction....................84

2.1.5 Mechanistic proposal - avoiding the CO poisoning....................89

2.2 Other important characteristics for an application in a PROX-stage....................93

2.2.1 Long-term stability....................93

2.2.2 Performance in more realistic reformates....................99

2.2.3 The water-gas shift activitiy of Pt_3Sn/Vulcan....................103

2.3 Summary on bimetallic Pt_3Sn catalyst....................105

3. An alternative for the low temperature conversion - Au/α-Fe_2O_3............................107

3.1 Mechanistic insight into the CO oxidation over gold catalysts....................................109

3.1.1 A short review..109
3.1.2 The „support-effect“..111
3.1.3 Oxygen supply from the FeO_x-support (Transient response measurements).......116
3.1.4 Proposed reaction scheme..121

3.2 The influence of structural parameters on the activity / selectivity..............................123

3.2.1 The dependence of the activity on the particle size...123
3.2.2 Influence of the calcination temperature..129
3.2.3 The dependence of the particle size on the sodium content.................................132

3.3 The CO coverage on Au and its influence on the kinetics..134

3.3.1 Kinetic observations..134
3.3.2 Comparison of the CO coverage on Pt/γ-Al_2O_3 versus Au/α-Fe_2O_3....................137
3.3.3 Temperature dependence..143

3.4 Deactivation behaviour..147

3.4.1 „Off-line deactivation“..147
3.4.2 „On-line deactivation“ during CO oxidation...148

a) Irreversible poisoning of more crystalline samples..150
b) Reversible deactivation on amorphous samples...155
c) Deactivation model...157

3.5 Effects of CO_2 and H_2O on the activity / selectivity..160

3.5.1 Selectivity enhancement by water..160
3.5.2 Performance in CO_2-containing mixtures..163

3.6 Reverse water-gas shift over Au/α-Fe_2O_3..170

3.7 Other support materials...172

3.8. Summary on gold catalysts...177

IV. Summary & future perspectives

V. References

VI. Acknowledgement

Appendix

A) Improved DRIFTS-cell design......198

B) Additional figures......204

C) English abstract......205

D) Deutsche Zusammenfassung (german abstract)......207

E) List of publications......209

F) Lebenslauf (curriculum vitae)......210

I. INTRODUCTION

1. The selective CO oxidation - reactions

The following work is concerned with a detailed mechanistic investigation of the selective (preferential) oxidation of CO over supported noble metal catalysts in hydrogen-rich gases. As will be specified in the following chapter, this reaction has an important commercial application for the purification of hydrogen feed gas streams for low temperature fuel cells produced by methanol steam reforming.

Although in the past years numerous studies on the pure CO oxidation (*i. e.*, in UHV, a nitrogen or a helium background) on noble metal surfaces have appeared (*e. g.*, [1-3] and many others) only a few pulications were concerned with effects arising from coadsorbates and parallely occuring surface reactions (*e. g.*, [4-7]). Moreover all the latter studies use a phenomenological approach by kinetics, but in most cases provide no mechanistic explanations for the observed reaction orders and rates, which consequently is one of the central intentions of this work.

For the preferential CO oxidation in H_2-rich gases two competing, parallely occuring processes have to be considered, the CO oxidation reaction

$$CO + \tfrac{1}{2} O_2 \rightarrow CO_2 \qquad ; \Delta H^0 = -283 \text{ kJ/mol [8]} \qquad \text{(I-1.1)}$$

and the H_2 oxidation reaction

$$H_2 + \tfrac{1}{2} O_2 \rightarrow H_2O \qquad ; \Delta H^0 = -242 \text{ kJ/mol [8]} \qquad \text{(I-1.2)}$$

The selectivity, S, indicates, which of the two reactions is favoured by the kinetics. For practical reasons it has been defined *via* the oxygen consumption:

$$S = \frac{r^{CO}}{r^{CO} + r^{H_2}} = \frac{\Delta O_2^{CO-\text{oxidation}}}{\Delta O_2^{CO-\text{oxidation}} + \Delta O_2^{H_2-\text{oxidation}}} \qquad \text{(I-1.3)}$$

r^X = oxidation rate of CO and H_2, resp.; ΔO_2^X = oxygen consumed by oxidation reactions

In principle for our complex reaction mixture, which contains CO, O_2, H_2 and the products CO_2 and H_2O, also a few other reactions must be taken into consideration, *e. g.*, methanation or methanol formation. Fortunately, on the catalyst systems, which are investigated in the following chapters, most of these secondary reactions occur only above the applied operation temperatures at a significant rate, *e. g.*, over Pt/γ-Al_2O_3 methanation sets in only for temperatures above 250°C, but the optimum temperature range for the selective CO oxidation is around 200°C [9]. The only interference worth noticing arises from the water-gas shift (denoted as „WGS“ in the following) reaction:

$$CO_2 + H_2 \leftrightarrow CO + H_2O \qquad ; \Delta H^0 = +41 \text{ kJ/mol [8]} \qquad \text{(I-1.4)}$$

Although the measured rates for the WGS reaction (forward and reverse direction) are at least 2 - 3 orders of magnitude smaller than the CO oxidation rates (see, *e. g*., chapter III-1.3.2), the reverse WGS sets the limit for the minimum CO concentration, which may be achieved by the selective CO Oxidation [10-12].

2. Technical application: PROX

An increasing awareness for environmental protection over the last two decades has lead to new efforts in order to reduce the exhaust emissions. For mobile applications a new generation of fuel cell power sources (*e. g.*, in the NECAR series by Daimler Chrysler [13]) is expected to replace the currently employed combustion engines. Most of the vehicles, based on PEM fuel cells (proton exchange membrane), gain power from the electrochemical oxidation of hydrogen. As a result the local emission of NO_x, CO and CO_2 is absent or, for the latter, at least significantly reduced [14]. Unfortunately, gaseous hydrogen has a very low energy storage density (1 kJ/cm³ for steel cylinders) [14]. Even if recently developed light-weight materials for gas cylinders are employed, the required volume and weight is still not acceptable for a mobile application in cars [13]. Liquid hydrogen would allow for a much more compact construction (10 kJ/cm³ [14]), but the necessary low-temperature tank wastes a lot of additional energy for cooling, decreasing the overall efficiency, and bears several technical problems, *e. g.*, an inevitable leaking of hydrogen or strictly required safety devices [15]. Other solutions for a direct storage of hydrogen, *e. g.*, nanotube materials or metal hydrides, are envisaged for the future but still require time for the development of suitable prototypes [16].

An alternative concept, which is currently envisaged as an intermediate solution, includes the „on-board“ production of a hydrogen-rich gas from liquid hydrocarbons or alcohols, which provide a superior energy storage density (17.7 kJ/cm³ for methanol), *e. g.*, by a steam reformation process [14, 17]. A suitable fuel is methanol, which requires rather low process temperatures for the reforming step (ca. 250 - 300°C over a Cu/ZnO catalyst), so that the number of side reactions is limited, and can be easily gained from various sources (methane, coal, bio-mass) [14, 16]. The steam reformation process provides a feed gas (reformate) which consists of ~75% H_2 and ~25% CO_2 (compostion of the dry part) and additionally 10 - 15% H_2O [18]:

$$CH_3OH + H_2O \rightarrow 3\,H_2 + CO_2 \quad ; \Delta H^0 = +131 \text{ kJ/mol [19]} \qquad \text{(I-2.1)}$$

Unfortunately, due the above mentioned reverse water-gas shift reaction (eq. I-1.4), up to 2% CO are contained in the reformate, which would poison the anode catalyst in a subseqently placed PEM fuel cell (see fig. I-1) and hence decrease the energy efficiency of the system to an unacceptable level [17, 20-22]. The maximum amount of CO tolerated by currently employed Pt catalysts at acceptable losses is ~20 ppm [18] and the recently introduced PtRu

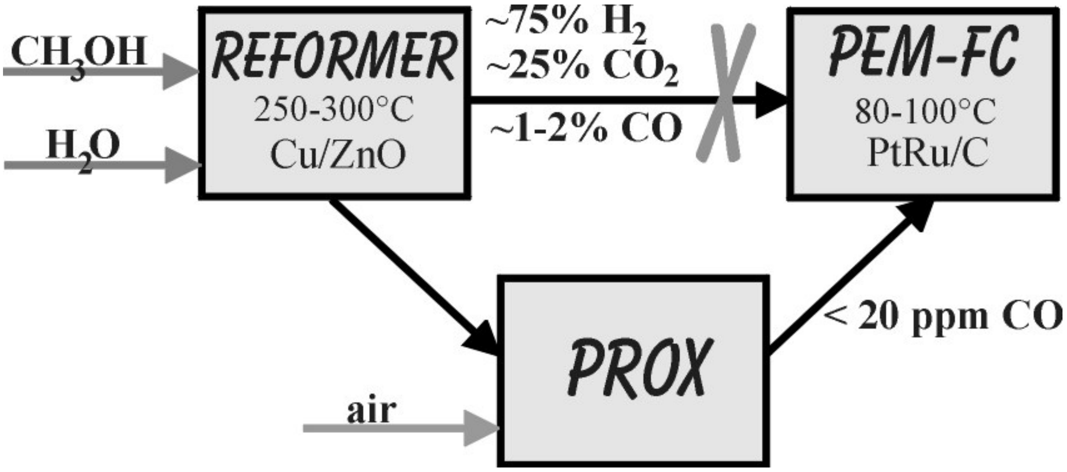

Fig. I-1: Setup scheme for an indirect methanol fuel cell power source.

anodes are hardly better (tolerance <100 ppm [16, 23]). A small fraction of the CO can be removed by dosing traces of oxygen over the anode catalyst (so-called „air-bleed“) [20], which extends the CO tolerance to 100 - 500 ppm but this technique induces also unwanted effects like sintering of the anode catalyst or ageing of the membrane [17, 18]. Consequently an additional purification stage is required, which reduces the CO content down to levels that are acceptable to the anode catalyst. Various concepts have been proposed, *e. g.*, selective methanation, pressure swing adsorption or diffusion membranes and also the preferential CO oxidation, which is named „PROX“ [17, 18, 24]. Currently the latter is preferred, since it allows for a rather space saving implementation compared to the other alternatives and the material costs are relatively low [17, 18].

Figure I-1 provides an overview scheme of the above described feed gas supply for a PEM fuel cell unit including a methanol reformer to produce the H_2-rich feed-gas and a subsequently placed PROX stage for the removal of carbon monoxide.

3. Intention of this work

The intention of this work is to grant mechanistic insight into the preferential CO oxidation over a few selected noble metal catalyst systems. Primary object is to explain the activity and selectivity behaviour, which was recorded in a parallel kinetic study by M. Kahlich [25]. Further aspects of interest are the long-term stability (stable steady-state or deactivation) under reaction conditions and effects arising from the use of different support materials. Finally, since the majority of kinetic experiments were performed in a simplified reaction atmosphere (*i. e.*, without water and CO_2; see, *e. g.*, [7, 26]), the influence of a more realistic atmosphere on the activity and selectivity is another central subject of this work. As a result the detailed understanding of these reaction processes might be helpful for the design of new catalyst systems and reactor concepts in future PROX applications.

The experimental priority is set on infrared spectroscopy, which allows for the *in-situ* observance of adsorbed surface species under reaction conditions. Nevertheless, a whole bunch of further methods, *e. g.*, reactor experiments, temperature programmed desorption, and X-ray diffraction, had to be additionally employed in order to develop comprehensive explanations for the observed phenomena.

After a short introduction on the experimental setup, we will start with the investigation of $Pt/\gamma\text{-}Al_2O_3$ (and later on also of other platinum catalysts), which was among the first catalysts proposed for the selective CO oxidation and still represents the basis for most of the currently employed systems [4, 10, 14, 18, 27, 28]. Consequently all other catalysts in this work are compared to it as a reference system. In the following chapter we will turn to a bimetal catalyst, a Pt-Sn alloy, to see, how the modification with another metal affects the activity / selctivity behaviour compared to the previously investigated pure platinum metal catalysts. The last catalyst under investigation is a system with a somewhat different CO oxidation scheme: supported gold, which was already proposed as an active system for PROX at very low operation temperatures [29-31]. Finally we will conclude the work with a comparative summary of the previously presented results.

Since large parts of this thesis are based on the results of a parallelly conducted kinetic study [25], some illustrations have been drawn from the latter work. These figures have been marked explicitely with „*{KAH}*“.

II. EXPERIMENTAL

1. Setup

Mixture	c [%]	purity degree	provider
H_2	100	5.0	MTI
N_2	100	6.0	MTI
CO	100	4.7	Linde / MG
CO in N_2	2	4.7 / 6.0	Messer Griesheim
CO in H_2	4	4.5 / 5.6	Mess. Gr. / MTI
CO in H_2	2	4.7 / 5.6	Messer Griesheim
CO in H_2	0.14	4.7 / 5.6	Messer Griesheim
CO_2	100	6.0	Messer Griesheim
O_2	100	5.0	MTI
O_2 in N_2	10	5.0 / 5.0 (CO-free)	Linde / MTI
O_2 in N_2	0.35	5.0 / 5.0 (CO-free)	MTI
O_2 in CO_2	10	5.5 / 6.0	Messer Griesheim
1%CO, 1% O_2, 1% CO_2, ½ % CH_4, 75% H_2, rest N_2			AGA
1% CO, 1%O_2, 25% CO_2, rest H_2			AGA

Table II-1: Different gases used for the experiments.

1.1 Reaction gases & mixture facility

In order to simulate reaction atmospheres as close as possible to those produced by a real methanol reformer (see fig. I-1) and to be able to investigate the effect of each contained component in detail, we arranged a complex gas mixture assembly, which allows for the variation over a large concentration range for each reactant. The central mixture faciltiy (scheme shown in fig. II-1) consists of four mass-flow controllers (2 x 100, 1 x 50 and 1 x 20 Nml/min MFCs; Hastings HFC-202), which are set by an electronic control unit (Hastings power supply 400). Pure gases and commercially available gas mixtures (table II-1) are attached *via* steel and copper (for CO-containing gases) tubes (Dockweiler) and switched by three-way valves (Whitey or Parker). Water could be added in a concentration range between 0.6 and 1.5 kPa by bubbling the feed-gas stream through a tempered water vessel (see fig. II-1). For each gas the corresponding MFC was calibrated manually by a flow-meter to ensure accurate flow rates (for more detailed information see [9, 32]). All flows are given in „Norm-milliliters“ per minute (Nml/min), *i. e.*, standardized to 0°C and 1 atm (ideal gas behaviour

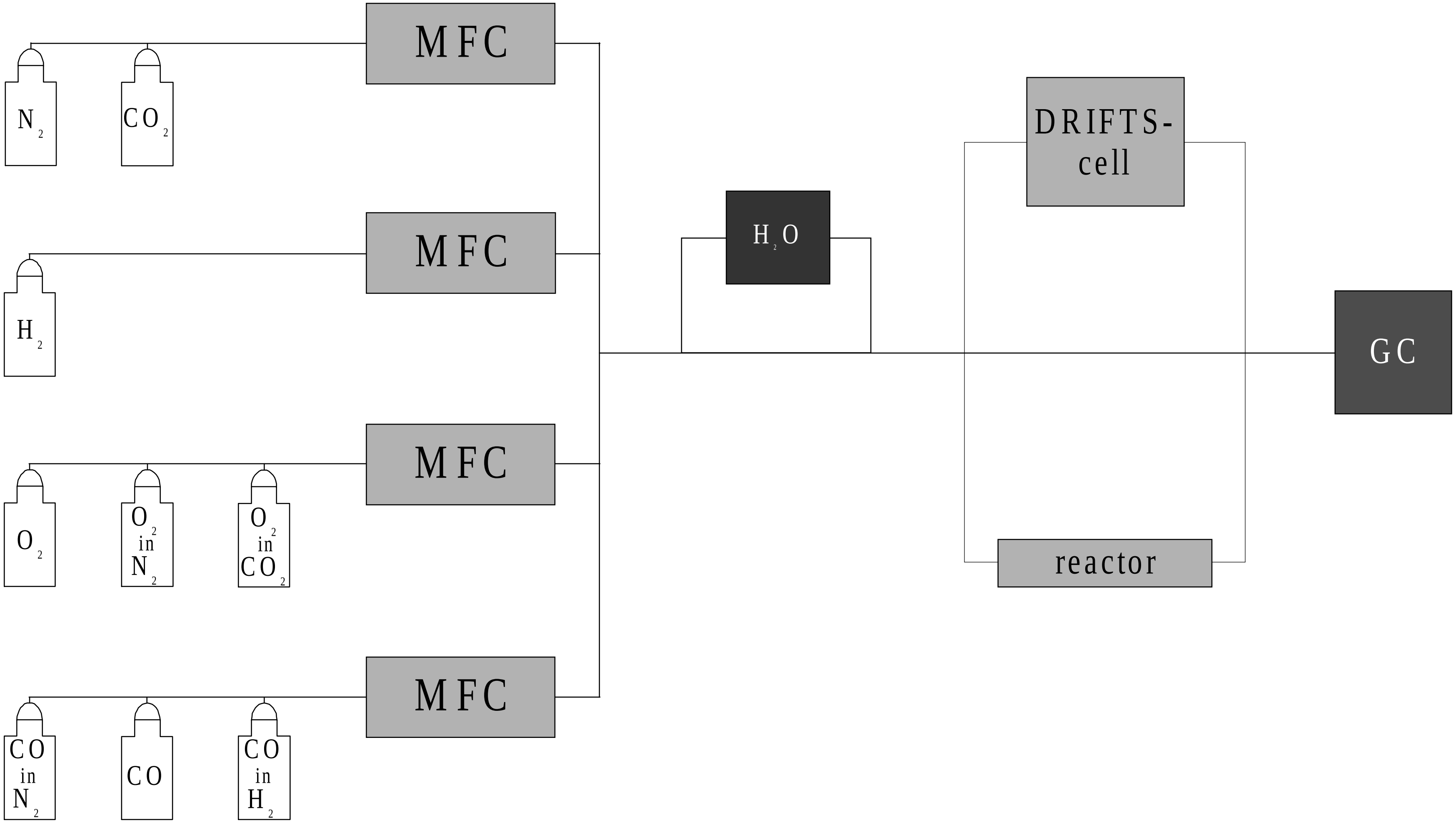
MFC
MFC
MFC
MFC
N_2
CO_2
H_2
O_2
O_2 in N_2
O_2 in CO_2
CO in N_2
CO
CO in H_2
H_2O
DRIFTS-cell
reactor
GC

__Fig. II-1__: Scheme of the gas supply setup.

term	applied for	CO [kPa]	O_2 [kPa]	H_2 [kPa]	CO_2 [kPa]	N_2 [kPa]	H_2O [kPa]	λ
„idealized reformate“	PROX	0.02-1.5	0.02-1.5	~75	-	rest	0-1.5	2 $^{1)}$
„more realistic reformate“	PROX	0.02-1.5	0.02-1.5	~75	rest	-	0-1.5	2 $^{1)}$
	reverse WGS $^{2)}$	-	-	~75	rest	-	1.5	-
	forward WGS $^{2)}$	1.0	-	-	-	rest	1.5	-

1) except indicated differently 2) WGS: water-gas shift reaction

Table II-2: Most frequently used reaction gas compositions

presumed). For most experiments flow rates between 80 - 135 Nml/min were applied, corresponding to a typical space velocity of 15 - 25 s^{-1}.

The most frequently used reaction gas mixtures are listed in table II-2. The term „idealized reformate“, which will be used frequently in the upcoming chapters, corresponds to a CO oxidation mixture with 75 kPa hydrogen and rest N_2 and was used, *e. g.*, for the majority of kinetic experiments [7, 9, 25, 26]. For a better overview the exact gas phase compositions, especially when differing from the standard mixtures, are indicated separately for each experiment. The partial pressure for the added oxygen in our experiments is expressed indirectly *via* the λ-value:

$$\lambda = 2 \cdot \frac{p_{O_2}}{p_{CO}} \qquad \text{(II-1.1)}$$

p_X = partial pressure of CO and O_2, resp. [kPa]

By three- and four-way valves the reaction gas mixtures may be directed either into the reactor tube (described in chapter 1.2), to the *in-situ* DRIFTS cell (chapter 1.3.2) or directly to the GC (chapter 1.4) for bypass-measurements, which were required as a reference standard for the calculation of the degree of conversion (fig. II-1).

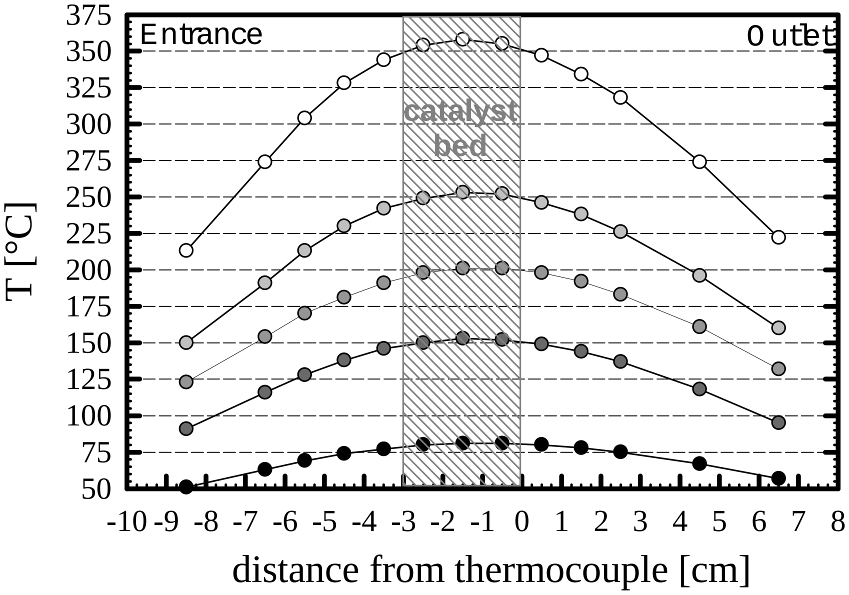

Figure II-2: Temperature-profiles inside the plug-flow reactor tube.

1.2 The plug-flow reactor

The test reactor consists of a small quartz tube (ID 4 mm; for the majority of shift and TPD-experiments also ID 10 mm), where the catalyst bed (ID 4 mm: ~100 mg, ID 10 mm: up to 1000 mg powder) is fixed in the middle by quartz wool plugs (see also [9]). A K-type thermocouple is attached on the tube above the catalyst bed by a ceramic paste (Polytech 905). The tube is placed inside a steel cylinder (ID 15 mm; endings sealded by steel plugs), whose temperature can be controlled by a facility for heating and cooling, via a resistant wire (Horst HSQ 900) wrapped around the cylinder and a parallely attached air cooling (1/8“ steel tube; Dockweiler). The latter is split up into two parts, both with the air entrance located at the ends of the steel cylinder. The addition of the cooling facility produced rather satisfying temperature profiles, with a stationary zone (± 2°C) reaching at least over 2-3 cm, which was sufficient for a standard catalyst bed (see fig. II-2). For thermal isolation the steel cylinder is embedded in a thick layer of quartz wool. Operation temperatures of up to 900°C may be applied to the reactor. On the other hand, when the cooling air is passed through a liquid nitrogen trap, the reactor may be cooled down to max. -100°C, which was necessary, *e. g.*, for the temperature-programmed desorption experiments on the bimetallic Pt-Sn catalyst (see chapter III-2.1.2).

For a plug-flow reactor it is assumed, that axial diffusion is negligible and that there are no radial variations of the flow rate [33]. The rates for the CO oxidation are calculated by a model, where the changes for a differential mass / volume element over the catalyst bed are considered *via*

$$\int_0^m \frac{dm}{\dot{V}_{CO_{in}}} = \int_0^{X_m} \frac{dX_{CO}}{-r_{CO}} \qquad \text{(II-1.2).}$$

m = mass of catalyst [g]; $\dot{V}_{CO_{in}}$ = volumetric flow [Nml/min];

X = conversion degree; r_{CO} = rate of CO oxidation [mol_{CO}/g*s]

For differential flow conditions (*i. e.*, at small conversion), where no major concentration changes occur and thus the rate becomes virtually constant along the catalyst bed, the average reaction rate may be calculated by integration of eq. II-1.1:

$$r = -X_m \cdot \frac{\dot{V}_{CO_{in}}}{m} \qquad \text{(II-1.3).}$$

Practically, differential flow conditions were fullfilled at conversion degrees below 20%. A more profund review on the plug-flow theory with a detailed derivation of eqs. II-1.2 and II-1.3, respectively, may be taken from ref. [9]. In order to guarantee differential conversion most of the catalyst samples had to be diluted with a non-reactive material. For most experiments α-Al_2O_3 (BET 4.7 m²/g) was used, since it also mitigates the pressure drop over the catalyst bed, thus any diffusional effects could be safely excluded. Only for the water-gas shift experiments, where the reaction proceeds at a much lower rate than the CO oxidation, the formation of a reactive interface by the mechanical mixing of the catalyst and the α-Al_2O_3 could have falsified the results significantly. Therefore for those measurements the catalysts were diluted either by a tempered low-surface-area version of the corresponding support material (SiO_2, MgO, TiO_2) or by SiC (Aldrich).

For a better comparison between different catalyst samples, in most plots and tables the rate was normalized to the number of available surface metal atoms and expressed as a turnover-frequency (TOF; [s]):

$$TOF = r_{CO} \cdot \frac{M_{met}}{D} \qquad \text{(II-1.4)}$$

M_{met} = atomic mass of noble metal [g]; D = metal dispersion

The reproducibility of the rates is strongly affected by the type of catalyst used and by possible deactivation effects during storage (see, *e. g.*, chapter III-3.4.1). For Pt/γ-Al_2O_3 the reproducibility was very good (rate less than ±20%, selectivity less than ±5%), for Pt_3Sn/Vulcan and the gold catalysts the deviations between measurements on different catalyst beds were sometimes larger, so that for many experiments an average over three or more experiments had to be taken in order to achieve a similar accuracy for the data.

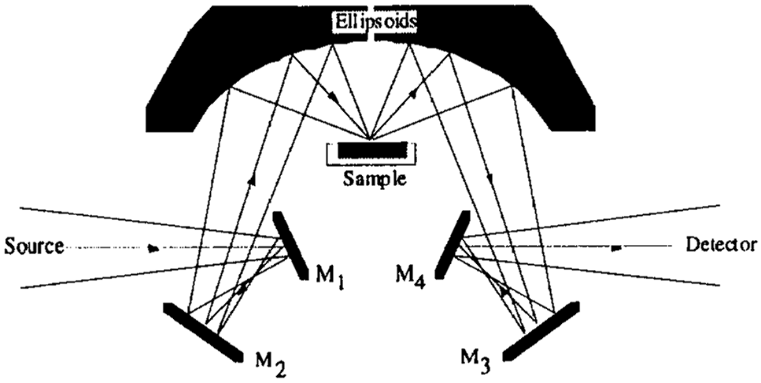

Fig. II-3: Scheme for the measurement of diffusely scattered light from a powder sample [40].

1.3 Infrared spectroscopy - DRIFTS

Infrared spectroscopy is one of the few methods that can be easily adapted for the *in-situ* characterization of surface species under non-vacuum conditions. The (selective) CO oxidation over noble metals is an excellently suited object for such studies, since the adsorbed CO has a large IR cross section (as well as possible by-products, *e. g.*, carbonates) and its absorbance frequency is very sensitive to both the local environment of the adsorption site [34] and the presence of other coadsorbed species [35]. This sensitivity is caused by small variations in the electron density of the substrate metal d-states, which results in an altered „back-donation“ of electrons from the metal to the 2π*-orbital of the CO, causing a corresponding shift in the absorbance freqency of the C-O bond [36]. Moreover, CO molecules adsorbed in close vicinity exhibit dipole-dipole coupling, which induces a slight coverage-dependent shift of the corresponding IR-bands to higher absorbance frequencies [37-39]. Therefore not only the absolute intensity (identical adsorption sites presumed) but also the position of the CO_{ad}-band serves as a good indicator for the surface CO coverage at the applied reaction conditions.

Especially the analysis of diffusely scattered light from powdered samples, DRIFTS (diffuse reflectance infrared Fourier transform spectrometry), has found a wide-spread use for heterogeneously catalyzed reactions. A fast increasing number of publications on apparative improvements (see *e. g.* [41, 42]) as well as many applications for catalytic studies (*e. g.* [32, 40, 43] have appeared in the last few years. The use of a diffuse reflectance setup (see scheme in figure II-3) allows for observations on powdered catalysts without any further sample preparation. Therefore corresponding structural changes, which, *e. g.*, may occur during the high-pressure formation of a KBr-pellet, required for transmissions FTIR spectroscopy, are avoided [41, 44, 45]. Moreover, the possibility to conduct high flow rate reactant streams through the sample, similar to a micro-kinetic reactor, along with the excellent control of environmental conditions in the used *in-situ* cells enables measurements under conditions very close to that of real technical applications and allows for studies at differential-flow conditions, which suffer less from the danger of mass-transport induced spectral artifacts. A major disadvantage of DRIFTS, however, is the unknown penetration depth of the incident beam, so that an absolute quantification as for transmission experiments is not possible. Thus for the calculation of, *e. g.*, the surface CO coverage some additional informations, *e. g.*, theoretical calculations *via* adsorption-desorption equilibria, are required as an calibration point (see, e. g., chapter III-1.1.3).

Figure II-3 shows a typical setup scheme for a DRIFTS measurement. With the help of mirrors the infrared beam is directed to a spherical mirror, which focusses the light onto the sample. A second spherical mirror collects the diffusely scattered light, which is further lead to the detector.

Since DRIFTS is not yet fully established as a standard method for applications in heterogeneous catalysis, we will provide a short review on the DRIFTS theory in the following section.

1.3.1 DRIFTS-theory

The basic equation for describing the intensity of any diffusely scattered light from a powder sample is given by the radiation transfer equation [46]:

$$-\frac{dI}{\kappa \rho dS} = I - \frac{j}{\kappa} \qquad \text{(II-1.5)}$$

I = light intensity at wavelength λ; ρ = density

κ = attenuation coefficient (radiation loss from absorption and scattering);

S = optical pathlength; j = scattering function

This equation may be simplified and solved by introducing well-definded experimental conditions. For a supported metal catalyst the most suitable approach was shown to be the Kubelka-Munk theory [47], where the incident and scattered light are approximated by two opposite fluxes, which are perpendicular to the illuminated surface [48]. For an infinitely thick sample the diffuse reflection can be described as a function of an apparent absorption and an apparent scattering coefficient in the so-called Kubelka-Munk equation [46, 49-51]:

$$f(R_\infty) = \frac{(1-R_\infty)^2}{2R_\infty} = \frac{k}{s} \qquad \text{(II-1.6)}$$

R_∞ = diffuse reflection from an infinitely thick sample;

k = absorption coefficient; s = scattering coefficient

The coefficients k and s are in priciple characteristic for each material under investigation, but it should be mentioned that the scattering coefficient, s, is a not only an intrinsic material function, but also , *e. g.*, dependent on the particle size, the particle distribution, the packing density and the humidity of the sample, which even for a known penetration depth would make an absolute quantification impossible [51, 52].

The required criterium of infinite depth is strongly dependent on the absorption of the sample. For a weak absorber (*e. g.*, Al_2O_3) a sample thickness of ca. 1 mm is necessary, for a strongly absorbing material like carbon the infrared beam penetrates only in the range of micrometers [53]. Additional experimental conditions for the use of the Kubelka-Munk function are [46]:

- a diffuse irradiation of the sample,
- isotropic light scattering,
- a low absorber concentrations (< 10% [53])
- a uniform absorber distribution

Since the thickness of the catalyst bed in all our DRIFTS cells is 3 mm or more and the absorber concentration is very low, due to the dilution with the support material, all pre-conditions are fullfilled and the Kubelka-Munk function should be well suited for evaluating our infrared spectra.

In order to avoid the measurement of absolute light intensities the reflection is related to a reference material, yielding the relative reflection, r_∞ [40]:

$$f(r_\infty) = \frac{(1-r_\infty)^2}{2r_\infty} = \frac{k}{s} \qquad \text{(II-1.7)}$$

For a weakly absorbing sample the absorption coefficient may be replaced by the extinction coefficient [49]

$$k' = 2.303 \cdot \varepsilon \cdot c \qquad \text{(II-1.8)}$$

ε = extinction coefficient; c = absorber concentration

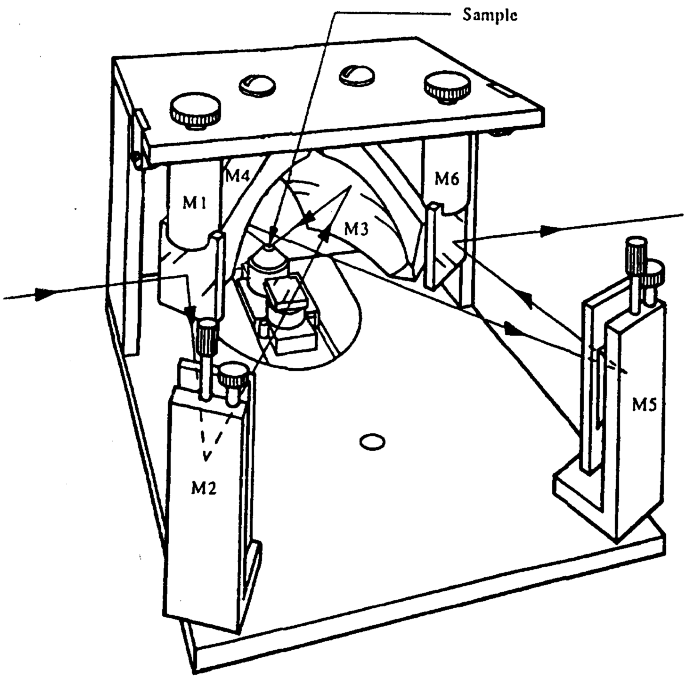

Fig II-4: „praying mantis“ mirror alignment [54].

and eq. II-1.7 is transformed into

$$f(r_\infty) = \frac{2.303 \cdot \varepsilon \cdot c}{s} = \frac{c}{k'} \qquad \text{(II-1.9)},$$

hence under these conditions the diffuse reflectance should be linearly related to the absorber concentration, which is indeed observed experimentally for absorber concentrations below 10% [53]. At higher concentrations, however, deviations due to specular and diffuse Fresnel reflection (*i. e.*, directly reflected light without penetration into any particle) and due to a decreasing penetration depth are noticed [55-57].

1.3.2 DRIFTS-setup

For our DRIFTS measurements we used a commercial mirror arrangement by Harricks in the so-called „praying mantis“ form (PM-DRA-2-XXX) to direct the infrared beam. The compartment is shown in figure II-4. The mirrors are aligned in an „off-axis“-geometry, *i. e.*, the interfering specular Fresnel reflectance is being faded out, which results in an extension of the linear concentration range for the Kubelka-Munk function [57].

We have employed three different *in-situ* DRIFTS cells. First we started with a commercial cell by Harricks (HV-DR2; see fig. II-5), but it was only used for a few of the adsorption experiments on the Pt/γ-Al_2O_3 catalyst (chapter III-1.1.1). The major part of work was done in a closely related imitation by our university workshop. For the latter model the gas leakage

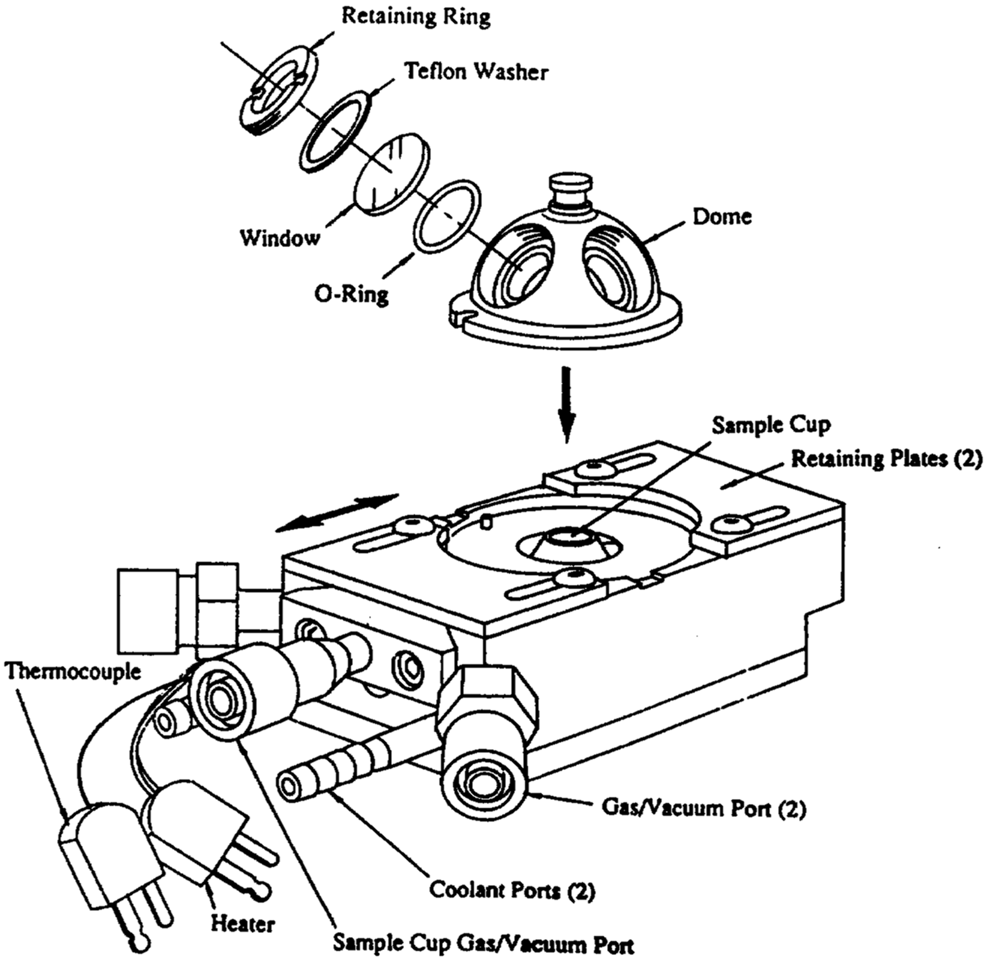
Retaining Ring
Teflon Washer
Window
O-Ring
Dome
Sample Cup
Retaining Plates (2)
Thermocouple
Gas/Vacuum Port (2)
Coolant Ports (2)
Heater
Sample Cup Gas/Vacuum Port

Fig II-5: Harricks DRIFTS-cell HV-DR2 [58].

problem, which is described in detail in appendix A, was reduced significantly, so that mass-transport related artifacts for spectra acquired during reaction could safely be excluded. The temperature for both cells is adjusted by an electronic controller (Watlow series 965), which controls a heating rod. The latter is mounted below the sample cup.

Later on, for measurements, which require the parallel recording of accurate kinetic data, we designed a completely new cell, which is introduced detailed in appendix A. The latter was used for our studies on the influence of increasing CO_2-contents on the selctive CO oxidation (see *e. g.* chapter III-3.5.2).

All cells allow for a continous gas flow through the catalyst bed (ca. 0.1g powder), which is placed on a small steel net. ZnSe had to be used as a window material, since the commonly employed KBr material was not resistant to the water produced in the H_2 + O_2 side reaction during the selective CO oxidation.

In order to achieve a reproducible packing density (which results in a more uniform scattering coefficient; see eq. II-1.7), we used a small weight to compress the freshly filled catalyst powder. Nevertheless, absolute intensities of spectra acquired on different catalyst beds should be compared with much reservation. Even if an identical catalyst is used, the tolerance for the signal intensity is more than ±10%. Consequently all experiments, where a sample is examined in different atmospheres were conducted in the form of „switch“-experiments, *i. e.*, the same catalyst bed was exposed subsequently to different mixtures. This procedure reduces the tolerance to 2 - 5%.

1.3.3 Processing of DRIFTS spectra

Spectra were acquired either with an Infinity AR 60 (Mattson) or on a Magna 560 (Nicolet) spectrometer, both equipped with a narrow-band MCT (mercury cadmium telluride) detector. The DRIFTS experiments were controlled and evaluated by the WinFIRST (Mattson) and by the OMNIC software package (Nicolet), respectively.

For each measurement several spectra were added in order to increase the signal to noise ratio (SNR). The number of coadded scans depended strongly on the penetration depth of the infrared beam into the powder, which is much larger for brightly coloured samples (*i. e.*, weak absorbers). Consequently, for Pt/γ-Al_2O_3 (chapter III-1) 300 scans, corresponding to a total scanning time of ca. 2.5 min., were sufficient. For the black Pt_3Sn/Vulcan catalyst (chapter III-2) measurements were only possible after dilution with a less strongly absorbing material (in most cases α-Al_2O_3; ca. 1:20). Nevertheless, at least 1200 scans were required, for very accurate measurements even up to 3000 scans (scanning time ca. 25 min.), in order to achieve an acceptable SNR. The experiments on Au/α-Fe_2O_3 yielded good results with 400 - 600 coadded scans (depending on the degree of dilution), corresponding to a total scanning time of up to 5 min..

In order to correct for the DRIFTS geometry, all spectra were evaluated as „diffuse spectra“ (designated by Kubelka-Munk units), following this standard procedure:

- At the beginning of each experiment one or more „background spectra“ (one for each envisaged measurement temperature - again averaged over the required number of single scans) are recorded on the freshly conditioned catalyst sample under a flow of pure nitrogen. Subsequently the „sample spectra“ at the applied reaction conditions are acquired. Both are recorded in the form of „single-beam spectra“, *i. e.*, as if the infrared light would be emitted directly from the sample (absolute IR intensity *vs.* wavelength)

- In the next step, a conventional „transmission spectrum“ is calculated by dividing the sample spectrum through the background reference,

$$T = \frac{I}{I_0} \qquad \text{(II-1.10)}$$

I = sample emissivity; I_0 = background emissivity

which is further transferred into the well-known form of an „absorption spectrum“:

$$A = - \log(T) \qquad \text{(II-1.11)}$$

Since the absolute intensity of the diffusely scattered light is highly sensitive to the position of the catalyst bed’s surface [32, 45, 59], the signal may decrease slightly during a measurement series as a consequence of a slowly occuring displacement of the surface (*e. g.*, by the increasing compression of the catalyst bed by the applied gas flow). In order to correct for such deviations, the sample spectrum is scaled to the background intensity at a „fixed point“, which is reproducible during the experiment (*i. e.*, where no IR bands are growing - in most cases between the gas-phase bands of CO and CO_2 at around 2250 cm^{-1}, as was proposed, *e. g.*, by Barth *et al.* for the CO adsorption on Pt/Al_2O_3 [60]). To exclude spectral artifacts in the final DRIFTS form arising from a cross-over of the sample and background spectra, since the Kubelka-Munk function (eq. II-1.6) produces absolute values and absorption bands in the negative range would be inverted [61], all sample spectra were multiplied by a factor 0.96 after the scaling procedure, so that the intensity of the sample spectrum is safely below the background for all measured wavelenghts.

- In the last transformation the Kubelka-Munk function (eq. II-1.7) is applied to the absorption spectrum:

$$\text{KM-spectrum} = \frac{(1-A)^2}{2A} \qquad \text{(II-1.12)}$$

- Finally the CO gas-phase signal was removed by scaling and subtracting a reference spectrum obtained under identical conditions over a non-reactive material (Al_2O_3, SiO_2 or SiC).

The adjusted nominal spectral resolution was 4 cm^{-1} (Mattson) or 8 cm^{-1} (Nicolet), respectively, corresponding to an effective reproducibility of roughly ± 0.1 cm^{-1} [59]. Higher resolutions werw not employed, since the ensueing unfolding of the rotational fine structure would make a proper subtraction of the gas-phase signal impossible [32].

Most catalysts had to be diluted, not only for an improvement of the sampling depth, but also to fullfill differential flow conditions. In analogy to our reactor measurements for most experiments α-Al_2O_3 was employed, which had been tested previously for its non-reactive character (unpublished results).

1.4 On-line GC analysis

The reactant/product mixture leaving the plug-flow reactor or the DRIFTS cell, respectively, is directed to a gas chromatograph for on-line analysis of the CO conversion and selectivity (fig. II-1). The GC (model CP9001; Chrompack) is equipped with two parallelly installed widebore capillary columns (∅ 0.53 mm). H_2 is used as carrier gas (18 Nml/min). The GC's oven temperature is adjusted to 60°C. A diagram of the column setup is provided in fig. II-6. After the sample volume (ca. 15 µl) has been introduced *via* a six-way walve (SV2), in the first step, CO_2 and water are separated from the less polar components by a Poraplot U type column (25 m, 20 µm coating; Chrompack). Subsequently, *via* a four-way valve (SV1) the remaining gases (N_2, O_2, CH_4, and CO) are directed to a Molesive 5Å column (30 m, 15 µm coating; Chrompack), where they are finally resolved into single peaks. The resulting total run time is ~8 min.. Each channel (Poraplot and Molsieve, resp.) is monitored by a thermal conductivity detector (Chrompack TCD 914). For the analysis of CO and O_2 „bypass measurements“ (*i. e.*, without passing the catalyst bed), acquired prior to the experiment, are used for calibration. The CO_2- and CH_4-contents (the latter would evolve from the parallely occuring CO + H_2 reaction) are evaluated *via* comparison to a „calibration gas“ of known composition. The GC measurements were controlled by the Maestro software package (Chrompack), which was also used for the integration of the resulting chromatograms.

The dectection limits for this setup are at least 10 ppm for each component. A reproducibility (standard deviation) of ±0.2% was calculated at the typical analyte pressure of 1 kPa.

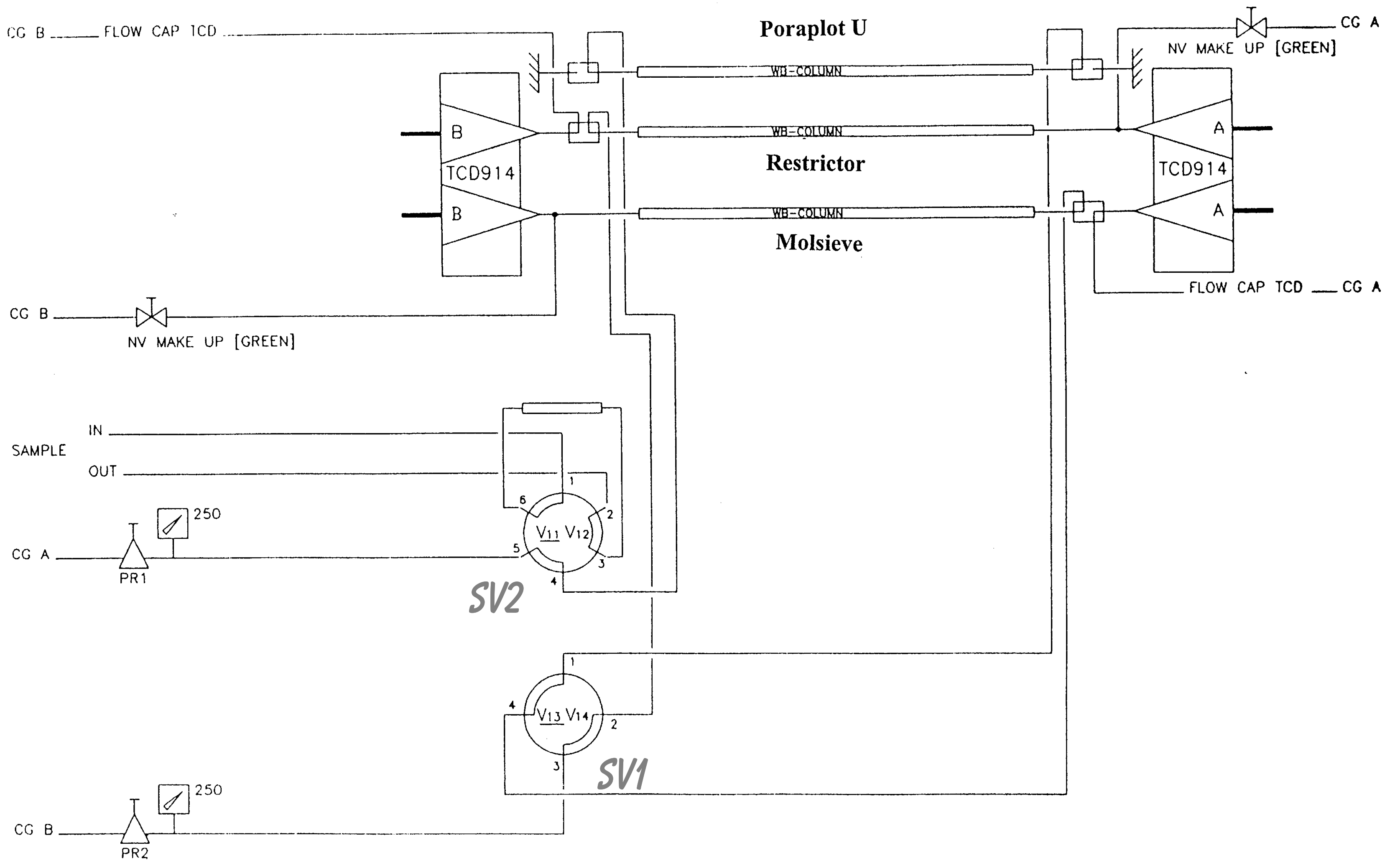
CG B
FLOW CAP TCD
Poraplot U
WB-COLUMN
NV MAKE UP [GREEN]
CG A
B
TCD914
B
WB-COLUMN
Restrictor
A
TCD914
A
WB-COLUMN
Molsieve
FLOW CAP TCD
CG A
CG B
NV MAKE UP [GREEN]
SAMPLE
IN
OUT
1
6
2
V11 V12
5
3
4
CG A
250
PR1
SV2
1
4
V13 V14
2
3
SV1
CG B
250
PR2

Figure II-6: GC-Setup.

1.5 Other methods used

1.5.1 XPS

The sample chamber for the XPS experiments has a base pressure of $5*10^{-9}$ kPa. It is equipped with a hemispherical analyzer (Specs EA 2000; ∅ 150 mm) and a standard dual anode source. The Al-Kα-line (1486.6 eV) was used for our experiments. The pass energy was set to 147 eV for survey scans and 88 eV for more detailed spectra, corresponding to a resolution of 1.4 and 1.2 eV, respectively, for the Ag($3d_{5/2}$) signal. Signals of Au($4f_{7/2}$) at 84.0 and Ag($3d_{5/2}$) at 368.3 eV were used for the calibration of the spectrometer. The spectra acquisition is controlled by the Spectra software package.

For the evaluation of the XP spectra a Shirley background subtraction routine was employed [62]. The signals were fitted by Gauß-Lorentz functions. In order to compensate for charging effects on the Au catalysts (chapter III-3), the C(1s)-signal was fixed to 284.6 eV. The Pt_3Sn/Vulcan catalyst (chapter III-2) showed no charging effects due to its excellent electric conductivity. For futher information the reader is referred to ref. [63].

1.5.2 On-line IMR-MS analysis

The TPD (chapter III-2) experiments on Pt_3Sn/Vulcan and the oxygen titration experiments on Au/α-Fe_2O_3 and Pt/γ-Al_2O_3 (III-3.1.3) were performed by on-line analysis with an IMR-MS (ion molecule reaction mass spectrometer). This type of mass spectrometer (Atomika IMR-MS SP89) employs low energy noble gas ions (Xe^+, Kr^+) for the ionization of the analyte gas, so that the fragmentation process is significantly reduced. Consequently it allows for the detection of CO on the mass 28 without any interference from, *e. g.*, nitrogen, which is not ionized under these conditions, or from CO_2, which is not fragmented [64].

The employed noble gases are dosed by a calibrated leak, resulting in a pressure of 10^{-5} kPa in the ionization chamber; the analyte gas is differentially pumped and then dosed separately *via* a 60 µm iris (10^{-6} kPa). The gate-time for analysis (quadrupole MS) was 2 s for each of the seven surveyed components (CO, CO_2, O_2, H_2O, CH_4, Kr, and Xe) in our TPD measurements. Together with an additional delay of 1 s, this corresponds to a sampling frequency of 4 datapoints per minute. For the CO titration experiments (chapter III-3.1.3) a shorter gate-time of 0.2 s (O_2, CO_2, CO, Kr, Xe) was chosen, equivalent to 1 datapoint per second. The resulting signals are detected by a SEV. For analysis all signals were normalized to the noble gas signals and calibrated with the help of reference gases of known composition. The measurements are recorded by a software package from Atomika. The integration of peaks was performed with the Sigma Plot software (Jandel Scientific). Further details on the analysis by IMR-MS may be taken from ref. [65]. For futher information on the setup see ref. [66].

1.5.3 Isotope studies / pulse experiments

The isotope / pulse studies were performed in a TAP-reactor (temporary analysis of products; model 1b, equipped with a high pressure assembly) at the Institute of Technical Chemistry, University of Bochum. A detailed description of a typical TAP-setup and the employed reactor type, which contained a mass of ca. 50 mg catalyst powder, is found in ref. [67]. All experiments were performed in the vacuum-flow mode (*i. e.*, with vacuum applied to one end of the catalysts bed), which is characterized by a very short contact time for the reactants (incoming flow rate ca. 1-2 Nml/min).

For our investigations on the Au/α-Fe_2O_3 catalyst (chapter III-3.1.3) we admitted pulses of isotopically labeled $^{36}O_2$ (Cambridge Isotope Laboratories; ca. 95% ^{18}O; diluted with Argon 1:5; ~$2*10^{15}$ molecules/pulse) to a continuously flowing reaction mixture for the selective CO oxidation (ca. 1.7% CO, $\lambda = 2$; 75% H_2, rest Ne).

1.5.4 XRD

XRD experiments were performed on a Siemens D5000 spectrometer at the ZSW (Center for Solar Energy and Hydrogen Research) in Ulm, Germany, using the Cu-K_α line (1.540 Å). The source beam is limited by a variable software-controlled slit. A further „scatter slit“ of 2 mm, which fades out the diffusely scattered light from the sample, a „receiving slit“ of 0.6 mm and a graphite monochromator were used for all measurements. The experiments are controlled and evaluated by software from Bruker. For peak fitting procedures pseudo-Voigt functions were applied. The determination of the particle size was done *via* the Scherrer-equation, where the halfwidth (FWHM) is inversely proportionally related to the particle diameter [68].

Since the very small metal particles on our gold catalysts (see tables III-10) are already close to the XRD detection limit, the latter is not a very accurate method for determining the corresponding dispersion. Therefore the calculated TOFs exhibit a rather large tolerance of up to ±50% for those samples which contain the smallest gold particles. Consequently for some samples additional TEM photographs were recorded for a more precise determination of the average particle size.

2. Catalyst characterization

Catalyst	**company / product**	**metal loading [wt-%]**	**Pt particle size [nm]**	**D [%]**	**$T_{conditioning}$ [°C]**
Pt/γ-Al_2O_3	Degussa F 213 XR/D	0.5	4 (CO-TPD) 1) 2.3 ±0.6 (TEM)	38 42 2)	350
Pt/MgO	Engelhard 41621	0.5	4.6 ±1.6 (TEM)	20 2)	350
Pt/SiO_2 3)		0.5	ca. 3 (TEM)	50	350 4)
Pt/TiO_2	Degussa F 700 XR/D	0.5		40 5)	350
Pt/Vulcan	E-TEK	20	3.7 ±1.0 (TEM)	26 2)	300
Pt black	Mateck	100	15.6 (XRD)	10	200

1) see ref. [9]; 2) particle size distribution (TEM) included for calculation of D;
3) preparation via colloid particles; 4) calcination for 90 min.
5) assumption for TOF calculations in chapter III-3.1.3

Table II-3: Pt-catalysts used for our experiemts

2.1 Platinum catalysts

Several different Pt-catalysts were employed in our study (table II-3). The majority of the experiments were performed over a commercial Pt/γ-Al_2O_3 catalyst (Degussa; F 213 XR/D), which is closely related to currently employed systems for PROX applications (*e. g.* [10, 16, 18]). Prior to the experiments all Pt-catalysts were pretreated oxidatively by 10 kPa O_2 in N_2 (20 Nml/min; 30 min.) and subsequently reduced in flowing hydrogen (20 Nml/min; 30 min.). The resulting platinum particle sizes and dispersions are included in table II-3.

2.2 Pt_3Sn catalyst

The carbon supported bimetallic PtSn catalyst (Pt_3Sn/Vulcan by E-TEK) was loaded with 20 wt% metal containing 75 at% Pt. The particle size distribution determined by TEM, with an average particle diameter of 3.8 ±1 nm after catalysts conditioning (see below), yields a dispersion of 0.27. The formation of uniform alloy particles with nominal composition is indicated in spot-resolved EDX measurements on the reduced sample.

For Pt_3Sn/Vulcan the best set of pretreatment parameters was evaluated in a series with different conditioning temperatures (200 - 350°C) and durations (up to 1 h), where the most active and selective catalyst was achieved after 30 min. calcination (20 Nml/min O_2/N_2) and reduction (20 Nml/min H_2), respectively, at 300°C.

2.3 Gold catalysts

All gold catalysts were synthesized (by V. Plzak; ZSW Ulm) in close accordance with standard procedures from literature (see *e. g.* [69-72]):

- Coprecipitation (*e. g.* for Au/Fe_2O_3, Au/Ni_2O_3, $Au/Mg(OH)_2$, Au/CeO_2):

  7 - 10 g catalyst were prepared by titrating a solution containing $HAuCl_4$ and the support metal nitrate with a Na_2CO_3-solution (all 1M) at a constant pH-value and (for most cases) a temperature of 60°C (volume ca. 1 liter). The exact precipitation conditions are provided in tables III-10 and III-12. Further details on this procedure may be taken from ref. [73].

- Deposition-precipitation (*e. g.* for Au/Fe_2O_3, Au/Co_3O_4, Au/MnO_2, Au/SnO_2):

  Differently from the above described coprecipitation procedure, in the first step only the pure support precursor was formed before the $HAuCl_4$ was added in a second step at changed precipitation conditions (pH near the isoelectric point; see also table III-10-A).

- Impregnation (*e. g.* for Au/TiO_2, Au/Al_2O_3):

  The support material (7 - 10 g) was suspended in a buffered aqueous solution of Na_2CO_3 (ca. 1 liter) and impregnated near its isoelectric point with chloroauric acid at 60°C.

The amount of employed $HAuCl_4$ was calculated in order to prepare samples containing ca. 2 at-% metal. The exact loading along with a detailed characterization of the freshly calcined catalyst is given in tables III-10 and III-12.

After filtration the wet samples were redispersed several times in water in order to remove residual chlorine and especially sodium, which was shown to cause a strongly enhanced sintering of the gold particles during the following calcination procedure (chapter III-3.2.3). Subsequently, the samples were dried overnight at 80°C and ground manually.

The resulting catalysts were pretreated by a calcination step with 10% O_2/N_2 at 400°C prior to all experiments (20 Nml/min, 30 min.). Differing pretreament procedures are indicated explicitely in the text.

III. RESULTS & DISCUSSION

1. The standard catalyst - Pt/γ-Al_2O_3

Alumina and silica supported platinum metals have been extensively studied for the CO oxidation in the past (see *e. g.* [74-77] and references therein). Consequently they were among the first catalysts proposed for the preferential oxidation of CO in an H_2-rich atmosphere (PROX) [4, 27, 78-80], which is one way for purifying the feed gas streams for polymer electrolyte fuel cells (PEM-FC) produced from steam reformed methanol [14, 18, 22]. Currently the Pt/Al_2O_3-system still represents the basis for the majority of commercially used catalysts in industrial applications [10, 16, 17, 28, 80, 81], although its performance has been improved over the years by modification with several promotors [80, 82].

Consequently, in our efforts to study the selective CO oxidation reaction over supported noble metal surfaces, we started from a commercial Pt/γ-Al_2O_3 catalyst (for characterization see chapter II-2.1). After evaluating the detailed kinetics and selectivity in idealized reformate for a variety of reaction conditions (Kahlich *et al.* - [9][7, 12, 83]), we tried to understand the exact nature of the reaction mechanisms, which are responsible for the observed properties.

In the following part we will try to relate the data obtained in the kinetic studies to surface species and processes and to characterize the influences, which additional components (H_2, H_2O, CO_2), constituting a real methanol steam reformate, exhibit on the basic CO oxidation reaction. We will begin with the determination of the CO_{ad} coverage on the metal particles under reaction conditions by *in-situ* DRIFTS experiments and demonstrate its close correlation to the selectivity before we further elucidate the role of coadsorbed hydrogen. In the subsequent chapter we will focus on effects arising from the presence of H_2O and / or CO_2 in the reactant feed gas and investigate, whether the simplified approach by idealized reformate in our kinetic studies is justified. In the last chapter we will compare various standard support materials with respect to the CO oxidation activity as well as to the water-gas shift reaction, which determines the minimum CO concentration achievable in a virtual PROX stage.

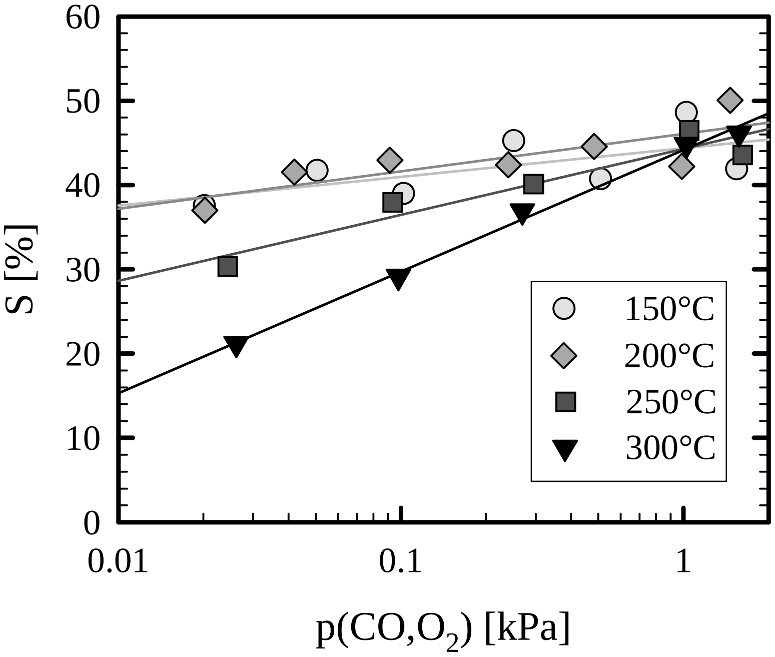

Fig. III-1: Selectivity over Pt/γ-Al_2O_3 in idealized reformate at λ = 2 for different temperatures. *{KAH}*

1.1. The influence of the CO coverage on the activity / selectivity

1.1.1 Selectivity & hydrogen induced rate enhancement

From an economic point of view it is crucial to waste as little hydrogen as possible in the PROX stage, thus the selectivity, S, which is defined by the ratio between the CO and H_2 oxidation rate, is of outstanding importance.

$$S = \frac{r^{CO}}{r^{CO} + r^{H_2}} = \frac{\Delta O_2^{CO-\text{oxidation}}}{\Delta O_2^{CO-\text{oxidation}} + \Delta O_2^{H_2-\text{oxidation}}} \qquad \text{(III-1.1)}$$

r^X = oxidation rate of CO and H_2, resp.; ΔO_2^X = oxygen consumed by oxidation reactions

On examining the detailed kinetics of the selective CO oxidation over Pt/γ-Al_2O_3 in idealized reformate it was found by Kahlich *et al.*, that the dependence of selectivity on the CO partial pressure changes markedly with temperature (figure III-1) [7, 25]. Whereas at 150 and 200°C the selectivity remains almost constant at 40 - 45 % over the whole CO partial pressure range from 1.5 to 0.02 kPa (at a constant λ-value of 2), it decreases significantly at 250°C down to 30% at 0.02 kPa CO. At 300°C the selectivity loss at lower CO partial pressure is even more pronounced, ending at only 20% for 0.02 kPa.

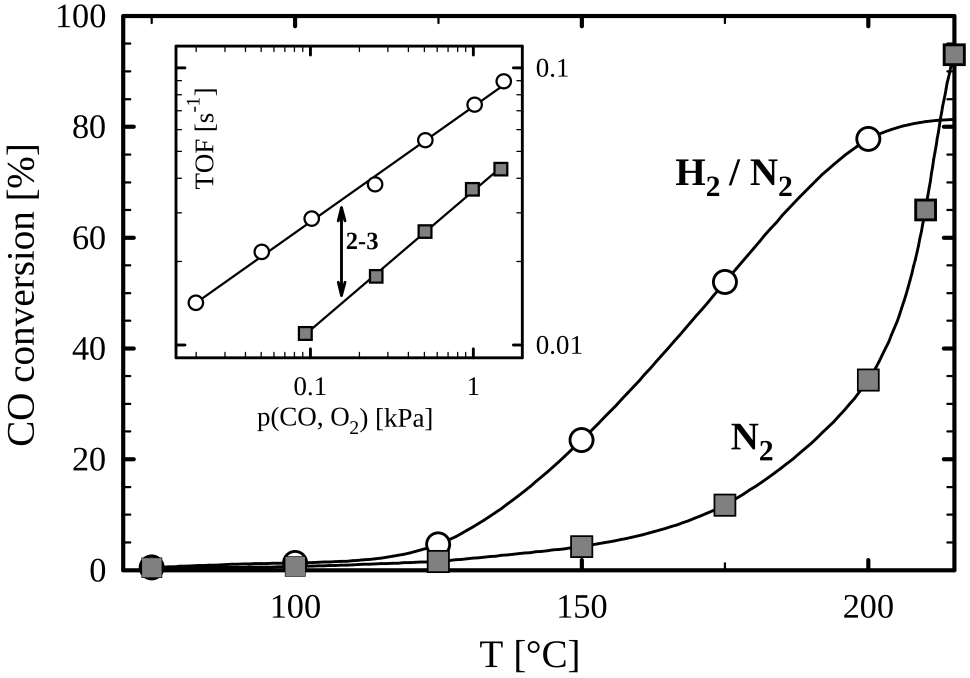

Fig. III-2: CO conversion of 1 kPa CO (λ = 2) at different temperatures in the presence of 75 kPa hydrogen (○; rest N_2) and in a pure nitrogen background (■), respectiveley (data taken after 15 min at each setpoint). *Inset*: Rate enhancement of the CO conversion at 150°C in the presence of 75 kPa hydrogen as a funcion of CO and O_2 partial pressure (λ = 2; data taken after 60 min at each point). *{KAH}*

Another interesting phenomenon, which was observed in the kinetic studies by Kahlich *et al.*, is a 2 - 3-fold enhancement of the CO oxidation rate, when switching at 150°C from a mixture of CO and O_2 in pure N_2 to idealized reformate, which additionally contains 75kPa H_2 (inset in figure III-2) [7, 32]. Consistent with this enhancement, the light-off temperature for the CO oxidation is shifted to lower temperatures ($\Delta T \approx 30 - 40$°C) in the presence of hydrogen (figure III-2) [7, 32]. But from the kinetic measurements it could not be clarified how this rate enhancement is established and if the effect should be attributed to either co-adsorbed hydrogen or the water, which is produced *in-situ* as a result of the $H_2 + O_2$ reaction. Muraki *et al.* also reported rate enhancing effects of similar magnitude on Pt/α-Al_2O_3 upon adding either 3 kPa water or 0.3 kPa hydrogen to 1 kPa CO ($\lambda \approx 0.9$) in the temperature range between 120 and 200°C [84]. In their DRIFTS spectra they observed a small downward shift of the band for linearly adsorbed CO and interpreted this as a perturbation of the surface CO_{ad}-layer induced by coadsorbed water, which would weaken the self-poisoning effect of the CO, but they could not further substantiate this proposal. In another kinetic study on the selective CO oxidation over γ-Al_2O_3-supported platinum metal catalysts Oh and Sinkevitch noted a 40°C downward shift in the light-off temperature for the CO oxidation reaction at 0.09 kPa CO (λ ≈

2) over Pt, when adding 0.9 kPa hydrogen [4]. Likewise similar effects of hydrogen have been reported in some other studies dealing with selective CO oxidation [5, 85, 86] and also, *e. g.*, by Dümpelmann *et al*. for the NO/CO conversion reaction on Pt/γ-Al_2O_3, where a blocking CO_{ad} layer limits the NO conversion rate in a similar way as will be shown for the PROX reaction [87]. All latter studies speculate on the formation of highly reactive H-CO intermediates on the metal surface, but yet there exists no direct prove for the formation of such species [3].

In the following we will investigate the relationship between CO coverage and selectivity behaviour on the basis of CO adsorption isotherms, recorded by DRIFTS at temperatures from 150 to 300°C. Subsequently, we will take a closer look at the influence of coadsorbed hydrogen and show that a hydrogen induced displacement in the CO_{ad}-layer may serve as a good explanation for the above described rate enhancement effects.

1.1.2 Experimental limitations - neglecting the reaction rate

Provided that the CO and H_2 oxidation reactions on platinum both follow a Langmuir-Hinshelwood mechanism [1-3, 88-91], these high selectivities of more than 40% (see fig. III-1) in a mixture with an H_2 to CO ratio of 50 and more can only be achieved if on the surface of the platinum particles a concentration ratio completely different from the gas phase exists. For the CO oxidation in a pure nitrogen background such a CO-rich surface would be typical for the so-called „low rate branch“, where the metal surface is covered predominantly with CO and dissociative O_2 adsorption is rate determining [1, 76]. Indeed, the kinetic studies by Kahlich *et al.* in idealized reformate revealed a negative reaction order for CO (-0.4; attributed to the self-poisoning effect of the CO_{ad} layer) and an oxygen reaction order close to 1 (+0.8), which are both typical for the „low rate branch“ [7]. This hypothesis was further supported by the comparison of DRIFTS spectra of 1 kPa CO in a pure N_2 background and during selective CO oxidation in idealized reformate (1 kPa CO, $\lambda = 2$) at 150°C [83]. The tall band in figure III-3 at ~2060 cm^{-1} is assigned to linearly bound CO on the platinum surface. It consists of at least two overlapping species: a low-frequency band band (~ 2050 cm^{-1}), which is assorted to CO_{ad} on step sites, and a high-frequency band (~ 2075 cm^{-1}), related to adsorption on extended terraces [92, 93]. The smaller band at ~1850 cm^{-1} represents bridge or multiply bonded CO (similarly consisting of at least two different species, probably also on terrace and step sites) [94]. In both spectra the integrated intensity of the adsorbed CO is practically constant within an experimental uncertainty of ± 5%. It is assumed, that in the CO / N_2

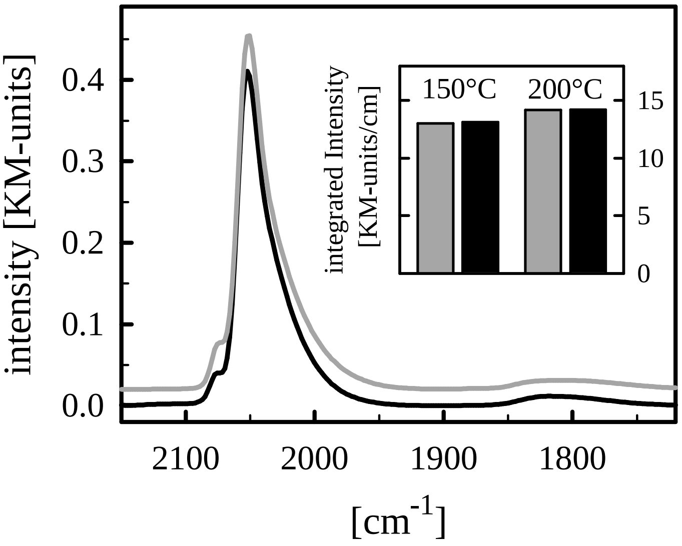

Fig. III-3: DRIFTS-spectra on Pt/γ-Al_2O_3 with 1 kPa CO in pure N_2 (——) and during selective CO oxidation (——; 1 kPa CO; λ =2; idealized reformate) at 150°C. *Inset*: Integrated intensities of the linearly bound CO_{ad} (also shown for same experiment at 200°C).

mixture the platinum surface is saturated by CO_{ad} (this will be essentially proven below), and hence the selective CO oxidation indeed proceeds on a platinum surface with a comparably high CO coverage under the applied conditions. The above experiment, however, covers just a single set of concentration and temperature parameters and needs to be verified generally.

Unfortunately the above described selectivity experiments could not be simply reproduced in the DRIFTS cell, since at temperatures above 200°C either the catalyst had to be diluted so much, that there was no sufficient IR-signal for quantification, or differential flow conditions were not fullfilled. A high background activity of the DRIFTS unit at low CO concentrations and temperatures above 200°C adds further limitations. An elegant way out, the validity of which will be shown in the following paragraph, is neglecting the reaction rate, *i. e.*, analysing the rates of carbon monoxide adsorption and desorption in the absence of oxygen. The steady state CO coverage can be expressed in terms of an adsorption / desorption balance:

$$r_{ad} = r_{des} + r_r \qquad \text{(III-1.2)}$$

r_{ad} = rate of adsorption; r_{des} = rate of desorption; r_r = reaction rate (turnover frequency)

T [°C]	r_{des} [s^{-1}]	r_r (TOF) [s^{-1}]
150	7.3 ... $3.2*10^4$	0.08
200	140 ... $4.1*10^5$	0.7
250	$1.4*10^3$ ... $3.2*10^6$	4
300	$1*10^4$ ... $1.8*10^7$	17
350	$5.1*10^4$ ... $7.5*10^7$	55

Table III-1: Comparison of the range for the desorption term r_{des} (see eq. III-1.2) with experimental and calculated turnover frequencies for the selective CO oxidation (1 kPa CO, $\lambda = 2$, idealized reformate; [7]) [95-98].

$$(1-\Theta)\cdot s\cdot\frac{N_A\cdot p}{\sqrt{2\cdot\pi\cdot R\cdot T\cdot M_{CO}}}\cdot\frac{1}{\rho}=\Theta\cdot\nu\cdot\exp\left(-E_A/RT\right)+r_r \qquad \text{(III-1.3)}$$

θ = relative CO coverage; s = sticking coefficient; N_A = Avogadro number;
p = partial pressure [Pa]; R = gas constant [J/g*K]; T = temperature [K];
M_{CO} = molecular weight of CO [g/mol]; ρ = surface density of Pt [atoms/m²];
ν = preexponential factor [s^{-1}]; E_A = activation energy [J]

The desorption term can be estimated theoretically from the adsorption energies and preexponential factors given in several CO adsorption studies on Pt single crystal faces. In table III-1 desorption rates at saturation coverage from those studies which represent the most extreme parameters of E_A and ν and thus should cover all possible values [95-98] are compared with the turnover frequency calculated from our kinetic data [7]. For the calculation of the r_r term it was assumed that the kinetics do not change markedly at high temperatures, which is indeed fullfilled over the whole range of conditions, where the above selectivity measurements have been taken [25]. For all temperatures the reaction rates are at least two orders of magnitude smaller than the desorption term, therefore the r_r term may well be neglected and a variation of the CO partial pressure in a CO / N_2 mixture should yield the same change of CO coverage as would be expected in the presence of O_2. In figure III-4 the integrated IR intensities of the linearly bound CO in different gas mixtures containing 1.5 kPa CO at 150°C are compared. The first two columns, representing the amount of adsorbed CO in a CO / N_2 mixture and during oxidation reaction ($\lambda = 2$) in a pure nitrogen background, are

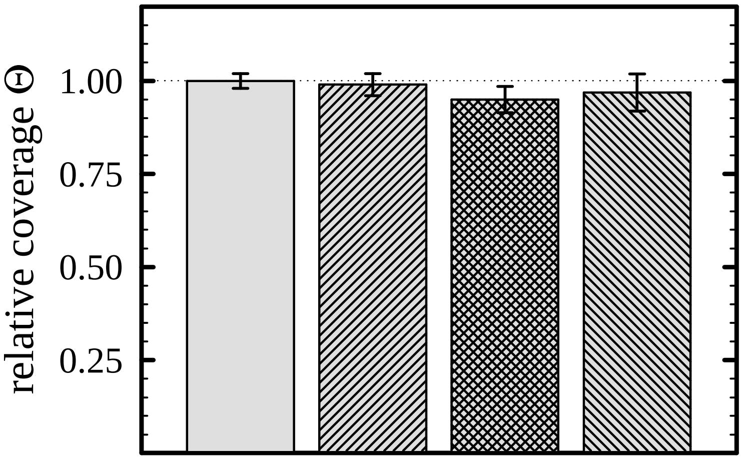

Fig. III-4: CO coverage (relative to saturation coverage) on Pt/γ-Al_2O_3 at 150°C in different atmospheres containing 1.5 kPa CO: ░ CO / N_2; ▨ CO / O_2 / N_2 ▩ CO / H_2 / N_2; ▧ CO / O_2 / H_2 / N_2 (PROX); (with H_2: 75 kPa; O_2: 1.5 kPa).

indeed almost identical within a measurement accuracy of ± 3%. This clearly verifies the above proposed simplifications.

1.1.3 Adsorption of CO in pure N_2

As was pointed out in chapter II-1.2.1, DRIFTS is only a relative technique, because an integration over the whole catalyst bed is not possible. Moreover, the CO coverage at a given partial pressure cannot be determined simply by a temperature raising experiment, because the IR cross section changes strongly with temperature, mainly caused by the reduced CO dipole coupling at elevated temperatures [40, 99] (compare also chapter III-2.1.2). Insofar some additional information is required as an absolute calibration point.

In table III-2 several studies on the adsorption of CO on different platinum single crystal faces are listed. With each set of parameters (sticking coefficient, s_0, preexponential factor and adsorption energy at high and low coverage) the relative CO coverage at a partial pressure of 1.5 kPa was calculated for temperatures between 150 and 350°C. For simplification purposes a constant sticking coefficient and a linear relationship between desorption energy and θ_{CO} were assumed. One should be aware, that the absolute saturation coverage of CO on platinum is around 0.7 ML [95] - the relative coverage of $\theta_{sat} = 1$, used in this work, which is calculated by the simplified model, corresponds to this absolute value. According to the results from table III-2 it is clearly justified to assume a saturation coverage at 150 °C. At 200°C the

Pt face	s_0	ν [s^{-1}]	E_a at θ_{sat} [$^{kJ}/_{mol}$]	E_a at $\theta \approx 0$ [$^{kJ}/_{mol}$]			θ_{CO} at			Method	ref.
					150°C	200°C	250°C	300°C	350°C		
111	0.67	10^{13}	135	154	1	1	1	1	1	TDS	[98]
111	1	10^{15}	84	139	0.99	0.93	0.83	0.72	0.60	TDS	[95]
111	0.84	$1.25*10^{15}$	103 $^{(1)}$	146 $^{(2)}$	1	1	0.97	0.90	0.78	TDS + MBS	[101]
111	0.83	(10^{13})	99	192	1	1	1	1	0.98	TDS	[102]
111	0.85	$2*10^{14}$ - $3.2*10^{7}$ $^{(3)}$	45	138	1	1	1	1	1	LI-TDS	[103]
111	0.76	(10^{13})	68	183	1	0.99	0.96	0.93	0.89	Calorimetry	[100]
111	(0.7)	10^{13}	101	139 $^{(2)}$	1	1	1	1	0.98	TDS	[104]
557	(0.7)	10^{13}	101	139	1	1	1	1	0.98	TDS	[104]
111	0.74	$2.9*10^{13}$	(90)	126	1	1	0.98	0.93	0.84	MBS	[105]
557	0.74	$7.9*10^{13}$	(105)	141	1	1	1	0.99	0.95	MBS	[105]
111	0.34	10^{13}	95	124	1	1	1	0.98	0.91	Flash-TDS	[106]
110	0.64	10^{13}	83	109	1	1	0.97	0.90	0.78	„	[106]
100	0.24	10^{13}	99	134	1	1	1	0.98	0.94	„	[106]
210	0.95	10^{13}	114	152	1	1	1	1	1	„	[106]
211	0.27	10^{13}	114	148	1	1	1	1	1	„	[106]
111	(0.7)	(10^{13})	(105)	139	1	1	1	1	0.99	TDS	[107]
211	(0.7)	(10^{13})	(130)	164	1	1	1	1	1	TDS	[107]
110	0.8	(10^{13})	135	160	1	1	1	1	1	TDS	[108]
110	0.7	$6*10^{14}$	130	148	1	1	1	1	1	TDS + MBS	[109]
321 $^{(S)}$	0.8	$2*10^{14}$	113 $^{(4)}$	151	1	1	1	0.99	0.97	TDS	[97]
321 $^{(T)}$	0.8	$2.5*10^{11}$	(60)	96	1	0.98	0.93	0.86	0.77	TDS	[97]
533 $^{(S)}$	(0.7)	$3*10^{12}$	120	134	1	1	1	1	1	TDS	[96]
533 $^{(T)}$	(0.7)	$7*10^{12}$	98	115	1	1	1	1	0.98	TDS	[96]

( ) = estimated values TDS = thermal desorption spectroscopy Flash-TDS = flash-desorption (50 - 100 K/s) LI-TDS = laser-induced TDS
MBS = molecular beam scattering (1) = extrapolated from 116 kJ at θ = 0.33ML (2) = including defect sites (3) here: $\nu = f(\theta)$
(4) extrapolated from 134 kJ at $\theta = 0.45*\theta_{max}$ (S) = step bound CO (T) = terrace bound CO

Table III-2: CO coverage for 1.5 kPa CO in a pure N_2 background at different temperatures calculated with eq. III-1.3 from literature data for several single crystal faces, assuming a linear relationship between E_a and θ.

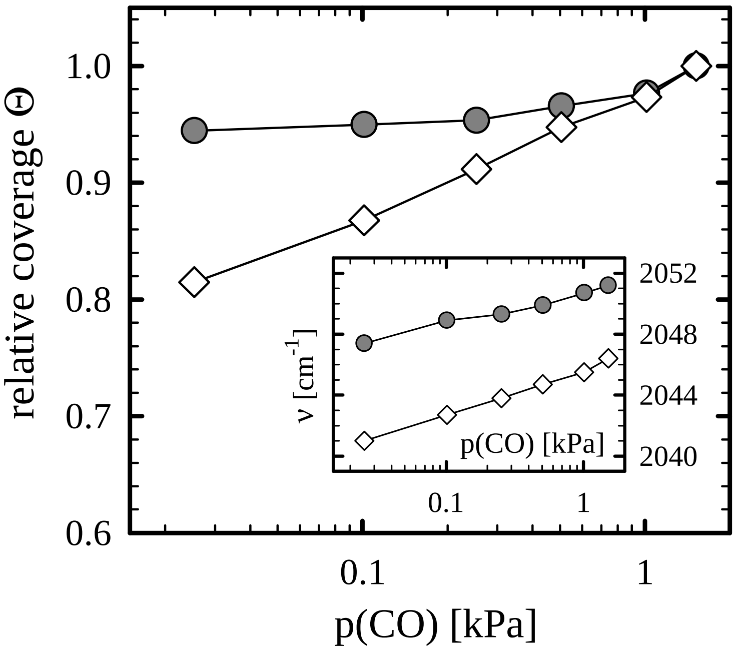

Fig. III-5: Change in the relative CO coverage on Pt/γ-Al_2O_3 with the CO partial pressure in a pure N_2 background at 150 (●) and 250°C (◇), resp. *Inset*: Corresponding positon of the infrared band for linearly adsorbed CO.

studies from Ertl *et al.* [95], Yeo *et al.* [100] and McClellan *et al.* [97] show deviations but the rest still indicates a Pt surface at saturation condition. At 250°C the number of deviations increases slightly (in most cases on the densely packed (111) crystal face, where the adsorption energy is by ~15% smaller than on the more open faces [107]), but from the vast majority of studies it should still be justified to assume $\theta = 1$. At higher temperatures, especially at 350°C, deviations become more severe so that clear conclusions on the coverage at 1.5 kPa CO cannot be drawn any longer from this table.

In our DRIFTS experiments the equilibrium surface coverage of CO is evaluated *via* the total integrated IR intensity of the linearly bound CO. Due to strongly increased half width values on supported catalysts compared to single crystals the two bands for terrace and step sites are very difficult to resolve and therefore treated as one in the following measurements. Anyway, at small particle diameters steps are the main type of adsorption site and terrace sites are just a small minority [40], which is supported by the dominating IR-signal of step bound CO in our spectra (see *e. g.* figure III-3). It is further assumed that the pressure-dependent changes in the coverage of the CO_{linear} species represent the overall changes of CO_{ad} in a satisfiying manner and that bridge bonded CO is only a minority species on our catalyst. According to Luo *et al.* at high CO coverages (the dominating) steps should be decorated exclusively with on-top species and their infrared signal is linearly related to the coverage [96]. In our DRIFTS measurements this is underlined by the extreme ratio of the integrated intensities of CO_{linear} and CO_{bridge} of 20 at 150°C and up to several hundred at higher temperatures.

Figure III-5 shows the experimentally evaluated CO equilibrium coverage in pure nitrogen at 150 and 250°C as a function of the CO partial pressure. The adsorption isotherms were recorded under a constant gas flow in an ascendig concentration sequence, waiting at least for 2 hours for equilibration at the lowest CO concentration (*i. e.*, 0.025 kPa) and then 30 min. at every other point before taking a spectrum. According to the calculations above both isotherms were scaled to the relative saturation coverage (*i. e.*, $\theta = 1$) at 1.5 kPa CO. Whereas at 150°C the coverage is near saturation coverage over the whole concentration range of two orders of magnitude, there is a significant drop in the CO coverage at 250°C down to 80% at 0.025 kPa. The small intensity increase between 1 and 1.5 kPa may be either due to an imperfect gas phase correction or, more likely, caused by a non-linearity of the IR signal due to strong coupling effects, which would increase with increasing coverage. However, in every case the same deviation would apply to all measured isothermes and not affect the relative differences. The peak position of the linearly bound CO (for the band associated with the step sites) is displayed in the small inset in figure III-5. In both cases a decrease of wavenumbers with falling CO concentration is noticed, which also points to a small decrease in the local CO density even at 150°C (Due to intensity shifts arising from coupling effects this decrease in wavenumbers is not necessarily linearly related to the coverage [110]). At 250°C the shift in peak position is slightly larger, which parallels the different slope of the adsorption isotherms. The frequency offset between 150 and 250°C of about 5 cm^{-1} at 1.5 kPa CO, where in both cases a saturation coverage has been calculated, is caused by the reduced coupling of CO dipoles at elevated temperatures, as described by Persson *et al.* [99] or Kappers [40].

For comparison purposes theoretically calculated adsorption isotherms for CO on Pt(111), derived from the values of Campbell *et al.* [101], and on Pt(321) (step sites) according to the study of McClellan *et al.* [97] are presented in figure III-6. Especially the coverages calculculated for Pt(111) (including defect sites) reflect our experimental values excellently, which demonstrates that the adsorption isotherms recorded by the DRIFTS signal of the linearly bound CO represent the true surface situation quite well. The fact that the Pt(111) surface even provides a better fit than the (321)-face, which theoretically should be closer related to small supported clusters, may likely be caused by the simplified calculations (eq. III-1), where a constant sticking coefficient (s_0) and a linear relationship between desorption

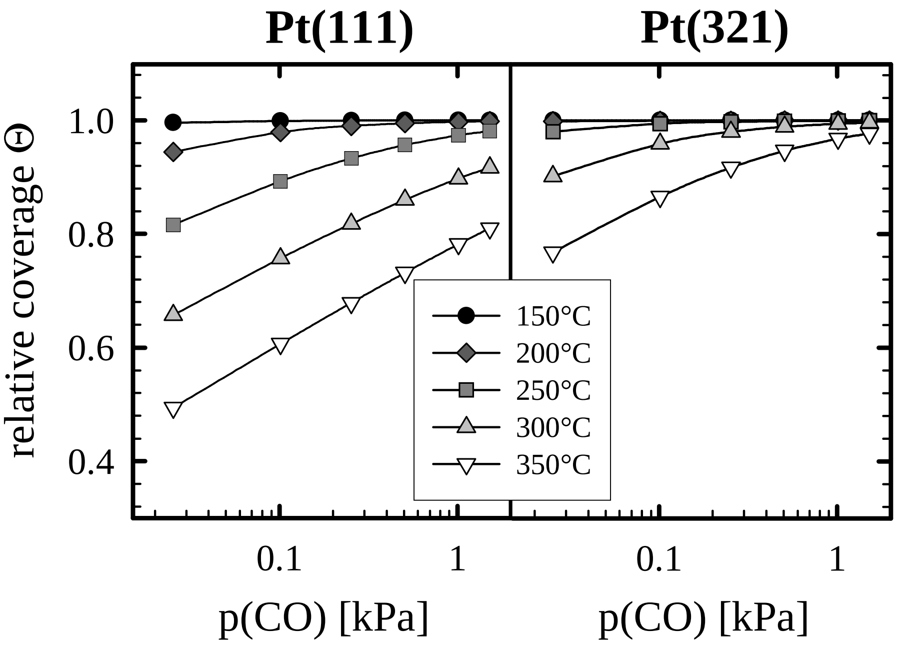

Fig. III-6: Adsorption isotherms for the Pt(111) and (321) face (step sites) calculated by the values from table III-2 using eq. III-1.3 [101, 97].

energy and coverage is assumed (which are both counteracting effects, but do not necessarily exactly outweight each other.

1.1.4 Adsorption of CO in H_2 / N_2

The question still remains if all of the above assumptions and simplifications can be applied if we proceed to a more complex matrix containing 75% hydrogen. First of all we should clarify whether we can expect an appreciable surface coverage of hydrogen at such high temperatures, since its adsoption energy is considerably smaller than that of CO [111, 112]. If we theoretically estimate coverages for pure H_2-adsorption by similar calculations as were performed for CO in table III-2, with the parameters provided in several previous studies [113-116], assuming second-order desorption kinetics, for every temperature level coverages greater than $\theta_H = 0.1$ are obtained at a partial pressure of 75 kPa hydrogen in the gasphase. Presumed, that the additional presence of CO_{ad} or O_{ad} does not affect the H_2 adsorption / desorption equilibrium significantly, we truly have a competition situation between CO and H_2 at the reaction conditions for selective CO oxidation.

Before we start a more detailed investigation of the coadsorption behaviour we will compare quantitatively the total integrated intensities of the CO_{ad} species in a pure nitrogen background (after 2 hours) and with 75 kPa H_2 (after one additional hour of equilibration). In figure III-4

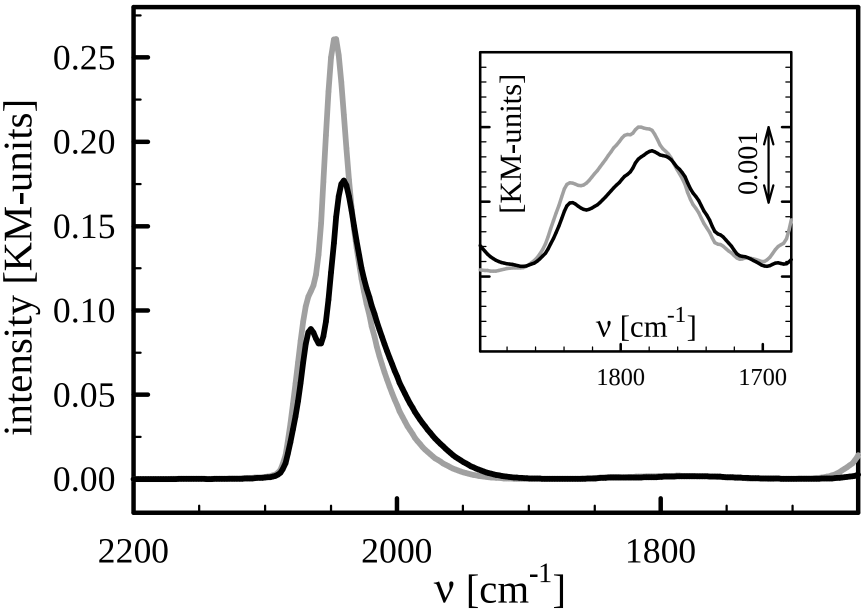

Fig. III-7: DRIFTS-spectra on Pt/γ-Al_2O_3 with 1.5 kPa CO in pure N_2 (▬) and in presence of hydrogen (▬; 1.5 kPa CO, 75 kPa H_2, balance N_2) at 250°C.
Inset: Zoom in the region for bridge bonded $CO_{ad.}$

the third column represents the integrated IR area of the linearly bound CO at 150°C in 1.5 kPa CO in 75 kPa H_2 / rest N_2. Compared to the hydrogen-free gas mixtures (first two columns) the IR signal of the linear bond CO is 5% smaller but, as will be explained in more detail in chapter III-1.2.5, this is compensated by an increase in the bridge bonded region. Thus it is rather a change in adsorption site than a significant decrease in θ_{CO}. So within the measurement tolerance of ± 3% we are still near saturation coverage with 1.5 kPa CO at 150°C in a H_2-rich gas mixture and the corresponding adsorption isotherm may again be scaled to the relative coverage $\theta = 1$.

The comparison between CO / H_2 / N_2 and selective CO oxidation in idealized reformate leads again to almost identical peak areas (columns 3 and 4 in figure III-4), which demonstrates that the above applied simplification of neglecting the reaction rate is also valid in the presence of hydrogen. It also clearly proves, that the catalyst operates near saturation coverage during selective CO oxidation, as was deduced from the kinetic measurements [7, 83] - at least within the increased measurement tolerance of ± 5%. A small loss in θ_{CO} of a few percent, however, which may be caused by the *in-situ* produced water, similar to the effects arising from the addition of water in the gas stream, described in chapter III-1.3.2, cannot be completely ruled out. Nevertheless, these results undoubtly confirm, that the selective CO

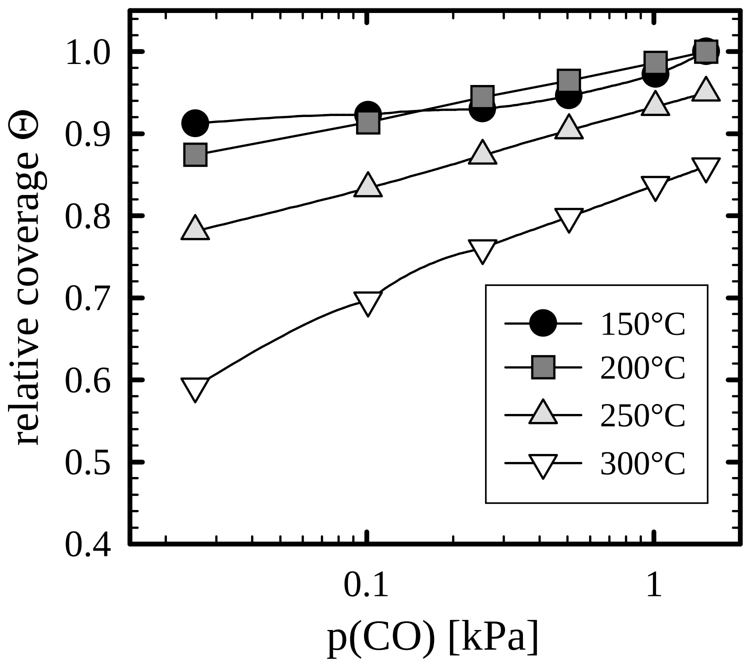

Fig. III-8: Change in the relative CO coverage with the CO partial pressure at different temperatures on Pt/γ-Al_2O_3 in a background containing 75 kPa H_2.

oxidation proceeds in the „low rate branch“ and therefore explains well the determined reaction orders.

Due to the lack of published data for calculations in a hydrogen-rich mixture, similar to those presented in table III-2, for calibration it is also necessary to compare the CO coverage at other temperatures with 1.5 kPa CO in pure N_2 and in CO / H_2 / N_2. For 200°C there was not much difference to the switching experiment at 150°C, so the CO coverage at 1.5 kPa CO in H_2 / N_2 is still at its saturation value (therefore not shown). For 250°C the corresponding IR spectra are shown in figure III-7 (The bridge bonded region is magnified in the inset window). Now there is a significant decrease in the linearly bonded region, which is – other than at 150°C – not compensated by an increase of bridge bonded CO. This represents a true loss in adsorbed CO, yielding a relative coverage of θ_{CO} = 95% in the presence of 1.5 kPa CO and hydrogen at 250°C. With view on the next chapter it should already be noted that mainly the step bound CO species (low frequency band) is affected, whereas the signal for the terrace bound CO is practically retained, although its desorption energy should be approximately 15% smaller [107]. This is explained with a strong dependence of the hydrogen adsorption upon site geometry [90, 117, 118], leading to a significant coadsorption of H_2 on step sites only.

In figure III-8 the experimental DRIFTS adsorption isotherms between 150 and 300°C of CO in a mixture of 75 kPa H_2 / rest N_2 over a concentration range of two orders of magnitude are shown. The data were recorded in the same manner as for the above measurement in pure nitrogen. Since from the theoretical calculations in chapter III.1.2.3 no absolute calibration point for the CO / N_2 isotherm at 300°C could be gained and therefore a switching experiment between a hydrogen-containing and a hydrogen-free mixture is of no use, the coverage at 1.5 kPa CO can only be estimated roughly with a tolerance of ± 5% on the basis of the coverage decrease in figure III-6 between 250 and 300°C.

Whereas at 150°C the coverage remains well above 90% of the saturation value, similar to the adsorption in a pure N_2 background, and for 200°C is only slightly less at low concentrations, at 250°C there is a significant coverage decrease at decreasing CO partial pressure, which is even more pronounced at 300°C. These adsorption isotherms exactly follow the same trend which was observed for the selectivity behaviour (fig. III-1) and show the same increasing slope at higher temperatures. Whereas near saturation coverage ($\theta > 0.9*\theta_{sat}$) the selectivity is between 40 - 45% and decreases hardly with decreasing CO partial pressure, indicating a situation with a relatively tight CO_{ad} layer, it soon drops down to smaller values below a critical value of $\sim 0.8*\theta_{sat}$. Below this point the local CO_{ad} density seems to be reduced to such an extent that hydrogen adsorption is strongly facilitated. The somewhat enhanced selectivity at 200°C at high CO partial pressures compared to 150°C may be explained by a CO coverage as high as at 150°C but a relatively lower H_{ad} coverage, due to a sticking coefficient that decreases with increasing temperature [103].

These measurements demonstrate that the selectivity is directly related to the CO coverage on the platinum particles. In view of the results on other catalysts (see chapters III-2.1.2 and III-3.3.2) this principle may be generalized for supported noble metal catalysts, that a high CO coverage (at least high compared to the hydrogen coverage, which is a crucial point for the Au-catalyst) causes high selectivity values in the PROX reaction.

1.1.5 Coadsorption behaviour of CO and H_2

Let us now take a detailed look at the coadsorption of CO and hydrogen on the platinum particles. Reviewing several studies from literature about coadsorption on platinum single crystal faces does not yield an uniform picture. The nature of the CO-H interaction seems to be very sensitive to the local surface geometry. Especially for step sites the results depend strongly on the orientation of the Pt single crystal.

On the (111)-face island formation is observed due to repulsive interactions between H and CO [111, 112, 119]. As a result of the compression into islands with a higher local density the adsorption energy of CO is decreased markedly [112]. It is very interesting that for very small H_2-pressures and coverages, respectively, which were not enough to keep up the compressed CO islands, Parker *et al.* could also observe a reduction in CO desorption energy of about 4 kJ/mol [120]. But it was not clear whether this was caused by an increased population of bridging CO at the expense of atop CO as a result of adsorbate-adsorbate interactions or due to a weak direct interaction of a similar type as in the case of alkali coadsorption as was proposed by Hoge *et al.* [119] – however, the latter could also generate such a diplacement effect in the CO population. The same island formation behaviour was observed upon H_2 adsorption on a CO precoverded Pt(997) face [118]. Henderson *et al.* investigated the coadsorption of H and CO on the step sites of a Pt(112) crystal by ESDIAD and LEED and reported likewise the formation of islands but in small one-dimensional structures consisting of tilted atop CO [121]. Whereas all the mentioned low-index planes behave in a quite similar way, a completely different situation was reported for the step sites of a Pt(533) crystal which differs by only one terrace row from the (112)-structure. After coadsorption with hydrogen, there seem to exist mixed regions of H and CO which have the same local density as for pure CO adsorption, along with one dimensional islands of pure CO [122, 123]. Within these mixed regions the site occupancy of CO is altered from atop places to bridging positions. The mixed phase is reported to show the same CO-CO distance as is found without hydrogen (*i. e.*, no compression occurs). For the on-top CO species at the edge sites only a small downward shift of a few cm^{-1} was observed in the EELS spectra, which was attributed rather to a change in the work function, Φ, caused by the adsorbed hydrogen, than to a change in the local coverage of CO. As a consequence, coadsorption may be possible at step sites even under conditions for a saturated CO_{ad}-layer. On the (111)-terraces of the Pt(533) crystal virtually no effect due to the coadsorption of hydrogen could be observed which encounters the studies on the Pt(111) faces. A possible explanation for this discrepancy, given by Wang *et al.*, is that in their experiment H built up from the step troughs and occupied sites that did not significantly affect the adsorbed CO [122]. Kim *et al.* reproduced these UHV results in aqueous electrochemical studies on a Pt(533) crystal and suggested that the hydrogen mainly coadsorbs at the step sites, since the observed effects on the IR absorbtion frequency for the terrace bound CO were again much smaller than on the step species [124]. Finally, in a study of coadsorption of H and CO on a polycrystalline Pt foil, which showed predominantly (110)

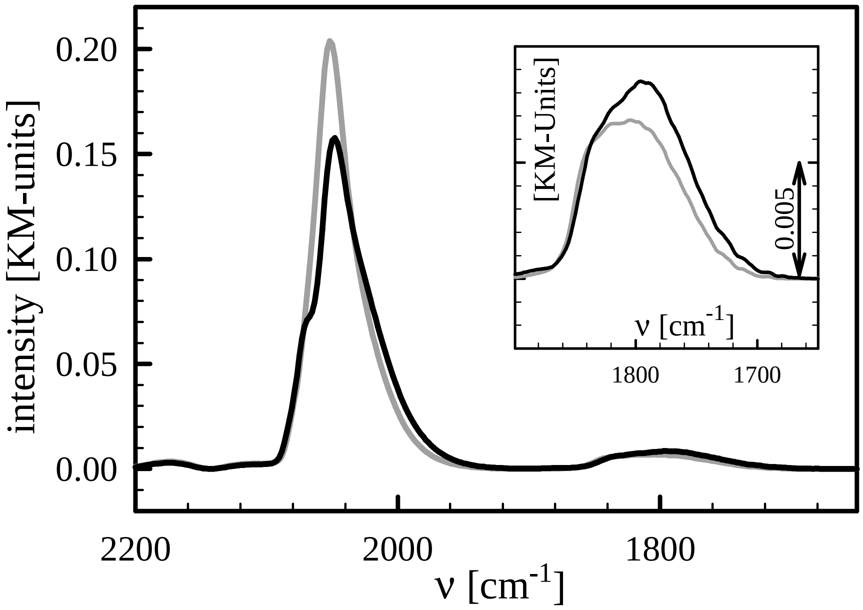

Fig. III-9: DRIFTS-spectra on Pt/γ-Al$_2$O$_3$ with 1.5 kPa CO in pure N$_2$ (▬) and in presence of hydrogen (▬; 1.5 kPa CO; 75 kPa H$_2$; balance N$_2$) at 150°C.
Inset: Zoom in the region for bridge bonded CO$_{ad.}$

characteristics, Thrush *et al.* also proposed the existence of mixed H-CO regions. In their TPD study a saturation coverage of CO completely blocked H$_2$-adsorption, but in the reverse experiment only two third of the CO was blocked. And at very low temperatures they observed coadsorption without desorption of the predosed species, which must have yielded a very crowded surface. Their results imply the idea that adsorption places exist which are only accessible to one of the adsorbents and coadsorption of one species may be possible without desorbing a corresponding fraction of the competing species. On the basis of this short literature review, coadsorption on terrace sites seems to be possible only at a low CO coverage, whereas a saturated CO$_{ad}$-layer effectively blocks the surface for hydrogen adsorption. But on step sites coadsorption of CO and H$_2$ may be expected by the formation of mixed structures.

In figure III-9 the infrared spectra of 1.5 kPa CO in pure N$_2$ and in 75% H$_2$, rest N$_2$, respectively, at 150°C are compared. Previously the catalyst was allowed to equilibrate in CO / N$_2$ for more than two hours before recording the first spectrum and then switching to the mixture containing 75% H$_2$, where the spectrum was taken after one hour on stream. The IR band from CO adsorbed linearly on step sites is shifted down for more than 3 cm^{-1} towards 2048 cm^{-1} in the presence of hydrogen and the peak is significantly diminished in height and broadened to lower wavenumbers. It is difficult to evaluate whether the high frequency band, assigned to on-top CO on terrace sites, changes its intensity, but from the analysis of the second derivatives it is obvious that it keeps its position with an accuracy of 1 cm^{-1}. The overall IR intensity of the linearly bound CO is reduced by approximately 5%. This reduction of linear bond CO is encountered by an increase in the bridge bound region of 22% (see inset). This band consists of at least two different species, too. There is a clear increase on the low frequency side (around 1790 cm^{-1}). Since the change in atop intensity was limited to step sites, the increased low frequency band at 1790 cm^{-1} is attributed to the corresponding bridge bond CO on steps, whereas the less affected higher frequency species at about 1820 cm^{-1} is assigned to CO$_{bridge}$ located on terrace sites. Although this site conversion phenomenon is most eyecatching at 150°C, since it is not accompanied by additional CO desorption as was seen at 250°C, it generally applies to all measured temperatures (150 - 300°C) that in a hydrogen-rich matrix the ratio between CO$_{linear}$ and CO$_{bridge}$ decreases by a factor of ~2 compared to CO adsorption in pure nitrogen, which corresponds to the displacement of a small fraction of CO$_{linear}$ to bridging sites.

Our results fully parallel the coadsorption behaviour studied on the Pt(533) face [122-124]: unaffected terrace bound CO, but a significant influence on step sites. Under our dynamic conditions (adsorption / desorption equilibrium) such a structure sensitive coadsorption behaviour may be most likely explained by the strong dependence of the hydrogen adsorption energy and sticking coefficient upon site geometry. Henderson *et al.* noticed a difference in adsorption energy between step and terrace sited of at least 29 kJ/mol in the presence of coadsorbed CO [121] and Christmann *et al.* showed that the initial sticking coefficient increases by a factor 4 on step sites [117]. Therefore a significant H-population is probably built up only on step sites. Another reason, why the step sites are affected exclusively, may be the unique coadsorption behaviour found for the Pt(533) step sites, which produces mixed structures with an unaltered CO density. As an interesting note, the parallel coadsorption behaviour of our supported catalyst with the Pt(533) single crystal face indeed justifies its frequent use as a model system for small particles (see *e. g.* [93])

In figure III-10 the adsorption isotherms in pure N$_2$ and with 75% hydrogen are directly compared (upper window). Obviously, in the H$_2$-rich gas the CO coverage is reduced by a few percent, even after regarding the site conversion to bridge bound species by scaling the relative coverage at 1.5 kPa CO at 150°C in both cases to $\theta = 1$. The more pronounced decrease of the local CO density with falling CO partial pressure in the presence of H$_2$ is also

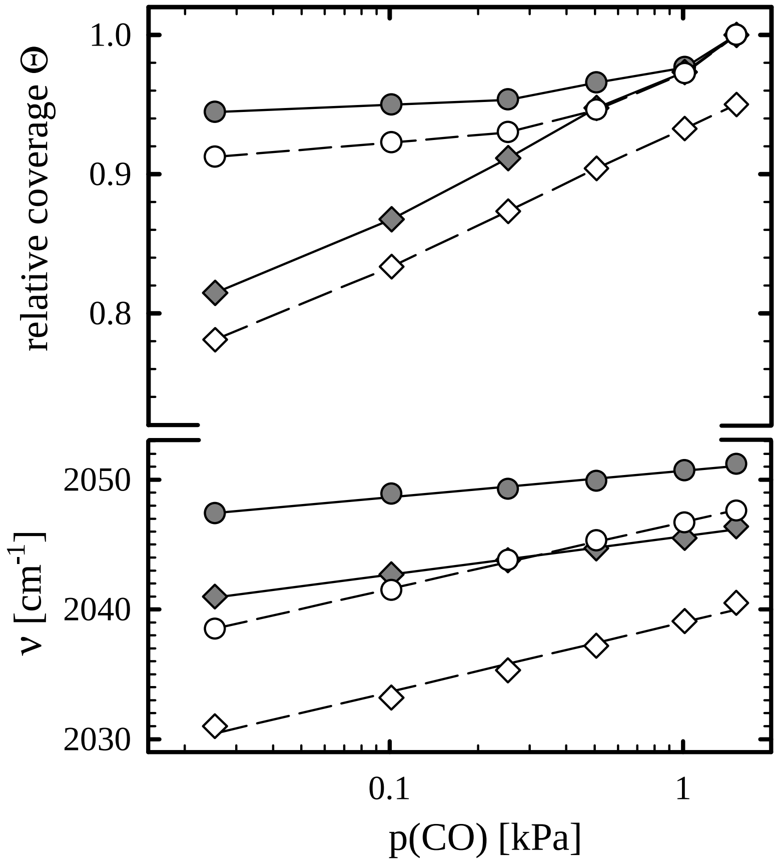

Fig. III-10: Change of the relative CO coverage (upper window) and of the corresponding band position (lower window; step sites) on Pt/γ-Al$_2$O$_3$ with CO partial pressure in pure N$_2$ at 150 (●) and 250°C (◆) and with 75% H$_2$ at 150 (○) and 250°C (◇).

indicated by the steeper slope in the evolution of band positions (lower window). Presumed that the carbon monoxide sticking coefficient and the preexponential factor (see eq. III-1.3) are not altered in the presence of hydrogen, the reduction in adsorption energy of CO, responsible for the increased desorption term, can be calculated from the relative coverages:

$$\Delta E_a = RT \cdot \ln\left(\frac{\Theta_{N_2} \cdot (1-\Theta_{H_2})}{(1-\Theta_{N_2}) \cdot \Theta_{H_2}}\right) \qquad \text{(III-1.4)}$$

ΔE_a = difference in adsorption energy [J];

θ_X = relative CO coverage in pure N$_2$ and with 75 kPa H$_2$, respectively

An average difference in adsorption energy of 2.0 ± 0.9 kJ/mol is calculated from the coverages estimated by DRIFTS. This is in fair agreement with the 4 kJ/mol decrease for CO adsorption on a Pt(111) face at low pressures in the presence of hydrogen, which was observed by Parker *et al.* [120]. It is also similar to the energetic difference for CO adsorption on atop and bridge sites on platinum [94], which now implies the hypothesis that the reduced desorption energy in our case is essentially caused by the observed transfer from linearly to bridge bound CO in the mixed H-CO structures at step sites. Possibly this effect originally emanates from direct electronic interaction between H and CO of the alkali-type as was proposed by Hoge *et al.* [119].

Since CO oxidation on platinum proceeds in the „low rate branch“ at our conditions, CO desorption is considered to be the rate limiting step. Therefore we expect the activation energy for this process to be similar to the activation energy for desorption [7, 88, 125]. If the turnover frequency is calculated theoretically using a power law approach

$$r = k \cdot \exp\left(\frac{-E_a}{RT}\right) \cdot p_{CO}{}^{\alpha} \cdot p_{O_2}{}^{\beta} \qquad \text{(III-1.5)}$$

r = reaction rate; k = constant; α, β = reaction orders for CO and O_2, respectively

the rate enhancing effect of the hydrogen coadsorption can be derived from a change in the activation energy, E_a, (presumed that $E_a \approx E_{des}$) *via*

$$\Delta r = \exp\left(\frac{-\Delta E_a}{RT}\right) \qquad \text{(III-1.6)}$$

Δr = enhancement factor in reaction rate

Although the determined effect on the desorption energy seems to be rather small, the change of 2 kJ/mol calculated from the adsorption isotherms is enough to account for a rate enhancement of a factor 1.8. Therefore the increased rate for the CO oxidation in the presence of hydrogen (see figure III-2) is almost solely attributed to the reduced CO adsorption energy caused by coadsorption of H_2 at step sites, and if, then only to a minor part to effects arising from the *in-situ* produced water, contrary to the hypothesis by Muraki *et al.* [84]. There exists also an analogous influence of water, added to the reaction mixture, on the rate for the CO oxidation over $Pt/\gamma\text{-}Al_2O_3$ [32]. In view of chapter III-1.3.2, however, this effect is more a direct consequence of the stabilization of the initial CO oxidation rate in the presence of water and not a true enhancing effect.

Our hypothesis, that the hydrogen and not the water is responsible for the rate enhancement, is also supported by experiments on Pt powder (for charcterization see chapter II-2.1), where a similar rate enhancement of even more than a factor five was observed for CO conversion at 150°C with 75 kPa hydrogen (idealized reformate; 1 kPa CO; λ = 2) compared to the oxidation in pure nitrogen. A concomitant decrease in the IR band positon upon the addition

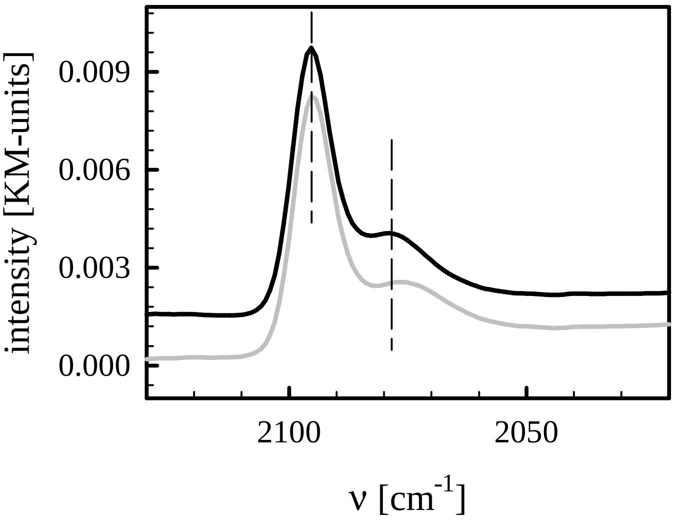

Fig. III-10a: DRIFTS-spectra on Pt-black during CO oxidation (1 kPa CO) in pure N_2 (━) and during selective CO oxidation (▬; 1 kPa CO; λ =2; idealized reformate) at 150°C.

of hydrogen from 2079.0 cm^{-1} to 2076.5 cm^{-1} for step bound CO is observed, indicating the reduction of this surface species (probably by conversion to bridge bound species as was shown for Pt/γ-Al$_2$O$_3$), and, which is again in analogy to Pt/γ-Al$_2$O$_3$, only a very small shift for the terrace bound CO (2095.4 cm^{-1} → 2095.0 cm^{-1}), underlining, that it is predominantly the step sites, which are affected by hydrogen coadsorption (figure III-10a). In contrast, the additional presence of 1.3 kPa H_2O showed absolutely no effect within the measurement tolerance on either of the CO species adsorbed on the Pt powder, demonstrating, that the influence of coadsorbed hydrogen is clearly different and has to be treated separately from any effects, which coadded (or *in-situ* produced) water may exhibit on the CO_{ad} layer and its reactivity (See also section III-1.3.2).

1.2. From idealized to more realistic reformates

After demonstrating qualitatively the dependence of the selectivity on the surface CO coverage in idealized reformate, the next step is to apply more realistic conditions, *i. e.*, the addition of water (up to 1.5 kPa) and CO_2 (up to 25 kPa) to the reaction mixture. Not only the immediate response upon switching to the new gas phase components is of interest, but also the long-time evolution of the catalyst's properties in an altered reaction atmosphere. If we think, *e. g.*, of mobile applications, an average life-time of up to 5000 hours would required for the PROX stage [23].

Here we will first summarize the long-term evolution in idealized reformate. A part of these investigations (*e. g.*, the *in-situ* DRIFTS measurements) has already been covered in the preceeding diploma thesis by Schubert [32]. Subsequently, in the two following chapters the influence of water and of carbon dioxide is examined in detail.

1.2.1 Self-poisoning by CO_{ad}

The typical time development of the activity / selectivity during selective CO oxidation over $Pt/\gamma\text{-}Al_2O_3$ at 150°C in idealized reformate (1 kPa CO; $\lambda = 2$) is shown in figure III-11. It is characterized by a continuous decrease in the turnover frequency of around 40% within 1000 min. on-stream. At the same time the corresponding selectivity increases slowly from around 36 to 42%. Exactly the same behaviour was found for the increased reaction temperature of 200°C. In anticipation of chapter III-1.3.1, such a permanent loss in activity, accompanied by an increasing selectivity, indeed applies to all platinum based systems during selective CO oxidation which have been evaluated in this work.

Such a loss of reactivity during reaction has often been reported in studies concerned with CO oxidation, both on single crystals [88] and on real catalysts [7, 74, 75, 126, 127]. For example, Cant and co-workers observed a reduction in the turnover frequency of around 50% after 1000 min. during CO-Oxidation at 180°C (2 kPa CO, $\lambda \sim 1$) for a Pt/SiO_2 catalyst [126, 128]. They also demonstrated that this deactivation was reversible, by simply flushing the catalyst at reaction temperature with He. Likewise, Nibbelke *et al.* noticed, that their $Pt/\gamma\text{-}Al_2O_3$ catalyst showed a higher CO oxidation rate after the daily startup of their reactor than after a few hours on-stream [127]. As an explanation Cant and Angove proposed a very slow change of the surface CO/O concentration eqilibrium, which initially depends on the ratio of sticking coefficients [128]. Based on the EELS/TPD experiments by Gland *et al.* [102], they assumed

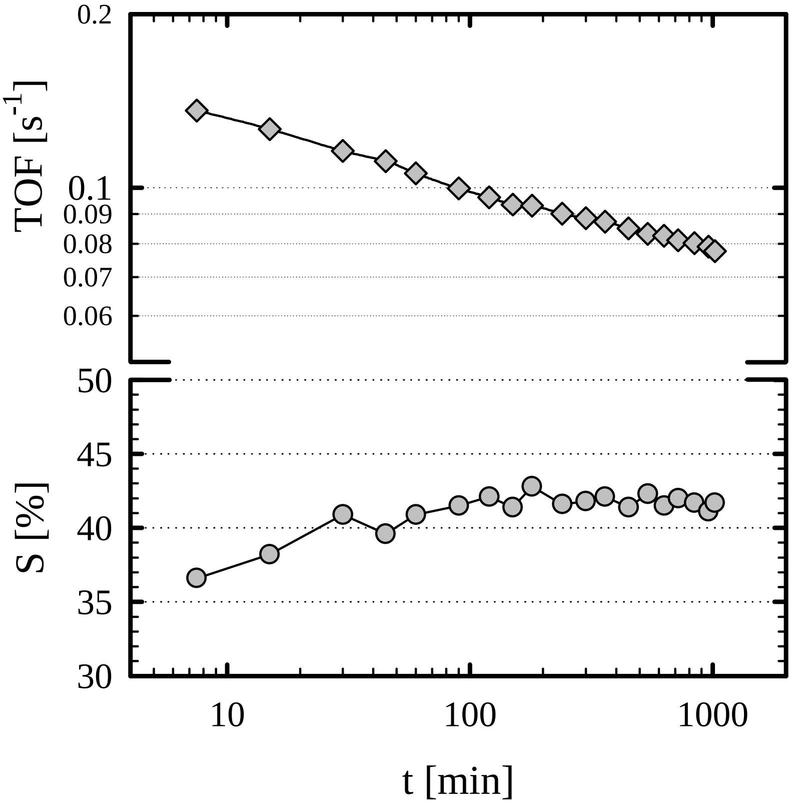

Fig. III-11: Time evolution of turnover frequency (upper window) and selectivity (lower window) during selective CO oxidation over Pt/γ-Al$_2$O$_3$ in idealized reformate with 1 kPa CO and λ = 2 at 150°C.

„unreactive“ O$_{ad}$ species at step sites as a possible reason for the unexpectedly slow replacement of O$_{ad}$ by CO. Recent studies with molecular beams indeed suggest the existence of a fraction of O$_{ad}$ species, which react only at higher temperatures, probably isolated O-atoms [129].

The deactivation characteristics for selective CO oxidation on Pt/γ-Al$_2$O$_3$ were already investigated in the diploma thesis of Schubert, where a concomitant slow increase in the IR-intensity of linearly adsorbed CO, accompanied by a small shift to higher wavenumbers of 1 - 2 cm^{-1}, during CO oxidation (in both cases, with and without H$_2$) at 200°C (1 kPa CO, λ = 2) was noticed. This was interpreted as a build-up of a more and more perfect CO$_{ad}$ layer with time [32]. On a more densely packed CO$_{ad}$ layer less oxygen and hydrogen adsorb on the surface, hence the reaction rate decreases by time, whereas the selectivity shows the opposite trend. This „self-poisoning“ by CO$_{ad}$ is easily reverted by flushing the catalyst for a few minutes with a non-reactive gas. Even after only stopping the reactant gas flow for a while or when changing the temperature level during our screening tests, where the temperature was increased by 25°C every 30 min., the initial activity was retained, which further confirmed, that the deactivation of platinum catalysts may be understood as a highly reversible slow approach to the real steady-state.

1.2.2 Influence of water

Although there exists a number of studies concerned with the reaction kinetics of CO oxidation on supported platinum metals in hydrogen-rich gases (*e. g.*, [4, 7, 16]), relatively little attention has been paid to the specific influence of water, although it constitutes up to 15% of the feed gas stream from a methanol reformer. In his diploma thesis Schubert noticed an increase in reactivity by a factor 2 for the CO oxidation in pure N_2 after adding 0.6 kPa H_2O in the feed gas stream (1 kPa CO, $\lambda = 2$, 150°C; addition of water after 30 min. of reaction; [32]). Muraki *et al.* found promoting effects (ca. factor 2 - 3) for both, hydrogen and water, on the CO oxidation over alumina suported platinum under steady state conditions at 150°C (1 kPa CO; $\lambda = 0.9$) and a small decrease of the activation energy from 55 to 45 kJ/mol in the presence of 3 kPa water [84]. Since additional CO_2 production *via* the water-gas-shift reaction could be excluded as an explanation due to the negligible water-gas shift rates (eq. I-1.4) below 200°C, they proposed that the self-poisoning induced by the blocking CO adlayer must have been reduced in some way. This was concluded from a small down-shift of the vibrational CO_{ad}-band upon admission of water. In their pulse experiments the presence of water accelerated the CO_2 production, which also pointed to a reduced CO inhibition in the oxidation reaction. Finally, Nibbelke *et al.* also mentioned a promoting effect (factor ~2.5) of 1 kPa water for the CO oxidation over $Pt/\gamma\text{-}Al_2O_3$ (0.9 kPa CO; $\lambda = 5$; 210°C), which decreases at higher temperatures. They speculated about O_2-dissociation on the support, enabled in the presence of OH-groups, analogous to what they proposed for ceria supports, but did not substantiate this hypothesis by experimental evidence [127]. Apart from that small enhancing effect, the water showed no further influence on their kinetics (CO and O_2 reaction orders).

In order to investigate the influence of moisture, we will first compare long-term experiments over $Pt/\gamma\text{-}Al_2O_3$ during CO oxidation without and in the presence of water. The upper part of figure III-12 diplays the activities for CO oxidation in pure nitrogen and in idealized reformate at different partial pressures of H_2O as a function of time (1 kPa CO, $\lambda = 2$; T = 150°C). For the CO oxidation in pure nitrogen without water a step in the activity behaviour is observed after 2-3 h. This step, the origin of which is still unclear, is absolutely reproducible, even after re-conditioning the catalyst. For a better comparison of the initial activity also the

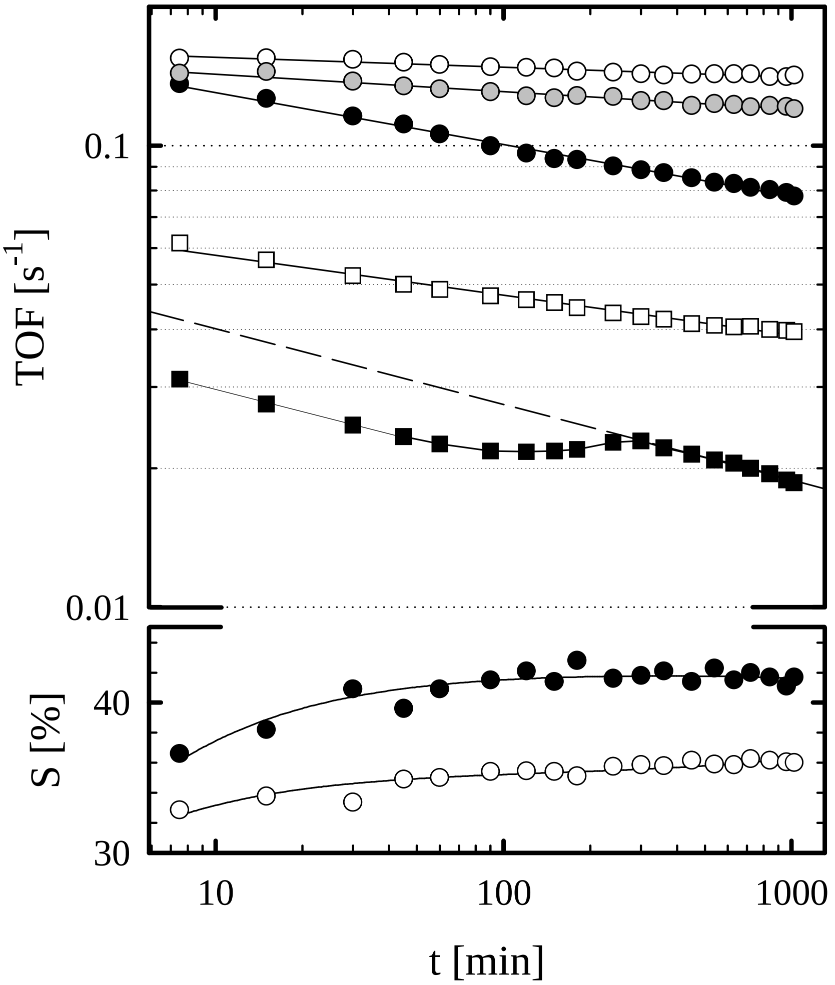

Fig. III-12: Time evolution of the turnover frequency (upper window) and selectivity (lower window) during oxidation of 1 kPa CO (λ = 2) at 150°C over Pt/γ-Al_2O_3 in pure N_2 (■), pure N_2 with 1.3 kPa H_2O added (□), idealized reformate (●; = 75% H_2), and idealized reformate with 0.65 kPa (◉) and 1.3 kPa H_2O (○) added, repectively.

extrapolation to the „steady-state“-activity after this step is included. Clearly, the initial activity is only moderately influenced by the presence of 1.3 kPa water (+15% for idealized reformate, +45% for the CO oxidation in pure N_2 – +100% if we regard the initial step). This is less than the influence of hydrogen (initial activity enhanced by a factor 3.2; x4.4 if the step is regarded), which was already discussed in the preceeding section. Analogous to the study of Muraki *et al.* [84] this „water-effect“ cannot be simply explained by the forward water-gas shift reaction,

$$CO + H_2O \leftrightarrow CO_2 + H_2 \qquad \text{(III-1.7)}$$

because the rate measured at 150°C (1 kPa CO, 1.3 kPa H_2O, Rest N_2) is only ~$9*10^{-7}$ $mol_{CO}/g_{Pt}*s$ (see also section III-1.3.2), which is more than two orders of magnitude less than the oxidation rates and a factor 60 smaller than the measured enhancement. And in the presence of 27 kPa hydrogen it is even one more order of magnitude lower, probably due to the simultaneously occuring reverse water-gas shift reaction. But what is striking now, is that the water seems to reduce the deactivation during time on-stream. In idealized reformate, the rate is almost stabilized on the initial level in the presence of 1.3 kPa water (As would be expected, with only 0.65 kPa water the effect is somewhat less pronounced). Thus the measured effect in „switch“-experiments crucially depends on the timing, leading to an increased apparent reactivity enhacement of water with preceeding reaction time. Therefore the (predominant) effect of co-added water during (selective) CO oxidation should better be named a „stabilizing effect“ rather than an „enhancement“. Of course, it is not possible to separate the influences of hydrogen and water on the CO oxidation completely, since in the first case water is always produced *in-situ* by the $H_2 + O_2$ side reaction, and in the latter case adsorbed water may dissociate on the support and produce H_{ad} on the platinum.

A second, very unpleasant effect arising from the addition of water during selective CO oxidation at 150°C over $Pt/\gamma\text{-}Al_2O_3$ is a decrease in selectivity, shown in the bottom part of figure III-12. With 1.3 kPa water in the gas mixture it is reduced from 42% down to 36% at „steady state“. Additional experiments by Kahlich in idealized reformate have shown, that this effect is clearly a function of the water partial pressure up to 5 kPa and then remains constant, leading to selectivities as low as 30% at 150°C and and 1 kPa CO ($\lambda = 2$) [25].

In order to gather more information on these water induced effects, we have performed „switch“-experiments in DRIFTS. Figure III-13 shows a typical result of such an experiment. First, spectra were recorded during selective CO oxidation over $Pt/\gamma\text{-}Al_2O_3$ at 150°C for 3 h (1 kPa CO, $\lambda = 2$) and then 1.3 kPa water was admitted to the gas mixture. In the left part of figure III-13 the infrared bands for linearly bound CO_{ad} after 60 min. in each atmosphere are shown. The position of the main peak is down-shifted by ca. 2.5 cm^{-1} and the integrated intensity is reduced by roughly 10% (±5%). Similar results were also obtained in mixtures without hydrogen. In the right part of figure III-13 the time evolution of the intensity (upper window) and the band position (lower window) are shown for the whole experiment. It may be noticed that the IR intensity (upper window) increases again after the switch to water, but now the peak position (lower window) shifts in the opposite direction while approaching the steady-state, indicating, that a new kind of equilibrium is installed on the catalyst surface. Due

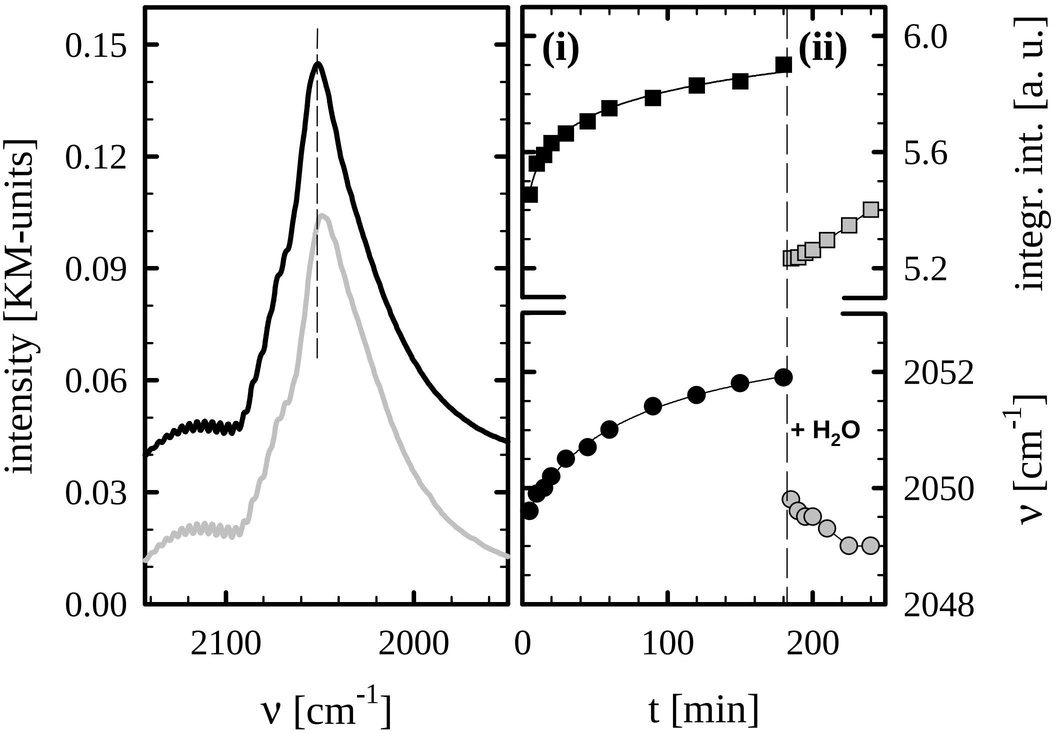

Fig. III-13: Comparison of DRIFTS spectra during selective CO oxidation in idealized reformate (1 kPa CO; $\lambda = 2$) over Pt/γ-Al_2O_3 at 150°C, first without water (black) and after 3 h with 1.3 kPa H_2O added (grey). *Left window*: IR CO_{ad}-bands after 60 min. in each atmosphere. *Right window*: Time-evolution of the integrated intensity (upper part) and of the band position (lower part).

to repulsive CO-O interactions the CO_{ad} is compressed into islands during CO oxidation, whose local coverage is independent from the island size [130, 131]. If there would simply be less CO on the surface, we would see the reduced intensity but probably no band shift, because the CO islands just get smaller. Hence in the presence of water also the locals density of the CO_{ad}-layer must have been reduced in some way.

To exclude artifacts arising from mass-transport or local temperature change effects, which cannot be completely ruled out with the used DRIFTS cell model, the influence of water was also investigated without reaction, *i. e.*, during CO adsorption (1 kPa; 150°C) in 75 kPa H_2, rest N_2 (figure III-14). Exactly the same phenomenon as for the „switch"-experiment during reaction is observed. When comparing the spectra acquired after 1 h in each atmosphere, we notice a downshift from 2053.3 cm^{-1} to 2050.9 cm^{-1} in the presence of 0.65 kPa water and a further shift down to 2049.9 cm^{-1} after adding 1.3 kPa H_2O (*i. e.*, 3.4 cm^{-1} overall shift).

But what else happens on the catalyst's surface after the admission of water during selective CO oxidation? If we take a look at other spectral regions, we notice, that upon the admission

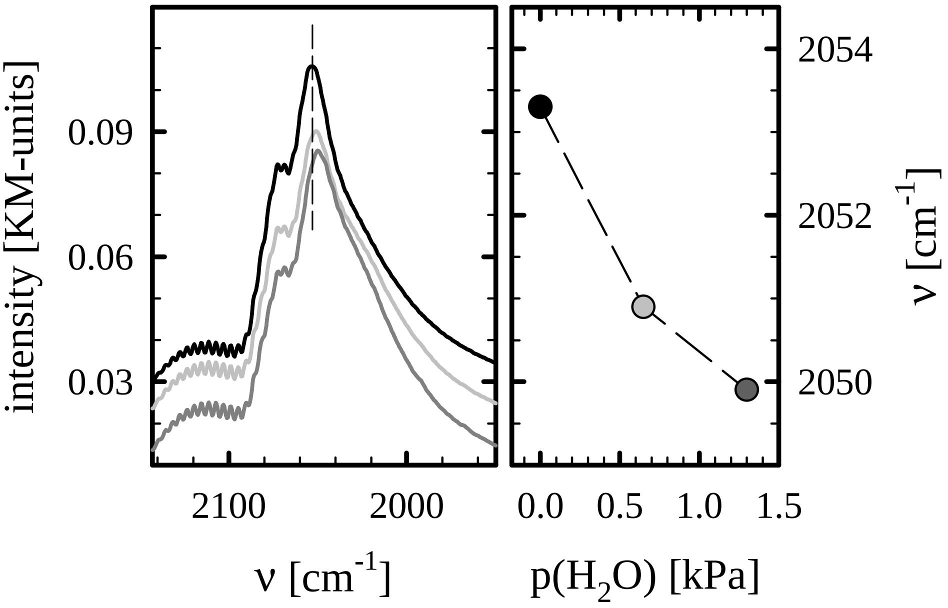

Fig. III-14: Comparison of DRIFTS spectra during adsorption of CO at 150°C on Pt/γ-Al$_2$O$_3$ (1 kPa; in 75 kPa H$_2$, rest N$_2$): dry (black), with 0.65 kPa (light grey), and with 1.3 kPa H$_2$O added (dark grey). *Left window*: IR CO$_{ad}$-bands after 60 min. in each atmosphere. *Right window*: Band position of main peak.

of water the growth of several bands in the region between 1700 cm^{-1} and 1300 cm^{-1} (and of a few small bands around 2900 cm^{-1}) is drastically increased. During reaction in a dry atmosphere formates (HCOO$^-$) were indentified, slowly accumulating on the support as is indicated by the IR bands at 1593 cm^{-1} ($\nu_{OCO/asym.}$), a doublet at 1375/1393 cm^{-1} (δ_{CH} and $\nu_{OCO/sym.}$) and a few peaks below 3000 cm^{-1} (ν_{CH} & some combination vibrations). The formates are most likely formed by insertion of CO$_{ad}$ in a neighbouring OH-group on the support at the metal/support interface (eq. III-1.8; [133])[134, 135].

The time-evolution of these bands during selective CO oxidation over Pt/γ-Al$_2$O$_3$ at 150°C for 3 h (1 kPa CO, $\lambda = 2$) can be followed by the grey spectra in figure III-15. Upon the addition of 1.3 kPa water to the reaction mixture the growth of bands in the region below 1700 cm^{-1} increases dramatically. Moreover, new bands arise, whereas the formate species are slowly reduced (black spectra in figure III-15). Bands at ~1660, ~1575, 1460, 1335 and 1395 cm^{-1} indicate carbonate (CO$_3^{2-}$), bicarbonate (HCO$_3^-$) and / or carboxylates species (CO$_2^-$), but an exact assignment of these bands is difficult [71, 136-139]. Even though different IR cross-sectios for formates and carbonates must be assumed, from the time-evolution of the IR band intensities is is obvious that the growth rate of these by-products is significantly enhanced in the presence of water. Of course, (bi-)carbonates could also arise from a reaction between the

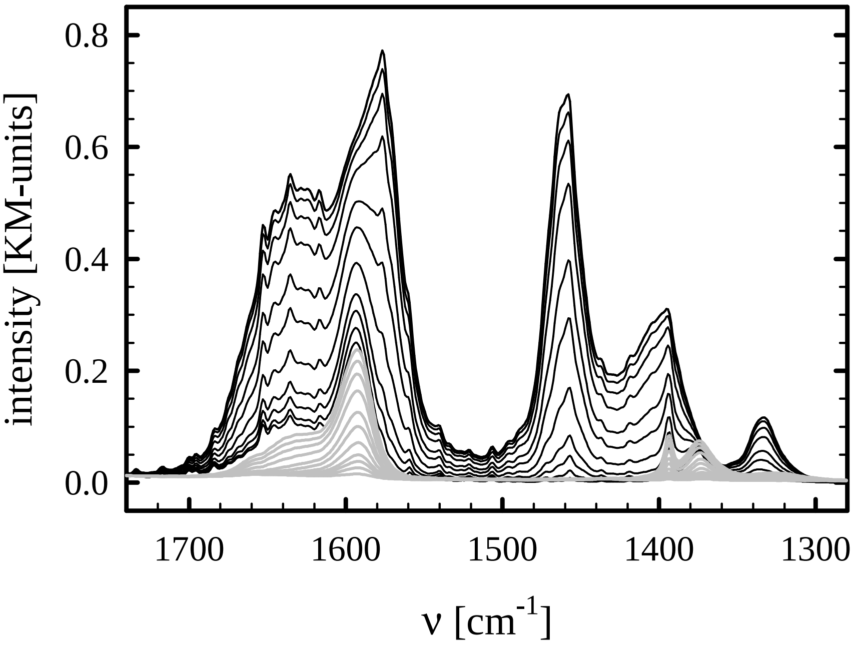

Fig. III-15: Time evolution of the spectral region between 1280 cm^{-1} and 1740 cm^{-1} over Pt/γ-Al_2O_3 in idealized reformate (1 kPa CO, λ = 2; 150°C) for 3 hours (grey) and then with 1.3 kPa H_2O added for another 3 hours (black). Spectra are acquired after 5, 10, 15, 20, 30, 45, 60, 120, 150, and 180 min.

produced CO_2 and support OH-groups, but as will be shown below, this is only a minority path and the majority of the by-products is formed indirectly from CO_{ad} *via* oxidation of formate species.

Possible reaction pathways are (compare *e. g.* [134, 138, 140, 141]):

$$CO_{ad} + OH^- \leftrightarrow HCOO^- \qquad \text{(III-1.8)}$$

$$HCOO^- + H_2O\,(OH^-) \leftrightarrow HCO_3^-\,(CO_3^{2-}) + H_2 \qquad \text{(III-1.9)}$$

$$HCO_3^- + OH^- \leftrightarrow CO_3^{2-} + H_2O \qquad \text{(III-1.10)}$$

These formates or bicarbonates decompose predominantly into CO_2 and H_2 when they are in contact with noble metals [134, 142-144], which was also indicated by our own temperature programmed experiments on the decomposition of either by-products accumulated during reaction or predosed formic acid ([145]; see Appendix B):

$$HCOO^- + H_2O\,(OH^-) \leftrightarrow CO_2 + H_2 + OH^-\,(O^{2-}) \qquad \text{(III-1.11)}$$

Consistently, they are also observed, when 1.3 kPa water is added during CO adsorption (1 kPa) in 75 kPa H_2, rest N_2 at 150°C. The complete reaction scheme for these products may be quite complex, but without going too much in detail, it can be concluded as a result, that upon the addition of water the formation of by-products on the support, produced from CO_{ad}, increases drastically. The new diffusion and reaction pathway may disturb the build-up of the steady-state coverage on the platinum surface, described in the preceeding section. CO is continuosly abstracted from the platinum surface and a new equilibrium between $CO_{ad(Pt)}$, $H_{ad(Pt)}$, $O_{ad(Pt)}$ and „$CO_{ad(Support)}$“ (= formates & (bi-)carbonates) is established. This leads to a relaxation of those CO islands which are in contact with the metal/support interface, which explains the lower band position observed in DRIFTS. The equilibration of the surface in presence of water seems to proceed more slowly, which is indicated by the „stabilized“ rates observed in our long-term experiments. The small rate enhancement along with the reduced selectivity in the presence of water may be caused by the somewhat lower steady state CO coverage along with a more disordered adsorbate layer, where the adsorption probability for hydrogen should be increased. Another contribution to the rate enhancement could arise from the dissociation of water on the support, with a subsequent spill-over of hydrogen to the platinum particles, leading to a small increase of the H_{ad} population, which in turn would decrease the adsorption energy of CO adsorbed in H-CO mixed reagions as was shown in section 1.2.4.

Consequently and as a final prove for our hypothesis, the water addition should show no effect for the CO oxidation on usupported platinum powder, where formate formation is not possible. Indeed, the rate, the deactivation behaviour and the selectivity (figure III-16, right part) for selective CO oxidation (1 kPa, $\lambda = 2$; 150°C) without and in the presence of 1.3 kPa water are identical after approximately three hours. The initial rate in the presence of water is even slightly lower, maybe caused by coadsorbed water, which is only slowly removed similar to the initially adsorbed oxygen species, which are held responsible for the deactivation (see preceeding section). The same applies to „switching“-measurements on the Pt powder, where the addition of 1.3 kPa water after several hours of selective CO oxidation (1 kPa CO, $\lambda = 2$; 150°C) shows absolutely no effect on the rate or selectivity (not shown here). In the left part of figure III-16 the corresponding DRIFTS spectra without and in presence of water (after 90 min. in each atmosphere) are compared. To avoid influences from a possible „mechanical“ interface between the platinum particles and the dilution material, which is commonly α-Al_2O_3 (apart from the need to guarantee differential flow conditions, especially for the DRIFTS-measurements it was necessary to dilute the black Pt powder with a brighter material, in order to achieve an acceptable SNR), SiO_2 was used as a dilutent for this

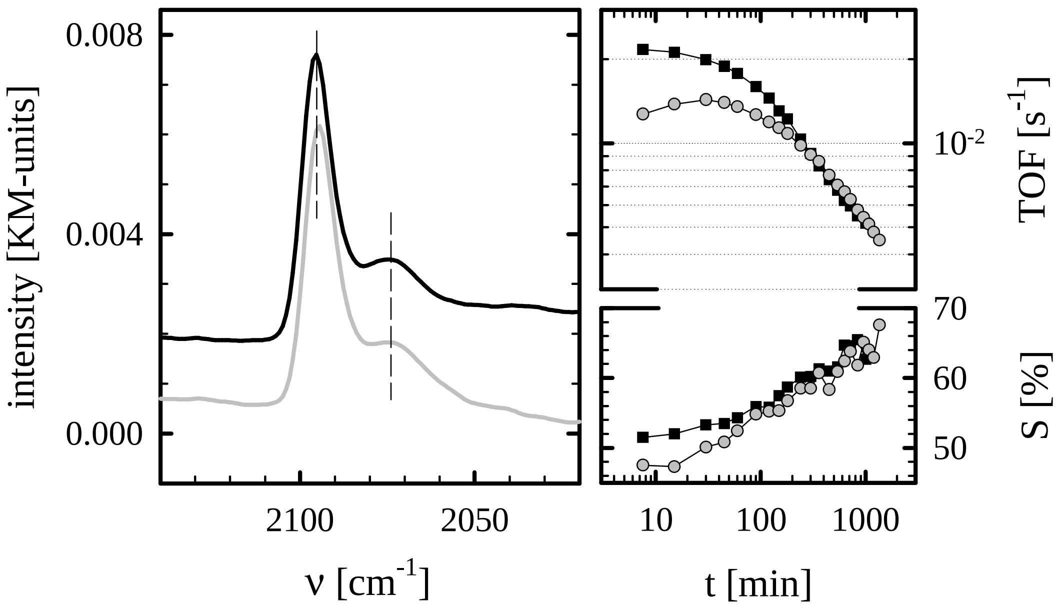

Fig. III-16: Selective CO oxidation over Pt powder in idealized reformate at 150°C (1 kPa CO, λ = 2; 150°C): *Left part*: Comparison of DRIFTS spectra (catalyst diluted with SiO_2) dry (—) and with 1.3 kPa H_2O added (—), after 1.5 hours in each atmosphere. *Right part*: Long-term activity (upper window) and selectivity (lower window) dry (■) and with 1.3 kPa water added (○).

experiment (see also below). During selective CO oxidation on the Pt powder two bands in the region for linearly adsorbed CO are recognized: One at 2095.4 cm^{-1}, assigned to extended low-index planes and one at 2074.8 cm^{-1}, related to defect sites [93]. Upon admission of 1.3 kPa water there is indeed only a small down-shift for the high frequency band of 0.9 cm^{-1} to 2094.5 cm^{-1}, and absolutely no shift for the low frequency band within the measurement tolerance for such a small and broad band (around ±1 cm^{-1}).

It should be noted that in analogy these results on Pt/SiO_2, where no by-products (at least not within the detection limit) are formed during selective CO oxidation, consequently there was also no downshift and no reduction of the integrated DRIFTS intensity of adsorbed CO observed upon the admission of water to the reaction mixture (1 kPa CO, λ = 2; 150°C; see Appendix B).

These results show clearly that the effects observed in the presence of water (rate stabilization, small enhancement of the initial rate and a reduced selectivity) are related to the γ-Al_2O_3 support, more specifically to the formation of formate / (bi-)carbonate species on the support. On unsupported platinum or on support materials, where those by-products are not formed to such an extent (*e. g.*, SiO_2), the water has practically no influence on the selective CO oxidation.

1.2.3 Performance in CO_2-rich gas

Up to now, we have simplified most of our experiments by using a matrix for the simulated reformate, which is made up from ~75% hydrogen and ~25% nitrogen. But a real feed gas produced from a methanol reformer consists of H_2 and $\underline{CO_2}$, therefore it is important to consider possible differences for the selective CO oxidation arising from the replacement of N_2 by CO_2. Unfortunately, there are very few literature data available on the influence of CO_2 on the (selective) CO oxdiation reaction over platinum metals. Nibbelke *et al.* mention that the addition of 1 kPa CO_2 had no significant effect on the CO oxidation activity over Pt/γ-Al_2O_3 (0.12-4 kPa CO; 0.12-2.5 kPa O_2; 163°C). In kinetic studies from our own group, where idealized reformate (0.01 - 1.5 kPa CO, λ = 0.5-10) has been compared to a realistic gas mixture, containing 25 kPa CO_2 (in the dry part) plus 10 kPa H_2O, virtually no difference for the rate and selectivity at 300°C was observed, whereas at 150°C the selectivity decreased by approximately 10% (absolute), attributed to the negative influence of the water, which was already discussed above [25]. The activity in the realistic reformate at 150°C was even slightly enhanced compared to the idealized mixture (factor 2 at 0.2 kPa CO, λ = 2). For both temperature levels the CO reaction order was slightly increased (from -0.44 to -0.14) in the presence of CO_2 and H_2O, whereas the oxygen reaction order remained practically the same (~ +0.8) [25, 132].

In this section we compare the influence of a more realistic gas mixture on the selective CO oxidation (1 kPa CO, λ = 2) at different temperatures between 100 and 250°C. Every data point was evaluated on a freshly conditioned catalyst bed after 90 min. on-stream, when the major deactivation period had been passed. The additional influence of 1.3 kPa water was investigated by „switch“-experiments, where after 2 hours of reaction with 25% CO_2 the water was added to the reactant flow (data taken after 1 additional hour).

In figure III-17 the CO oxidation activity in the different gas mixtures is compared in the form of an Arrhenius diagram. The activation energy in the presence of 25 kPa CO_2 is reduced from little less than 70 kJ/mol (± 4 kJ/mol) down to ~55 kJ/mol (± 4 kJ/mol). We also recognize a slight reduction of the turnover frequency for all levels above the light-off temperature for the selective CO oxidation (~130°C; see figure III-2), being more pronounced at higher temperatures. The maximum difference is a factor 2.5, observed at 250°C. At 100°C, below

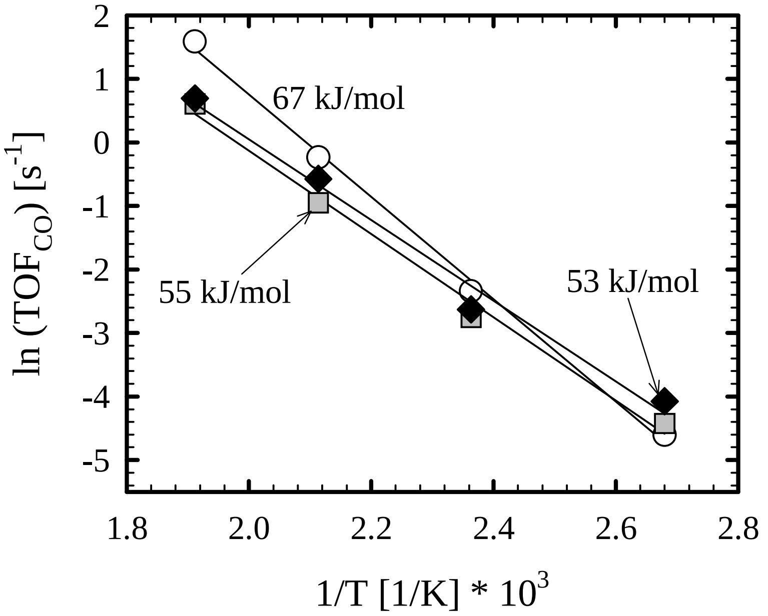

Figure III-17: Arrhenius diagram for the turnover frequency of CO oxidation over Pt/γ-Al_2O_3 in idealized reformate (○; 1 kPa CO, λ = 2), a mixture containing 25 kPa CO_2 (▨), and in a realistic reformate (◆; 25 kPa CO_2; 1.3 kPa H_2O).

the light-off temperature, even a small increase compared to idealized reformate is noticed. The decrease at higher temperatures indeed represents a real reduction of the CO oxidation activity and is not just an effect of the reverse water-gas shift (eq. III-1.7), which would lead to a re-creation of CO from CO_2, since the observed differences in the turnover frequencies for mixtures with and without CO_2 are for all temperature levels at least one order of magnitude above the shift rates (see also chapter III-1.3.2). Adding 1.3 kPa water to the CO_2-mixture exhibits only a very small effect on the CO oxidation rate, represented by a slight increase of the activity of 15 - 45%, similar to the enhancement of the initial rates for the idealized reformate, which was investigated in the preceeding section, but does not change the activation energy. hour).

The effect of CO_2 / H_2O on the hydrogen oxidation reaction (calculated *via* selectivity; figure III-18, left window) is shown in figure III-18 (right window). In the presence of 25 kPa CO_2 we find similar tendencies as were observed before for the CO oxidation reaction. The turnover frequencies are slightly decreased, with the effect being more pronounced at higher temperatures (maximum difference: factor 3 at 250°C). The activation energy decreases to the same value (~55 ± 6 kJ/mol) as for the CO oxidation reaction. This absolutely parallel behaviour implies that both oxidation reactions are still coupled by the same rate limiting step. The activation energy for CO (H_2) oxidation in idealized reformate of around 70 kJ/mol

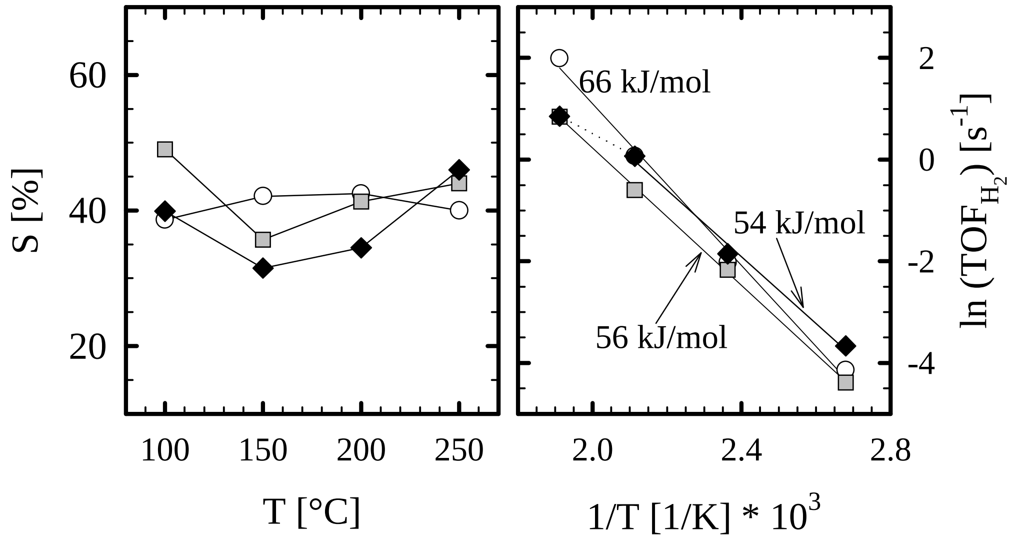

Figure III-18: (a) Selectivity and (b) Arrhenius diagram for the calculated turnover frequency of H_2 oxidation over Pt/γ-Al_2O_3 in idealized reformate (○ ; 1 kPa CO, λ = 2), a mixture containing 25% CO_2 (▨), and in realistic reformate (◆ ; 25 kPa CO_2; 1.3 kPa H_2O).

reflects the CO desorption energy, which is of the same magnitude in the high coverage range [1, 125]. The decreased activation energy in the presence of CO_2 in principle strongly suggests a reduction of the CO „self-poisoning“, which would be consistent with the observed change of the CO reaction order, from -0.44 to -0.14 [25, 132]. Such an effect could either be caused by a reduced CO desorption energy or by a new oxygen-supplying path on the catalyst surface. Both suggestions, however, would be expected to induce a marked enhancement of reactivity, but in our experiments just a slight opposite effect is observed. The only explanation left is that CO_2 may indeed reduce the CO poisoning by some way, but exhibits a second poisoning effect itself which more than compensates the expected rate enhancement.

Up to 200°C the additional admittance of 1.3 kPa water to the CO_2-mixture shows a small enhancement for the turnover frequency of the hydrogen oxidation as was found for the CO oxidation reaction, probably being caused by the same reasons discussed in the preceeding section. Again the activation energy compared to the dry „CO_2-mixure“ is not changed. Interestingly, at 250°C the „water-effect“ has vanished – equally, for the CO oxidation reaction at 250°C the measured effect of water was also very small: just +10%. This is consistent with the observations by Kahlich, that water shows no effect on the rate and selectivity at 300°C [25, 132]. It is consequent to take a look at the thermal stability of the by-products accumulated on the support. Temperature-programmed reaction (TPR) experiments by Schubert *et al.* have demonstrated, that the maximum build-up rate of formates during selective CO oxidation (1 kPa CO, λ = 2) is at ~170°C, whereas above 200°C the steady state coverage decreases strongly due to a very rapid decomposition [32]. Hence, if a similar temperature window applies also to the (bi-)carbonates and carboxylates, a possible explanation, why the „water-effect“ is only observed at temperatures below 200°C, may be, that at elevated temperatures there is not such an extended „$CO_{ad/Support}$“ coverage (in the form of formates and the other by-products) formed, which could stay in equilibrium with molecules adsorbed on the platinum surface and hence affect the rate / selectivity.

As a consequene of the two overlapping effects from CO_2 onto the H_2 and CO oxidation reactions, *i. e.*, reduction of the adsorption energy but also reduction of the activity at elevated temperatures, a quite complex selectivity behaviour results, which is shown in the left window of figure III-18. Whereas without CO_2 the selectivity is constant around 40% over the whole investigated temperature range, it is slightly enhanced at 100 and 250°C, remaines almost identical for 200°C and is somewhat reduced around 150°C in the more realistic mixtures. But most changes induced by CO_2 are quite small, also with view on the measurement tolerance of about ±3-4% for this graph. The additional admittance of 1.3 kPa water to the gas mixture again causes a drop in selectivity of 5-10% (with the exception at 250°C as was discussed already above), but the general trends are again not changed compared to the dry CO_2-containing mixture.

In order to investigate the above proposed hypothesis of two overlapping effects (one enhancing and one, which poisons the reaction) exhibited by the CO_2 onto the CO oxidation, additional *in-situ* DRIFTS measurements were performed. After starting by 60 min. of reaction in idealized reformate (1 kPa CO, $\lambda = 2$; 200°C; 0.2 kPa CO_2 as a result of CO conversion) the nitrogen was gradually replaced by CO_2 (1.2, 3.6, 11.1 and 23.4 kPa CO_2; each mixture subsequently for 30 min.). In figure III-19 the results from this combined DRIFTS / GC measurement are displayed. For the linearly bound CO_{ad}-band a blue-shift (window b), in dependence of the CO_2 partial pressure, is recognized, but it is not accompanied by any significant change in the integrated IR intensity of this band (window a). Nevertheless, the ratio between linearly and bridge bound CO increases very strongly with increasing CO_2 partial pressure. The corresponding DRIFTS-spectra are shown in window c. In the right part of figure III-19 the turnover frequency (window d) and selectivity (window e; data taken after 30 min. in each mixture) are displayed. The somewhat low overall selectivity compared to the kinetic measurements may well be attributed to leaking in the used DRIFTS-cell model, where a part of the reactant stream may pass at the side of the catalyst bed (See appendix A). Although a slight downward trend for the reactivity and an upward going

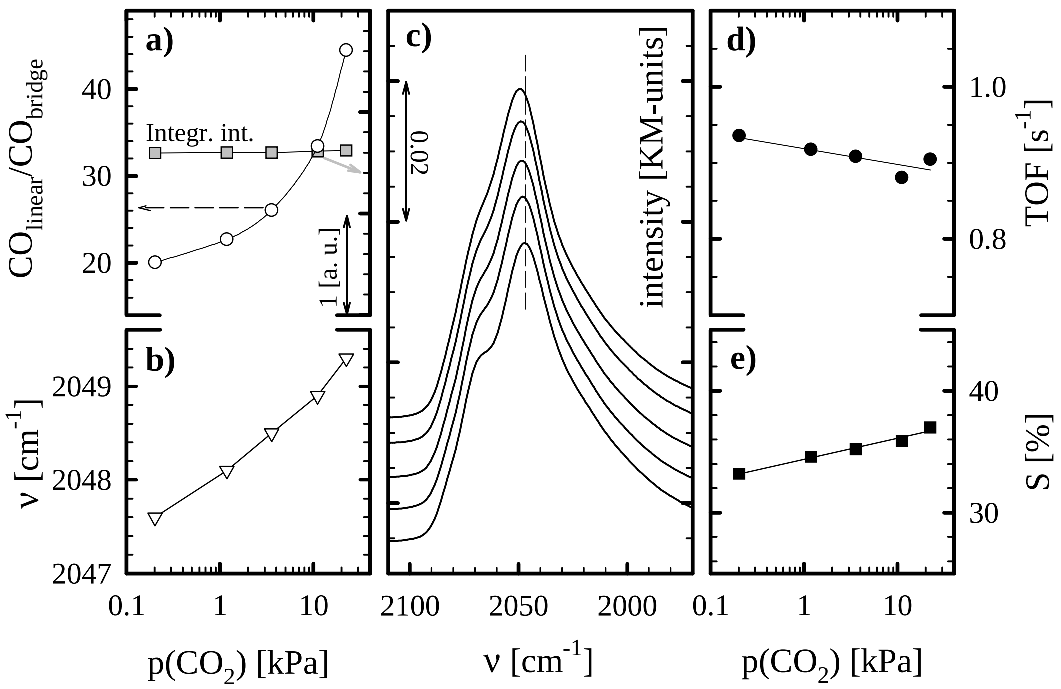

Figure III-19: CO_2 influence on the selective CO oxidation over Pt/γ-Al_2O_3 (1 kPa CO, λ = 2; 200°C): *a)* ratio between adsorbed CO_{linear} and CO_{bridge} (○) and total integrated IR intensity of CO_{linear} (▣), *b)* peak position of CO_{linear} (▽), *c)* DRIFTS-spectra of CO_{linear} region with 0.2, 1.2, 3.6, 11.1 and 23.4 kPa CO_2 (from bottom to top), *d)* turnover frequency (●) and *e)* selectivity (■).

tendency for the selectivity are noticed, these changes are very small (TOF within 6%, selectivity within 4%). Hence, in accordance with the preceeding experiments, it can be noted, that the CO_2 effectively exhibits only a small influence on the activity / selectivity at 200°C. Nevertheless, from the DRIFTS spectra a significant effect on the adsorbed CO is noticed.

When oxygen is admitted to a CO-mixture over platinum catalysts, in accordance with previously published studies [128, 131, 139, 146], generally a blue-shift (3 cm^{-1} and more on our catalyst) is noticed as a consequence of the increased dipol-dipol interactions arising from the compression of CO_{ad} into island structures [32]. This shift is usually accompanied by an increase in the IR intensity of the linearly bound CO_{ad} (around 10% for a mixture of 1 kPa CO and oxygen in a N_2 background over Pt/γ-Al_2O_3) and of the ratio between linearly and bridge bound CO (on our catalyst from 20 to 30), which indicates an increased local density of the CO_{ad}-layer, characterized by the greater amount of occupied on-top sites [32].

Hence, as a possible explanation for the observed CO_2-induced blue-shift, we propose the dissociation of CO_2 (either on platinum or, which is more likely, since CO_2 dissociates only at higher temperatures over Pt metal [147], at the metal-support interface [148]), which would produce O_{ad} (and CO_{ad} as well) and therefore enrich the platinum surface with oxygen. This is supported by the concomitant increase of the linear/bridge CO ratio, which indicates an

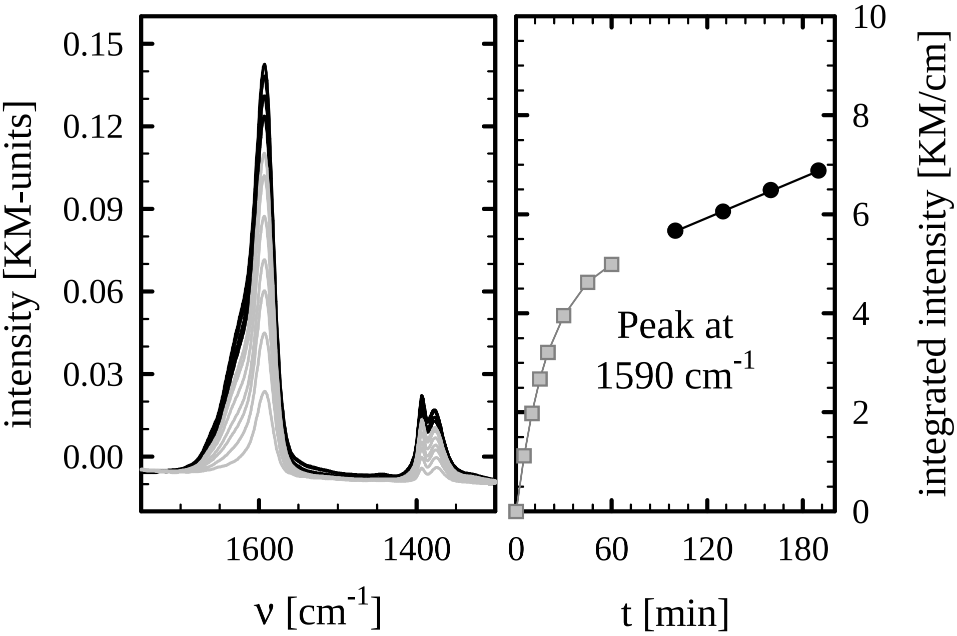

Figure III-20: CO$_2$ influence on the build-up of support-bound by-products on Pt/γ-Al$_2$O$_3$: *Left part*: DRIFTS spectra - first during CO oxidation in idealized reformate for 60 min. (1 kPa CO, λ = 2; 200°C; grey lines: aquired after 5, 10, 15, 20, 30, 45 and 60 min.), then with progressing replacement of N$_2$ by CO$_2$ (0.2, 1.2, 3.6, 11.1 and 23.4 kPa CO$_2$; black lines: spectra aquired subsequently after 30 min. in each mixture). *Right part*: integrated intensity of the IR-band at 1590 cm^{-1}.

increase in the local CO density. The missing increase in the IR intensity for the linearly bound CO may be explained by a small reduction of the overall CO coverage, which would compensate the expected effect. Since CO adsorbs into oxygen islands for reaction, but not *vice versa* [76, 129, 149], such an increase of the steady-state oxygen coverage is expected to reduce the „self-poisoning“ by CO$_{ad}$ and as a consequence theoretically increase the reactivity enormously. This scenario is consistent with the reduced CO reaction order (ca. -0.14), which was observed in the presence of CO$_2$ [25, 132], as well as with the lower activation energy, which is now less dependent on the desorption energy of CO$_{ad}$.

In analogy to the last section, it may also be interesting to take a short look at the spectral region of by-products (support bound species) in the presence of CO$_2$. In figure III-20 (left window) the DRIFTS spectra recorded during selective CO oxidation in idealized reformate (1 kPa CO, λ = 2; 200°C) over Pt/γ-Al$_2$O$_3$ for 60 min. and after subsequent replacement of background nitrogen by increasing amounts of CO$_2$ (1.2, 3.6, 11.1 and 23.4 kPa CO$_2$; each mixture for 30 min.) are shown. But neither the formation of new species (apart from a very small band at 1450 cm^{-1}, which may be assigned to bicarbonates, HCO$_3^-$, or carboxylates,

CO_2^-) nor any major deviation from the usual growth rate of the formate bands in idealized reformate (represented by the integrated IR area of the band at 1590 cm^{-1}; right window) are observed.

In summary, although the apparent influence of CO_2 on the rate and selectivity is small, the DRIFTS spectra show significant changes for the platinum steady-state surface equilibrium. For consistence there must exist a second, poisoning, effect of the CO_2, which compensates the expected rate enhancement. With the applied methods, however, it could not be identified yet. Our model explains well the kinetic changes (reaction order, activation energy) observed by Kahlich [25, 132], but of course, the hypotheses in this section are based only on two different methods (DRIFTS + microkinetic reactor measurements) and, not least due to the lack of data from previous studies, are rather speculative. The CO oxidation in presence of CO_2 should be tested in further experiments, especially on UHV model systems, to gain further insight into this quite complex behaviour.

In total, the influence of water (small concentrations) and / or CO_2 on the selective CO oxidation over $Pt/\gamma\text{-}Al_2O_3$ is rather moderate, causing deviations for the rate and selectivity of only a few percent, but not of any order of magnitude, so that our measurements in idealized reformate indeed are an appropriate first approach to real feed gas from a methanol reformer.

1.3 Other support materials

This chapter is focussed on the influence of the support material on the performance characteristics of platinum catalysts for the PROX reaction, especially, in order to evaluate a catalyst with a better turndown ratio for the load following behaviour in mobile applications, which is limited by the simultaneously occuring reverse water-gas shift reaction [10, 11]. In the first section we will compare the activity and selectivity of various platinum catalysts supported on conventional supports (γ-Al_2O_3, MgO, SiO_2, TiO_2, and carbon) at a standard temperature of 150°C. The second chapter is concerned with the influence of the support on the reverse water-gas shift activity and closes with a short summary on the PROX / shift ratios at 150°C.

1.3.1. Comparison of activity / selectivity

In principle we may think of three possible ways, how the support could influence the CO oxidation. First, Mojet *et al.* proposed a direct electronic interaction between the metal and the support, which would alter the adsorption energy of the carbon monoxide and lead to changes in the IR frequency of the CO_{ad}-band and in the CO_{linear}/CO_{bridge} ratio [150]. But such a phenomenon should be expected only for very small platinum cluster sizes. Second, the support may induce a restructuring of the Pt particles, forcing the exposure of new crystal faces and changing the site composition on the metal surface, which may lead to different reaction rates, since, *e. g.*, the CO oxidation on stepped single crystal faces has turned out to be a structure sensitive reaction [107, 151]. Unfortunately, we do not have access to methods, which could elucidate such theories, hence we cannot confirm or exclude the additional influence of restructuring phenomenons in the following context. Third, the support provides a reactive chemical interface to the metal particles, causing, *e. g.*, CO_{ad} to spread on the support *via* formate or carbonate species (see chapter III-1.2.2) [133].

To our best knowledge, no studies exist, which investigate the support influence upon CO oxidation on platinum metals extensively. For the „high rate branch“ (0.01-0.1 kPa CO, 0.5 kPa O_2) as well as for the „low rate branch“ (> 0.3 kPa CO, 0.5 kPa O_2) Fuchs *et al.* measured similar turnover frequencies of around $1*10^1$ s^{-1} for Pt/α-Al_2O_3 and Pt/ZrO_2 at 300°C [152]. The same activity applied to a polycrystalline Pt foil. When comparing Pt/SiO_2 and Pt/Al_2O_3, Mergler *et al.* noticed a fivefold higher activity of the latter system ($7.2*10^{-4}$ s^{-1} compared to $3.6*10^{-3}$ s^{-1} at 2.7 kPa CO, $\lambda = 1$; 150°C) [77], whereas Sarkany *et al.* recognized a somewhat enhanced performance (factor three) for the silica-supported catalyst ($1.5*10^{-3}$ s^{-1} and $0.5*10^{-3}$

Catalyst	**TOF_{CO} [s^{-1}] *10^{2} $^{1)}$**	**S [%] $^{1)}$**	**TOF_{H_2} [s^{-1}] *10^{2} $^{1)}$**
Pt/γ-Al_2O_3	9.6 (15.3)	42 (36)	13.3 (27.2)
Pt/MgO	15.5 (22.2)	53 (40)	13.7 (33.3)
Pt/TiO_2	3.5	1.1	315
Pt/SiO_2	2.4	58	1.7
Pt powder	2.0 (1.7)	56 (55)	1.6 (1.4)
Pt/Vulcan (freshly cond.)	0.68 (1.0) $^{2)}$	87 (57) $^{2)}$	0.10 (0.75) $^{2)}$
Pt/Vulcan (recond.)	0.88	43	1.2

() = with 1.3 kPa water added *1*) after 2 h on-stream *2*) after 1000 min.

Table III-3: Turnover frequencies for CO and H_2 oxidation and selectivities over various Pt catalysts in idealized reformate (1 kPa CO, $\lambda = 2$) at 150°C.

s^{-1}, respectively, at 3 kPa CO, $\lambda = 1$; 100°C; data taken after 60 min) [75]. The discrepancy, which is relatively small anyway, probably arises from large tolerances for the determination of the dispersion. Moreover their absolute TOFs seem to be very low compared to other studies concerned with CO oxidation over such systems, hence should be considered with care, anyway. Muraki *et al.*, *e. g.*, reported a TOF of $1.1*10^{-2}$ s^{-1} over Pt/γ-Al_2O_3 (1 kPa CO, $\lambda = 0.9$; 150°C) [84], Cant and co-workers found TOFs of around 1.3-$4*10^{-2}$ s^{-1} for Pt/SiO_2 (1.3-2 kPa CO, $\lambda = 0.8$-1, 177°C) [74, 126, 153]. For single crystal faces Hardacre *et al.* observed a conversion of $3*10^{-2}$ s^{-1} (0.9 kPa CO, $\lambda = 1$; 157°C) over Pt(111) [154] and Berlowitz *et al.* reported a TOF of $1.5*10^{-2}$ s^{-1} (2.1 kPa CO, $\lambda = 1$; 150°C) over Pt(100) [88]. The similar magnitude of the measured values for supported and unsupported systems implies that the support does not exhibit any major effects upon the CO oxidation reaction (at least not in absence of hydrogen).

In figure III-21 the activities (as a turnover frequency, upper part) and selectivities (lower part) of several platinum catalysts are compared for the selective CO oxidation in idealized reformate (1 kPa CO, $\lambda = 2$) at 150°C. The characteristic parameters for the various catalysts (Pt/γ-Al_2O_3, Pt/MgO, Pt/SiO_2, Pt/TiO_2, Pt/Vulcan and Pt powder) are summarized in chapter II-2.1. For comparison the dispersion of Pt/TiO_2, which was not known, was estimated to be 40% in order to calculate the TOF roughly. To provide a better overview, the TOFs and selectivities after 2 hours on-stream are put together in table III-3. Included are also the rates with 13 kPa water added for some catalysts as well as the hydrogen oxidation rates calculated *via* selectivity.

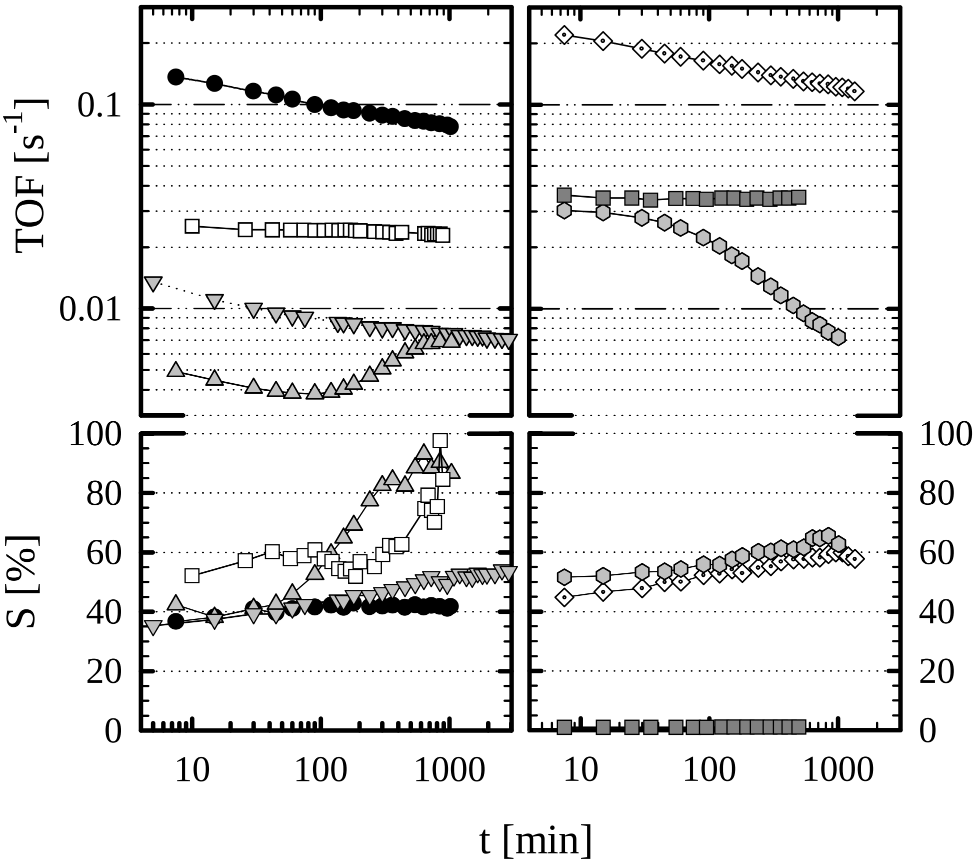

Figure III-21: Time evolution of turnover frequencies (upper part) and selectivities (bottom) over various platinum catalysts in idealized reformate (1 kPa CO, λ = 2) at 150°C: ●Pt/γ-Al$_2$O$_3$; □ Pt/SiO$_2$; △Pt/Vulcan (freshley conditioned); ▽ Pt/Vulcan (after re-conditioning); ◇Pt/MgO; ■ Pt/TiO$_2$; ⬡Pt powder.

The Pt/γ-Al$_2$O$_3$ catalyst possesses a relatively high activity - one order of magnidute higher than reported in the above cited references, which may be largely ascribed to the enhancement in presence of hydrogen and of *in-situ* produced water (see chapters III-1.1.5 and III-1.2.2). The conversion over Pt/MgO is even larger (+60%). The TOFs on Pt/SiO$_2$ and Pt/TiO$_2$ are about a factor three below that of Pt/γ-Al$_2$O$_3$. The apparently more stable conversion rates on these catalysts may be caused by organic residuals after the conditioning procedure from the colloid precursor shell, which were removed slowly during the reaction and counteract the „normal“ deactivation, for Pt/SiO$_2$ and by the strongly enhanced water production (extremely low selectivity), which may prevent an approach to the steady-state for Pt/TiO$_2$, repsectively. The activity over Pt powder is again slightly smaller and shows a strongly decreasing tendency with time on-stream, which is probably caused by the faster approach to the steady state, since no support bound species participate in the equilibration process. The Pt/Vulcan catalyst shows a large initial „step“ for the activity. If we regard the rate after ~1000 min., when the

„step“ has been passed, it is slightly higher than on the unsupported platinum. Interestingly – different from the „step“ on Pt/γ-Al_2O_3, which was observed for CO oxidation in a pure nitrogen background (see figure III-12) – , after a second conditioning procedure the „step“ has vanished and the catalyst shows the „normal“ deactivation behaviour as it would be expected. Therefore, we correlate this „step“ to the build-up of thermally rather stable species on the carbon support (*e. g.*, OH-groups or COO^--species) during the reaction, which facilitate the CO oxidation reaction, similar to what has been observed for OH-groups on the Pt/γ-Al_2O_3 catalyst (see chapter III-1.2.2). As a general summary, we may claim the following order of reactivity for the selcective CO oxidation:

Reactivity: Pt/MgO ≈ Pt/γ-Al_2O_3 > Pt/TiO_2 ≈ Pt/SiO_2 ≈ Pt/Vulcan ≈ Pt powder

But indeed the effects are relatively small (within one order of magnitude), as was already expected from the small differences between the literature TOF’s, cited above.

The selectivity are relatively similar, except for the Pt/γ-Al_2O_3, which shows a relatively low value. The latter effect may be ascribed to the very small particles (see table II-3), which should favour hydrogen adsorption and oxidation due to the greater number of step sites, where the hydrogen coverage builds up preferably (chapter III-1.1.5). Another, much clearer exception is Pt/TiO_2 with an extremely low value, where the H_2 + O_2 reaction is probably catalyzed by a redox-mechanism on the titania support ($Ti^{4+} \leftrightarrow Ti^{3+}$). The selectivity over the re-conditioned Pt/Vulcan catalyst was also surprisingly small, probably a direct consequence of the species formed during the preceeding reaction.

Selectivity: Pt/Vulcan ≈ Pt powder ≈ Pt/SiO_2 ≈ Pt/MgO > Pt/γ-Al_2O_3 >> Pt/TiO_2

From an economic point of view Pt/MgO seems to be a good alternative to Pt/γ-Al_2O_3. The reactivity is somewhat higher and the selectivity is slightly enhanced, hence the required mass of catalyst for a PROX stage should be less. The reason for the superior conversion on these two catalysts is probably the large amount of OH-groups on the support surface along with the stronge basicity, which enables the extensive formation of by-products and therefore increases the conversion rate (see chapter III-1.2.2).

1.3.2. The water-gas shift - limiting the CO conversion

For the envisaged employment of PROX as a purification stage for methanol reformer gas in vehicles the requirements are quite restrictive. Currently used anode catalysts (Pt, PtRu) in

PEM fuel cells are poisoned by only traces of carbon monoxide in the feed gas. The maximum concentration, which is tolerated, is around 100 ppm CO [11, 23], especially when a so-called air-bleed is employed (oxygen dosage over the anode catalyst) [20], but ideally should be less than 20 ppm [18, 155]. For such extreme demands also the simultaneously occuring (reverse) water-gas shift reaction must be considered:

$$H_2 + CO_2 \leftrightarrow H_2O + CO \qquad \text{(III-1.12)}$$

The re-creation of CO *via* the WGS reaction, which parallels the CO oxidation, but is negligible under oxidation conditions, becomes significant as soon as the oxygen is used up. It limits the achievable minimum CO concentration from a PROX stage [10, 156] and, as a consequence, determines the maximum turndown ratio for the load following behaviour in vehicles, which depends on the ratio between the CO oxidation reaction and the reverse water-gas shift reaction [25].

Therefore we investigated the shift rates over various platinum catalysts at temperatures, which result in good selectivities and activities for the primary CO oxidation reaction, *i. e.*, between 150 and 300°C [7, 25], and with the simultaneous addition of water, as it would be found in real methanol reformates.

The exact mechanism of the water-gas shift reaction is still subject of an ongoing debate (see, *e. g.*, [138, 157-160]). In principle there are two possible pathways: The „associative mechanism“, which proceeds *via* intermediates (usually formates, $HCOO^-$):

$$CO + H_2O \leftrightarrow \text{intermediate} \leftrightarrow CO_2 + H_2 \qquad \text{(III-1.13)}$$

and the „regenerative“ or „redox mechanism“ [157]:

$$H_2O + \breve{\ } \leftrightarrow H_2 + O_{ad} \qquad \text{(III-1.14)}$$

$$O_{ad} + CO \leftrightarrow CO_2 + \breve{\ } \qquad \text{(III-1.15)}$$

Chinchen and Spencer suggested that for catalysts and conditions, which allow the regenerative mechanism to operate, this mechanism is the faster one [161] and therefore would be applicable to our platinum systems.

Unfortunately, there are only few reference data available concerned with the WGS over platinum catalysts, since commercially employed catalysts are based on other metals (*e. g.*, copper), which yield much higher rates [162, 163]. Grenoble *et al.* investigated the forward water-gas shift reaction over different Pt-catalysts at 300°C (24.3 kPa CO, 31.4 kPa H_2O) and

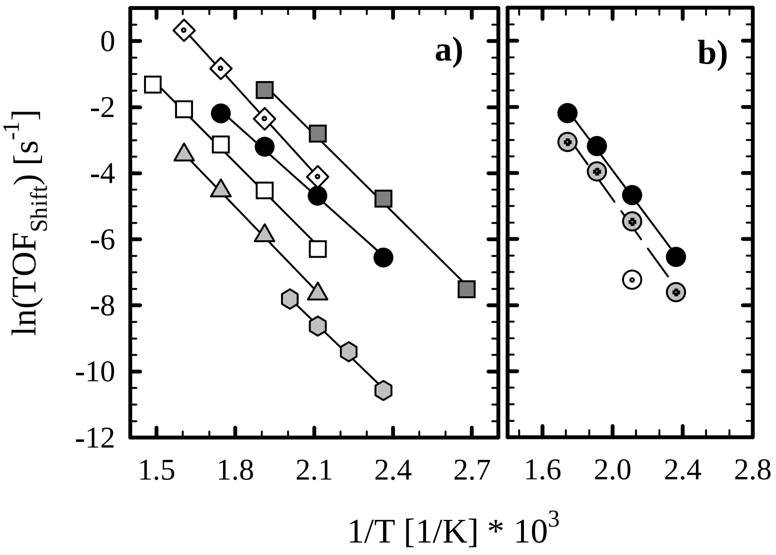

Figure III-22: *a)* Arrhenius diagram for the reverse water-gas shift activity over platinum catalysts over various supports (~25 kPa CO_2, ~ 74 kPa H_2, 1.3 kPa H_2O): ● Pt/γ-Al_2O_3; □ Pt/SiO_2; △ Pt/Vulcan; ◇ Pt/MgO; ■ Pt/TiO_2; ⬡ Pt powder; *b)* comparison of shift-rates over Pt/γ-Al_2O_3: ● reverse WGS; ⊛ forward WGS (1 kPa CO, 1.5 kPa H_2O); ⊙ forward WGS with 27 kPa H_2 added.

noticed a marked influence of the support material [162]. Pt/Al_2O_3 (TOF $6.35*10^{-2}$ s^{-1}) was one order more active than Pt/SiO_2 ($6.1*10^{-3}$ s^{-1}) and two orders more than Pt/C ($7*10^{-4}$ s^{-1}). They attributed this effect to the different ability of the support materials in activating the H_2O dissociation. Wolf *et al.* investigated the reverse water-gas shift reaction (2 - 6 kPa CO_2 and H_2, resp.) over platinum powder and Pt/MgO, but at much higher temperatures of 800-950°C, and ascribed the enhanced activity (×25-50) of the latter system to the facilitated CO_2 dissociation at the metal/support interface [148]. For iridium catalysts Erdöhelyi *et al.* registered an outstanding activity for the forward reaction over the titania supported catalyst, which turned out to be a factor of ten more active than Ir/Al_2O_3 and Ir/MgO and an additional factor three more than Ir/SiO_2 (8 kPa CO, 16 kPa H_2O; 350°C) [160].

On our platinum catalysts (for characterization see chapter II-2.1) we tested the reverse WGS reaction in an atmosphere as close as possible to a real methanol steam reformate, consisting of ~25 kPa CO_2, ~74 kPa H_2 and 1.3 kPa H_2O. Figure III-22a provides an overview in the form of an Arrhenius diagram. The values at 150°C (as mass-specific rates) as well as the determined activation energies are enclosed in table III-4. For all data points the CO_2 conversion was so small that the resulting CO concentration was well below the thermodynamic equilibrium concentration. The activity for the reverse water-gas shift reaction follows in principle the same trend as for the H_2 oxidation and with the exception of the more active Pt/TiO_2 also that of the CO oxidation reaction (see table III-3):

Catalyst	**r^{PROX} at 150°C [1)] [mol_{CO}/g_{Pt}*s]**	**r^{Shift} at 150°C [2)] [mol_{CO}/g_{Pt}*s]**	**$^{PROX}/_{Shift}$ ratio**	**E_a^{Shift} (± 5) [kJ/mol]**
Pt/Al_2O_3	$1.9*10^{-4}$	$2.8*10^{-6}$	70	62
Pt/MgO	$1.6*10^{-4}$	$3.0*10^{-6}$	55	74
Pt/SiO_2	$6.8*10^{-5}$	$9.2*10^{-7}$ [3)]	75	69
Pt/TiO_2	$7.2*10^{-5}$	$1.7*10^{-5}$	4	69
Pt/Vulcan	$9.1*10^{-6}$ [4)]	$8.3*10^{-8}$ [3)]	110	69
Pt-Black	$1.0*10^{-5}$	$1.7*10^{-8}$	600	65
Pt/Al_2O_3 [5)]	$1.9*10^{-4}$	$9.6*10^{-7}$	200	67

1) after 2 hours on-stream *2*) after 30 min *3*) extrapolated 4) after 1000 min *5*) forward WGS

Table III-4: Comparison of PROX and reverse WGS activities over several platinum catalysts and determined activation energies of the shift reaction.

$Pt/TiO_2 > Pt/MgO > Pt/\gamma\text{-}Al_2O_3 > Pt/SiO_2 > Pt/Vulcan > Pt$ powder.

The order of reactivity as well as the relative differences between the various supports matches excellently the tendency that would be expected from the above cited references. The titania supported catalyst is by far more active than the other oxide supported catalysts, analogous to the outstanding activity, noticed for the hydrogen oxidation, which again points to an active role of this support in the reaction process.

As a consequence of the same order of reactivity for the oxidation and shift reaction, the ratio between both remains at a rather constant level for the different supported platinum catalysts (except Pt/TiO_2). The only significant improvement in the turndown ratio of the load following behaviour would be established for unsupported platinum, but its generally poor activity and the strong deactivation for the CO oxidation vote unequivocally against a commercial employment.

Although a rather narrow distribution for the activation energy of the reverse water-gas shift, ranging between 55 and 90 kJ/mol for oxides as well as for most supported noble metals, is a generally observed phenomenon [157], the striking similarity of the values in table III-4, including also the unsupported platinum, implies an identical reaction pathway on all of these catalysts. The lacking stability of intermedate oxygenates on pure platinum [143, 164] strongly suggests the regenerative mechanism to be operative as was predicted by Chinchen *et al.* [161]. Nevertheless the support exhibits a marked effect on the reaction rate, possibly due to a facilitated CO_2 dissociation on the oxidic supports (or metal-support interfaces).

In figure III-22 b the reverse water-gas shift over Pt/γ-Al_2O_3 is compared to the forward reaction (1 kPa CO, 1.5 kPa H_2O, rest N_2). Both rates are of the same order of magnitude with the latter being slightly (factor 3) smaller. The activation energy (67 kJ/mol) for the forward reaction – slighly lower than the 82 kJ/mol observed by Grenoble *et al.*, but the latter was measured at much higher reactant concentrations (24.3 kPa CO, 31.4 kPa H_2O) [162] – is also of the same magnitude as for the reverse reaction.

After adding 27 kPa hydrogen, the forward WGS turnover freqency decreases by approximately one order of magnitude, probably due to the simultaneously starting reverse reaction, which clearly proves that under typical PROX conditions the contribution of the forward water gas shift is very small compared to the CO oxidation reaction and may well be neglected for simulations (see, *e. g.*, [12]).

As a comprehensive result, the magnesia supported catalyst may be considered as a possible alternative due to its high rate and good selectivity. The slightly higher PROX / shift ratio, however, favours the employment of Pt/γ-Al_2O_3.

1.4 Summary on platinum catalysts

In the preceeding chapters we have seen, that the selectivity for the PROX reaction is closely coupled to the CO_{ad} coverage on the metal surface under reaction conditions. With the help of adsorption isotherms, recorded by DRIFTS, the existence of an almost saturated CO_{ad}-layer on Pt/γ-Al_2O_3 was directly confirmed for temperatures up to 250°C and over a large variety of CO partial pressures. This demonstrates that the selective CO oxidation proceeds in the „low rate branch“, which explains the observed reaction orders on platinum catalysts as well as the independence of the selectivity from the CO partial pressure. The enhanced reactivity compared to a hydrogen-free reaction mixture was traced back to the coadsorption of hydrogen at step sites, which would displace the CO on bridging positions and lower the desorption energy of the latter by approximately 2 kJ/mol.

During time on-stream the Pt/γ-Al_2O_3 catalysts looses activity due to the build-up of a more and more perfect CO_{ad}-layer, which increasingly blocks the dissociative oxygen adsorption. This deactivation process is reduced in the presence of water due to the extensive formation of oxygenate species on the support, which reduce the local CO-density on the metal surface and alter the approach to the steady-state surface equilibrium. Unfortunately, the lower CO_{ad} coverage allows for an enhanced adsorption of hydrogen (and oxygen) on the platinum, leading to a decreased selectivity, which must be taken into consideration for serious calculations on PROX reactors employed for the purification of methanol steam reformates.

CO_2 exhibits a two-sided effect on the selective CO oxidation when compared to mixtures, where the CO_2 had been replaced by nitrogen. The activation energy is lowered for both, CO and H_2 oxidation, from ~70 to ~55 kJ/mol, which suggests that the strong poisoning effect of the CO is reduced, as was already implied by the more positive CO reaction order in realistic reformate, determined by Kahlich [25]. DRIFTS measurements suggest a relative increase in the O_{ad} coverage, most likely as a direct consequence of the CO_2 dissociation at the metal-support interface. But the rate enhancement, which would be expected, is obviously masked by an additional poisoning effect of the CO_2 on the reaction, which could not be identified yet. In the end, the effects of CO_2 and water on the reaction kinetics were found to be of a minor magnitude, which justifies our initial approach by the simplified model of idealized reformate [7, 12, 25].

When comparing different support materials, only Pt/MgO turned out to be a possible alternative, due to its slightly higher activity and selectivity for the CO oxidation.

The generally small PROX-shift ratios over platinum catalysts cause a low turndown ratio for the load-follwing behaviour in mobile applications, hence allowing only a rough purification (down to several hunderd ppm CO) of methanol steam reformates at temperatures, which guarantee a satisfying mass-specific activity of the catalyst [12]. As a consequence, for most of the recent PROX concepts, based on a two-stage system [11, 156, 165], the $Pt/\gamma\text{-}Al_2O_3$-based catalyst is useful only for the first (high temperature) reaction stage and other catalyst systems (*e. g.*, supported Au [29, 30]), which exhibit a better PROX-shift ratio at relatively low λ-values, must be empolyed for the final removal of the carbon monoxide [12].

2. Improved performance on bimetallic systems - Pt_3Sn/Vulcan

As was pointed out in the preceeding chapters, alumina supported platinum metals (Pt, Rh, Ru) were proposed and successfully tested as PROX catalysts by several groups (see, *e. g.*, [4, 6, 14]. There is still a need, however, for improved performance under dynamic conditions and for lowering the operating temperature to the PEM fuel cell level of about 80°C. The latter offers advantages in system integration, including improved cold start properties for mobile applications [166] and the possibility of implementing the catalyst directly into the fuel cell, in form of a double layer anode [155, 167, 168] and also reduces the role of the reverse water gas shift reaction [12].

PtSn alloys are already known as good catalysts for the electrooxidation of CO in sulfuric acid solution [169, 170], and have also been proposed as active catalysts for gas-phase CO oxidation [171, 172]. Very closely related systems, Pt catalysts supported on SnO_2, have been demonstrated in extensive studies to be good catalysts for low temperature CO oxidation (see, *e. g.*, refs. [173-178].

A general objective for the use of alloyed metals in heterogeneous catalyzed reactions is to improve the activity or selectivity of the originally employed metal by mixing it with another element. The second component either induces an electronic (or ligand) effect due to the formation of metal-metal bonds, which, *e. g.*, for platinum metal causes a modification of the reactive d-orbitals, leading to a modified adsorption energy for the reactants / products, or it blocks distinct reaction sites (ensembles), where unwanted side-reactions occur (geometric or ensemble effect) [179-182]. Moreover, on some alloys the second metal may also actively participate in the reaction process, equivalent to the formation of a real bifunctional surface.

In the following chapters we will examine in detail how the addition of Sn improves the PROX characteristics of a Pt catalyst, so that it is now able to match the stringent requirements of a highly active low-temperature system, capable of reducing the CO content of feed gas made up from steam reformed methanol down to a level, which is acceptable to currently used anode catalysts (Pt, PtRu).

In the following chapter we will present first kinetic results on the activity and selectivity of our vulcan supported PtSn catalyst for the PROX reaction, supplemented by temperature programmed CO desorption (CO-TPD), infrared spectroscopic (diffuse reflectance infrared Fourier transform spectrometry - DRIFTS), and photoelectron spectroscopic (XPS) data. For comparison similar data for a standard Pt/γ-Al_2O_3 catalyst obtained in a previous study are included [7]. Based on these results and by comparison with similar data from other systems such as Au/α-Fe_2O_3 and Pt/SnO_2 catalysts, we will suggest a mechanistic model to explain the selectivity behavior of the Pt_3Sn/Vulcan catalyst. In a further chapter, we will evaluate its suitability for the envisaged application in a low-temperature PROX stage by investigating the long-term stability as well as the performance in more realistic reformate gas mixtures and finally demonstrate its superior water-gas shift characteristics. Further details of the reaction kinetics, in particular their dependence on reactant partial pressures, are currently determined and will be published in a parallel thesis by M. Kahlich [25].

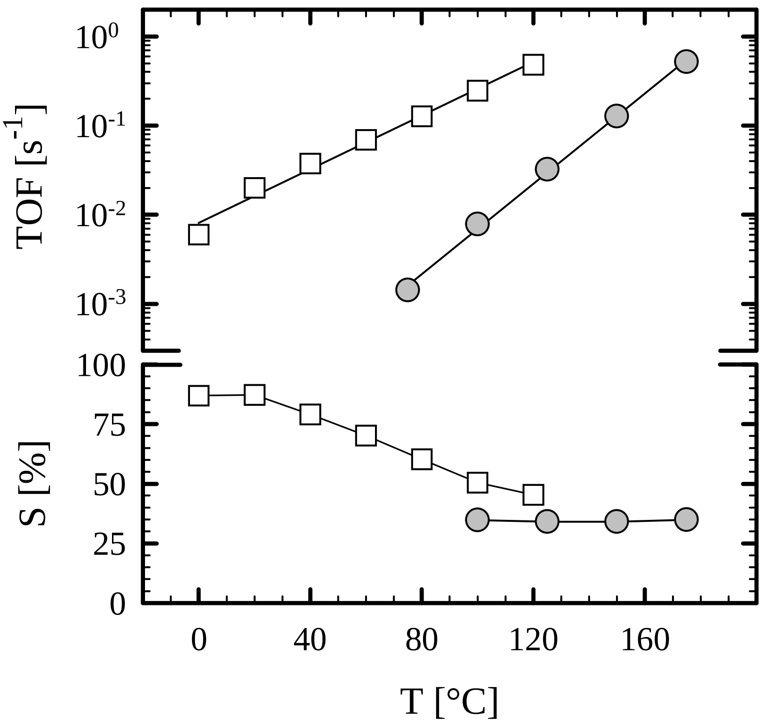

Fig. III-23: Turnover frequency (*upper window*) and corresponding selectivity (*lower window*) for selective CO oxidation over Pt_3Sn/Vulcan (□; data acquired after 90 min. on-stream) and Pt/γ-Al_2O_3 (●; after 20 min) in idealized reformate (1 kPa CO; λ = 2).

2.1. Low-temperature CO oxidation over Pt_3Sn/Vulcan

2.1.1 Superior performance on Pt_3Sn/Vulcan vs Pt/γ-Al_2O_3

Results on the activity (top) and selectivity (bottom) of the Pt_3Sn/Vulcan and, for comparison, of the Pt/γ-Al_2O_3 catalyst in idealized reformate (1 kPa CO, λ = 2) at different temperatures between 0° and 175°C are presented in figure III-23. Data for the Pt catalyst were recorded consecutively on the same catalyst bed, waiting for 20 min. at each temperature, so that the system was close to stationary conditions. Nevertheless, since complete steady state had not been established yet, the rates on the Pt catalyst are slightly higher, between 0% at 200°C and 50% at 150°C, than those reported in ref. [7]. For Pt_3Sn/Vulcan each point was measured on a freshly conditioned catalyst bed because of the more pronounced tendency for irreversible deactivation (see also chapter III-2.2.1). These data were recorded after 90 min. on-stream, where most of the loss in reactivity has already occurred. Figure III-23 clearly reveals the superior performance of the PtSn catalyst for the PROX reaction: Over the entire temperature range investigated the activity of the bimtallic PtSn catalyst is significantly higher than that of the Pt catalyst. At 80°C (PEM fuel cell operating temperature) the difference in turnover

System	**D**	**T** [°C]	**p(CO)** [%]	**p(O_2)** [%]	**r^{CO}** x10^5 [mol/(s·g_{Pt})]	**TOF** x10^3 [s^{-1}]	**Ref.**
0.98% Pt-SnO_2/ α-Al_2O_3	0.6	60	0.8	1	2.2 (11)	7.3 (70)	[177]
2.8% Pt-SnO_2/SiO_2	-	35	1	0.5	0.4② (4.6)	-	[176]
0.46% Pt-SnO_2/ Cordierite	0.6	60	1	6	1.7 (11)	6.5 (70)	[175]
3% Pt-SnO_2	~0.2	150	1.6	1.8	3.7 (~200③)	39 (~1300③)	[174]
2% Pt-SnO_2	-	75	5	5	11① (15)	-	[173]
2.7% Pt-Sn/SiO_2	-	50	16	8	13① (7.1)	-	[171]

① evaluated at high conversion ② with 8% CO_2 added ③ extrapolated

Table III-5: Comparison of published data for CO oxidation rates at atmospheric pressure in the absence of H_2 on similar catalysts. Experimental conditions are listed above. Data from fig. III-23 at the respective temperature and p(CO) = p(O_2) = 1 kPa , 75 kPa H_2, balance N_2 are given in parenthesis.

frequencies is about two orders of magnitude, 0.15 s^{-1} on Pt_3Sn/Vulcan *vs* 2×10^{-3} s^{-1} on Pt/γ-Al_2O_3. The activity of the PtSn catalyst at 80° is reached only at 150°C by the Pt catalyst. This reactivity can be compared with that of another low temperature PROX catalyst, Au/α-Fe_2O_3, where under identical conditions (80°C) a TOF of 0.7 s^{-1} was determined [26].

For the CO oxidation on the chemically rather similar Pt/SnO_2, in the absence of H_2, significantly lower activities, by about one order of magnitude, were reported for similar reaction conditions (see lines 1 - 4 in table III-5). On our PtSn catalyst we noted an increase in CO oxidation activity by a factor of 2 - 3 in the presence of H_2 (see chapter III-1.1.1), nevertheless, a difference by a similar factor remains which must be attributed to differences between the catalysts. Only for higher reactant concentrations [173] activities of comparable magnitude were observed (table III-5).

A plot of ln(r^{CO}) *vs* 1/T (fig. III-24; idealized reformate with 1 kPa CO, λ = 2) yields an apparent activation energy of 31 (±4) kJ/mol on Pt_3Sn/Vulcan, which is clearly less than the 76 (±5) kJ/mol determined on Pt/γ-Al_2O_3. Likewise, activation energies of around 49 (±5) kJ/mol on the bimetallic PtSn catalyst and 77 (±7) kJ/mol on Pt/γ-Al_2O_3 are determined for the concomitant hydrogen oxidation (r^{H_2} calculated *via* the selectivity), where the latter value is essentially identical to the activation barrier for the CO oxidation. Note that the values for

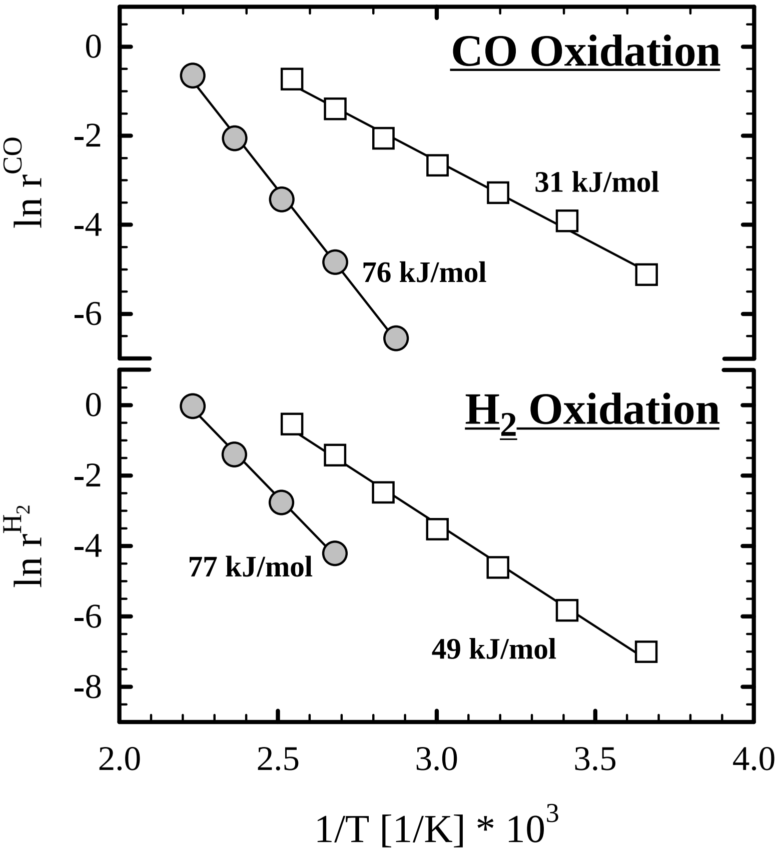

Fig. III-24: Arrhenius diagram of turnover frequencies for CO oxidation (*upper window*) and H_2 oxidation (calculated *via* selectivity; *lower window*) over Pt_3Sn/Vulcan (□) and Pt/γ-Al_2O_3 (●) in idealized reformate (1 kPa CO; λ = 2).

the activation barrier refer to an effective barrier for the complete process, in the presence of the respective other species (CO or hydrogen), rather than to a specific reaction step.

Similar to the reactivity discussed above also the selectivity and its temperature dependence (Fig. III-23, bottom) differ significantly between the two catalysts. On Pt_3Sn/Vulcan the selectivity more or less steadily decreases with temperature, starting from a very high value of about 85% in the low temperature regime around 0 - 20°C to about 45% at 120°C (Note that because of the very low hydrogen oxidation rates at 0°C the experimental uncertainty is rather high, so that the seemingly constant selectivity at 0° and 20°C should not be overinterpreted). In contrast, on Pt/γ-Al_2O_3 the selectivity is much lower, around 35%, but constant up to 175°C. Only at temperatures above 200°C the selectivity was reported to decay in this system ([7]; see also chapter III-1.1.1). The constant selectivity and small turnover frequencies at low temperatures on the Pt catalyst were explained by assuming the platinum surface to be fully covered by CO. In that temperature regime CO desorption controls the dissociative adsorption of oxygen and is rate limiting, and the steady state coverages θ_H and θ_O are very low ([7]; see also chapter III-1.1.1). This situation is characteristic for the so-called 'low rate branch' for CO oxidation [1]. The decay in selectivity sets in at temperatures where these conditions no longer hold true, *i. e.*, at temperatures where the CO desorption rate is sufficient to cause a decline in the CO coverage under steady state conditions, allowing the hydrogen and/or oxygen coverage, θ_H and θ_O, to build up. If similar mechanistic explanations are valid also for PtSn, then the CO adsorption energy should be significantly reduced on the Pt_3Sn/Vulcan catalyst as compared to Pt, at similar conditions, so that the decrease in CO coverage would already occur above room temperature as compared to above 200°C on Pt/γ-Al_2O_3. This hypothesis is tested in the next section by a CO desorption experiment.

2.1.2 Alloying effects

The freshly conditioned Pt_3Sn/Vulcan catalyst was cooled down to -48°C and exposed to a flow of 10 Nml/min CO for 5 min.. After purging the reactor with nitrogen the sample was heated up linearly at 5°C/min (10.4 Nml/min of nitrogen). Again a CO-TPD on Pt/γ-Al_2O_3 is shown for comparison [7].

The CO-TPD spectra in the top part of figure III-25 allow the following conclusions. First of all the onset of desorption from the PtSn catalyst is shifted to lower temperatures, from about 50°C on Pt to about -20°C on Pt_3Sn/Vulcan. For desorption from Pt/γ-Al_2O_3 two peaks at 110°C and 220°C are found, which are commonly assigned to CO adsorbed on terrace and step sites, respectively [92, 123]. The additional high temperature peak from the Pt/γ-Al_2O_3 catalyst at around 280°C is probably due to the decomposition of formates, which accumulate on the support during adsorption [133]. For Pt_3Sn/Vulcan, the first maximum appears at around 45°C, followed by a shoulder at ~105°C and another maximum at 215°C. From the analogy in desorption temperatures the two latter states are tentatively assigned to CO desorption from small clusters of Pt surface atoms on the alloy particles. The low temperature peak at 45°C, which is only observed on Pt_3Sn/Vulcan, is attributed to CO desorption from Sn modified Pt sites. Ross explained the lowering of the CO adsorption energy on the Sn modified Pt sites by an electronic effect due to metal-metal interactions between Pt and Sn, which would result in a downshift and narrowing of the platinum d-states, so that the overlap with the $2\pi^*$-orbitals of the adsorbed CO molecules and hence the CO adsorption energy is reduced [183]. This qualitative picture was confirmed by recent calculations in the group of J.

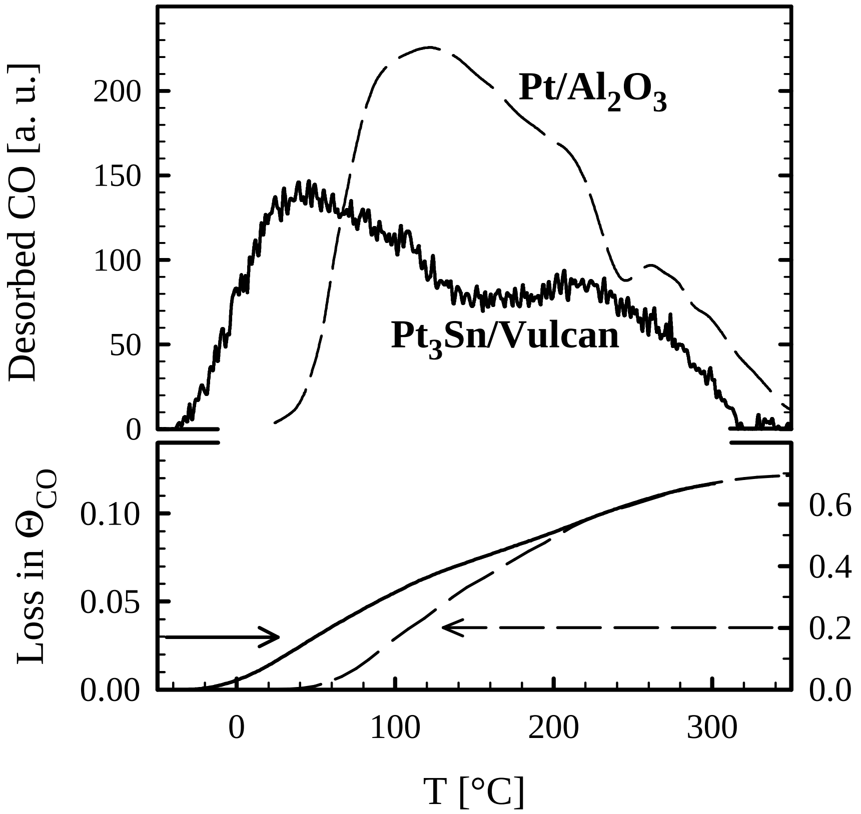

Fig. III-25: *Upper window*: temperature programmed desorption of pre-adsorbed CO over Pt_3Sn/Vulcan (——; 5°C/min, 10.4 Nml/min N_2) and Pt/γ-Al_2O_3 (- - - - ; 3°C/min, 15 Nml/min He [7]; size scaled); *lower window*: calculated loss of CO in monolayers fractions of metal surface.

Nørskov, which demonstrated the close correlation between the position of the d-band and the CO adsorption energy [182].

Assuming first order desorption kinetics and a (coverage independent) preexponential of 10^{13} s^{-1} we can estimate an activation energy of $E_{des} \approx 110$ kJ/mol for CO desorption on Pt/γ-Al_2O_3 (for the first maximum) and around 90 kJ/mol for the first maximum on the Pt_3Sn/Vulcan catalyst, which corresponds to a reduction of E_{des} by roughly 20 kJ/mol for the alloyed surface. Similar results were reported by Ross, who determined a temperature shift of 50°C compared to pure platinum in CO desorption experiments on an ordered Pt_3Sn single crystal, equivalent to a decrease in the desorption barrier of about 20 kJ/mol [183, 184], or by Paffett *et al.*, who reported desorption maxima at 60°C - 80°C and 110°C resulting in desorption barriers of 100 - 105 kJ/mol and 122 kJ/mol for ordered PtSn surface alloys and pure platinum, respectively [185] (For these calculations the authors assumed a prexponential of $4*10^{15}$ s^{-1}). In total, the (surface) alloy formation leads to an appreciable reduction in the onset of desorption at high coverages. For the present purpose, however, it is decisive to estimate the change in steady state coverage under reaction conditions. Using the desorption parameters determined above and sticking coefficients between 0.1 and 1, we can calculate that the reduction in CO coverage is negligible at 60 - 80°C and 1 kPa CO partial pressure. Hence it is unlikely that the PtSn system is operated in a low coverage situation at these temperatures, contrary to findings for Au/α-Fe_2O_3 [186]. Theoretically, for a similar reaction mechanism on Pt_3Sn/Vulcan as on Pt/γ-Al_2O_3 the decay in selectivity should begin at temperatures around 120°C as concluded from the difference in the onset of desorption, while based on experimental findings this onset of a decaying selectivity must be below or at 20°C (see Fig III-23), pointing to additionally effects contributing to the change in selectivity behavior as well.

In addition to the change in adsorption energy also the CO saturation coverage on the metal particles differs significantly. Because of the different catalyst loading and dispersion in the two TPD experiments we also plotted the integrated desorption curves, corrected for these differences and normalized to adsorbate coverages on the total metal surface, in the bottom part of figure III-25. Assuming a saturation coverage of 0.7 monolayers (ML) on the Pt particles [7], we obtain an absolute coverage of slightly more than 0.1 ML on the PtSn particles. This is by a factor of 5 below the saturation coverage extrapolated for a surface with Pt_3Sn composition, if we assume the same saturation CO density on the Pt surface atoms. The latter assumption was put forward and confirmed in UHV experiments on ordered single-crystal PtSn alloy surfaces (*e. g.*, [184, 185, 187]). Hence, the CO adsorption capability of the PtSn particles must be significantly reduced. Most plausibly the surface has become strongly enriched in Sn during the pretreatment procedure. Similar effects, significant Sn surface segregation of PtSn-alloys during annealing (or) in the presence of oxygen, were indeed found in earlier studies [171, 188-190]. Most likely the calcination step during conditioning (20 Nml/min of 10 kPa O_2 in N_2 for 30 min. at 300°C) causes a massive segregation of Sn to the surface, forming SnO_x clusters or a (partial) SnO_2 overlayer, which are not completely reverted during subsequent reduction in H_2. A situation with 80% of the surface covered by Sn or an oxidic species after the conditioning sequence does not appear unrealistic (see also next section). This is supported by our XPS results, where the calculated Pt:Sn ratio on the freshly conditioned catalyst is only 2.0 (table III-6), pointing to a strong surface enrichment of tin of more than 50%.

Note that the CO TPD experiment does not account for a possible influence of the coadsorbed hydrogen, which is present under steady state conditions during selective CO oxidation, on the CO desorption kinetics. Although we found that the influence on θ_{CO} is rather small in the

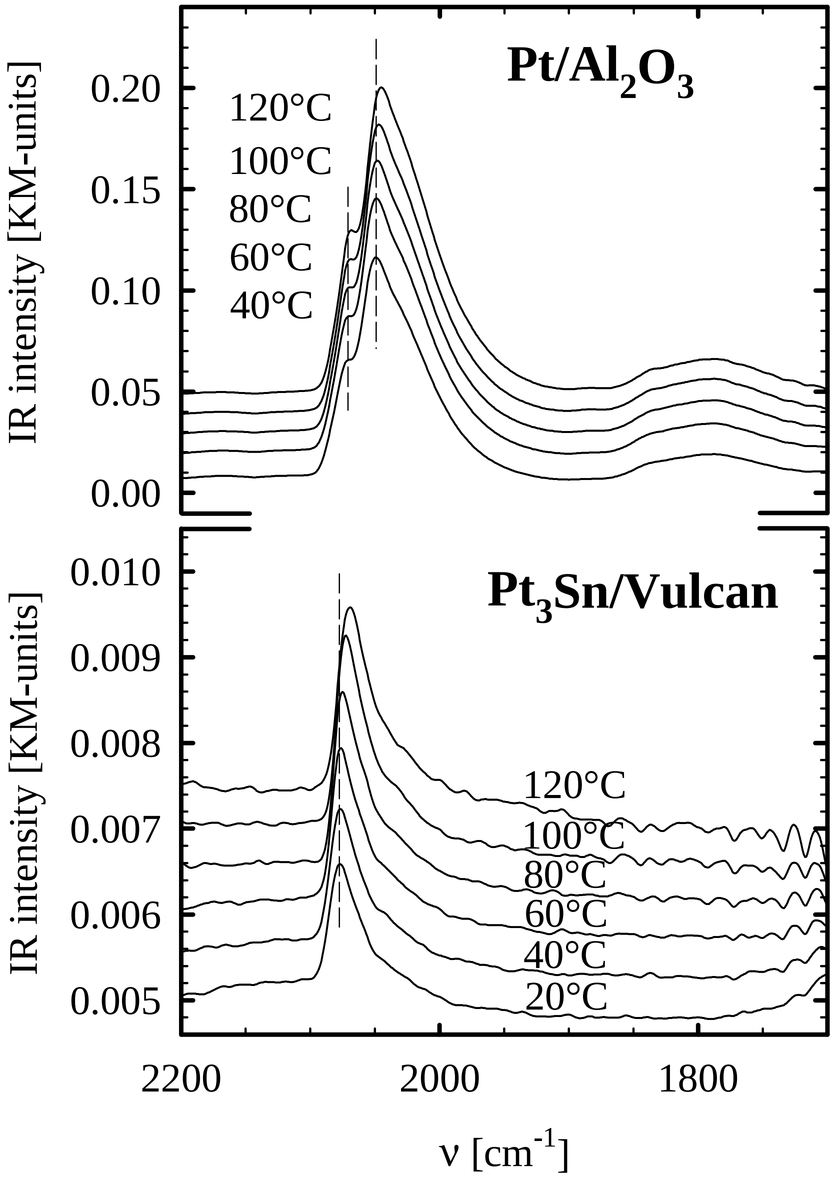

Fig. III-26: DRIFTS spectra (region for linearly adsorbed CO) in idealized reformate (0.1 kPa CO; λ = 2) at varying temperatures over Pt/γ-Al_2O_3 (*upper window*) and Pt_3Sn/Vulcan (*lower window*).

case of Pt/γ-Al_2O_3, where the adsorption energy of CO is lowered by only 2 kJ/mol in the presence of coadsorbed hydrogen (chapter III-1.1.5), this may be different for the PtSn system. Similar effects could also play a role for the CO oxidation kinetics.

More detailed statements require precise knowledge of the temperature dependent CO coverage under steady state conditions. This will be topic of the DRIFTS experiments described in the following section.

2.1.3 Coverage dependence of the selectivity

The use of infrared spectroscopy for the determination of temperature dependent changes in the CO coverage is based on earlier observations, showing that the exact position of the C-O stretch vibration, on an identical adsorption site, changes both with coverage and with temperature [38, 39]. The former shifts result from static changes in the C-O bond, due to direct and indirect adsorbate-adsorbate interactions, and from a coverage dependent dynamical coupling between neighboring dipoles. Temperature dependent shifts, at constant coverage, arise from thermal decoupling, *i. e.*, from a temperature induced reduction in dynamical coupling [40, 99, 191]. Monitoring the evolution of the C-O stretch frequency with temperature should therefore allow conclusions on the temperature dependent coverage behavior.

For these experiments IR spectra were recorded on a freshly conditioned catalyst in an atmosphere of 0.1 kPa CO, 75 kPa H_2, and rest N_2 for 90 min. at increasing temperatures, starting at 20°C and staying for 60 min. at each temperature. The spectra obtained on both catalysts are reproduced in figure III-26, the shift of the band position with increasing temperature, in the temperature range between 20°C and 120°C, is plotted in figure III-27. As evident from figure III-26, the overall shape of the spectra does not change significantly with temperature. On Pt/γ-Al_2O_3 two distinct CO species appear in the region of linearly adsorbed CO. A large band at around 2050 cm^{-1}, which is attributed to CO at step sites, and a shoulder at around 2073 cm^{-1}, which is assigned to a small fraction of CO on extended terraces [133]. Both bands reveal a small shift to lower wavenumbers of 3 - 4 cm^{-1} in the temperature range investigated. From parallel adsorption measurements on the Pt/γ-Al_2O_3 catalyst we know that the platinum surface is fully saturated with adsorbed CO over the entire temperature range at the conditions of figure III-23 (chapter III-1.1.4). Therefore this IR-shift is attributed solely to a thermal reduction of the dipole coupling at constant coverage. Alike conclusions were also drawn in very similar earlier experiments on Pt/Al_2O_3 catalysts by Anderson [191] or Primet [39].

Previous studies had shown that for adsorption on PtSn alloy surfaces the CO band is slightly shifted to lower frequencies (up to 20 cm^{-1}) compared to pure platinum (at a corresponding metal dispersion), which was mainly attributed to a dilution effect, which reduces CO coupling, and an additional small electronic influence (ca. 5 - 10 cm^{-1}) of the tin [192-194]. The band at around 2075 cm^{-1} found in the present study on the bimetal-PtSn catalyst is there-

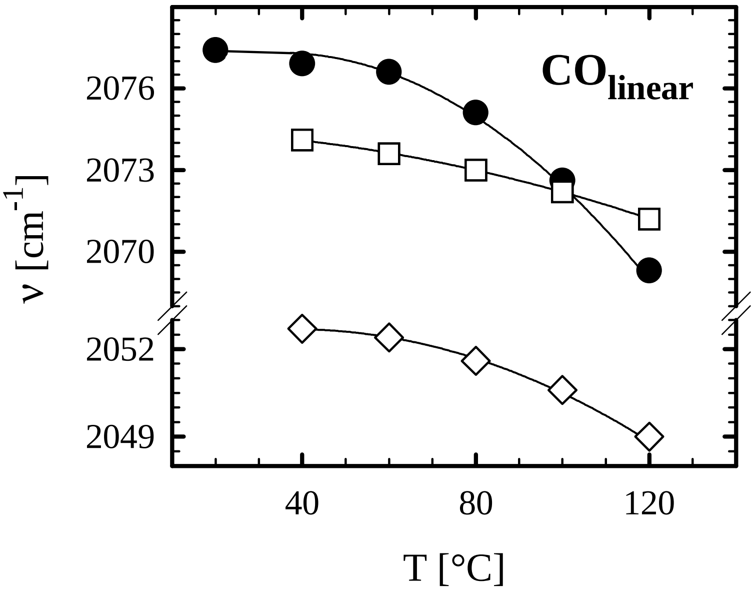

Fig. III-27: Position of the IR band for linearly adsorbed CO in idealized reformate (0.1 kPa CO; λ = 2) as a function of temperature over Pt_3Sn/Vulcan (●) and Pt/γ-Al_2O_3 (□ terrace bound CO and ◇ edge bound CO).

fore associated to linearly bound CO on Pt sites on the alloyed surface. With increasing temperature the band shifts by about 9 cm^{-1} to lower wavenumbers.

For comparison, Balakrishnan *et al.* reported in a similar study on a $PtSn/Al_2O_3$ catalyst containing 1% Pt and 0.1% Sn an infrared band at 2068 cm^{-1} at room temperature (after saturation with 101 kPa CO), which down-shifted about 25 cm^{-1} as the coverage decreased at higher temperatures [193]. Likewise, de Ménorval *et al.* observed an IR band at 2072 cm^{-1} on their $PtSn/Al_2O_3$ catalyst (1.4% Pt, 0.2% Sn; D = 64%), shifting to 2043 cm^{-1} after desorption at 200°C [195]. For samples containing more tin (up to 1%) the downward shift was significantly smaller (~12 cm^{-1}), indicating that the coupling is reduced by the dilution with tin [193].

If the contribution of direct thermal effects is around 3 cm^{-1}, similar to Pt/γ-Al_2O_3, the additional shift of about 6 cm^{-1} must be attributed to a reduction in CO coverage with increasing temperature. Comparison with the cited literature data ([193-195]) implies, that the present shift of 6 cm^{-1} would correspond to a coverage decrease of ca. 20%, assuming a linear relationship between the band position and θ_{CO}.

Based on these results the CO coverage on the Pt_3Sn/Vulcan catalyst drops continuously with increasing temperature under steady state conditions, especially above 60°C. Even if we take into account that the kinetic data were recorded under oxidizing conditions and at a somewhat higher CO content of 1 kPa (a concentration which could not be realized in the IR

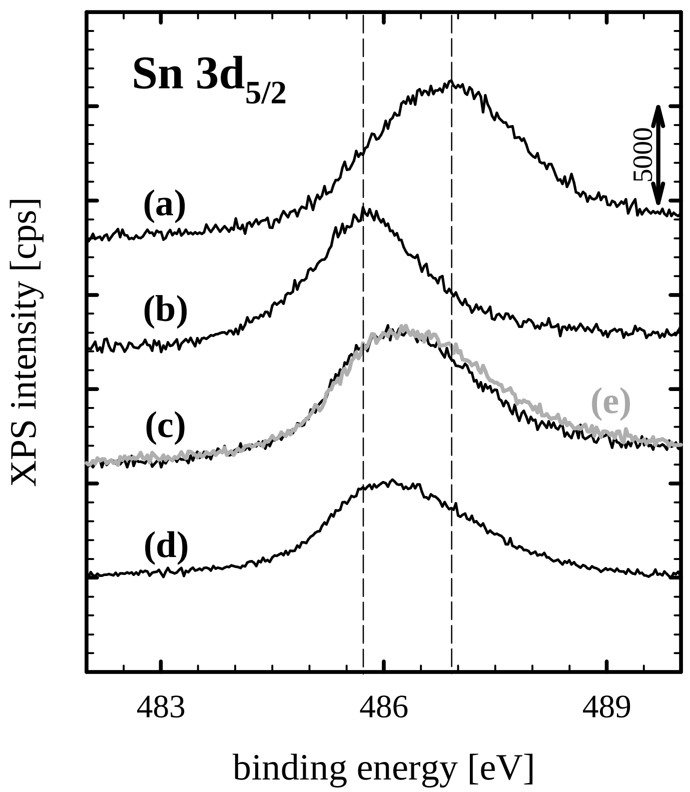

Fig. III-28: XPS spectra of the Sn $3d_{5/2}$ level on Pt_3Sn/Vulcan during conditioning (*a)* first 30 min. with 10 kPa O_2 in N_2, then *b)* 30 min. H_2; both 300°C), *c)* after exposure of the freshly conditioned catalyst to air (20°C; 15 min.) *d)* after 16 h of CO oxidation in pure nitrogen and *e)* after 1 h PROX in idealized reformate (spectra d & e with 1 kPa CO; $\lambda = 2$; 80°C; with subsequent exposure to air at 20°C, ca. 15 min.).

experiments, since under these conditions the gas phase CO signal completely covered the CO_{ad} band on the carbon supported catalyst), this infrared experiment confirms the conclusions from the TPD experiment, that the steady state CO coverage decreases significantly in the temperature range 60 - 120°C, which in turn would serve as a good explanation for the decay of selectivity under PROX conditions in fig. III-23. On the other side, both experiments indicate that the coverage decrease is small, if at all existing, at temperatures below 40 - 60°C, pointing to another contribution to the increasing selectivity in this temperature range.

2.1.4 Catalyst state during conditioning & reaction

In addition to alloy formation Sn can affect the reaction also by forming SnO_x, which may cover part of the metal particles. Therefore information on the oxidation state of the Sn component, under reaction conditions, is a precondition for understanding the reaction mechanism. This question was investigated by XPS measurements. XP spectra were recorded

Treatment	**Pt($4f_{7/2}$) [eV]**	**Sn($3d_{5/2}$) [eV]**	**„Sn^0“ [%]**	**Pt/Sn-ratio**
conditioning:				
10 kPa O_2 at 300°C	71.6	486.9	9	1.6
+ 10 kPa H_2 at 300°C	71.7	485.8	≡ 100	2.0
+ exposure to air at 25°C	71.6	486.1	57	1.8
after reaction (ex-situ):				
1 h id. reformate (1 kPa CO, $\lambda = 2$; 80°C)	71.6	486.3	39	1.7
20 h id. reformate (1 kPa CO, $\lambda = 2$; 80°C)	71.6	486.3	37	1.7
16 h CO oxid. in pure N_2 (1 kPa CO, $\lambda = 2$; 80°C)	71.6	486.1	52	1.8

Table III-6: XPS results on our Pt_3Sn/Vulcan catalyst after treatment in different atmospheres (C(1s) at 284.6 eV).

on the freshly conditioned catalyst and on a used catalyst, after 1 and 20 h reaction, respectively. Since these measurements cannot be performed *in-situ*, we also characterized a catalyst conditioned in a high pressure cell of the XP-spectrometer (30 min. 10 kPa O_2 + 30 min. 10 kPa H_2, both at 300°C) for comparison, avoiding subsequent transport through air. The spectra (Sn($3d_{5/2}$) peak) recorded after the different treatments are shown in figure III-28.

The reactive treatments lead to the following results (also listed in table III-6): After oxidation in the high pressure cell the Sn($3d_{5/2}$) signal appears at a BE of 486.9 eV (spectrum (a) in fig. III-28), the subsequent reduction cycle causes a down-shift to 485.8 eV. Furthermore, compared to the rather large width of spectrum (a) (full width at half maximum (FWHM) 2.3 eV) the latter spectrum is significantly narrower, with a FWHM of 1.8 eV. From a comparison of the positions to those given in previous studies, which were obtained on various supported and unsupported PtSn and Sn samples (listed in table III-7; the BE-range for the $3d_{5/2}$ signal of Sn in its different states is also graphically illustrated in figure III-29), we attribute the latter spectrum to Sn in its metallic state (which is slightly shifted upward for alloys and small films when compared to bulk Sn [196, 197]), whereas after the calcination treatment $Sn^{2+/4+}$ species dominate the spectrum. The latter are hardly distinguished by XPS [198, 199]. The large peak width of 2.3 eV, however, points to contributions from different oxidation states. Hence Sn oxidation is still incomplete, in agreement with previous findings that oxidation of PtSn alloys is very slow, much slower than for metallic Sn [196, 200].

After the subsequent reduction cycle, the BE's are reduced but still slightly higher than those reported in the literature for alloy surfaces/particles. Since significant particle size effects are

System	Pretreatment	Pt(4f) [eV]	$Sn(3d_{5/2})$ [eV] $^{1)}$	Other	Ref.
Pt_3Sn	sputtering	70.9	484.6		[189]
Sn/Pt(100)	annealed at > 600 K $^{2)}$	70.9	~485.0		[202]
Pt_3Sn	air (25°C)	71.5	485.0 $^{3)}$/ 486.4		[203]
	+ H_2 (300°C)	71.7	485.3 / 486.4 $^{4)}$		
PtSn foil	250 kPa H_2 (375°C)	72.0	484.9 $^{(88)}$ / 486.7 $^{(12)}$		[204]
	O_2 (500°C)		486.0		
PtSn $^{5)}$			485.3		[196]
	+ 200 kPa O_2 (25°C)		485.7 $^{6)}$		
Pt_3Sn	air (25°C)	71.2	484.7 / ~486.0 $^{4)}$		[205]
Sn/Pt(111)	500 L O_2 (50°C)		484.8 / 485.9		[185]
$PtSn/SiO_2$	O_2 (400°C)	71.4 $^{(61)}$ / 72.5 $^{(39)}$	484.0$^{(6)}$ / 485.4$^{(11)}$ / 487.6$^{(83)}$	Si(2p) = 103.4 eV	[171]
	+ CO/O_2 (300°C)	71.2	485.5$^{(21)}$ / 487.3$^{(79)}$		
$PtSn/SiO_2$ $^{7)}$	250 kPa H_2 (375°C)	71.5	484.8 $^{(49)}$ / 487.0 $^{(51)}$	Si(2p) = 103.7 eV	[204]
	O_2 (500°C)		487.4		
$PtSn/SiO_2$	+ H_2 (300°C)		483.6$^{(16)}$ / 484.9$^{(66)}$ / 486.8$^{(18)}$	Si(2p) = 103.4 eV	[206]
$PtSn/Al_2O_3$	+ H_2 (300°C)	71.3	483.9$^{(20)}$ / 484.9$^{(52)}$ / 486.8$^{(28)}$	Al(2p) = 74.7 eV	
$PtSn/Al_2O_3$ $^{7)}$	250 kPa H_2 (375°C) $^{8)}$	72.1	484.0 $^{(49)}$ / 486.6 $^{(51)}$	Al(2p) = 74.7 eV	[204]
	O_2 (500°C)		487.0		
$PtSn/Al_2O_3$	air (500°C)		~483.6 $^{(33)}$ / ~486.9 $^{(67)}$		[194]
PtSn/C	H_2 (350°C)	71.8	~486.3 $^{(15)}$ / 487.7 $^{(85)}$	C(1s) = 284.9 eV	[207]
Sn/Al_2O_3	reduced by ion beam / atomic H	-	484.8 / 486.6 $^{9)}$	Al(2p) = 74.3 eV	[199]
Sn	sputtering	-	484.7		[198]
	+ air (25°C)	-	484.7 + 486.4		
Sn		-	484.9		[196]
	+ 200 kPa O_2 (25°C)	-	485.0 / 486.4		

1) $^{(x)}$ = in at% 2) formation of PtSn surface alloys 3) low-BE shoulder 4) high-BE shoulder 5) prepared by vapor deposition of Sn (0.28 ML Sn)
6) + broadening to high BE 7) Pt:Sn = 1:2.7 8) forming an Pt_3Sn alloy phase 9) similar values were obtained on an air-exposed Sn-foil

Table III-7: XPS literature data obtained on various PtSn or Sn systems.

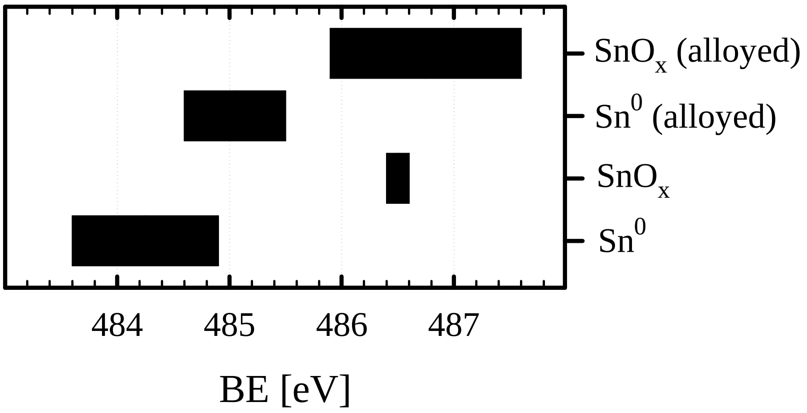

Fig. III-29: Binding energy range for the Sn($3d_{5/2}$) peak of various Sn and PtSn samples in literature studies [171, 185, 189, 196, 198, 199, 202-206]

unlikely at an average particle size of 3 - 4 nm, the higher BE might reflect an incomplete reduction of the particles. Similar effects have in fact been observed, during reduction of an Al_2O_3 supported PtSn catalyst at 500°C in a H_2 flow, where EXAFS spectra recorded *in-situ* showed significant Sn coordination to oxygen atoms [201]. On the other hand, for a SiO_2 supported PtSn catalyst the same procedure led to a more complete reduction and alloy formation. Similar conclusions have been reached in numerous other studies, which confirmed that after reduction in H_2 a significant fraction of the Sn in Al_2O_3 supported catalysts was involved in PtSn alloy formation, but a large fraction, presumably unreduced tin oxides, remained unaffected on the surface [193, 204, 206, 208-211]. For carbon supports the situation appears to be similar: After reduction part of the Sn is metallic and dissolved in PtSn alloy particles, another part of it is still in an oxidic state, adsorbed on the PtSn particles and presumably also on the support material [207, 212]. Likewise, the increased Pt:Sn ratio measured after reduction, which indicates diffusion of Sn into the alloyed metal particles, underlines the formation of a real bimetallic catalyst after our conditioning procedure. Because of the ten times higher H_2 partial pressure during reduction in the reactor the degree of Sn reduction for the conditioned catalyst prior to reaction may be somewhat higher than after the *in-situ* reduction in the XP-spectrometer.

Next we compare with spectra recorded on the catalysts after conditioning in the reactor and after 1h reaction in idealized reformate (1 kPa CO, $\lambda = 2$; 80°C), respectively (fig. III-28 c,d), and subsequent transfer into the spectrometer. For better comparison these spectra are overlaid on top of each other. The Sn(3d) peaks in these spectra are almost identical, both with respect to their peak position, with binding energies (BE's) of 486.1 and 486.3 eV, respectively, as well as to the Sn(3d)/Pt(4f) intensity ratio. The only significant difference is a shoulder on the high BE side of the spectrum, which is more pronounced after reaction than after conditioning, which may be attributed to either an enhanced amount of oxidized Sn species or, more likely (since the broadening is not observed after CO oxidation in a pure N_2 background), to the formation of $Sn(OH)_x$ species, which can be expected as a consequence of the parallely occuring $H_2 + O_2$ reaction. A virtually identical spectrum was obtained on a catalyst after 20 h reaction (see table III-6).

The rather wide peaks (FWHM 2.3 eV) can be deconvoluted into and fitted by contributions of the 'reduced' and the 'oxidized' component in figs. III-28 a and b (Note that the 'reduced' component is presumably also partly oxidized.) The apparent shift of 0.3 eV and the increase in peak width from spectrum (III-28b) to spectrum (III-28c) reflect an increase in the oxidized component, which is caused by the sample transfer. The relatively low increase in oxidation is consistent with findings from previous studies on the oxidation of PdSn and PtSn (surface) alloys, which reported only slight peak shifts of below 0.5 eV for oxygen exposures around 10^{11} L (1 L = $1.33 \cdot 10^{-6}$ mbar s) [196, 200], much less than obtained for bulk Sn or thick Sn films [185].

In contrast to the tin component, the Pt($4f_{7/2}$) signal remains constant at a BE of 71.6 eV for all treatments, indicating a fully reduced state. The somewhat higher BE compared to the values listed for pure Pt (ca. 71.2 eV [213]) is probably an effect of the Pt-Sn alloy formation [214].

In total these results indicate that the working catalyst, under reaction conditions, contains partly oxidized Sn on the surface. Similar conclusions were reached in additional *in-situ* XANES measurements on the Pt_3Sn/Vulcan catalyst during reaction in idealized reformate (The results will be published in detail in an upcoming article). This formation of SnO_x species during CO oxidation was also confirmed in *post-mortem* AES experiments by Logan *et al.* for a Sn overlayer on a Pd(100) substrate (reaction at 1 kPa O_2, < 0.2 kPa CO; ~200°C) [215]. Nevertheless, part of the tin in our catalyst is present as metallic Sn^0 in form of PtSn alloys. The close similarity of the spectra (III-28c) and (III-28d) indicates that during the reaction the catalyst largely keeps the morphology and (surface) composition it had after conditioning, with a slight increase in the amount of oxidized Sn species. After the oxidative treatment, more highly oxidized SnO_x surface species are formed, accompanied by reaction induced Sn segregation. Similar conclusions can also be drawn from a quantitative analysis of the Sn(3d)/Pt(4f) intensity ratios. Moreover, the XPS data support the strong Sn surface enrichment on the freshly conditioned catalyst when compared to the nominal composition (Pt_3Sn), as was already indicated by the low saturation coverage of CO in our TPD experiment. This is also in agreement with a recent study of de Miguel *et al.*, who reported extreme surface compositions of Pt:Sn = 1:16 and more on a PtSn/C catalyst after reduction at 350°C [207].

2.1.5 Mechanistic proposal - avoiding the CO poisoning

From the data presented above, the mechanism for preferential CO oxidation on carbon supported PtSn catalysts, at 1 kPa CO and 1 kPa O_2, must satisfy the following conditions:

i) The rate for CO oxidation is much higher on Pt_3Sn/Vulcan than on Pt/γ-Al_2O_3, by about 2 orders of magnitude at 80°C; it is close to that observed on Au/α-Fe_2O_3 under identical conditions.

ii) The effective activation energy for CO oxidation on Pt_3Sn/Vulcan is much lower than on Pt/γ-Al_2O_3, and closely similar to that observed on Au/α-Fe_2O_3 under identical conditions. It is also much lower than the CO desorption barrier on this surface, implying that CO desorption is not the rate limiting step.

iii) The low temperature selectivity of 85% on the PtSn catalyst is much higher than that obtained for the common Pt catalyst (35%) in the temperature range where this is active. It decreases with temperature above 20°C.

iv) CO adsorption on the PtSn alloy surface exhibits an additional low temperature state not existent on Pt, which reduces the onset for CO desorption by 60 - 70°C at saturation coverage. Despite of the resulting decrease in steady state CO coverage with temperature the reaction proceeds at a substantial local CO coverage on the free Pt surface sites, much higher than for Au/α-Fe_2O_3, but below saturation coverage.

v) Under reaction conditions part of the Sn is oxidized, while the remaining part is metallic, forming PtSn alloy particles. A large fraction of the surface, about 80%, is blocked for CO adsorption, by both SnO_x patches and alloyed Sn atoms on/in the surface.

These requirements are met by the following tentative mechanistic picture for the PROX reaction on the Pt_3Sn/Vulcan catalyst in the parameter range investigated here: During reaction the catalyst operates at high CO coverages, which may reach saturation in the low temperature regime between 0° and 40°C and decreases steadily with increasing temperature. But even at 120°C the CO coverage is still considerable (reduced by approximately 20% based on the infrared results). Areas covered by SnO_x as well as Sn surface sites are not accessible for CO adsorption. These areas are active, however, for oxygen adsorption. Since the sticking probability of oxygen on a CO covered PtSn surface, even with only Pt sites being occupied, is expected to be low, oxygen adsorption will be dominated by adsorption on small SnO_x islands. Oxygen adsorption on Pt sites vacated by reacting or desorbing CO molecules, which is the rate limiting step on pure Pt, is still possible, but is much less efficient than on the SnO_x areas. CO oxidation takes place by reaction between CO adsorbed on the Pt areas/sites of the catalyst particles and O_{ad} adsorbed on adjacent SnO_x islands/Sn sites or by spill-over of one the species and subsequent reaction to CO_2. Since oxygen adsorption is not limited by CO desorption, the activity of the PtSn catalyst is much higher than that of Pt catalysts, at least in the regime of high CO coverages. A rather similar mechanism had been proposed for low temperature CO oxidation on Pt/SnO_2 catalysts by Lintz and coworkers [177], explaining the high activity at low temperatures by adsorption of oxygen on the tin-dioxide and subsequent reaction with CO adsorbed on Pt sites. The still lower activity of the SnO_2 supported Pt catalysts as compared to the present system (see table III-5) can be understood from the higher dispersion of the SnO_x component, if this material is present on the surface of the active metal particles. The reduced CO adsorption energy and hence decreased steady state coverage of CO, which work in the same direction, would not be sufficient to explain the rather high reaction rates even at the lowest temperatures, around 0 - 20°C. Since CO desorption is no more a precondition for oxygen adsorption and subsequent reaction, the activation energies for CO oxidation and CO desorption on the PtSn catalyst are distinctly different, in contrast to pure Pt catalysts, where the creation of vacancies by CO desorption is the rate limiting step, at least in the 'low rate branch', and the barriers for CO oxidation and CO desorption, in the high coverage limit, are of similar size [1, 216].

The hydrogen oxidation reaction, in the presence of small amounts of CO in the gas phase, seems to be dominated by hydrogen adsorption on Pt surface sites. The much higher selectivity of the PROX reaction on PtSn than on Pt results from the much higher rate for CO oxidation, while the enhancement of the hydrogen oxidation rate is less pronounced. This points to a low steady state coverage of H_{ad}, which is most easily explained by a hydrogen adsorption path where hydrogen adsorption on PtSn proceeds in the same way as on Pt, by adsorption into vacancies of the CO adlayer. This way hydrogen adsorption is effectively inhibited at high CO coverages. Hydrogen adsorption on SnO_x areas, being the dominant route for oxygen adsorption, does not seem to play a role. Furthermore, even in the absence of CO the sticking coefficient for hydrogen adsorption on the PtSn surface is significantly lower than on a pure Pt surface [185], probably a geometric effect, which reduces the number of reactive Pt ensembles [195, 217, 218].

In that picture it is straightforward to explain the much higher selectivity on the bimetallic PtSn catalyst as compared to the pure Pt catalyst and the steady decrease of the selectivity with temperature. At low temperatures (and high CO coverages) hydrogen adsorption and oxidation are practically inhibited, since limited by CO desorption. With increasing temperature at least at temperatures above 40 - 60°C, the CO coverage decreases on PtSn, while on Pt it remains practically constant up to much higher temperatures. Consequently the hydrogen oxidation rate increases steadily, leading to a steady decline in selectivity. For Pt/γ-Al_2O_3, in contrast, the selectivity is constant over a wide temperature range and decays only above 200°C (chapter III-1.1.1).

These effects are reflected in the activation energies measured for the two oxidation reactions. While on Pt/γ-Al_2O_3 the apparent, measured activation energies for CO and H_2 oxidation are practically identical, the latter is significantly higher than the former one on Pt_3Sn/Vulcan, in accordance with the observed decrease in selectivity with temperature. It is important to note that these activation energies are not simple barriers for the individual oxidation step, *i. e.*, for the reaction between adjacent CO_{ad} and O_{ad} (or H_{ad} and O_{ad}), but rather result from a complex interplay between different processes, each of them exhibiting a different temperature dependence, with considerable consequences for the overall reaction process. For instance for PtSn, where oxygen adsorption is possible also on Sn areas, CO desorption is no longer rate limiting and the apparent barrier for reaction (31 kJ/mol) is much lower than that for CO desorption (~70 - 90 kJ/mol). In that case the actual reaction step is likely to be rate limiting, with the measured activation barrier actually describing the activation energy of this reaction step. For the hydrogen oxidation rate on Pt_3Sn/Vulcan, on the other side, the measured activation barrier must include also effects from the decline in CO coverage with increasing temperature. On pure Pt the hydrogen oxidation rate is directly coupled to that for CO removal, *i. e.*, CO desorption, CO oxidation and H_2 oxidation exhibit the same apparent activation energies, at least up to 200 °C [7].

At last we compare the reaction mechanism for CO oxidation on PtSn with that on another low temperature CO oxidation catalyst, on Au/α-Fe_2O_3. The latter catalyst is very different from PtSn in that on the Au surface CO adsorption is much weaker, leading to a very low steady state CO coverage at operating temperatures between 40° and 80°C ([186]; compare also chapter III-3.3). On the other side, despite of the low CO coverage oxygen adsorption on Au is practically not possible because of the very low sticking coefficient for dissociative oxygen adsorption on Au [219, 220]. Existing reaction models therefore assume oxygen adsorption on the FeO_x support, followed by diffusion to the perimeter of the Au particles and subsequent reaction either at the perimeter, or, after a spill-over process of one of the components, on the adjacent Au or support areas (see chapter III-3.1). Hence, also in this case CO desorption is not rate limiting, at least not for the supply of oxygen, and this catalyst shows reaction characteristics similar to the present Pt_3Sn/Vulcan catalyst, with the selectivity decreasing with temperature [26, 186]. In this case, however, the competing adsorption and oxidation of hydrogen is not inhibited by a CO adlayer on the metal particle, but by the high activation barrier for the dissociative hydrogen adsorption on Au [221-223].

Finally we would like to note that if the mechanism suggested above is correct, one would expect for the PROX reaction on PtSn catalysts that in the parameter range investigated here the selectivity is independent of the O_2 partial pressure in the low temperature regime, where oxygen adsorption is limited to adsorption on the SnO_x islands, and decreases with CO partial pressure, at least at temperatures above 40°C. These proposals are currently investigated and will be presented in a parallel thesis work by M. Kahlich [25].

2.2 Other important characteristics for an application in a PROX-stage

Not only a high activity and selectivity are decisive for an employment in a real PROX application, there are other important factors, which have to be considered as well, *e. g.*, the long-term stability or effects arising from a more realistic composition of the reaction gas mixture.

The currently employed Pt/γ-Al_2O_3 system showed a quite satisfying long-term stability in our tests in idealized reformate, characterized by a rather moderate and highly reversible decline of activity (chapter III-1.2.1). But due to its high operation temperature (150 - 250°C), which is necessary in order to ensure a sufficient mass-related activity, its performance suffers strongly from the reverse water-gas shift reaction occuring at the same time in presence of CO_2, which limits the CO purification level achievable in a PROX stage (see, *e. g.*, [11, 12]; compare also chapter III-1.3.2).

Similar to the procedure for Pt/γ-Al_2O_3 in the preceeding part of this work, in the following context, we will first investigate the long-term performance of our Pt_3Sn/Vulcan catalyst before we subsequently discuss effects arising from a more realistic reformate containing CO_2 and / or H_2O. Finally we will evaluate the activity for the water-gas shift reaction and compare it to the standard Pt/γ-Al_2O_3 catalyst.

2.2.1 Long-term stability

The evolution of the CO oxidation activity over Pt_3Sn/Vulcan during time-on stream in various gas mixtures (all 1 kPa CO, $\lambda = 2$; 80°C) is displayed in figure III-30 and compared to the deactivation behaviour of the Pt/γ-Al_2O_3 catalyst in idealized reformate at 150°C (black circles). The deactivation over the bimetallic PtSn catalyst (diamonds) in idealized reformate (46% within 1000 min.) is almost identical to that of the Pt catalyst. But due to the different reaction mechanism, where the oxygen supply is not limited by the CO desorption but occurs *via* the Sn component, the activity loss on Pt_3Sn/Vulcan cannot be simply traced back to a slow „self-poisoning“ by a more and more perfect CO_{ad}-layer as was proposed for Pt/γ-Al_2O_3 ([32, 128]; see also section 1.2.1). For the CO oxidation in pure nitrogen this deactivation is strongly enhanced (86%; triangles). Moreover, the activity is significantly lower (factor 2 for the inital TOF), which is in analogy to the pure Pt catalysts and probably caused by a similar effect of coadsorbed hydrogen on the adsorption energy of CO in idealized reformate (Chapter III-1.1.5). On the closely related Pt/SnO_2 system Gardner *et al.* observed a similar severe

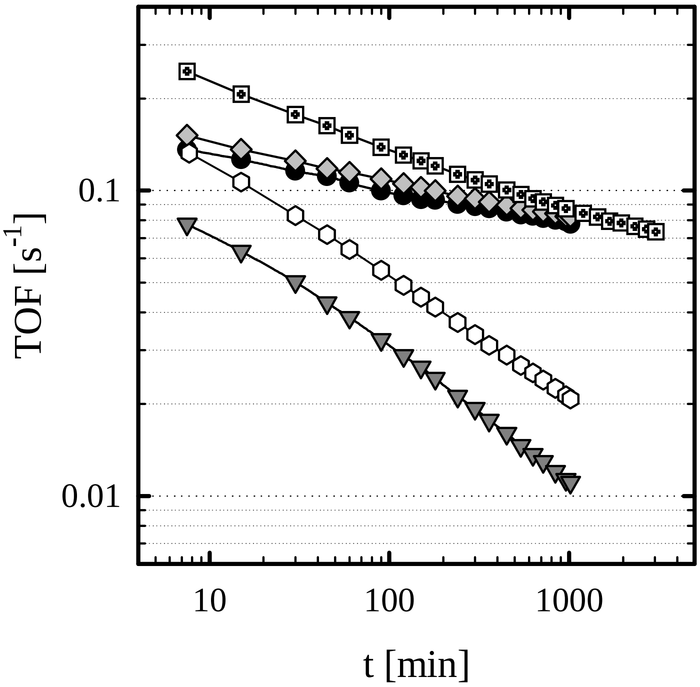

Figure III-30: Long-term activity of Pt_3Sn/Vulcan (80°C) in idealized reformate (◇ ; 1 kPa CO, $\lambda = 2$), in idealized reformate + 1.3 kPa H_2O (⊞), during CO oxidation in a pure N_2 background (▽) and in pure N_2 with 1.3 kPa H_2O added (⬡); for comparison: Pt/γ-Al_2O_3 in idealized reformate at 150°C (●;1 kPa CO, $\lambda = 2$).

deactivation of roughly 70% within 1000 min. (1 kPa CO, $\lambda = 1$; 55°C) [224]. The addition of water (1.3 kPa; hexagons) to the hydrogen-free mixture increases the activity slightly (+40%), which is again similar to Pt/γ-Al_2O_3 and also in accordance with alike observations by Croft *et al*. on a Pd/SnO_2 catalyst (5 kPa CO, $\lambda = 8$; 60°C) after the addition of 2.8 kPa H_2O [225], but it does not alter the deactivation behaviour markedly. Such an increase of the initial activity is also noted for idealized reformate in the presence of water (square symbols), but here the effect is slowly reduced with proceeding time on-stream, leading to an asymptotic approach to the data obtained in the dry mixture (see next section).

The reversibility of this activity loss on Pt_3Sn/Vulcan (in idealized reformate) was investigated in subsequent long-term measurements, which are shown in fig. III-31. Other than for Pt/γ-Al_2O_3 the activity is not fully restored after intermediate purging with pure nitrogen at 80°C (*i. e.*, at reaction temperature; 20 Nml/min for 1 h) and 170°C, respectively. Just 65 - 70% of the initial rate are regained by this procedures. Only after an intermediate purging step at 270°C (inset window in fig. III-31), which is already close to the conditioning temperature, the initial activity is restored to the full extent.

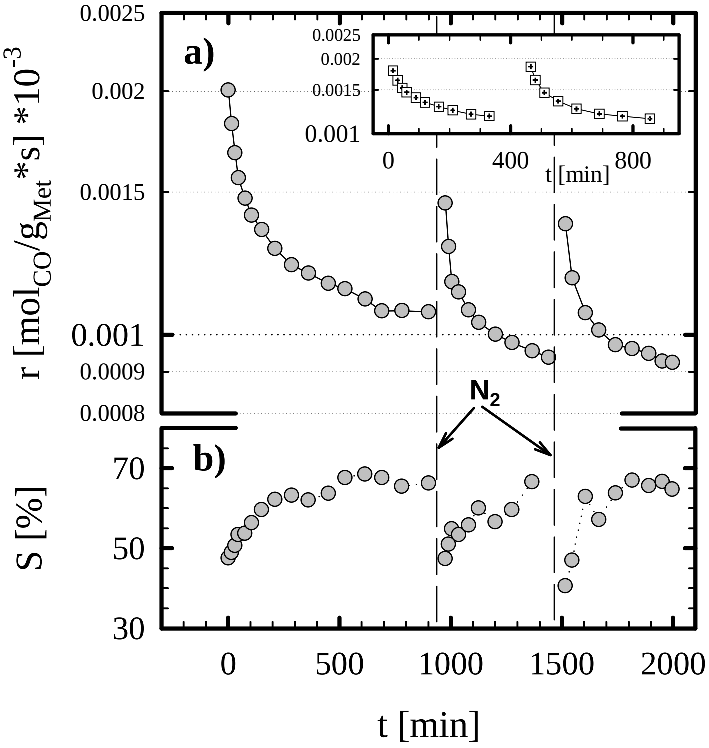

Figure III-31: "Regeneration-tests" over Pt_3Sn/Vulcan after reaction in idealized reformate at 80°C (1 kPa CO, $\lambda = 2$): first by intermediate purging with nitrogen for 1 hour at reaction temperature, then at 170°C - *a)* reaction rate and *b)* selectivity; *Inset*: Regeneration-test" by purging with N_2 at 270°C (1 h).

At the beginning of the experiment and after each purging step the selectivity starts from a low level (ca. 45%) and then slowly increases to its final value (ca. 67%), a behaviour which is well known from our experiments on the Pt/γ-Al_2O_3 system. On the latter, this phenomenon was explained by a CO_{ad}-layer approaching its final steady state coverage only very slowly and hence initially allowing more hydrogen to adsorb on the surface. The fact, that the same effect exists for the bimetallic PtSn surface, too, underlines that we indeed operate at a rather high θ_{CO} at our reaction conditions (at least high enough to block the H_2 adsorption) as was already suspected in the preceeding chapter. It furthermore confirms clearly that CO and H_2 still compete for the same (Pt) adsorption sites and that the latter does not additionally adsorb on the tin component.

Since we may exclude the „CO-poisoning“ model as an explanation for the observed activity loss on the Pt_3Sn/Vulcan catalyst, in principle two other models must be take into account. First, by-products may form on the catalyst surface during reaction and block active sites, as was demonstrated, *e. g.*, for the carbonate species, which accumulate on a Au/α-Fe_2O_3 catalyst during time on-stream (see chapter III-3.4). Second, the surface composition, which has

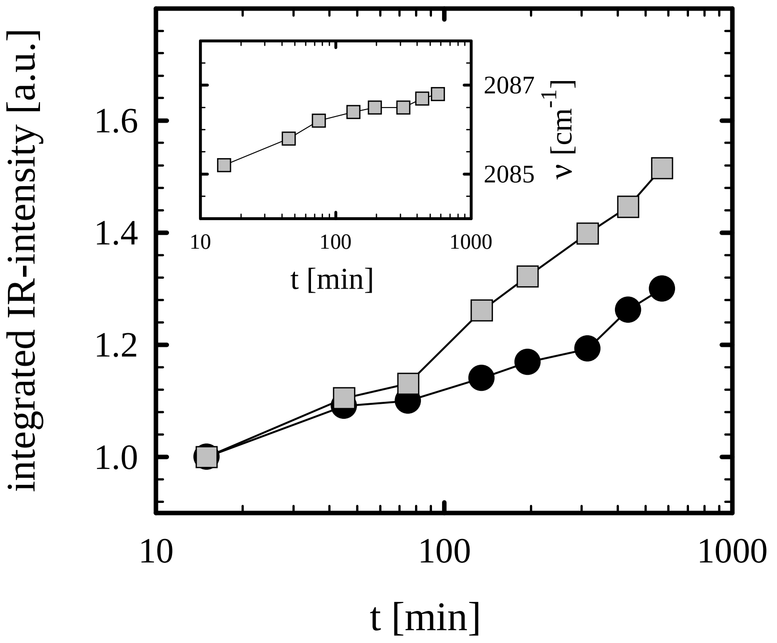

Figure III-32: Time-evolution of the IR-band for linearly bound CO on Pt_3Sn/Vulcan in idealized reformate (▨) and during CO oxidation in a pure nitrogen background (● ; 1 kPa CO, λ = 2; 80°C).
Inset: Time-evolution of the band position in idealized reformate.

shown to be rather dynamic during the conditioning process, may change gradually in order to approach a new enthalpy minimum in the employed reaction atmosphere. For this model it is quite difficult to predict which metal would be expected to accumulate in the surface layer in idealized reformate: On the one hand CO and H_2 would favour a platinum enrichment, on the other hand oxygen as well as the *in-situ* produced water support the segregation of tin to the surface [188, 189, 203, 226]. The following DRIFTS and TPD experiments were recorded in order to confirm or refute the above hyphotheses.

First, we acquired DRIFTS spectra during several hours of CO oxidation in idealized reformate and in a pure nitrogen background, respectively (1 kPa CO, λ = 2, 80°C). In figure III-32 the time-evolution of the integrated IR area of the band for linearly bound CO (at around 2085 cm^{-1}) is shown. For a better comparison the initial value (acquired after 15 min. of reaction) is scaled to one. Quite clearly, in both experiments the CO_{ad} signal grows significantly during time on-stream. Moreover, this effect even accelerates with progressing reaction time instead of slowly approaching a steady-state value, which would be expected for a simple equilibration of adsorbed species as was observed on Pt/γ-Al_2O_3 [32] (and would would give rise to changes the intensity by less than 10%, anyway). Since for a bimetallic PtSn surface the CO adsorbs exclusively on the platinum under our conditions [227, 228], the

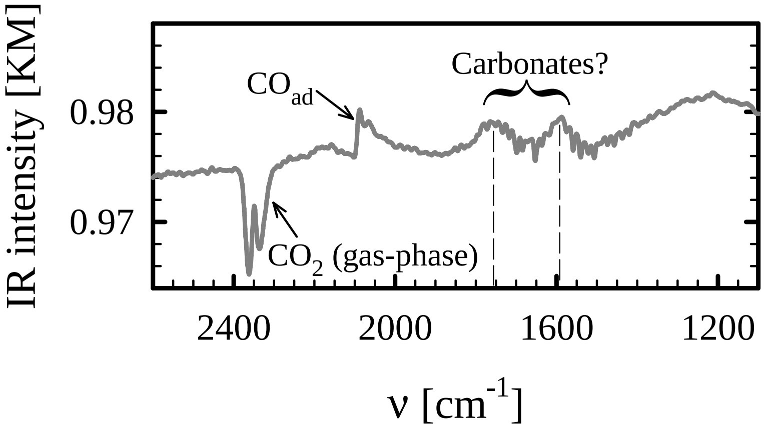

Figure III-33: Difference spectra on Pt_3Sn/Vulcan obtained in idealized reformate (0.5 kPa CO, λ = 2; 80°C) between a spectrum acquired after 15 min. and after 10 hours, respectively - Upward bands: increase; downward bands: loss.

intensity increase in our DRIFTS spectra strongly suggests that the platinum is enriched at the surface of the alloyed particles during CO oxidation. The parallel increase of the wavenumber (fig. III-32, inset window) likewise suggests a gradual reduction of the small electronic effect of tin, which for alloyed particles originally down-shifts the band position compared to pure Pt particles [192-194].

Nevertheless, the much more pronounced IR-effect in idealized reformate, obviously a consequence of the high H_2-content in this gas mixture, contrasts the more moderate deactivation compared to the hydrogen-free mixture, which was found in our long-term experiments (fig. III-30). Hence the observed segregation effect cannot be responsible for the activity loss on Pt_3Sn/Vulcan (at least not for the reversible, major part).

Next, we investigated the formation of by-products in DRIFTS. But due to the very small penetration depth of the infrared beam into the black coloured catalyst powder, the spectral region below 1800 cm^{-1} was hardly accessible, resulting in an extremely low signal-to-noise ratio (even at a total scanning time of more than 20 min.). The only information, which could be obtained from a long-term measurement in idealized reformate (0.5 kPa CO, λ = 2; 80°C) over a Pt_3Sn/Vulcan catalyst diluted with diamond powder (which should be a completely inert material), is that upon dividing the spectra acquired after 15 min. and 10 h on-stream, respectively, a slight growth of bands at 1590 and 1750 cm^{-1} appears (fig III-33), which indeed suggests the accumulation of byproducts (most likely carbonates, CO_3^{2-}) on the surface during the reaction.

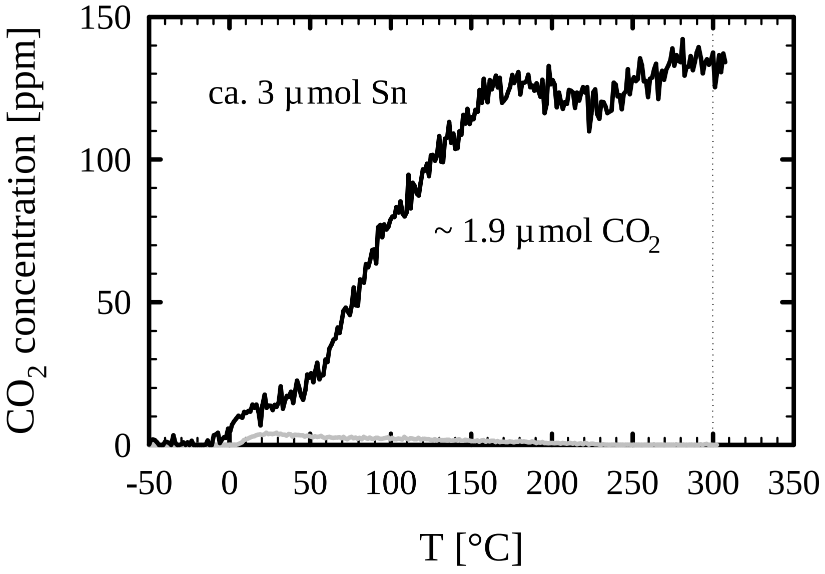

Figure III-34: TPD experiment (8 Nml/min N_2; 5°C/min) after 12 hours of reaction over Pt_3Sn/Vulcan in idealized reformate (0.6 kPa CO; $\lambda = 2$; 80°C) and the subsequent oxidative removal of the CO_{ad} at -20°C (━━). For comparison: CO_2-TPD over freshly conditioned Vulcan support - Both plots are normed to the employed mass of support material (──).

In order to confirm this idea, we performed a temperature programmed desorption (TPD) experiment *post mortem*, which is shown in figure III-34 (a CO_2-TPD on the pure Vulcan support is included for comparison). After approximately 12 hours of reaction in idealized reformate (0.6 kPa CO, $\lambda = 2$, ca. 40 kPa H_2; 80°C), we cooled the catalyst bed down to -20°C, removed the adsorbed CO by purging with 10 kPa O_2 in N_2 (ca. 5 min.; 20 Nml/min) and then slowly increased the temperature (5°C/min) in a flow of nitrogen (8 Nml/min). Indeed some CO_2 evolved at elevated temperatures, with two broad maxima at ~170°C and ~280°C. The measurement was cut off at 300°C, since at temperatures above the conditioning temperature large contributions from residual catalyst impurities cannot be excluded. From the parallel TPD experiment on the pure support (grey line in fig. III-34) as well as from the negligible CO_2 signal (up to 300°C) during our CO-TPD experiment in the last section (fig. III-25), we infer, that the CO_2 evolution on the used catalyst is indeed related to by-products, which are formed during the selective CO oxidation over Pt_3Sn/Vulcan. The amount of ca. 1.9 µmol CO_2 is slightly less than the total amount of Sn in the catalyst (3 µmol; but of course not all Sn is at the surface) and hence implies the location of these by-products on the tin component (probably on the SnO_x patches). These results strongly suggest, that an accumulation of by-products is responsible for the observed deactivation by blocking the oxygen adsorption on the Sn / SnO_x sites. But this deactivation model obviously only holds true for the easily reversible part of the activity loss, since according to our CO_2-TPD at a purging temperature of 170°C (see fig. III-31) the major part of the by-products should have been removed. Hence, the more irreversible rest of deactivation must be attributed to other reasons.

Consequently, the rather moderate deactivation in a hydrogen-rich gas compared to the CO oxidation in pure N_2 is traced back to a less pronounced accumulation of by-products (*e. g.*, by a faster decomposition in idealized reformate), but without further experimental data it is difficult to speculate for reasons.

The deactivation part, which is reverted only at temperatures close to the initial formation temperature (at 270°C), may indeed be caused by a superposed segregation effect, as was inferred by the DRIFTS experiment. Only at very high temperatures the surface composition is restored closely to the state of the freshly conditioned catalyst.

Very similar conclusions were reached in a study by Hoflund *et al.* on a Pt/SnO_x/SiO_2 catalyst, where the largest part of the observed deactivation could be reverted by heating or exposing the sample to vacuum, which was accompanied by the evolution of CO_2 and therefore attributed to the accumulation of carbonates during reaction [176]. Yet a portion of the decay remained irreversible, which they attributed to changes in the surface morphology / composition.

Finally it should be noted that this section of course was based only on a very limited set of data, since the Pt_3Sn/Vulcan catalyst is hardly accessible by DRIFTS. Hence the developed model should be considered only as a suggestion. Additional methods (*e. g., in-situ* XRD, XAFS) are required in order to ultimately confirm or refute our proposal and are currently employed on our catalysts. The results will be published later.

2.2.2 Performance in more realistic reformates

At the beginning of this section we will first investigate the effect of the addition of water only to our idealized reformate on the performance of our Pt_3Sn/Vulcan catalyst, before we proceed to more realistic reformate mixtures, where the balance nitrogen has been replaced by CO_2.

In figure III-35 two long-term measurements in idealized reformate are shown (1 kPa CO, $\lambda = 2$; 80°C), one in a dry gas mixture and the other with 1.3 kPa water added. The initial activity is slightly enhanced in the wet mixture, but this effect diminishes with proceeding time on-

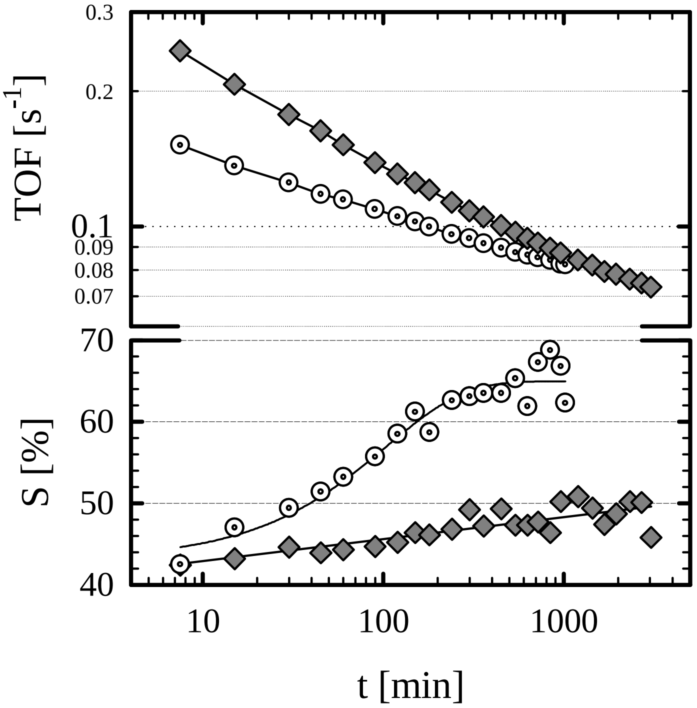

Figure III-35: Activity (*upper window*) and selectivity (*lower window*) over Pt_3Sn/Vulcan in idealized reformate (1 kPa CO, $\lambda = 2$) in idealized reformate at 80°C: dry (⊙) and with 1.3 kPa H_2O added (◆).

stream. In analogy to Pt/γ-Al_2O_3 (see chapter III-1.2.2) we attribute the enhancement to an extensive by-product formation (probably on the tin component, most likely on SnO_x-patches) in the wet gas mixture. The latter enables the CO_{ad} to spread on a larger area and in turn causes a more disordered surface layer with a somewhat lower local coverage on the platinum component, hence allowing more oxygen (and hydrogen) to adsorb. An additional contribution may arise form the dissociative adsorption of water on the Sn / SnO_x, which, after a subsequent spill-over of hydrogen to the platinum, would lead to a slightly reduced adsorption energy of CO due to the displacement of CO from on-top to bridge sites by coadsorbed H_{ad}, as was shown in section III-1.1.5 for Pt/γ-Al_2O_3. An analogous enhancement of the CO oxidation rate (without presence of H_2) by water (2.8 kPa) of even one order of magnitude has been observed in earlier studies by Croft *et al.* over a Pd/SnO_2 sample (5 kPa CO, $\lambda = 8$; 60°C) [225].

At prolonged reaction time, the H_2O induced enhancement is constantly reduced, probably a saturation effect, resulting from the limited number of tin (oxide) sites available for the by-products formation. Indeed, CO_2-TPD measurements on Pt_3Sn/Vulcan, which were conducted after PROX reaction in idealized reformate in order to confirm the formation of by-products, revealed exactly the same quantity of CO_2 after ~12 hours (see preceeding section) and after

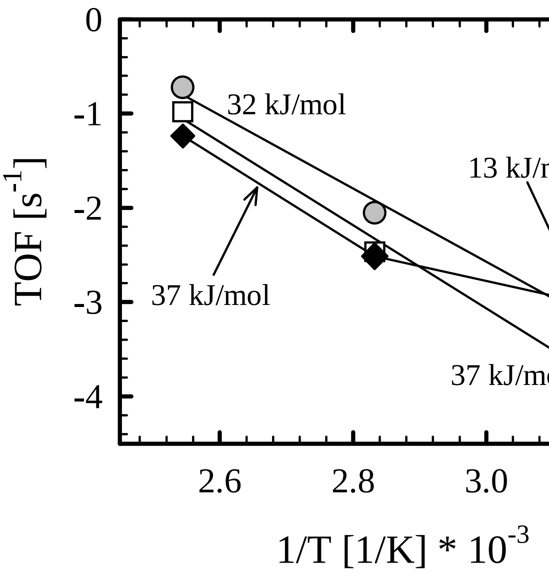

Figure III-36: Arrhenius diagram for the turnover frequency of the CO oxidation over Pt_3Sn/Vulcan in idealized reformate (●; 1 kPa CO, $\lambda = 2$), a mixture containing 25 kPa CO_2 (□), and in a more realistic reformate (◆; 25 kPa CO_2; 1.3 kPa H_2O).

~60 hours of reaction (not shown for brevity), respectively, which strongly supports the idea of a saturation effect.

The time-evolution of selectivity resembles also very closely the observations on the Pt/γ-Al_2O_3 catalyst (chapter III-1.2.1). It increases slowly with time on-stream, due to a tighter CO_{ad}-layer, which blocks the hydrogen adsorption (but this time not the oxygen adsorption on the bimetallic metal!). Again in the wet mixture the selectivity is significantly lower (up to 15% with 1.3 kPa H_2O), but other than on Pt/γ-Al_2O_3 on Pt_3Sn/Vulcan this effect cannot be related to an enhanced / stabilized conversion rate (after ~1000 min.). The fact that (at advanced reaction time) solely the hydrogen and not the CO oxidation rate is affected, shows that the equilibrium suface coverage on the Pt has not been altered. This in turn implies, that the presence of water (probably in the form of OH-groups) catalyzes a second $H_2 + O_2$ reaction pathway on the support material or at the Pt-SnO_x interface, as will be essentially shown in the following context (compare also fig. III-37).

The kinetic effects on the CO oxidation reaction arising from a replacement of the balance nitrogen in the idealized reformate (1 kPa CO, $\lambda = 2$) by CO_2 are shown in figure III-36 (data taken after 90 min.; each set of temperatures was measured on a new catalyst bed). The rates are slightly reduced in a CO_2-containing mixture, but the effect is very small (decrease by 25 -

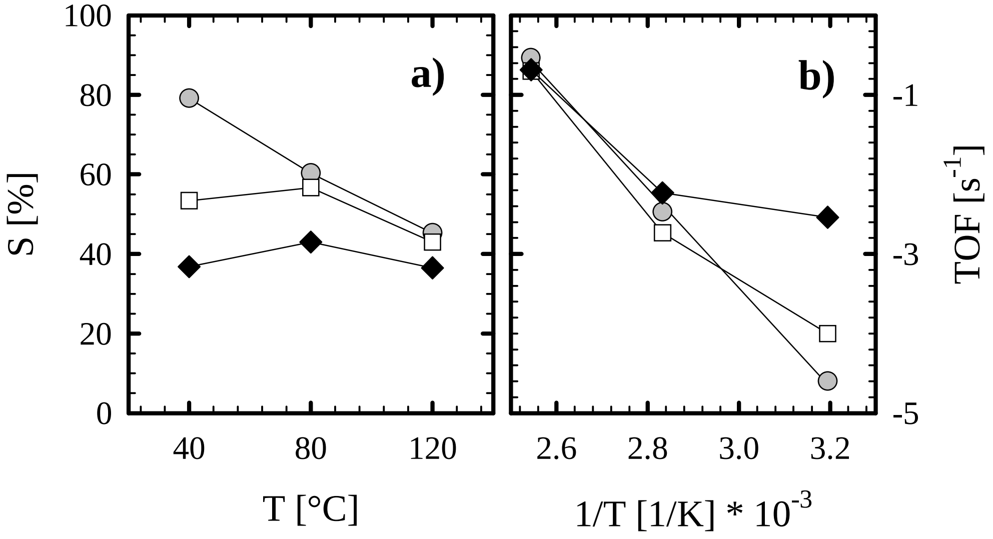

Figure III-37: (a) Selectivity and (b) Arrhenius diagram for the calculated turnover frequency of the H_2 oxidation over Pt_3Sn/Vulcan in idealized reformate (● ; 1 kPa CO, $\lambda = 2$), a mixture containing 25 kPa CO_2 (☐), and in a more realistic reformate (◆; 25 kPa CO_2; 1.3 kPa H_2O).

40%). Consequently the activation energy of 32 ± 6 kJ/mol in idealized reformate remains quite constant for the CO_2-containing mixture (37 ± 6 kJ/mol).

This result was surprising, since Arana *et al.* noticed a complete inhibition of the CO oxidation in a pure argon matrix (16 kPa CO; $\lambda = 1$; 25°C) in the presence of 32 kPa CO_2 for their $PtSn/SiO_2$ catalyst [171]. They suggested a site blocking of CO by CO_2, which, *e. g.*, lead in their infrared experiments to a significant intensity reduction of the CO_{ad}-band after the previous adsorption of CO_2 [229]. Likewise, Hoflund and co-workes mention a negative influence of 8 kPa CO_2 on the performance of their $Pt/SnO_x/SiO_2$ catalyst (1 kPa CO, $\lambda = 1$; 35 and 55°C, resp.) [176, 230]. At the moment we are not able to explain the discrepancy to our measurement, but it is interesting to note that in the same study from Arana *et al.* a $PdSn/SiO_2$ sample also showed no effect at all upon the addition of up to 48 kPa CO_2, which would resemble the behaviour of our Pt_3Sn/Vulcan catalyst much more closely [171].

The additional presence of 1.3 kPa water in the CO_2-containing reformate showed virtually no effect for 80 and 120°C, respectively. But at 40°C the activity is significantly enhanced (~ factor 2), which results in a strongly decreasing activation energy at lower temperatures, getting smaller than 13 kJ/mol. This probably indicates a change in the reaction mechanism at low temperatures in a wet atmosphere. We could think, *e. g.*, of a second pathway, becoming dominant for these conditions, which involves support OH-groups as oxidizing agents as was

Catalyst	**$r^{PROX\ 1)}$ [mol_{CO}/g_{Met}*s]**	**r^{Shift} at 150°C $^{2)}$ [mol_{CO}/g_{Met}*s]**	**$^{PROX}/_{Shift}$ ratio**
Pt/γ-Al_2O_3	$1.9*10^{-4}$	$2.8*10^{-6}$	70
Pt/Vulcan	$9.1*10^{-6\ 4)}$	$8.3*10^{-8\ 3)}$	110
Pt_3Sn/Vulcan	$2.3*10^{-4}$	$4.7*10^{-10\ 3)}$	49000

1) after 2 hours on-stream at 80°C (Pt_3Sn/Vulcan) and 150°C (pur Pt catalysts), resp.

2) after 30 min. at 80°C (PtSn) and 150°C (Pt), resp. *3*) extrapolated

4) after 1000 min

Table III-8: Comparison of PROX and reverse WGS activities over Pt_3Sn/Vulcan and pure platinum catalysts.

proposed by Schryer *et al*. for the CO oxidation on their Pt/SnO_x catalyst at temperatures around 80°C [231]. This would be well compatible with our observations.

The hydrogen oxidation reaction (TOFs calculated *via* selectivity in fig. III-37a) follows in principle a similar scheme (fig. III-37b). At 120°C we observe almost identical rates in all three gas mixtures, at 80°C the activity is slightly enhanced for the wet mixture (+65% compared to the dry CO_2-containing mixture) and at 40°C we notice very strong enhancing effects of both CO_2 (+80%) and H_2O (additional factor 4) on the H_2 oxidation. This would again be consistent with a second reaction pathway, which becomes dominant at low temperatures and which is promoted by the presence of CO_2 and especially H_2O.

As a consequence of this „low-temperature“ mechanism the selectivity becomes very poor at 40°C for CO_2-containing mixtures, whereas it is hardly affected at higher temperatures, where the „normal“ CO oxidation mechanism operates (see preceeding chapter). With the additional presence of water this effect is intensified and now applies already to 80°C and explains clearly the very low selectivity values in wet gas mixtures (compare also fig. III-35).

2.2.3 The water-gas shift activitiy of Pt_3Sn/Vulcan

In analogy to our measurements on Pt/γ-Al_2O_3, the reverse water gas-shift activity (eq. III-1.12) over Pt_3Sn/Vulcan, which finally is the decisive factor for the minimum CO concentration achievable at the reactor outlet [11, 12], was tested in an atmosphere as close as possible to a realistic reformate mixture, containing ~74 kPa H_2, ~25 kPa CO_2 and 1.3 kPa H_2O (compare chapter III-1.3.2). Since the Pt_3Sn/Vulcan catalyst had to be diluted in order to avoid diffusion effects, we used SiC this time instead of the α-Al_2O_3, which was usually employed for the PROX measurements, (see also chapter II-1.2), in order to avoid any effects

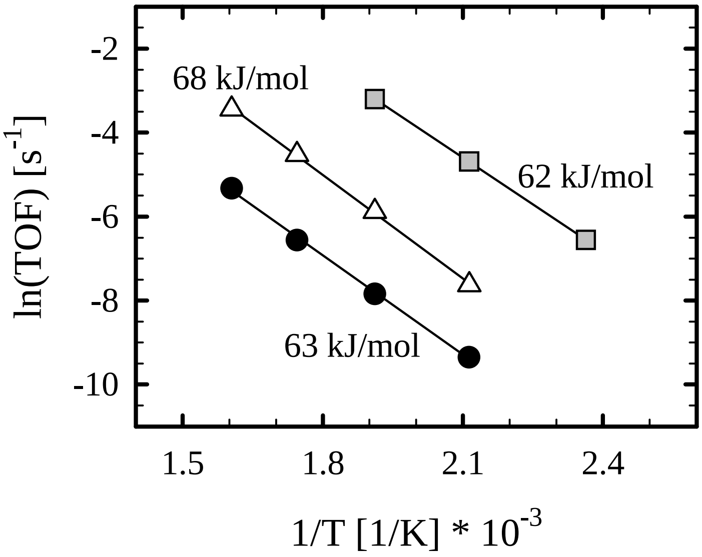

Figure III-38: Arrhenius diagram for the reverse water-gas shift activity over ▨ Pt/γ-Al_2O_3, △ Pt/Vulcan and ● Pt_3Sn/Vulcan (ca. 74 kPa H_2, ca. 25 kPa CO_2, 1.3 kPa H_2O).

due to a mechanically formed interface by the mixing procedure). The same applied to the Pt/Vulcan catalyst, which is used as a comparison in the following.

In figure III-38, the shift activity of Pt_3Sn/Vulcan is compared to that of Pt/γ-Al_2O_3 and Pt/Vulcan in an Arrhenius diagram. The results are also summarized in table III-8. The observed activation energy is close to that of the pure platinum catalysts, which suggests an identical reaction mechanism (*i. e.*, the „regenerative mechanism“, which includes the direct dissociation of CO_2 on the metal surface [157]; eq. III-1.14 and III-1.15). Nevertheless, the absolute TOF on Pt_3Sn/Vulcan is significantly smaller, even when compared to the Pt/Vulcan catalyst (factor 50). This may be rationalized by a „geometric“ effect of the alloyed tin atoms, reducing the number of active Pt-ensembles for the H_2 and probably also CO_2 dissociation, similar to what has been proposed for PtSn surface alloys [185, 217, 218].

When we compare the PROX/shift ratios calculated for the envisaged operation temperatures, 80°C for Pt_3Sn/Vulcan and 150°C for the pure platinum catalysts, we notice an improvement of almost four orders of magnitude for the bimetallic PtSn system (table III-8). Consequently, much higher degrees of purity should be obtained for a reformate cleaned over Pt_3Sn/Vulcan at 80°C than for a conventional platinum catalyst operating at temperatures of 150°C and above, which was indeed demonstrated experimentally by M. Kahlich [25].

2.3 Summary on bimetallic Pt_3Sn catalyst

In the preceeding sections we have seen that the performance of our bimetallic Pt_3Sn/Vulcan catalyst in idealized reformate (1 kPa CO, $\lambda = 2$) is superior compared to that of a commercial Pt/γ-Al_2O_3 system. This was explained by a bifunctional surface, where the oxygen can adsorb also on Sn / SnO_x sites and its supply therefore is not limited by the CO desorption from the platinum metal. Another contribution to its outstanding low-temperature activity arises from an electronic alloying effect, which reduces the CO adsorption energy by ca. 20 kJ/mol, as was shown by our TPD experiment. Unfortunately, this effect causes a significant shift of the on-set temperature for the selectivity decay to much lower temperatures due to a reduced CO coverage, which progressively deviates from the saturation value at increasing temperatures under our conditions. Nevertheless, the selectivity, though steadily decreasing with temperature as a consequence, is remarkably high, with 85% at low temperatures around 0°-20°C and even at 120°C it is with 45% still higher than that of standard Pt catalysts. XPS measurements indicate that under reaction conditions only part of the Sn is reduced, included in PtSn alloy particles, while another part is in an oxidic state, forming SnO_x islands on and presumably also aside the active particles.

Our observation that CO desorption is not rate limiting and that the selectivity decreases with increasing temperature, are consistent with a mechanistic model involving separation of the reactant adsorption sites (bifunctional surface), with competing CO and hydrogen adsorption on Pt sites/areas and oxygen adsorption predominantly on SnO_x islands on/adjacent to the active PtSn particles. The reaction takes place at the perimeter of these islands or by invoking a spill-over process. Due to the possibility of oxygen adsorption also at high CO coverages CO desorption is not rate limiting, as evidenced by the very different barriers for these processes, while hydrogen adsorption on the Pt sites/areas is effectively inhibited by the CO adlayer.

A small drawback for the commercial employment of Pt_3Sn/Vulcan, is the irreversible activity loss, which could not be recovered completely after purging procedures at the operation temperature level and was traced back to surface segregation effects during reaction. The largest part of the deactivation, however, which we suspected to arise from the accumulation of by-products, was easily reverted, similar to the Pt/γ-Al_2O_3 catalyst.

When we change from idealized reformate to more realistic mixtures, containing CO_2 and / or water, we have seen that at higher temperatures (>80°C) neither CO_2 (25 kPa) nor water (1.3

kPa) exhibit significant effects on the selective CO oxidation. At lower temperatures a second mechanistic pathway for both, the CO and H_2 oxidation reaction, seems to become dominant (probably *via* OH^-groups and carbonate-like intermediates on the SnO_x or at the Pt-SnO_x interface), which is catalyzed by the presence of CO_2 and especially of H_2O and leads to drastically reduced selectivity values. The resulting optimum operation temperature (maximum selectivity) on our Pt_3Sn/Vulcan catalyst in more realistic reformates (for 1 kPa CO and $\lambda = 2$) is therefore around 80°C.

Its excellent performance along with the extremely low reverse water-gas shift activity makes Pt_3Sn/Vulcan a very interesting candidate for the fuel gas purification in low temperature fuel cell technology (PEM-FC).

3. An alternative for the low temperature conversion - Au/α-Fe_2O_3

Gold has long been disregarded for catalytic reactions due to the inert nature of bulk surfaces, caused by a high activation barrier for the dissociative adsorption of molecules like O_2 or H_2 [182, 221, 223, 232, 233]. However, when it is in a highly dispersed state supported on metal oxides it exhibits a surprisingly high activity for several reactions – not only CO oxidation [234],[71, 235-238] but also, *e. g.*, catalytic hydrogenation [72, 233, 239, 240], partial oxidation of hydrocarbons [233, 240, 241], hydrochlorination of ethyne [242] or the NO/CO conversion [233, 240, 241]. According to Haruta and co-workes, gold clusters supported on certain reducible oxides (Fe_2O_3, TiO_2, NiO_x or CoO_x) and on Group II metal-hydroxides ($Mg(OH)_2$, $Be(OH)_2$), respectively, are able to oxidize CO even at temperatures as low as -70°C at reasonable conversion rates [234, 243], which led to first applications in gas sensors, filters or for the recombination in CO_2 lasers [71, 233, 235, 244].

Moreover, since the hydrogen oxidation rate is enhanced to a much smaller extent than the CO oxidation, when compared to pure gold powder [71, 234], these catalysts recently have gained attraction for the preferential oxidation of CO in H_2-rich gas (PROX) [26, 29-31, 240, 244]. The obtained mass-specific reaction rates [$mol_{CO}/(g_{Au}\cdot s)$] on supported Au catalysts are indeed equally high at 80°C, and even lower temperatures, as compared to standard PROX catalysts such as Pt/γ-Al_2O_3 [28, 28, 156] and Ru/γ-Al_2O_3 [245] at their operating temperature of 150° - 200°C [16]. This, in principle, improves the cold-start properties in a fuel cell system [166] and also allows for a thermal (and spatial) integration of the PROX unit with the PEM fuel cell stack in form of a thin second layer placed on top of the anode-side of the membrane electrode assembly (MEA) [155]. Since the efficiency, in particular with respect to the load-following behavior, of the PROX unit critically depends upon the rate of CO back-formation from CO_2 *via* the reverse water-gas shift reaction, a significantly improved performance is expected at low temperatures, where the shift equilibrium becomes more favorable [12].

In our own group, we started with a Au/α-Fe_2O_3 catalyst, which was initially studied extensively for its kinetic properties during selective CO oxidation in idealized reformate (M. Kahlich [12])[25, 26]. In this work it is the priority purpose, to gain mechanistic insights into the (preferential) CO oxidation, in order to explain the kinetic observations (reaction orders, selectivity) as well as the deactivation behaviour or the influence of additional components in the reaction mixture, which are present in a real reformate (H_2, H_2O and CO_2).

Hence, in the first chapter we will turn to the molecular level of the CO oxidation on gold catalysts and show that the support is involved in the reaction for some of the systems. Subsequently we focus closer on the Au/α-Fe_2O_3 catalyst, by investigating the dependence of activity / selectivtiy upon the Au particle size and the detailed properties of the iron oxide support. The third chapter is concerned with the metal CO coverage under reaction conditions and establishes its influence on the selectivity and the reaction order. Thereupon we will examine the long-term stability of our gold catalysts, where the observed deactivation will be related to a poisoning by surface carbonate / carboxylate species, which are produced during the PROX reaction, before we investigate the influence of water and CO_2 on the reactivity / selectivity. In the next chapter we will take a short look onto the water-gas shift reaction and show that the oxidation / shift ratio is much more favourable than, *e. g.*, for the commercially employed Pt/γ-Al_2O_3 system, before we finally compare the activity and selectivity of several gold catalysts supported on various metal oxides, to see, if there are other promising candidates for the envisaged application.

All of the Au catalysts presented in the following chapters were prepared by V. Plzak (ZSW Ulm). The preparation / pretreatment procedures are given in chapter I-2.3.

3.1 Mechanistic insight into the CO oxidation over gold catalysts

3.1.1 A short review

Due to the inability of large bulk surfaces to adsorb oxygen (or hydrogen) dissociatively at temperatures below 200 - 300°C [219, 232, 246], which is traced back to a high dissociation barrier arising from the completely filled d-states of gold [182, 223], the high reactivity of small supported clusters for the CO oxidation is not straight-forward.

There is a general agreement, that the CO is adsorbed on the gold, characterized by an infrared band at ~2110 cm^{-1} (which is not present on pure Fe_2O_3) and that the reaction follows a scheme, where both reactants are adsorbed on the catalyst's surface [26, 71, 186, 236, 247-253]. But many details, especially concerning the oxygen adsorption and activation, are still highly controversial: Where does the oxygen adsorption take place? Is it dissociatively adsorbed or in a molecular form? Where does the reaction take place? Does the reaction proceed directly or *via* intermediate species?

When we start from UHV studies over gold single crystals, we notice that the CO oxidation reaction only takes place readily when atomic oxygen (produced, *e. g.*, from ozone [254] or by a hot filament [220, 246]) is preadsorbed on the metal [220, 255]. But oxygen offered in its molecular form does not adsorb dissociatively over gold single crystal faces up to temperatures of more than 400°C and consequently no reaction occurs [219, 246, 256]. On the other side the activation energy for desorption is quite large, leading to desorption maxima in TPD studies as high as 280°C on Au(111) [120], or 280°C [255] and ~380°C [246] on Au(110), respectively, corresponding to an E^*_{des} between 120 and 160 kJ/mol.

Several models have been proposed in order to explain why small supported gold clusters work for the CO oxidation even at temperatures as low as -70°C, in spite of the inhibited oxygen dissociation. For a better overview the various proposals are visualized in figure III-39.

The first models were based on intermediates adsorbed on the support, which were observed by IR spectroscopy. Knell *et al.* postulated the reaction over a Au/ZrO_2 catalyst to proceed *via* the formation of a formate species ($HCOO^-$), formed by the insertion of CO into support OH-groups, followed by the oxidation to carbonate species (CO_3^{2-}), which finally decompose to give CO_2 [236]. But the presence of formates was solely based on IR bands, which cannot be assigned unambigously, hence this pathway must be considered with some reservation.

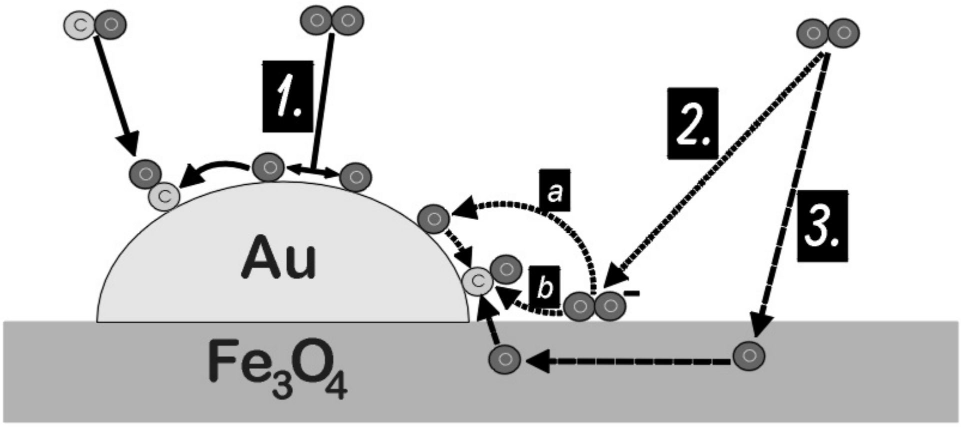

Fig. III-39: Different mechanisms proposed for the CO oxidation over gold supported on reducible metal oxides (here Fe_3O_4, which is the active phase during reaction in simulated reformate for our Au/α-Fe_2O_3 catalysts).

Anyway, we exclude this mechanism for our Au/α-Fe_2O_3 system, since we never detected formate bands during our DRIFTS measurements (Therefore this pathway is not included in fig. III-39). The Haruta group initially proposed a mechanism *via* carbonate-like intermediates, which would form at the metal-support interface from a reaction between CO adsorbed on the gold and oxygen adsorbed on the support (probably in the form of O_2^--species, similar to pathway 2b in fig. III-39). But subsequent studies with isotope labelled oxygen demonstrated that the carbonates (other than the CO_2-product), which were observed over Au/ZnO and Au/TiO_2, predominantly originate from a reaction of CO with (unmarked) support lattice oxygen and not with the atmospheric oxygen offered for the reaction [248, 257]. Therefore, in the more recent papers Haruta and co-workers distanced themselves from their initial model and assumed, that the latter is just a slow secondary pathway, which is not relevant for the overall oxidation rate [233, 240].

In analogy to the initial „Haruta-model“ most of the recent papers, the majority of which is dealing with Au/TiO_2 systems, propose the adsorption of oxygen to occur on the support [249, 253, 258-260], probably on oxygen vacancies [250], which are abundant on semiconductor materials like TiO_2, Fe_2O_3 or ZnO [261], especially in the proximity of Au clusters due to the formation of a Schottky-junction effect at the interface [262]. Iwasawa and co-workers favour the adsorption to proceed *via* superoxide species (O_2^-; reaction pathway no. 2 in fig III-39), which were observed in ESR measurements, but did not specify, whether these dissociate at the interface to give O_{ad} (pathway no. 2a) or react directly with adsorbed CO (pathway no. 2b; which would probably include a carbonate-like intermediate as in the first „Haruta-model“)

[250, 258]. Fukushima *et al.* and Grunwaldt *et al.* agree in principle with the spatially separated adsorption of the reactands but assume that the oxygen dissociates on the support (producing „lattice oxygen"; pathway no. 3 in fig. III-39) with a subsequent reaction at the interface or after the spill-over of oxygen to the gold metal [249, 260].

Based on infrared measurements on Au/TiO_2 and Au/ZnO, where Boccuzzi *et al.* noticed a significant blue-shift for the CO_{ad}-band when oxygen was admitted to the catalyst (a similar effect was also noticed in our own DRIFTS measurements on $Au/\alpha\text{-}Fe_2O_3$; see chapter III-3.3.2), which implies a spatial proximity of the adsorbed reactants, *i. e.*, both are adsorbed on the gold particles (pathway no. 1 in fig. III-39) [248], the more recent papers from the Haruta-group now assume a direct adsorption of oxygen on the gold clusters (This model was also favored in the recent publications by Valden *et al.* [263, 264]). The oxygen bond cleavage was suspected to be induced either by the formation of a four-center surface complex including CO and O_2 being adsorbed on a common Au site, which would form a labile precusor state [240], or to occur on metal surface defect sites [233]. According to this theory, the role of the support material would be limited to the production of gold particles as small as possible or to promote the appearance of highly reactive gold sites or crystallite faces.

3.1.2 The „support-effect"

First we want to clarify, how the choice of the support material influences the reactivity of a gold catalyst for the CO oxidation. In table III-9 numerous previous studies are evaluated (rates and TOFs are extrapolated to our standard reaction temperature of 80°C) and compared to our own results.

It is evident that relatively high activities can be obtained on any support material (even on pure gold), even on those, which are not explicitly known for exhibiting extensive oxygen adsorption or storage properties at such low temperatures, such as Al_2O_3, MgO, SiO_2 or ZrO_2. Therefore it is a logical consequence that the oxygen adsorption and dissociation must be possible directly on the gold metal for these systems (Corresponding to pathway 1 in fig. III-39).

Nevertheless, there are noticable differences in the reactivity between gold on such „inert" materials and on those catalysts, which are supported on reducible transition metal oxides (Fe_2O_3, TiO_2, and NiO_x). The TOF of the latter seems to be enhanced by up to one order of magnitude. The existence of such a „support effect" was also demonstrated by Tsubota *et al.*, who

catalyst	preparation 1)	Au : Me [at-%]	d_{Au} [nm]	p(CO) [kPa]	$p(O_2)$ [kPa]	r ($*10^4$) [$mol_{CO}/g_{Au}*s$]	TOF 2) [s^{-1}]	E_a [$^{kJ}/_{mol}$]	ref.
Au/α-Fe_2O_3	DP	~1	2.6 - 7	1	1	39 3)	1.3 - 3	29	this work
	DP	~1	2.6 - 7	1	20	74 4)	2.9 - 6.7	-	this work, [26]
	DP	2.0	3.6	0.2 - 6 5)	1 - 20 5)	13	0.7	35	[71]
Au/NiO_x	CP	1.7	4.8	1	1	20	1.3		this work
	CP	2.0		0.5	10	0.4 - 1.2 6,7)			[265]
Au/TiO_x	IMP	1.7	4.6	1	1	33	2.0	21	this work
	IMP 8)	0.4	33	4.9	4.9	8.1	4.5 9)	29	[253]
	DP	1.3	2.9	1	20	33	1.3	27	[233]
	DP 10)	1.8	3	1	20	20 7,11)	0.8		[258, 266]
	DP 10)	1.2	30	1	20	2.0	0.7	12	[258, 267]
	IMP 12)	0.7	2.0 - 2.5	0.25	0.25	0.7 7)	~0.03	~ 25 13)	[256, 268]
Au/$Mg(OH)_2$	CP	1.3	< 4	1	1	14	0.5 - 0.9		this work
	DP	1.5	0.6 - 1.2	1	20	> 51 14)	> 1.2		[269]
Au/Al_2O_3	IMP	1.7	~ 4	1	1	6.3	0.3		this work
	DP	0.2	2.4	1	20	13	0.5	32	[270]
Au/ZrO_2	IMP 12)	1.1	2.0 - 2.5	0.25	0.25	0.12 7)	~ $5*10^{-3}$	~ 25 13)	[256, 268]
Au/SiO_2	CVD	2.1	6.6	1	20	1.3	0.1	17	[270]
	DP 15)	0.6	30	4.9	4.8	0.08	0.04	15	[237]
Au powder	-	100	20	1	20	~ 0.001 7)	~ $3*10^{-4}$	~ 20 13)	[71, 234]
Au sponge	-	100		5	5	0.006		2.1	[271]

1) DP = deposition-precipitation, CP = coprecipitation, IMP = impregnation, CVD = chemical vapor deposition 2) spherical particles assumed, except where reported other
3) statistical average of DP-catalysts in table III-10 4) calculated *via* O_2 reaction order of 0.27 [26] 5) reported reaction orders were zero
6) extrapolated from $r = 1.5*10^{-5}$ $mol/g_{Au}*s$ at 20° with $15 < Ea < 30$ kJ/mol 7) measured at high conversion 8) pre-reduced at 200°C in H_2 after calcination
9) ca. 2.3 s^{-1}, when calculated for 1 kPa CO and $\lambda = 2$ with the reported reaction orders of 0.5 (CO) and 0.08 (O_2) at 30°C 10) with phosphine-stabilized Au complex
11) extrapolated from $r = 9.6*10^{-3}$ $mol/g_{Au}*s$ at 28°C with $E_a = 12$ kJ/mol 12) gold colloids 13) activation energy estimated from conversion data
14) extrapolated from $r = 1.2*10^{-4}$ $mol/g_{Au}*s$ at -70°C with $E_a > 15$ kJ/mol 15) pre-reduced at 450°

Table III-9: Comparison of kinetic data on Au catalysts with values calculated from literature studies (extrapolated to 80°C).

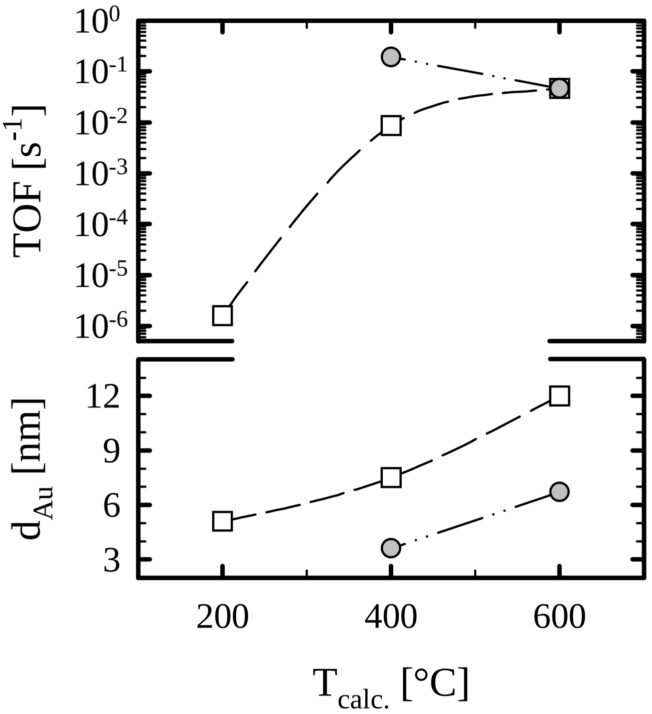

Figure III-40: TOFs (*upper window*) and Au particle diameters (*lower window*) of Au-TiO_2-samples (1 kPa CO, λ = 40, 0°C) *vs* calcination temperature: □ physical mixture of Au-colloid and TiO_2 powder, ● Au/TiO_2 prepared by deposition-precipitation method [272].

mechanically mixed Au-colloids with TiO_2 and noticed an increasing activity at increasing calcination temperature (although the gold particles were sintering rapidly!), caused by the progressing development of the reactive metal-support interface ([272]; see figure III-40). Whereas after calcination at 200°C the TOF of the mixture was very low – similar to pure Au powder –, it matched the initially superior reactivity of a conventionally prepared (DP) Au/TiO_2 catalyst after calcination at 600°C. The enhancing effect of titania for the CO oxidation can be also inferred from catalyst samples prepared by Grunwaldt *et al*. (see table III-9), where the TOF of the titania supported sample is one order of magnitude higher than the one on zirconia [256, 268] (The generally much lower TOFs in their study are likely to be caused by the low calcination temperature for the colloid precursors, so that the reactive interface has not been developed fully yet, as was proposed by Feldmeyer *et al.* [273]). Likewise, Bollinger and Vannice demonstrated, that a subsequently added titania coating increases the reactivity of a gold powder considerably [253].

If we take a closer look, we find another interesting difference between the two groups. For „inert“ support materials the activity of the catalyst seems to depend very critically upon the

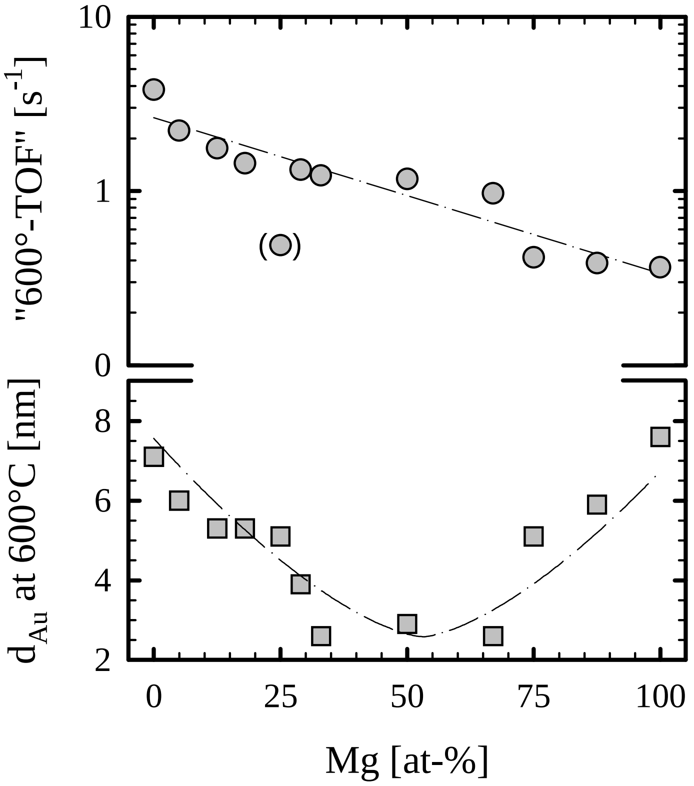

Figure III-41: Au particle size (*lower window*) at 600°C and activity (*upper window*) in idealized reformate (1 kPa CO, λ = 2; 80°C), normed to the dispersion calculated for 600°C, on Au/Fe_2O_3*MgO mixed-oxide-support catalysts.

particle diameter of the gold crystallytes and only extremely small particles yield highly active samples. This illustrates, why our own catalysts (Au/γ-Al_2O_3 and Au/$Mg(OH)_2$) are slightly less reactive than those in the previous studies. It is worth noticing, that a higher conditioning temperature (400°C instead of 300°C, *i. e.*, the „Au/MgO“-sample) consequently lead to a reduced TOF on our Au/$Mg(OH)_2$ catalyst (see chapter III-3.7). This dependence of catalysts with „inert“ support was also observed by Okumura *et al.* for Au/SiO_2, where a sample with 20 nm particles showed no measurable activity [270], as well as by Cunningham *et al.* for the Au/MgO system [269]. It may be speculated, if the small clusters simply feature more reactive defect sites (edge, kink or step sites) [43] or if a gradual change in the electronic structure with decreasing size is responsible for the high reactivity as was suspected, *e. g.*, in the studies by Valden *et al.* [263, 264] and Cunningham *et al.* [269].

In contrast, the size of the metal component seems to play only a minor role, when an „active“ oxide like TiO_2 is used. From the references cited in table III-9, it is obvious, that even gold particles as large as 30 nm still exhibit a surprisingly large reactivity. This effect was confirmed for conventionally prepared Au/TiO_2 catalysts by Bollinger and Vannice, who noticed equally high TOFs for 33 and 4.5 nm particles [253], as well as by Iwasawa and co-workers for their samples (30 *vs* 3 nm), produced from phosphine-stabilized precursors ([258] and references therein). Although we did not cover such a large range of particle sizes with our Au/α-Fe_2O_3 catalysts (∅ between 2.8 and 11 nm), the same tendency applies, since all samples exhibit a similar high TOF within ± 50% (see following chapter). But, as will be shown later on, the microscopic structure of the interface plays a crucial role for the overall activity of the catalyst.

In order to demonstrate that similar enhancing effects can be expected for iron oxide, a catalyst with a mixed support, MgO*Fe_2O_3, in varying compositions was prepared (ZSW Ulm; preparation by coprecipitation - the exact parameters are not listed here for the observance of secrecy because of patent applications). The reactivity, which is calculated from the rate in idealized reformate after calcination at 400°C (1 kPa, $\lambda = 2$; 80°C) and this time normalized to the number of surface atoms after calcination at 600°C (presumed that the sintering behaviour is similar for all support compostions, the particle growth at the higher temperature level allows for a much preciser size determination by XRD; $d_{Au} \sim \pm 1$ nm) is displayed in figure III-41 (upper window) along with the measured size of the gold particles (lower window). The growth of the support material particles during calcination directly governs the sintering of the attached gold clusters [274]. For the mid-range of the „Mg-concentration“ MgO and Fe_2O_3 form a non-stochiometric hydrotalcite-like precursor, namely Pyroaurite ($Mg_{6-x}Fe_{2+x}CO_3(OH)_{16}*4.5H_2O$) [275], which incorporates the gold in its layer structure (spacing 2.3 nm [276]) after preparation. Therefore the gold precursor is fixed during the thermal reduction of AuO_x to Au^0 (> 350°C; TGA results by V. Plzak; to be published later), which obviously causes the production of very small gold particles for the freshly conditioned samples in the mid-range of „Mg-concentrations“. On the „Mg-rich“ side as well as on the „Fe-rich“ side the sintering is increasingly governed by the growth of the pure oxide components, resulting in larger gold particles. The determined reactivity for the „Mg-rich“ catalysts (> 50-60% MgO) indeed decreases with increasing particle size, as would be expected from the above context (The lines included in fig. III-41 are just to guide the eye and do not intend to imply any calculated dependencies). But in the the opposite direction with increasing amounts of Fe_2O_3, the activity is even enhanced in spite of the growing Au cluster size, demonstrating that the iron oxide support also enhances the reactivity of attached gold particles as was shown above for TiO_2 (The sample with 25% MgO yielded a somewhat too low activity - probably a consequence of a non-uniform gold distribution, with the major part attached to the magnesia, which is indicated by a very strong deactivation during time on-stream, typical for pure Au/MgO catalysts).

Hence it seems that for gold catalysts based on these transition metal oxides (TiO_2 and Fe_2O_3, probably also NiO_x), the support ensures the oxygen supply for the reaction and that the direct dissociative adsorption on the gold particles is no longer the limiting factor. The following transient response experiments were conducted in order to elucidate this oxygen supplying role of the iron oxide support further.

3.1.3 Oxygen supply from the FeO_x-support (Transient response measurements)

In order to investigate the reaction mechanism over Pt/SnO_x, another system which shows a high low-temperature activity for the CO oxidation, Grass and Lintz performed titration experiments with one of the reactants, either CO or O being preadsorbed on the catalysts surface [177]. Whereas they observed a sharp CO_2 peak when the CO was predosed (t_{max} at 0.6 min. and FWHM = 0.5 min.), the resulting response was much slower (t_{max} at 1.5 min.), very broad (FWHM = 1.5 min.) and the signal decayed with a pronounced tailing over 2 - 3 h with preadsorbed O_{ad}. The observed difference was interpreted in terms of CO_{ad} being adsorbed on the platinum metal, which would react very fast with the incoming oxygen. On the contrary, the predosed oxygen is also adsorbed (dissociatively) on the support oxide and its slow diffusion to the reaction sites (on the platinum or at the interface) causes the retarded reaction to CO_2.

In the following we present similar CO-Titration experiments with and without preadsorbed oxygen on our $Au/\alpha\text{-}Fe_2O_3$ system (sample no. 051198; see table III-10) at 80°C and compare the result to a commercial $Pt/\gamma\text{-}Al_2O_3$ catalyst (at 150°C, so that the TOFs in idealized reformate are of a similar order of magnitude), where it is known that the oxygen adsorbs exclusively on the metal surface, as well as to a pure $\alpha\text{-}Fe_2O_3$ support. From these titration experiments we will not only gain qualitative information, if there are any differences in the time scale for the CO_2 evolution, but we will also be able to roughly quantify the amount of reactive, preadsorbed oxygen. Prior to the experiment the catalysts were conditioned as usual (see chapter II-2.3). For the $Pt/\gamma\text{-}Al_2O_3$ the reactor (containing ca. 2.76 µmol Pt) was cooled down to 150°C, then saturated with 10 kPa O_2 in N_2 for 10 min. (20 Nml/min) and purged with nitrogen (20 Nml/min) for ca. 5 min. in order to remove the residual gas-phase O_2. Subsequently, a stream of 2 kPa CO in N_2 (10 Nml) was admitted and the resulting response

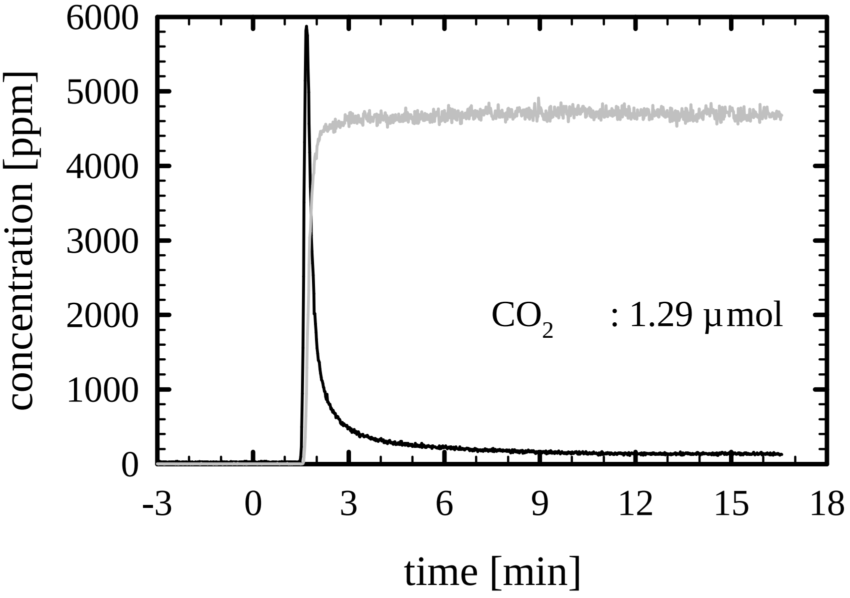

Figure III-42: CO_2-response (——) over Pt/γ-Al_2O_3 (ca. 1.2 µmol surface metal) upon reaction of predosed oxygen at 150°C with 2 kPa CO (——; *0.25) in N_2 at a flow of 10 Nml/min.

recorded by IMR-MS (ion molecule reaction mass spectrometer) on-line analysis, which allows for the selective detection of CO in a nitrogen containing background. The resulting CO_2 peak (See figure III-42) shows its maximum at 1.67 min. and is quite sharp (FWHM = 0.26 min.) as would be expected for a fast reaction. The calculated amount of adsorbed oxygen is ~1.3 µmol, which corresponds fairly good to the number of surface metal atoms (ca. 1.2 µmol). The small excess may be atributed to the formation subsurface oxygen species [277] (The off-set in the baseline after admission of the CO is caused by CO_2- and O_2-impurities in the feedstream and was corrected for integration).

For comparison the pure support, α-Fe_2O_3 (ca. 18 µmol Fe), was calcined at 400°C just like the gold catalysts (30 min. 10 kPa O_2 in N_2 at 20 Nml/min) and after cooling down in pure nitrogen titrated with 2 kPa CO in N_2 at our standard reaction temperature of 80°C (figure III-43, window a). Indeed a small fraction of surface lattice oxygen reacts after a while ($t_{max} \approx$ 12.3 min.; FWHM ≈ 6 min.), corresponding to a partial conversion (ca. 17%) of the α-Fe_2O_3 to Fe_3O_4, which is also the stable iron oxide phase formed during the PROX reaction in H_2-rich gas (determined by TGA; ZSW Ulm). After a subsequent pre-adsorption of oxygen at 80°C no further CO_2-evolution could be detected upon switching to the CO-mixture, demonstrating that the Fe_3O_4-phase was not re-oxidized at this temperature level (not shown here for brevity).

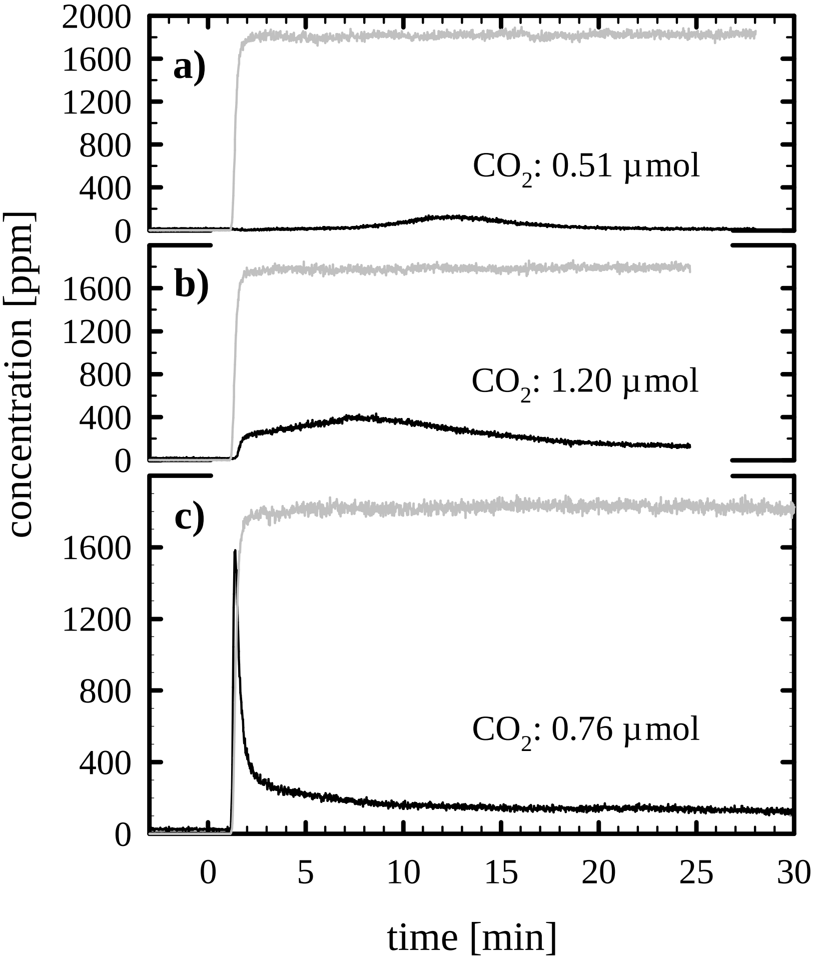

Figure III-43: CO_2-response (——) at 80°C to a flow of 10 Nml/min of 2 kPa CO (——; *0.1) in N_2: *a)* on pure α-Fe_2O_3 after calcination at 400°C and pre-dosing oxygen at 80°C, *b)* on Au/α-Fe_2O_3 (no. 051198; 0.25 µmol total metal) after calcination at 400°C and *c)* after subsequent predosing oxygen on the partly reduced "Au/Fe_3O_4" at 80°C.

The identical sequence was repeated on the Au/α-Fe_2O_3 catalyst (ca. 17 µmol Fe and 0.25 µmol Au). After calcination the catalyst was cooled down to 80°C in N_2 and then the CO/N_2-mixture admitted to the reactor (window b). As for the pure support we observe a rather broad CO_2 response, but this time the production increases very fast (after ca. 1.7 min.) and shows its maximum already at ~7.5 min. along with a pronounced tailing (FWHM ca. 10 min.). The calculated amount of reactive oxygen is also much larger (corresponding to ca. 43% conversion of α-Fe_2O_3 to Fe_3O_4). It seems, that the presence of gold clusters accelerates the reduction of the α-Fe_2O_3 support, probably due to the additional CO adsorption on the gold component.

On this partially reduced catalyst („Au/Fe_3O_4“), which should be rather close to the „real“ state during PROX reaction, we pre-adsorbed oxygen (at 80°C; 20 Nml of 10 kPa O_2 in N_2 for 10 min.) and after purging with nitrogen switched again to the CO-mixture (window c). This time we observe an extremely sharp peak (t_{max} = 1.38 min; FWHM = 0.38 min.), very similar to the reaction on the $Pt/\gamma\text{-}Al_2O_3$ catalyst (even slightly faster) and no further slowly reacting oxygen species as on the freshly conditioned sample are found, which was already expected from the lacking reaction on the pure support. This titration sequence could be duplicatd repeatedly after the renewed preadsorption of oxygen, even when simulated reformate was admitted to the reactor in the meantime in order to fully establish the steady state of the catalyst. From its extremely high reaction rate, we infer, that this oxygen, which is believed to be the active species for the CO oxidation, is not a „normal“ lattice oxygen (O^{2-}), as would be characteristic for a reaction sequence including oxygen dissociation on the support and the subsequent transport to the gold interface by the oxide (scheme no. 3 in fig. III-39). Due to the large amount (ca. 3 times more oxygen than Au atoms are available), it cannot be solely adsorbed on gold sites but must be necessarily located (at least the major part of it) on the support.

We think, that superoxide species (O_2^-), as were observed by Liu *et al.* on their Au/TiO_2 during reaction by ESR measurements, would indeed serve as a good explanation for the fast reaction (= high mobility) of the pre-adsorbed oxygen as well as for the large amount [250]. As a result of these step-response experiments, we believe that pathway no. 2 (fig. III-39) describes best the oxygen adsorption over $Au/\alpha\text{-}Fe_2O_3$ and that the enhancing effect of the support originates from this additional oxygen reservoir on the metal oxide.

Perhaps an even more elegant way to distinguish between the different kinds of oxygen adsorption (and diffusion) would be monitoring the CO_2-response after pulsing isotopically labelled oxygen ($^{36}O_2$) during the CO oxidation in idealized reformate, which would undoubted guarantee the correct steady state of the support material. We tried to realize this experiment in a TAP reactor (temporary analysis of products; see, *e. g.*, ref. [67]), but unfortunately, it did not yield clear results due to the extremely strong readsorption of the CO_2-product on the support material, leading to an enormous broadening of the observed response signal. Nevertheless, a few other aspects from this experiment are worth noticing. First, no isotopic scrambling of oxygen,

$$^{36}O_2 + {}^{32}O_2 \leftrightarrow 2\,{}^{34}O_2 \qquad \text{(III-3.1)},$$

was observed at our reaction temperature between 76 and 99°C, which fully parallels the findings of Liu *et al.* on Au/TiO_2 [250]. This is a further hint, that the oxygen either does not dissociate immediately after adsorption (corresponding to the existence of O_2^- species) and / or that the desorption step after dissociation is governed by a high energy barrier (as would be characteristic for O_{ad} on the gold metal). Second, no doubly marked product, $C^{18}O^{18}O$, was observed. This is in in strong contrast to the experiments of Boccuzzi *et al.* over Au/ZnO and Au/TiO_2, who noticed the appearance of all possible products, $C^{16}O^{16}O$, $C^{16}O^{18}O$, $C^{18}O^{18}O$ and even $C^{18}O$, upon reaction of $C^{16}O$ with ${}^{36}O_2$ at room temperature [248, 257]. But due to the strong interaction of CO_2 with our support, which was noticed during our TAP experiments, we attribute this scrambling to the readsorption on the support, followed by oxygen exchange, which for CO_2 occurs very fast according to Liu *et al.* [250]. For our own experimental setup, subsequent reactions of the product are of minor importance due to the extremely small contact times in the TAP reactor, which clearly explains the difference in the results. But the fact that no doubly marked CO_2 is observed, now rules out any reaction pathway, which includes the direct reaction between molecular oxygen species and CO *via* a carbonate-like intermediate (or transition state):

e. g., $C^{16}O + {}^{36}O_2^{-} + e^{-} \leftrightarrow [$ 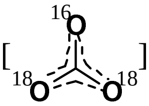 $]^{2-}$ (III-3.2)

For such a carbonate-like molecule the cleavage of each oxygen bond in the following decomposition step, to give CO_2, should have the same probability, which as a consequence would lead to the formation of 33% doubly marked CO_2. Therefore, from the missing appearance of the latter product, we infer a reaction pathway, where the superoxide molecules dissociate at the metal-support interface in a first step, probably followed by the subsequent spill-over to the gold, corresponding to reaction scheme no. 2a in fig III-39. The presence of O_{ad} on the gold is also indicated by our DRIFTS measurements, where we noticed a significant blue-shift (8 cm^{-1}) for pre-adsorbed CO upon the admission of oxygen to the cell (see chapter III-3.3.2), which was also observed by other workgroups [43, 248]. Iwasawa and co-workers did not notice such a IR shift, however, their IR spectras were rather diffuse and therefore a change would be rather difficult to recognize [278].

3.1.4 Proposed reaction scheme

From the preceeding context along with a few other hints we may draw the following picture for the CO oxidation over supported gold catalysts:

- The reaction takes place between CO_{ad} and O_{ad} on the gold surface. This is also mirrored by the very similar activation energies on the various support materials as well as for the reaction of pre-adsorbed CO with atomic oxygen on a Au(110) single crystal (38 kJ/mol) [279].

- With „inert“ support materials, such as SiO_2, Al_2O_3 or MgO also highly active gold catalysts can be prepared, but only, if the gold is in an extremely high dispersed state. For these systems the oxygen adsorption probably occurs directly on the gold clusters, either on defect sites (steps, edges, kinks) or facilitated by variations in the electronic structure of small metal particles. These catalysts show a strong dependence on the metal particle size and loose their activity soon with increasing diameters of the gold particles. The additional role of residual impurities from preparation, which would show a much stronger impact for small clusters, should also be taken into consideration.

- Some transition metal oxides (FeO_x, TiO_x, NiO_x) enhance the reactivity of the gold particles significantly by supplying the oxygen, necessary for the CO oxidation. This leads to a relative independence of the turnover frequency from the gold particle diameter (see also next chapter), but makes the performance very sensitive upon the microcrystalline structure of the metal-support interface. The latter explains, why the activity of such systems, often depends crucially upon the pretreatment method (see, *e. g.*, [237, 280]). Of course, the argument for a constant TOF should only holds true for low metal loadings, where the gold particles are sufficiently distant from each other and the oxygen supply rate is not rate-limiting.

- The oxygen adsorbs in large quantities on these „active“ support materials in the form of a superoxide (O_2^-) species, which possess a sufficiently high mobility so that the diffusion to the gold particles is not the rate-limiting step. Liu *et al*. proposed the adsorption on oxygen vacancies [250], which should be abundant numerously in the vicinity of the gold clusters, due to the Schottky junction effect between the gold and the n-semiconducting support materials [262]. For the reaction it dissociates probably at the metal-support interface to produce O_{ad}, adsorbed on the gold. Therefore, these superoxide species may be designated as a precursor species for the dissociative adsorption on catalyst’s surface. However, a reaction scheme including the oxidation with molecular oxygen species cannot be ruled out if other transition states than the carbonate-like type are assumed and which would not give rise to isotopic scrambling.

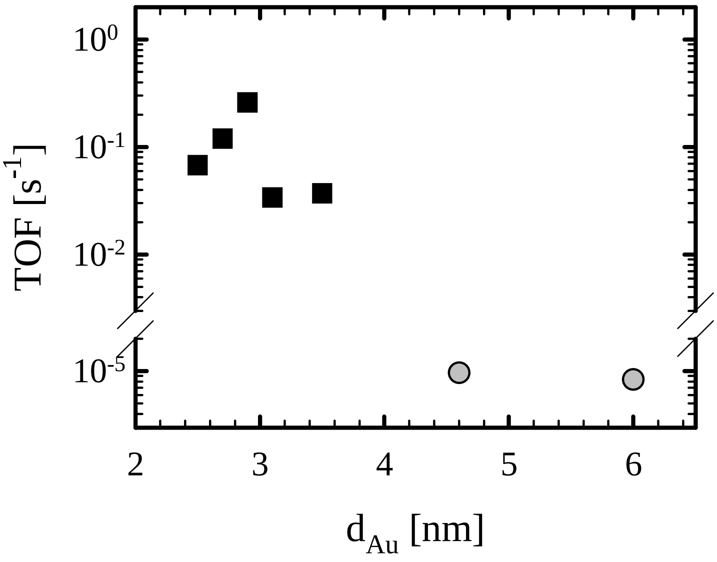

Fig. III-44: Turnover frequency of the CO oxidation on several Au/TiO_2 catalyst samples at room temperature (1 kPa CO in air) as a funcition of the Au particle diameter according to Haruta [240]: Preparation by deposition-precipitation (■) and by photodeposition(●).

3.2 The influence of structural parameters on the activity / selectivity

There is an ongoing debate about the influence of morphological parameters (especially of the Au cluster size, but also concerning the support particle size or the predominant support crystal phase) of gold catalysts on the reactivity of those systems (see, *e. g.*, [258] and references therein). Hence, within this chapter, we will first summarize the measured properties of our different Au/α-Fe_2O_3 samples and try to derivate regularities, which relate the activity and selectivity to structural parameters. Subsequently, the influence of different conditioning temperatures will be evaluated. The final section focusses on the role of residual impurites (especially of sodium), left from the preparation procedure.

3.2.1 The dependence of the activity on the particle size

Whereas in former publications based on the early work of the Haruta group (see [71] and references therein) an inverse proportional relationship between the TOF and the Au particle size (in the range of 2 - 15 nm) was assumed, Valden *et al.* proposed in a recent study, that for particle sizes below 2.5 - 3 nm the activity decreases due to increasing non-metal characteristics [263, 264] (It should be mentioned that there exist some contradictory studies, where it was shown that the characteristics remain almost unchanged for gold clusters sizes above ~15 atoms [281]). For illustration, the turnover frequencies for the CO oxidation on several Au/TiO_2 catalysts observed by the Haruta group are presented as a function of the Au particle size in figure III-44(data taken from [240]). The maximum acitvity was observed for particles which are little less then 3 nm. At smaller (down to 2.5 nm) and larger (up to 3.5 nm) diameters the measured activity was by about one order of magnitude less. Finally, with a more strongly increased particle size (up to 6 nm) the activity dropped by several orders of magnitude. But one should be aware that the latter samples were prepared by a different method (named „photodeposition“) so that not only the particle size but also the form of the Au crystallites and the nature of the Au-Fe-interface may have changed which can lead to drastic changes in the reactivity [71]. A similar activity dependence was obtained by Valden *et al*. on planar Au/TiO_2 model systems leading to a slight difference in reactivity by a factor of three when comparing Au particles of 6 and 3 nm. Hence, within this section we will, after summing up the characteristics for a major part of the samples, try to find out, whether equivalent correlations between the morphology of our Au/α-Fe_2O_3 catalysts and their activity or selectivity may be drawn.

In table III-10-A the preparation methods and some characteristic parameters (Au loading, BET, predominant FeO_x-phases in the dried precursor at 80°C and the TEM-results) of the freshly conditioned (400°C, 30 min synthetic air) catalysts are summarized. Table III-10-B provides an overview on the Au-particle sizes determinded by XRD after conditioning at 400 and 600°C, respectively, the sodium content after preparation and the results of our activity tests in idealized reformate (1 kPa CO, $\lambda = 2$) at 80°C. Unfortunately, especially with very small particles there is a large tolerance for the size determination, because only a small fraction of the Au crystallites is visible in the XRD (The considered fraction is calculated by comparing the Fe_2O_3: Au XRD peak ratios after conditioning at 800°C, where 100% of the Au should be visible, due to the increased particle size, and at 400°C or 600°C, respectively). Such an effect could arise from either an inhomogeneous particle size distribution with a fraction of very small particles or be caused by extremely flat shaped Au crystallites as were observed, *e. g.*, by Blick *et al.* on Au/MgO [282]. Hence the given particle sizes and the calculated turnover frequencies contain a quite large tolerance (maximum deviation ± 50% for the TOF).

With the deposition-precipitation method ($T_{d/p}$ = 80/60 or 60/60°C, pH ca. 7.8 - 8.2; see also chapter II-3.2), used for most of the recent catalyst samples, the smallest achieved average particle size was 2.8 nm (no. 061197), which is comparable to the Au/TiO_2 catalysts prepared

Sample no.	Preparation 1) / T [°C]		Au loading [wt%]	BET after condit. [m²/g]	FeO_x-phases / XRD: HM at 400°C [nm] 2)	TEM: Au at 400°C [nm]	D [%] from TEM
100996	CP / 50 - 60		3.20	61	FH / 13.7		
300996	CP / 50 - 60		2.70	60	FH / 11.9		
201196	CP / 75 - 80		3.15	54	FH + HM / 13.7		
210897	CP / 80	Wet storage for 10h (80°C)	4.55	35	HM + FH / 20.0		
061197	DP / 80 + 60		2.30	63	FH (+HM) / 16.5	2.8 (3.2 3))	49 (37 3))
101297	DP / 80 + 60		2.52	56	FH (+HM) / 16.4	3.3 (3.8 3))	43 (31 3))
260598N	DP / 80 + 60		2.75	74	FH (+HM) / 16.3		
260598K	DP / 80 + 60	Wet storage for 10h (80°C)	2.50	35	HM / 25.8		
280598N	DP / 80 + 60		2.55	47	FH (+HM) / 18.8		
070798	DP / 80 + 60		1.31	46	FH (+HM) / 15.8		
280798	DP / 80 + 60		2.69	40	FH + HM / 17.3		
280798Na		$NaNO_3$-impregnated	2.69		FH + HM / 16.2		
031198	DP / 80	treated with $NaBH_4$ at 20°C	2.43	61	GT (+FH +HM) / 16.1		
051198	CP / 60		3.57	64	FH / 14.0		
100399_W4	DP / 60	four redispersion steps	2.76	46	FH / 14.6		
100399_W2	DP / 60	two redispersion steps	3.30	55	FH / 15.6		
100399_W0	DP / 60	no redispersion step	3.69		FH / 14.0		
120499	CP / 80		3.47		FH (+HM) / 14.9		
110599	CP / 60	pH 8.5	2.71	55	FH / 15.4		
180599	CP / 80		3.90	42	HM + FH / 20.9		
230899	DP 3) / 25 + 60	pH 6.7 + 7.7 - 8.1	3.92	66	GT / 11.2		
230899H		pre-reduced with H_2O_2	3.92		GT / 11.1		

(1): CP = Coprecipitation, DP = Depostion-precipitation (2): precursor phases after drying at 80°C: FH = Ferryhydrite $Fe_5(OH)_8{*}4H_2O$, HM = Hematite α-Fe_2O_3, GT = Goethite α-FeOOH

(3): regarding the particle size distribution (4): Goethite formed by bubbling air through a solution of $FeCl_2$ at room temperature

Table III-10-A: Several Au/α-Fe_2O_3 catalysts prepared by the ZSW Ulm: preparation & characterization (see also section II-2.3)

Sample no.	**XRD: Au at 400°C [nm]**	**XRD-considered Au-fraction at 400°C [%]**	**XRD: Au at 600°C [nm]**	**XRD-considered Au-fraction at 600°C [%]**	**AAS: Na [wt%]**	**rate after 2 h. [$mol_{CO}/g_{Au}*s$] $*10^4$**	**S [%]**
100996	9.2	73	13.0	93	2.08	20	62
300996	6.8	65	11.2	88	3.51	11	
201196	6.4	8	12.3	80	3.66	9.9	65
210897	5.8	23	8.0	51	1.14	6.4	73
061197	< 4		7.5	72	0.02	61	64
101297	4.7	28	7.0	63	0.08	33	63
260598N	4.5	23	9.2	56	0.44	24	62
260598K	11.5	17	11.3	33	0.37	12	68
280598N	7.6	26	10.3	71	0.06	42	60
070798	5.9	18	8.0	65	0.26	33	67
280798	5.6	18	7.5	56	0.03	38	71
280798Na	6.0	19	9.0	57	1.18	9.9	76
031198	9.7	83	11.1	70	0.02	~ 1.5	
051198	7.0	17	7.5	61	0.01	40	67
100399_W4	6.8	21	7.7	69	0.10		
100399_W2	6.6	37	8.7	59	1.37		
100399_W0	8.8		14.5		9.05		
120499	7.8	34			1.72	11	63
110599	5.5	22	6.7	69	0.16	46	63
180599	6.6	13	7.6	43	0.00	41	62
230899	4.9	30	8.5	68	0.00	30	65
230899H	10.5	70	12.8	86		11	46

Table III-10-B: Several Au/α-Fe_2O_3 catalysts prepared by the ZSW Ulm: characterization & activity / selectivity at 80°C.

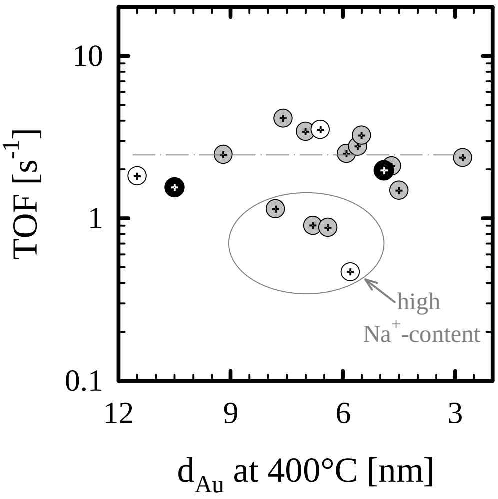

Fig. III-45: CO conversion rate (80°C, idealized reformate, 1 kPa CO, $\lambda = 2$) of various Au/α-Fe_2O_3 samples (see Table III-10) as a function of the Au particle size obtained by XRD after conditioning at 400°C (synthetic air; 30 min). Predominant precursor support Fe-phase: Ferrihydrite (⊕), Hematite (⊕), and Goethite (●).

by Haruta and co-workers by similar procedures [71, 233]. The mass-specific activity (in mol_{CO}/g_{Au}*s) indeed shows an increasing trend at smaller XRD-determined particle sizes. But upon investigating the dependence of the turnover frequency, which is normalized to the dispersion of the freshly conditioned samples (for the calculation a (hemi-)spherical droplet form was assumed for simplification; $r_{Au} = 0.144$ nm), on the particle diameter (figure III-45), it becomes evident that this trend is predominantly arises from the increased fraction of exposed Au surface atoms at decreasing particle size, since the calculated TOF's remain surprisingly constant within ±50% (average value ca. 2.5 s^{-1}) for particles ranging from 2.8 up to 11 nm, which is in contrast to the activity dependence claimed by Haruta [240] or Valden *et al.* [263]. The strong scattering is probably caused by the different sodium contents of the samples (see below): The four samples which deviate significantly in fig. III-45, having a TOF lower than 1 s^{-1}, are those with extremely large Na^+-contents (samples no. 201196, 300996, 100896 and 120499). Exactly the same tendency is recognized, when the TOF for our catalyst samples is related to the number of exposed surface atoms after calcination at 600°C (see table III-10-B), which would yield much more precise values due to the larger fraction of XRD-considered Au particles (not shown here for brevity). Other than in the above cited references we find no pronounced particle size effect. Likewise, Bollinger and Vannice could not find any significant differences between the reactivities of Au/TiO_2 samples with 4.5 and 33 (!) nm particles, respectively [253]. This independence of the TOF on the particle diameter agrees well with our reaction model (oxygen supply *via* the support), which was developed in the preceeding chapter. But unfortunately, we have only few samples with Au particles smaller than 4.5 nm so it cannot be completely excluded, that there may exist a narrow maximum for the reactivity around 3 nm as was observed by the Haruta group on Au/TiO_2 (see figure III-44; [240]).

Moreover, there seems to be little influence of the iron oxide precursor phase (after drying the freshly prepared catalyst) on the resulting TOF. This is not very surprising, since in all cases α-Fe_2O_3 is formed after calcination at 400°C. But when starting from a Ferrihydrite ($Fe_5(OH)_8*4H_2O$) precursor, samples with smaller gold particles could be prepared than on a support consisting of major parts of Hematite (α-Fe_2O_3) or Goethite (α-FeOOH). Obviously, for the Ferrihydrite precursor phase, sintering of the oxide particles is less favourable during the calcination process. Consequently, with this type of catalysts the smallest gold clusters are achieved, since the sintering of the support strictly governs the growth of the attached Au particles, as was shown by detailed XRD measurements after calcination at various temperature levels [274]. We also tried to pre-reduce the Au on some of the catalyst samples by adding H_2O_2 or $NaBH_4$ to the catalyst suspension, but this resulted not only in much larger gold particles (*e. g.*, sample no 230899H), but also in a very poor performance for the $NaBH_4$-treated samples (= lower TOF; see table III-10). Probably on these samples the established Au-FeO_x-interface must have been smaller or less reactive [283]. Those results demonstrate once more that the activity for this type of catalysts crucially depends on the pretreatment procedure.

Similar effects of different FeO_x precursor phases were also observed by Kozlova *et al.*, who suggested that stronger Au-support interactions on very amorphous FeO_x phases indeed reduce the sintering of Au particles [278, 284].

It is interesting to note that Wagner *et al.* reported a significant dependence of the reactivity on the type of the used iron oxide with Ferrihydrite-supported catalysts being superior to Hematite- and Goethite-supported catalysts, which seems to contrast our results. But they investigated uncalcined samples, where the original support phase should be largely retained during CO oxidation, whereas for our catalyst the resulting phase after calcination is uniformly α-Fe_2O_3 [285]. Hence these results should be compared with reservation.

Haruta and co-workers claimed that other than for the CO oxidation, the H_2 oxidation rate is almost independent from the Au particle diameter (and also from the kind of support), which, according to their model, would lead to an increased selectivity at smaller particle sizes as a consequence [270, 286]. But on our catalyst the selectivity shows no discernible trend, varying between 60 and 75% on the different samples for particle sizes up to 11 nm (it should be mentioned that these deviations are well outside the measurement tolerance of < 5%!). Nevertheless, from our data in table III-10-B (and also from the results in the next section) we can exclude that it is just a simple function of the gold particle size.

It is interesting to note, that the pre-reduction treatment by H_2O_2 (sample no. 230899H) led to a strong decrease in the selectivity, when compared to the untreated, identically produced fraction (no. 230899), but yet we cannot offer a satisfying explanation for this behaviour at the moment.

As a result it may be concluded, that the exact nature and morphology of the interface affects the reactivity of our catalysts very strongly, whereas the particle size of the gold crystallites seems to have no or little impact on the performance. It is interesting to note that Vannice and co-workers noticed a very similar trend for the other highly active system (see preceeding chapter), Au/TiO_2, where the activity seemed to depend in a very subtle manner upon the nature of the support phase (and its interface to the metal) for the conditioned catalysts, but not on the size of their gold clusters [72, 237, 253, 287]. Our results underline that for this type of gold catalysts the support plays an active role in the CO oxidation reaction, probably as an oxygen supply as discussed in the preceeding chapter.

3.2.2 Influence of the calcination temperature

For the Au/α-Fe_2O_3 sample no. 110599 the long-term stability (fig. III-46a, c), the activity (window b) and selectivity (window c) were tested for different conditioning temperatures (calcination in 10% O_2 in N_2 for 30 min.; each experiment with a new catalyst bed).

When going from 200°C to 300°C, the CO oxidation rate increases significantly, but then drops again at higher calcination temperatures. This is in excellent agreement to observations by Haruta *et al.* on a coprecipitated Au/α-Fe_2O_3 catalyst employed for the CO oxidation in air (1 kPa; -70°C). At 200°C the gold, which is initially in an ionic state, is probably not yet reduced to the full extent. This would be constistent with XPS-measurements of Sze *et al.*, Haruta *et al.* and Kozlova *et al.* on Au/α-Fe_2O_3 catalysts, where after calcination at 200°C the Au(4f) BE is still located at 84.1-84.2 eV (normed to the C_{1s}-peak at 284.6 eV) [234, 278, 288], which is somewhat above the position for metallic Au of ~83.8 eV [235, 246, 278]. Likewise, for this low temperature pretreatment Park and Lee recorded a very broad XP

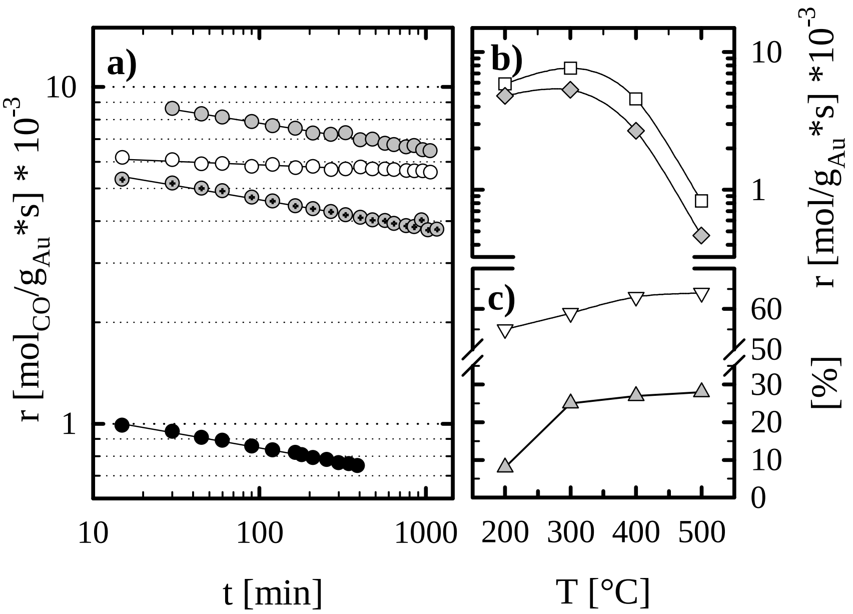

Fig. III-46: *a)* Comparison of the selective CO oxdiation in idealized reformate (1 kPa CO, $\lambda = 2$; 80°C) over Au/α-Fe_2O_3 after calcination at different temperatures: ○ 200°C, ◉ 300°C, ⊛ 400°C, and ●500°C; *b)* Activities for CO (□) and H_2 oxidation activity (◇; calculated *via* selectivity) after 120 min.; *c)* Selectivity (▽) and loss of reactivity between 30 and 1000 min. (△ ;extrapolated for 500°C data).

spectrum on an impregnated Au/α-Fe_2O_3 catalyst, which they attributed to the parallel presence of ionic and metallic Au species [289]. Moreover, the ferrihydrite precursor is not yet converted to its final Hematite form [71]. We therefore attribute the lower activity of our catalyst after the low temperature calcination to both of these missing structural transformations. An additional role of residual carbonate (originating from the preparation procedure), which is not fully decomposed after calcination at 200°C (TGA results by V. Plzak) and was shown to decrease the activity (see chapter III-3.4.2), cannot be excluded.

At elevated temperatures (> 300°C) the gold is probably reduced to its metallic state, Unfortunately, in the above cited XPS studies, there is a slight disagreement about the resulting gold state after calcination at 300°C. Whereas Sze *et al.* and Park *et al.* observed already metallic Au^0 (83.8 - 83.9 eV; normalized to the C1s peak at 284.6 eV), Haruta and co-workers still claim ionic contributions, which dissappeared only at 400°C (83.9 eV). At higher temperatures the gold particles probably increase significantly in size, which is responsible for the corresponding decrease of the mass-related activity rate after calcination at 400 and 500°C, respectively.

It should be mentioned, that there is an intense debate, in which state the gold is in its most active form. Whereas, *e. g.*, Minico *et al.*, Visco *et al.* and Park and Lee propagate a superior performance of positively charged Au species [251, 289, 290], the results from Dekkers *et al.*, Boccuzzi *et al.* and Haruta and co-workers [71, 269, 291, 292] and our own data as well suggest, that ionic gold is a less reactive species. In the former studies the most active catalysts were the samples calcinated at 200°C and below, whereas in the latter publications the catalysts only gained high activity after formation at 300°C and above. We cannot solve this obvious contradiction finally here, but it is noteworthy that even for our own Au/α-Fe_2O_3 catalysts the optimum conditioning temperature was not identical for all samples. No. 061197 showed, *e. g.*, its highest activity after conditioning at 400°C (Therefore, 400°C had been chosen as a general calcination temperature for our standard activity tests and the kinetic measurements). This indicates that the activity is not solely a function of the oxidation state of gold alone, but probably also of other factors like, *e. g.*, the structure (quality) of the Au-FeO_x interface, which depends in a very subtle manner on the preparation method. For example Park and Lee produced their catalysts by impregnation of freshly prepared Hematite [289], whereas on our catalysts this support phase was formed only at higher temperatures, starting initally from a ferrihydrite precursor. Most likely such differences in preparation account for the observed differences in the optimum pretreatment procedure.

The hydrogen oxidation activity (window b; grey diamonds in fig. III-46) follows in principle an identical trend - but is slightly enhanced at lower calcination temperatures, relative to the CO oxidation rate, leading to somewhat lower selectivities at decreasing calcination temperatures (window c; white triangles), which in turn implies that on positively charged gold particles (which are still present after the low-temperature calcination procedure) the $H_2 + O_2$ reaction is more favoured. Similar conclusions were reached in the early work of the Haruta group [234].

With respect to chapter III-3.4, where we will explicitly examine the deactivation behaviour, it is interesting to compare the long-term stability after the different pretreatment temperatures. In figure III-46c (grey triangles) the reactivity loss (in %) between 30 and 1000 min. (extrapolated for the „500°C“-measurement) is illustrated. The deactivation behaviour is essentially identical for the three higher temperatures (-30%), only at 200°C the rate decreases by less than 10%. This is in contrast to the study by Sze *et al.* on CO oxidation in air at 60°C, where they noticed a continuous, strong increase in activity loss with increasing pretreatment temperature for all levels above 300°C, which may be attributed to the somewhat different reaction atmosphere they used (*e. g.*, absence of hydrogen) [288]. For our series the stabilized rate at 200°C is likely to be caused by a simultaneous slow reduction of the less reactive ionic gold species to their metallic state, which would counteract the „normal“ deactivation process and as a consequence yield an apparently stabilized rate.

3.2.3 The dependence of the particle size on the sodium content

We also investigated the possible influence of impurities on the formation and activity of our gold catalysts. The preparation starts from $HAuCl_4$, Na_2CO_3 is used for the precipitation step. Hence Na^+ and Cl^- are likely to be included. Other impurities than these were never observed in XPS or EDX measurements, but of course for both methods the dectection limit is quite high. Whereas there is a broad agreement that chloride probably acts as a poison for the CO oxidation and leads to increased Au particle sizes after conditioning [233, 237, 286, 293, 294], there is no consistence upon the influence of Na^+ impurities. Haruta reported reduced activity and a more pronounced deactivation of the Na-containing samples [233]. In contrast, Yuan *et al.* even noted a rate enhancement in the presence of Na^+ in their study on Au/Fe_2O_3 catalysts [294].

In fact, the chloride was removed quite well from our gold catalysts after several washing steps, so that only for one sample (no. 120897) traces of Cl^- were established by EDX measurements. Due to the lack of sufficient statistical data we can not draw any conclusions concerning the Cl-influence on Au/α-Fe_2O_3.

The Na^+ was somewhat more difficult to remove: In a series of samples which differed only by the cleaning procedure (no. 100399; see tables III-10) four redispersion steps at 80°C, following the precipitation-deposition procedure, were required to reduce the Na-content down to 0.1 wt-%. Figure 47a clearly shows that there is just a very moderate negative influece of sodium on the turnover frequency of Au/α-Fe_2O_3 (only ferrihydrite-precursor catalysts are regarded for this figure). An increase of almost three orders of magnitude in the Na-content reduces the activity by only a factor of 3 - 4, nevertheless, this may well explain the large scattering in the TOFs in fig. III-45. But there is a striking effect of sodium impurities on the formation behaviour during calcination. From figure III-47b it is obvious that above a critical content of approximately 0.2 wt% Na^+ promotes the sintering of the gold clusters. In this figure the particle diameter after conditioning in synthetic air (30 min.) at 600°C is displayed, since at this temperature level the XRD already covers the major part of particles and the uncertainty hence decreases (see table III-10-B). Nevertheless the same tendency applies as well for the data obtained at 400°C.

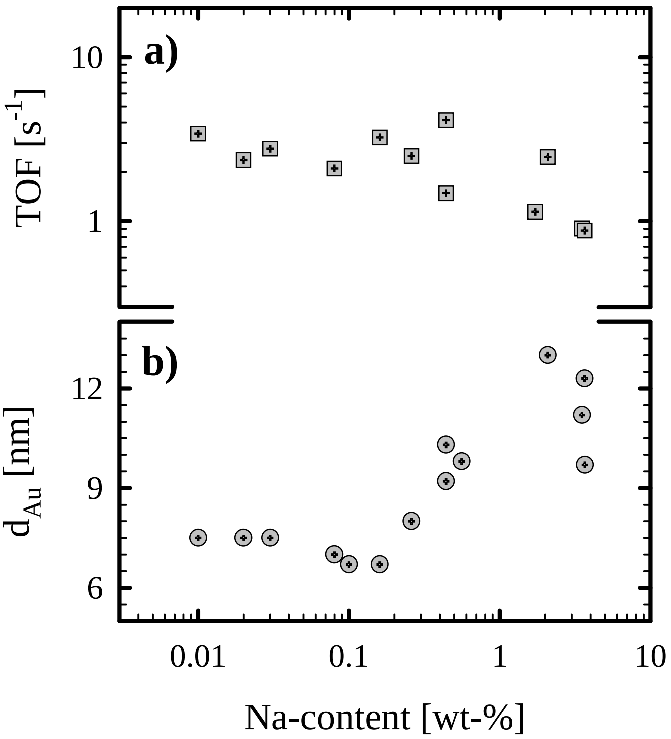

Fig. III-47: a*)* Turnover frequency for CO conversion (80°C; idealized reformate; 1 kPa CO; λ = 2) of various Au/α-Fe_2O_3 samples (see tables III-10-A,B) as a function of the Na-content. *b)* Average Au particle diameters (determined by XRD) after conditioning in sythetic air at 600°C (30 min) as a function of the Na-content after the final washing step.

Kang and Wan claim the observation of a similar phenomenon for zeolite supported gold catalysts, where the resulting particle size of the conditioned catalyst shows a slightly increasing tendency with increasing NaOH addition during preparation [295]. At the moment we can just speculate for reasons, but a possible explanation may be the simple blocking of anchoring sites for gold particles on the support by Na^+-ions, so that they possess a higher mobility during the formation process, leading to larger agglomerates.

3.3 The CO coverage on Au and its influence on the kinetics

The general suitability of the Au catalysts for the PROX reaction was investigated in a previous studiy on a Au/α-Fe_2O_3 catalyst, where Kahlich *et al.* determined the CO oxidation rates and selectivity in H_2-rich gas [26]. These studies revealed drastic differences in the reaction kinetics as compared to the PROX reaction over a Pt/γ-Al_2O_3 catalyst, which we had studied earlier [7, 12, 83]. While the selectivity remained constant on Pt/γ-Al_2O_3 for operating temperatures ≤200°C, it decreased strongly with decreasing CO partial pressure (1.5 - 0.02 kPa) and increasing temperature (40° - 120°C) on the Au/α-Fe_2O_3 catalyst. It was proposed that these differences result from different steady state CO coverages on the two catalysts during the reaction, with the Pt catalyst operating at very high CO coverages, practically at saturation coverage (see chapter III-1.2), while the Au catalyst was expected to run at low CO coverages. Direct proof for the latter assumption, which is crucial for the mechanistic understanding of the reactions, however, is still lacking.

In this section, we will first compare basic kinetic data on the PROX reaction on both catalysts. We then present *in-situ* DRIFTS measurements, during CO adsorption/selective oxidation at varying CO partial pressures, which yield direct information on the steady-state CO coverage under PROX operating conditions. These data show unambiguously that the steady state CO concentration is low on the gold particles compared to platinum. This difference is shown to lead to the observed strong decrease of the selectivity on Au with decreasing p_{CO}, while it remains independent on Pt. Finally, we show DRIFTS data recordedat lower temperatures which support the above conclusions and also rationalize the experimentally observed changes in the CO reaction order with temperature. All data in this section were obtained on the Au/α-Fe_2O_3 catalyst no. 201196 (See tables III-10).

3.3.1 Kinetic observations

Figure III-48 compares the turnover frequencies and selectivities of both catalysts at their envisaged operating temperatures during selective CO oxidation in idealized reformate at a constant λ-value of 2, demonstrating the high activity of Au/α-Al_2O_3 at 80°C and its superior selectivity at high CO partial pressures (figure taken from [25]). Assuming a simple power-law model for the CO oxidation kinetics, the slope in fig. III-40a corresponds to the sum of the reaction orders with respect to $p(O_2)$ and p(CO) [7].

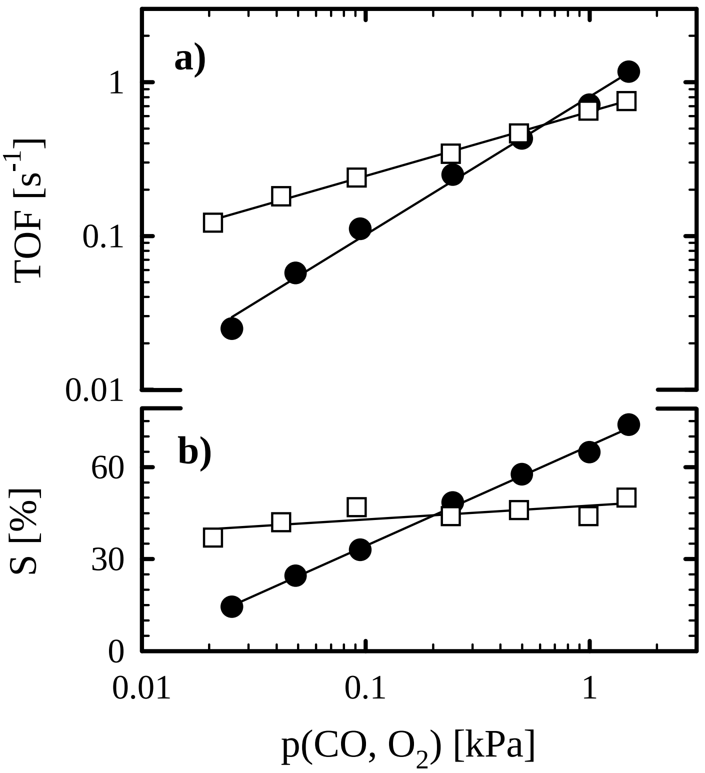

Fig. III-48: Selective CO oxdiation in idealized reformate ($\lambda = 2$) over Pt/γ-Al_2O_3 at 200°C (□) and Au/α-Fe_2O_3 at 80°C (●): *a)* CO oxidation activity; *b)* selectivity. *{KAH}*

In microkinetic studies on the preferential CO oxidation over Pt/γ-Al_2O_3 at 150-250°C, the reaction orders with respect to p(CO) and p(O_2) were determined to be -0.4 and +0.8, respectively [7], which is consistent with the selective CO oxidation reaction occurring in the so-called „low-rate branch“, where the Pt surface is thought to be completely covered by CO under reaction conditions [83]. Consequently, the oxidation rate of co-adsorbed hydrogen is also rate-limited by the same step (dissociative O_2 adsorption), so that the CO and H_2 oxidation rates are coupled, effecting an essentially constant selectivity of ca. 40% (Fig. III-48b) on Pt/γ-Al_2O_3 over the entire range of CO and O_2 partial pressures at temperatures below 250°C ([7]; see also section III-1.2.1).

As was already mentioned, the Au/α-Fe_2O_3 catalyst shows a comparable activity at the much lower temperature of 80°C. However, from the different slope in Fig. III-48a it is already apparent that the reaction orders, *i.e.*, the reaction kinetics, are very different on the gold catalyst. The reaction orders with respect to p(CO) and p(O_2), determined in microkinetic studies in idealized reformate, were +0.55 and +0.23, respectively [26]. In terms of a mechanistic model, the positive CO reaction order suggests that there is no self-poisoning of the CO oxidation reaction by adsorbed CO, contrary to what is observed for the Pt catalyst.

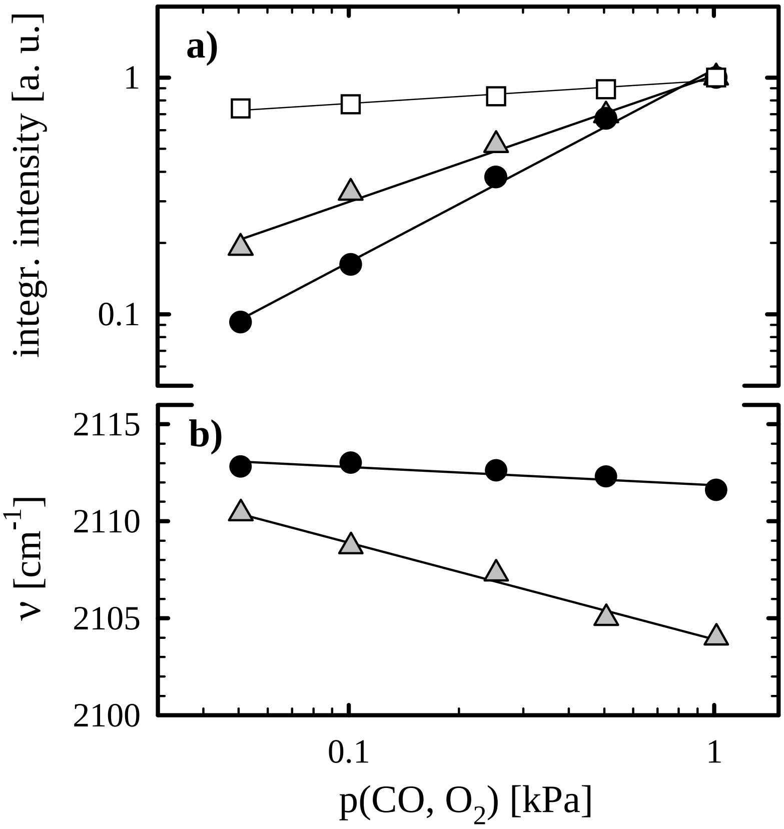

Fig. III-49: *a)* Integrated IR intensity and *b)* band position of the linearly bound CO_{ad} in idealized reformate (λ = 2) over Pt/γ-Al_2O_3 at 200°C (□) and Au/α-Fe_2O_3 at 80°C (●) and during CO adsorption in pure N_2 over Au/α-Fe_2O_3 at 80°C (△).

Boccuzi *et al.* [248] proposed that the reaction follows a Langmuir-Hinshelwood type mechanism where both reactants are adsorbed on the Au surface (see also chapter III-3.1), as it is well established for CO oxidation on platinum metal surfaces [1]. In this case the positive CO reaction order implies that under reaction conditions the CO coverage is significantly below saturation and hence a decrease of the CO partial pressure decreases the reaction probability for CO oxidation. The relatively high selectivity of the Au catalyst, particularly at high CO partial pressures (Fig. III-48b), can be rationalized by the very low dissociative sticking probability for H_2 on a gold surface [219, 223, 223]. Assuming low CO coverages under PROX conditions, hydrogen dissociation would be expected to be essentially unperturbed by adsorbed CO, so that the H_2 oxidation rate (at constant p(O_2)) should be independent from the CO oxidation rate which, indeed, is experimentally observed [26]. Consequently, a decrease in p(CO) with a concomitant decrease in the CO oxidation rate results in the loss of selectivity shown in Fig. III-48b, a striking difference to the behavior of the Pt/γ-Al_2O_3 catalyst.

The following in-situ DRIFTS experiments were conducted to support the suggested low CO coverage conditions during the PROX reaction on Au/α-Fe_2O_3.[26, 83]

3.3.2 Comparison of the CO coverage on Pt/γ-Al_2O_3 versus Au/α-Fe_2O_3

Since the DRIFTS signal depends on the penetration depth of the infrared beam into the powder catalyst sample and is a strong function of the support material, the particle size, and the packing density, a direct quantitative determination of the CO coverage from the DRIFTS spectra is generally not possible [50, 51]. Therefore, the experimental CO adsorption intensities measured during the PROX reaction by *in-situ* DRIFTS will be referenced to the CO_{ad} intensities produced by CO adsorption in a pure N_2 background. For the latter, we showed in section III-1.2.3, that the CO-coverage on the Pt catalyst can be estimated using first order Langmuir adsorption-desorption kinetics for CO. For a CO partial pressure of 1 kPa and temperatures up to 200°C CO coverages are in all cases are close to saturation ($\theta_{CO} > 0.9*\theta_{sat}$; see also table III-2). We also proved that under reaction conditions the reaction rate can be neglected compared to the desorption term (see table III-1). Therefore, on the basis of equation III-1.2 (and assuming that the IR cross-section of CO_{ad} is not significantly altered by the presence of O_2 and H_2), essentially identical CO_{ad} intensities were predicted and observed (see Fig. III-3) for CO in a pure nitrogen background and in idealized reformate. This, in conjunction with the above estimated CO coverage based on the pure adsorption experiments provides strong evidence that the PROX reaction under our reaction conditions (1 kPa CO, $\lambda = 2$; $T \leq 200°C$) does, ideed occur at saturation coverage on Pt/γ-Al_2O_3.

Based on equation III-1.2 we can estimate that the CO coverage on Pt/γ-Al_2O_3 remains close to saturation during the reaction in idealized reformate even at much lower CO partial pressures ($\lambda = 2$; 200°C), reflecting the adsorption-desorption behavior in the high pressure regime of a Langmuir isotherm. This is confirmed by the DRIFTS measurements in fig. III-49 (square symbols), which show that the IR intensity and hence the steady-state CO coverage (see above) decreases by less than 20% as the CO partial pressure is reduced from 1 to 0.05 kPa. At the same time, the CO frequency remained almost constant at 2050 cm^{-1} (not shown). Despite the slight loss in CO coverage the adlayer is still sufficiently dense to efficiently inhibit the adsorption of H_2 (and O_2) during the reaction, explaining the small loss in selectivity (Fig. III-48, square symbols). Hence, over the entire pressure range in fig. III-48 the selectivity in the PROX reaction on Pt/γ-Al_2O_3 catalyst is controlled by the high CO coverage

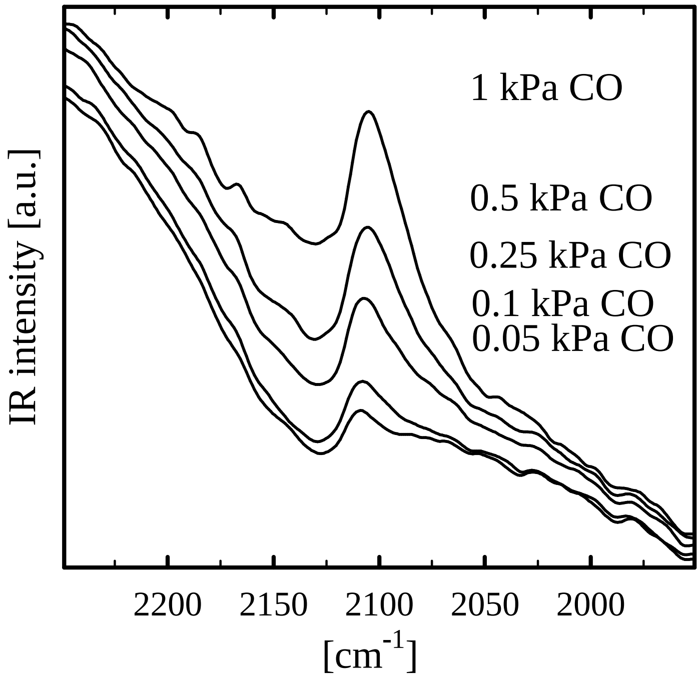

Fig. III-50: In-situ DRIFTS spectra (region 1950 - 2250 cm^{-1}) of linearly bonded CO recorded at adsorption-desorption equilibrium on Au/α-Fe_2O_3 at varying CO partial pressures between 0.05 and 1 kPa in pure N_2 at 80°C.

The IR vibrational spectra of the Au/α-Fe_2O_3 catalyst during CO adsorption or oxidation are characterized by a CO band at ca. 2110 cm^{-1} (see fig. III-50), which is generally assigned to linearly adsorbed CO on single crystalline gold surfaces [296] and supported Au particles [257]. An assymetric tailing on the low frequency side was interpreted by Boccuzzi *et al.* in terms of a second CO adsorption state at the perimeter places on their Au/ZnO catalyst [248, 248, 257]. However, since such a tailing could also emanate from a heterogeneous particle dispersion, we will refer to the band at ~2110 cm^{-1} as deriving from a single CO adsorption species. Additional CO species, such as CO adsorbed on (partly) ionic Au atoms (stabilized by the support) as it had been assigned to the high frequency bands on Au/TiO_2 and Au/ZnO at 2130 - 2150 cm^{-1} [248, 291, 292] as well as on Au/Fe_2O_3 at around 2138 and 2159 cm^{1} [251], were not observed under our experimental conditions. The absence of these species is probably related to different catalyst pretreatment conditions and/or the presence of H_2 during our CO oxidation experiments.

Similar to the above analysis of the CO adsorption characteristics of the Pt/γ-Al_2O_3 catalyst during the PROX reaction, we will first examine the adsorption of CO on the Au/α-Fe_2O_3 catalyst in the absence of reaction, *i.e.*, in a pure CO/N_2 mixture at the PROX operating tem-

system	**T [K]**	**pressure range**	**vib. shift [cm^{-1}]**	**θ_{sat} 1)**	**ref.**
Au(332)	92	$2.5*10^{-10}$ - 10^{-6} kPa	2124 - 2110	0.17	[296]
	105	$2.5*10^{-10}$ - 10^{-6} kPa	2125 - 2113		
Au powder	273	0.7 - 3 kPa	-	~ 0.2 2)	[297]
Au film on Al_2O_3	2	0.01 - 0.8 L 3)	2125 - 2108		[298]
Au/SiO_2	298	0.034 - 10.9 kPa	2120 - 2110		[299]
Au/SiO_2	298	$1.7*10^{-4}$ - 59 kPa	2129 - 2106	0.17 4)	[247]
Au/ZnO	298	0.0002 - 5 kPa	2116 - 2106	0.22	[257]
Au/Fe_2O_3	353	0.05- 1 kPa	2111 - 2104		this work

1) $\theta_{sat} = \theta$ at highest pressure and lowest ν_{CO}
2) calculated from their adsorption isothermes using an atomic density of 10^{19} m^{-2}
3) CO dosing in UHV
4) coverage at 2 kPa

Table III-11: CO vibrational frequency shifts as a function of CO partial pressure (and CO dosing) reported for unsupported and supported gold particles and estimated CO coverages for the maximum indicated saturation pressure.

perature. DRIFTS spectra obtained at different CO partial pressures at 80°C are reproduced in fig. III-50; the resulting CO adsorption intensities and the corresponding IR frequencies are plotted in fig. III-49a and b, respectively (triangular symbols) as a function of the CO partial pressure (balance N_2). Upon increasing the CO partial pressure from 0.05 to 1 kPa, the CO_{ad}-intensity increases by nearly one order of magnitude. Assuming a roughly linear relationship between signal intensity and absorber concentration, this represents a significant increase of the CO coverage on the gold particles. The conclusion is supported by a concomitant decrease in wavenumber from 2111 cm^{-1} to 2104 cm^{-1} (Fig. III-49b) since ν_{CO} on gold surfaces is know to decrease with increasing θ_{CO}, contrary to what is observed for platinum metals [247].

For comparison, the CO coverage dependency of the IR vibrational frequency of CO_{ad} on various gold surfaces reported in the literature is summarized in Table III-11. In contrast to platinum, neither the adsorption temperature nor the dispersion (*i.e.*, particle size) seem to have a significant influence on ν_{CO}. The highest values are between 2120 cm^{-1} and 2130 cm^{-1} for the low coverage regime and generally decrease to slightly below 2110 cm^{-1}. The maximum coverage under the conditions listed in Table III-11, which corresponds to the lowest wavenumbers, does not exceed $\theta_{CO} \approx 0.2$. This relatively low saturation value even at high pressures may be due to a strong decrease in adsorption energy at higher adsorbate densities [296]. Therefore, a simple comparison of band positions suggests that the equilibrium CO coverage in 1 kPa CO (balance N_2) on the Au particles of our catalyst should not exceed $\theta_{CO} \approx 0.2$.

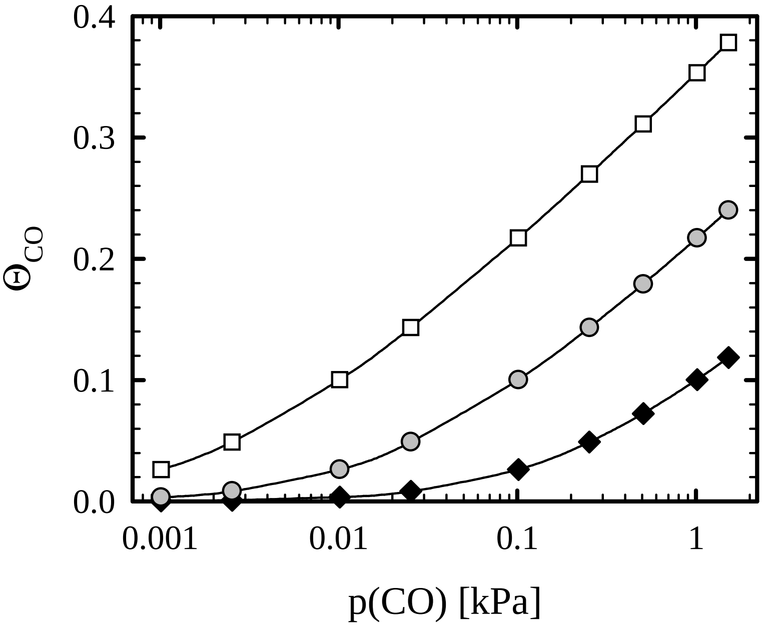

Fig. III-51: Adsoption isotherms calculated *via* Langmuir-kinetics for CO on gold in a pure nitrogen background at 80°C based on the data by Ruggiero *et al.* [296]. assumptions: $s_0 = 1$ and $\nu = 10^{13}$ (□); $s_0 = 1$ and $\nu = 10^{15}$ (◆); $s_0 = 0.1$ and $\nu = 10^{13}$ (●).

The low CO coverage under our conditions (1 kPa CO) is consistent with the data by Iizuka *et al.*, who for pure gold powder determined a coverage of ~0.2 at a partial pressure of 3 kPa CO and 0°C [297]. It is furthermore consistent with an estimate based on Langmuir adsorption-desorption kinetics for CO, in conjunction with published CO adsorption energies on Au surfaces (reconstructed Au(100): 58 kJ/mol [300]; polycrystalline Au: 55 kJ/mol [301]; Au(332): 55 kJ/mol [296]; Au(110): 33 kJ/mol [220] and 40 kJ/mol [302], resp.), preexponential factors between 10^{13} and 10^{15} s^{-1}, and maximum sticking coefficients of 0.1-1. Calculations (analogous to fig. III-6) based on the values given by Ruggiero *et al.* on Au(332) [296] are shown in figure III-51. The resulting CO coverages for 1 kPa CO are indeed in the range between 0.1 and $0.35*\theta_{sat}$ for all applied conditions.

In contrast to the approach used for the Pt/γ-Al$_2$O$_3$ catalyst, where the CO intensity for the pure adsorption case (CO/N$_2$ mixtures) was directly compared to the intensity observed under PROX conditions, this direct comparison is not possible for the Au/α-Fe$_2$O$_3$ catalyst. In the latter case the support phase changes from α-Fe$_2$O$_3$ (Hematite) to Fe$_3$O$_4$ (Magnetite) in the presence of H$_2$, concomitant with a change in the DRIFTS signal due to a different penetration depth. Therefore, a comparison of the absolute CO intensities in CO/N$_2$ with those measured during selective CO oxidation in idealized reformate (λ = 2) is meaningless. We therefore

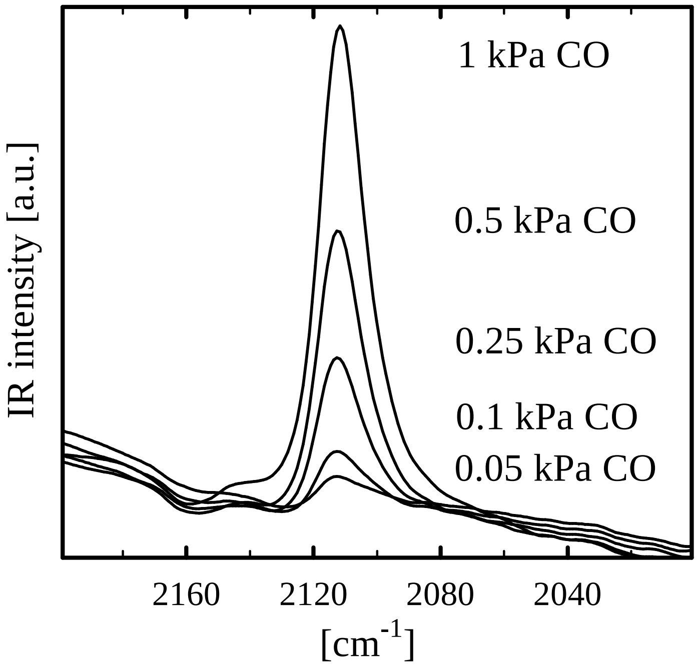

Fig. III-52: In-situ DRIFTS spectra (region 2000 - 2200 cm^{-1}) of linearly bound CO recorded during CO oxidation in idealized reformate ($\lambda = 2$) on Au/α-Fe_2O_3 at varying CO partial pressures between 0.05 and 1 kPa in pure N_2 at 80°C.

estimate the steady state coverage during the PROX reaction under our experimental conditions from the adsorption/reaction kinetics. As in the case of Pt, r_{des} (eq. III-1.2) is several orders of magnitude larger (using the above kinetic parameters) than the TOF for the gold catalyst (see fig. III-48a), so that the CO coverage in a pure N_2 background should be the same as during the PROX reaction, *i.e.*, ≤ 0.2 ML (assuming that the CO adsorption properties of the Au particles do not change in the presence of O_2 and H_2). To reflect the similar coverages, the CO intensities were normalized to each other at the highest CO partial pressure in fig. III-49a.

Consistent with a low CO coverage even at the highest CO partial pressure of 1 kPa (filled circles in fig. III-49a), the CO intensity (and therefore the CO coverage) decreases with decreasing CO partial pressure. This coverage dependence fits also to the observed positive reaction order with respect to p(CO), owing to a reduced reaction probability at reduced θ_{CO}.

The p(CO)-dependence of the CO vibrational frequency during the selective CO oxidation ($\lambda = 2$) is shown in fig. III-49b (filled circles), the associated DRIFTS spectra are displayed in fig. III-52. Compared to the case of CO adsorption from a pure CO/N_2 mixture (Fig. III-50), the CO_{ad} frequency under PROX conditions is now shifted to significantly higher wavenumbers and barely changes with decreasing CO partial pressure (2113 - 2111 cm^{-1}). A

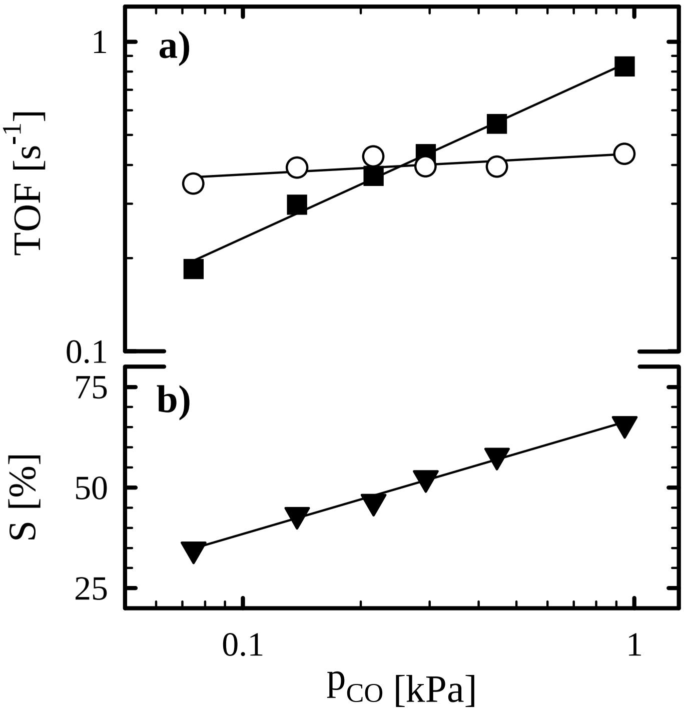

Fig. III-53: *a)* Turnover frequencies of CO (■) and H_2 oxidation (○) and *b)* selectivitiy (▼) over Au/α-Fe_2O_3 at 80°C and p_{O_2} = 1 kPa in idealized reformate. *{KAH}*

very similar blue-shift of the CO_{ad} band (1 kPa CO partial pressure) upon admission of oxygen (partial pressure not given in reference) of ~10 cm^{-1} was noted by Boccuzi *et al.* on the closely related Au/TiO_2 system [248].

This increase in ν_{CO} is assigned to the coadsorption of oxygen and its effect of decreasing the electron density in the gold particles. Since the bonding of CO to gold surfaces is dominated by the 5σ orbital [247], electron donation to the metal becomes more favorable under these conditions. Owing to the weak antibonding effect of the 5σ orbital with respect to the C-O bond, the IR band frequency would increase for a reduced electron density of the gold surface. Since fig. III-52 was recorded at a constant value of $\lambda = 2$, p(O_2) decreases in the same way as p(CO), so that the up-shifting effect of O_2 is expected to become smaller at lower partial pressures. The nearly zero net shift observed in fig. III-52 (see also filled symbols in fig. III-49b) can be understood as a result of these two counteracting effects (decreasing ν_{CO} with increasing θ_{CO}, but increasing wavenumber ν_{CO} with increasing p(O_2)). A similar effect may also exist for the IR cross-section, which would explain the more pronounced decay of the intensity with smaller coverages for the PROX reaction as compared to CO adsorption.

Under the above hypothesis of low CO coverages during the PROX reaction even at the highest CO partial pressure of 1 kPa examined in our study, it is reasonable to assume that the

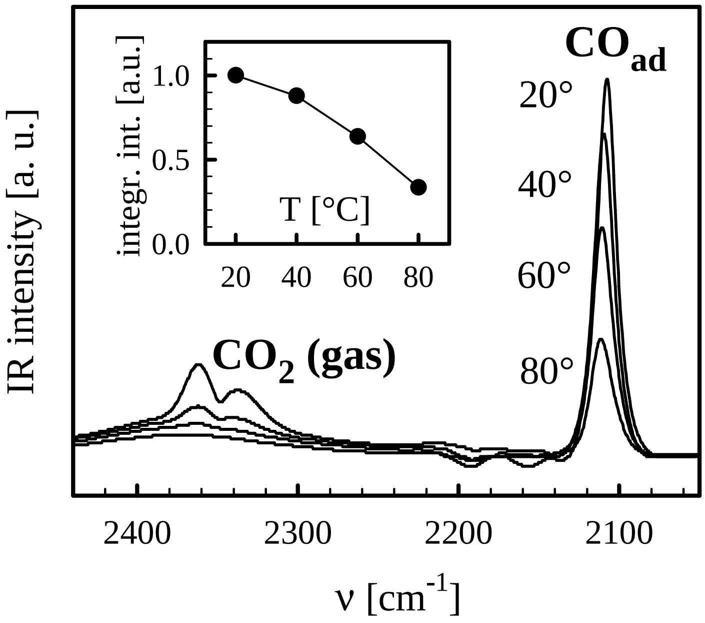

Fig. III-54: *In-situ* DRIFTS spectra on Au/α-Fe$_2$O$_3$ in idealized reformate (1 kPa CO; $\lambda = 2$) at different temperatures. *Inset*: Integrated IR intensities of the linearly bound CO *versus* temperature.

dissociative adsorption of hydrogen on the Au surface is not significantly perturbed by the presence of CO. Therefore, one would expect that the H_2 oxidation rate is independent of the CO partial pressure if the O_2 partial pressure remains constant. This, indeed, is confirmed by kinetic measurements (taken by M. Kahlich) on both CO and H_2 oxidation rates over Au/α-Fe$_2$O$_3$ in idealized reformate at 80°C and $p(O_2) = 1$ kPa at 80°C, shown in fig. III-53 [26]. While the CO turnover frequency decreases with decreasing CO partial pressure owing to a decrease in CO coverage, the H_2 oxidation rate remains essentially constant (Fig. III-53a). This demonstrates that r^{CO} and r^{H_2} are completely decoupled, contrary to what is observed for the Pt/γ-Al$_2$O$_3$ catalyst. As a consequence, the selectivity of the Au catalyst decreases with decreasing p(CO) (Fig. III-53b). Since the dissociative sticking probability for H_2 on a gold surface is very low [219], due to a strongly activated adsorption process [223], the overall selectivity is still rather high. This is different from the case of the Pt/γ-Al$_2$O$_3$ catalyst, where the high selectivity is only caused by the nearly complete blocking of the surface with adsorbed CO.

3.3.3 Temperature dependence

In this section we finally present and discuss *in-situ* DRIFTS data recorded during the PROX reaction on Au/α-Fe$_2$O$_3$ at varying temperatures, which will provide a final piece of evidence for the hypothesis that the CO coverage under PROX conditions at 80°C is very low, far below saturation. These data will rationalize the observed decrease in the CO reaction order during selective CO oxidation with temperature, which was found to change from +0.55 at 80°C down to +0.35 at 40°C [26]. A similar behavior was observed also by Lin *et al.* on a 2.3 wt% Au/TiO_2 catalyst, with a decrease in the CO reaction order from 0.6 to 0.2 as the temperature was decreased from 87° to 37°C in a H_2-free gas mixture ($p_{CO} = 0.1\text{-}2.5$ kPa, $p_{O_2} = 0.1\text{-}2$ kPa, balance He) [237]. Figure III-54 shows *in-situ* DRIFTS spectra recorded in idealized reformate (10 kPa CO, $\lambda = 2$) at 20°, 40°, 60° and 80°C, respectively (all spectra taken after 30 min. of equilibration). Clearly, the amount of linearly adsorbed CO decreases by a factor of three (see inset in fig. III-54) with increasing temperature. It cannot be excluded that a part of this apparent coverage variation may also be caused by changes in the O_{ad} coverage, which would influence the band position and probably also the IR cross section of CO_{ad} (see below). Nevertheless, a strong decrease of the CO coverage with temperature resembles the behavior expected in the steep, middle regime of a Langmuir adsorption-desorption isobar, where the CO coverage is far below saturation, which in turn gives further credence to the hypothesis that the CO coverage under PROX conditions at 80°C is rather low on the $Au/\alpha\text{-}Fe_2O_3$ catalyst. Such a strong variation of the steady-state CO_{ad} concentration fits well to a reaction scheme where the CO supply is increasingly rate limiting, which qualitatively rationalizes the increase in CO reaction order with increasing temperature.

Consequently, one would expect a more moderate decrease of θ_{CO} with p_{CO} at lower temperatures, *i. e.*, at 40°C. In figure III-55 the integrated intensity and peak position of CO_{ad} in idealized reformate are shown as a function of the CO and O_2 partial pressure ($\lambda = 2$; 40 and 80°C, respectively). While at 80°C the CO_{ad} band is reduced by a factor 11 as p_{CO} is decreased from 1 to 0.05 kPa, at 40°C only a lowering by a factor 6 is observed. Exactly the same trend applies for CO adsorption in a pure N_2-background (not shown here for brevity): At 40°C the difference in band area between the highest and lowest CO partial pressure is only a factor 3 compared to factor 6 at 80°C. This observed reduction in the CO partial pressure dependence of θ_{CO} at lower reaction temperatures implies a somewhat larger absolute coverage at 40°C (as was already suspected from the temperature-experiment above), which explains the observed decrease of the CO reaction order from +0.55 at 80°C down to +0.35 at 40°C [26].

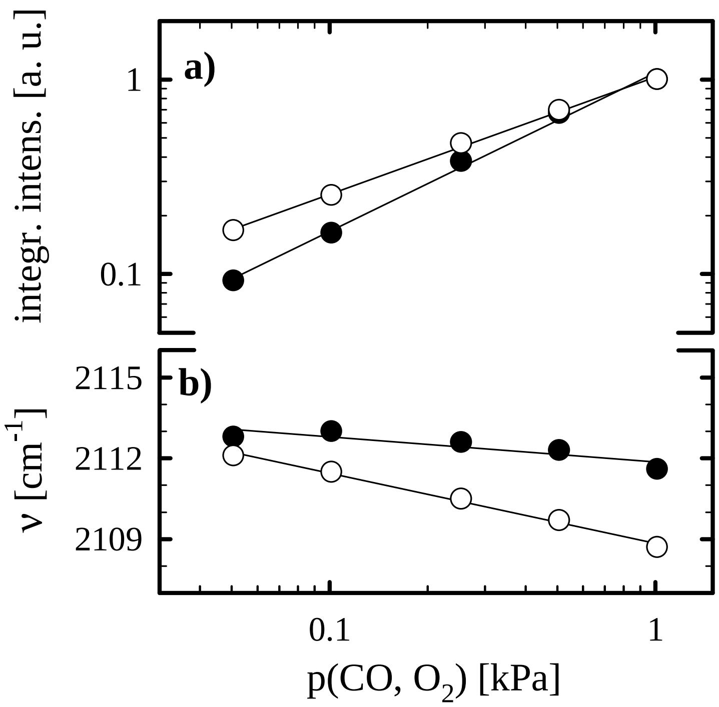

Fig. III-55: *a)* Integrated IR intensity and *b)* band position of the linearly bound CO_{ad} over Au/α-Fe_2O_3 at 80°C (●) and at 40°C (○) in idealized reformate (1 kPa CO, $\lambda = 2$).

In contrast to 80°C, where due to the simultaneously occuring oxygen coadsorption the CO-band position remained almost constant over the whole examined partial pressure range (see figure III-49b), at 40°C we notice a stronger dependence on the CO partial pressure. It now resembles more closely the behaviour during CO adsorption in pure N_2. The observed blue-shift upon switching from 1 kPa CO in N_2 to idealized reformate ($\lambda = 2$) is also reduced to only 3 cm^{-1} at 40°C (at 80°C: 10 cm^{-1}). Consequently, the influence (*i. e.*, relative amount) of coadsorbed oxygen must have been reduced at this lower temperature level, implying that the CO_{ad} : O_{ad} ratio must have been increased at 40°C.

In summary we have seen in this chapter by direct *in-situ* DRIFTS observations that under typical reaction conditions the reaction kinetics and the selectivity in the PROX reaction on Au/α-Fe_2O_3 are largely determined by the steady-state CO coverage on the active metal surface. θ_{CO} changes significantly with temperature or CO pressure, yielding coverages below 0.2 ML at 80°C and at 1 kPa CO. The CO coverage and its variation with partial pressure and temperature not only parallel the selectivity behavior in the kinetic measurements by M. Kahlich, *i. e.*, a pronounced loss of selectivity at lower CO partial pressures on Au/α-Fe_2O_3. It also rationalizes the observed CO oxidation reaction orders with respect to CO and O_2 and their temperature dependence as well as the independence between the H_2 and CO oxidation over Au/α-Fe_2O_3 (and the coupling over Pt/γ-Al_2O_3, respectively).

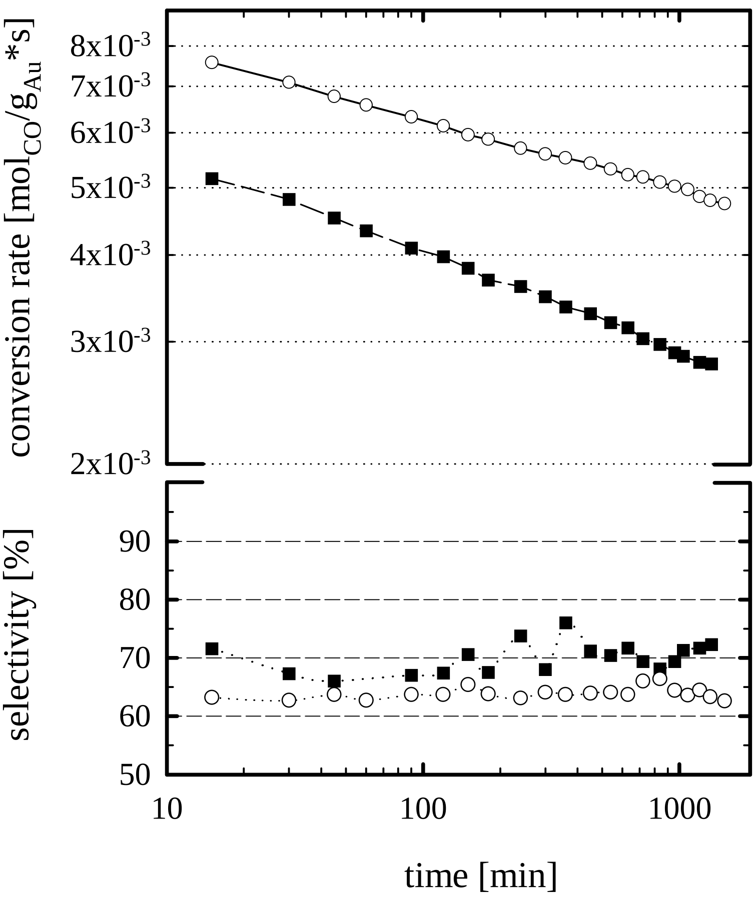

Figure 56: Activity (upper window) and selectivity (bottom) of Au/α-Fe_2O_3 (061197) at 80°C in idealized reformate (1 kPa CO, $\lambda = 2$) four month after catalyst preparation (○) and one year later (■).

3.4 Deactivation behaviour

3.4.1 „Off-line deactivation“

For the gold catalysts we have to distinguish two different kinds of deactivation. The loss of reactivity during reaction („on-line deactivation“), which is the object of the forthcoming sections, and a deactivation during storage (in air at room temperature), which occurs over a time-scale of month and years („off-line deactivation“).

In figure III-56 two long-term measurements in idealized reformate (1 kPa CO, $\lambda = 2$; 80°C) are compared, one within four months after preparation of the sample (no. 061197) and another, which was recorded with a temporal seperation of ca. 11 months („aged“ catalyst). The initial activity of the latter is reduced by more than 30%, but without any major consequences for the selectivity. The deactivation during reaction is also somewhat enhanced (46% instead of 36% within 1300 min. at equal absolute conversion rates). This „off-line deactivation“ applies in the same way for all other „aged“ Au/α-Fe_2O_3 samples, *e. g.*, sample no. 280598 lost ~45% activity within 11 months. This irreversible deactivation is probably caused by a slow recrystallization process of the initially amorphous support, which induces a parallel growth of the attached gold clusters, now leading to larger particle sizes after conditioning. This hypothesis is substantiated by XRD measurements on the 061197 sample, which indeed showed sharper bands on the „aged“ catalyst (~16 months after preparation), indicating larger particles (unpublished results). Of course an additional influence of contaminations from the surrounding atmosphere, *e. g.*, sulfur, cannot be generally excluded. As will be shown explicitely in the next section, the enhanced „on-line“ deactivation of the „aged“ catalyst is related to the increased cristallinity of the support phase.

3.4.2 „On-line deactivation“ during CO oxidation

Apart from this „off-line“ deactivation during storage, all Au/α-Fe_2O_3 samples suffered from a strong activity loss during our standard screening tests in idealized reformate (1 kPa CO, λ = 2; 80°C) under differential flow conditions, which, *e. g.*, amounts to ~40% of the initial activity after 1000 min. on-stream for the 061197 sample (see figure III-56). But we noticed a qualitative difference in the deactivation behaviour between our initially prepared samples, *e. g.*, no. 201196, which were produced by coprecipitation at temperatures >60°C, with the support consisting of larger hematite parts after drying, leading to a more crystalline structure after calcination, and the more recent samples, *e. g.* no. 061197. The latter were prepared by deposition-precipitation or coprecipitation at only 60°C, resulting in a very amorphous iron oxide structure after the conditioning procedure (see also table III-10-A). Whereas the first samples loose their activity very fast and it is hardly regained by any purging procedure, on the latter the deactivation is much more moderate and the initial rate is fully restored after a simple flush of the catalyst bed with an inert gas at reaction temperature. Therefore, in the subsequent sections we will treat the deactivation phenomenon separately on both catalyst types (investigated exemplary for the samples no. 201196 and 061197, respectively), before we finally develop a comprehensive model, which explains the activity loss on our Au/α-Fe_2O_3 catalysts during the PROX reaction.

For most supported gold catalysts, which were examined in numerous previous studies for the low-temperature CO oxidation, a similar permanent deactivation during time on-stream was recognized. Lin *et al*. noticed, *e. g.*, a reduction of 40 - 60% of the inital activity within 1000 min. on a Au/TiO_2 catalyst (0.5 kPa CO, λ = 2; 40°C) [237], Torres Sanchez *et al*. reported a reactivity decrease of roughly 30% during 90 min. of selective CO oxidation over a Au/MnO_x catalyst (1 kPa CO, $\lambda = 2$, rest H_2; 16°C) [31] and the model systems (Au particles on thin TiO_2 films) studied by Valden *et al*. even lost 80% activity after only 150 min. reaction (0.9 kPa CO; $\lambda = 10$; 27°C) [263, 264].

Since the CO_{ad} coverage on gold under our reaction conditions is much lower than on platinum metals (see preceeding chapter), we can safely exclude a CO „self-poisoning“ effect as is generally observed on the latter systems (compare chapter III-1.2.1).

Several models were proposed in order to rationalize the loss of reactivity during reaction: In a study on a $Au/Mg(OH)_2$ catalyst during CO oxidation in air (1 kPa CO; -70°C) Haruta.and co-workers blamed a slow recrystallization process of the gold clusters, which initially are not deposited in their thermodynamically most stable form, to be responsible [269, 303]. But this model could not be transferred to a Au/TiO_2 catalyst, where the Au particles exist in the stable fcc geometry from the beginning on [283]. Other studies suggest the blocking of reactive (interface) sites by the slow accumulation of by-products on the support. Cunningham *et al*. claimed that carbonate species were the reason for deactivation on a Au/Co_3O_4 catalyst (1 kPa in air; -76°C), whereas Knell *et al*. suspected formate species, indicated by IR-bands around 1590 and 1370 cm^{-1}, which were exclusively observed in mixtures with excess oxygen (0.25 kPa CO, $\lambda = 2$ and 80, resp.; 100°C) on their Au/ZrO_2 catalyst [236]. Interestingly, in a stochiometric reaction mixture ($\lambda = 1$) no deactivation (and consequently no formate bands) was noticed over a period of 1000 min.. Furthermore in several studies on uncalcined or initially not fully reduced samples the slow transformation from ionic gold species to metallic gold was held to be responsible for a slow decrease of the activity [251, 280, 290, 304], but on the contrary recent studies have shown that the positivized gold intrinsically owns no superior activity [291, 292]. Anyway, this type of deactivation should not be relevant for our $Au/\alpha\text{-}Fe_2O_3$ system, since the gold is metallic after calcination at 400°C as is indicated by several XPS studies on Au/Fe_2O_3 catalysts [234, 278, 288] (compare also section III-3.2.2).

Other possible aspects that should be seriously taken into consideration are a slow crystallographic or chemical transformation of the iron oxide support during time on-stream, which may affect the metal-support interface structure or the oxygen adsorption properties of the catalyst. If oxygen vacancies on the support material play an important role in the mechanism of CO oxidation, also a high oxygen content of the gas phase may exhibit a negative effect due to the complete saturation of these vacancies [262], which could be

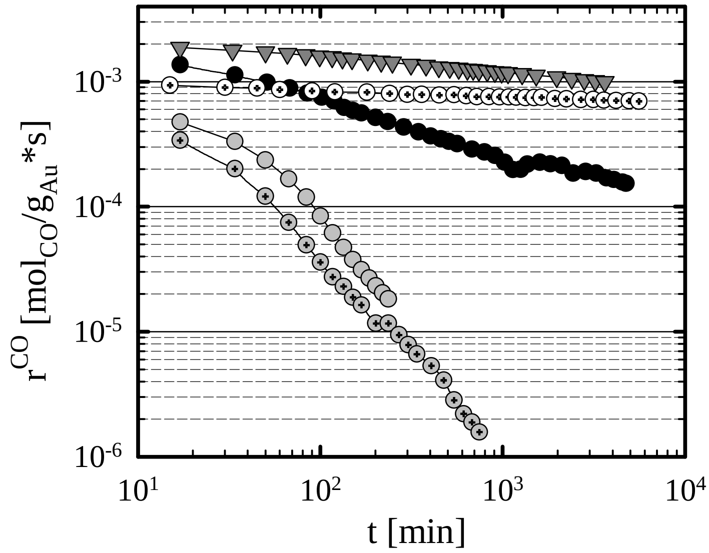

Fig. III-57: Long-term deactivation over Au/α-Fe_2O_3 (no. 201196) during CO oxidation (1 kPa CO, λ = 2 ;80°C) in different atmospheres: in idealized reformate (containing 75 kPa H_2), ● dry and ⊕ with 1.3 kPa water added, resp.; ○ in a pure N_2-background; ⊕ in a pure N_2-background at λ = 0.5.
For comparison: ▼ idealized reformate over Pt/γ-Al_2O_3 (1 kPa CO, λ = 2; 200°C).

another explanation for the strong activity decay observed by Knell *et al.* in O_2-rich reaction mixtures over Au/ZrO_2 [236]. But the latter theory should be ruled out for the deactivation during the PROX reaction on our Au/α-Fe_2O_3 catalyst, since we operate in a much more reductive atmosphere (containing 75% hydrogen), which would rather favour the existence of oxygen vacancies.

a) Irreversible poisoning of more crystalline samples

Figure III-57 provides an overview on the deactivation behaviour of Au/α-Fe_2O_3 (no. 201196) in different reaction atmospheres (all 1 kPa CO, λ = 2; 80°C). For comparison also the activity loss on the standard catalyst Pt/γ-Al_2O_3 is displayed, which is around 37% within the first 1000 min. in idealized reformate (triangle symbols; 1 kPa CO, λ = 2; 200°C). In an identical gas mixture (containing 75 kPa H_2) the gold catalyst clearly deactivates much more severely than the platinum catalyst, losing almost one order of magnitude of its initial rate (-83% in 1000 min.; black circles). Likewise, all other deactivation values, given in %, in the following context are calculated for the first 1000 min. on-stream. In a hydrogen-free gas mixture the deactivation on Au/α-Fe_2O_3 is even more pronounced (-99.7% = more than two orders of magnitude; grey circles), independent of the CO:O_2 ratio (tested for λ = 2 and 0.5, resp.), demonstrating, that the deactivation on our catalysts cannot be traced back to a „self-

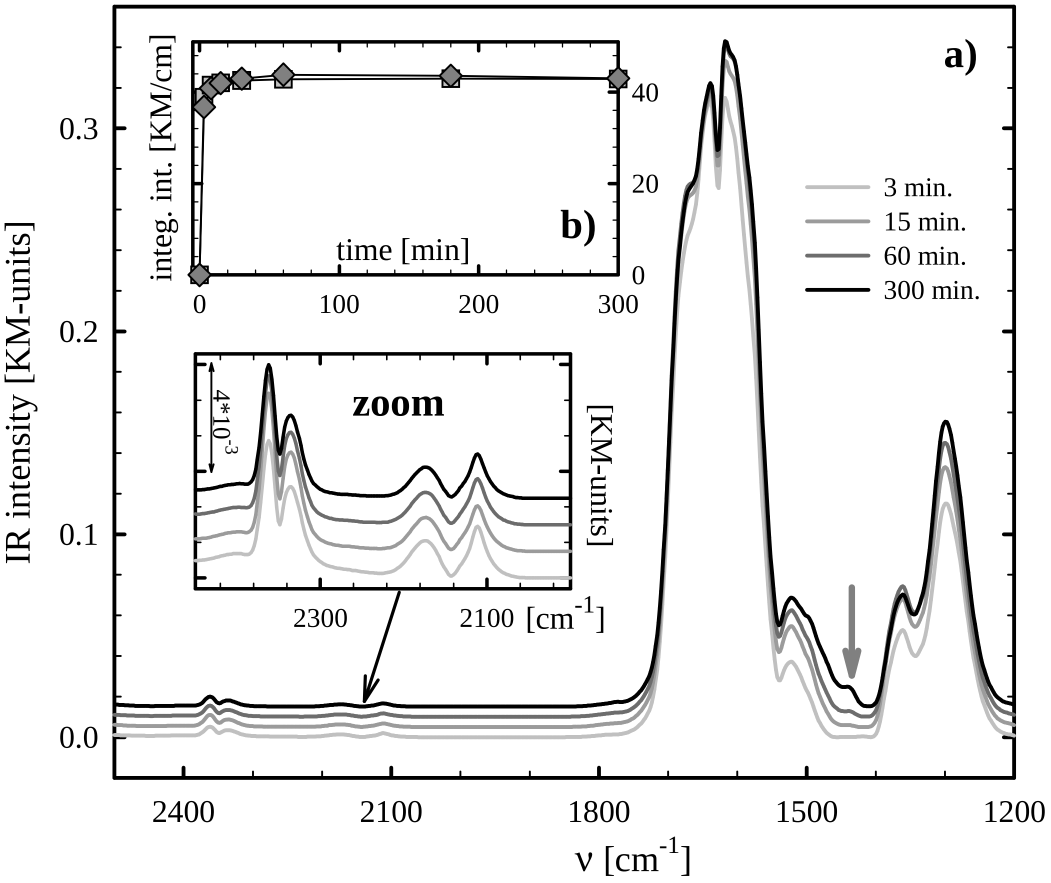

Figure III-58: *a)* Time evolution of DRIFTS spectra during CO oxidation in idealized reformate (1 kPa CO, $\lambda = 2$; 80°C) over Au/α-Fe$_2$O$_3$ (no. 201196); *b)* time-evolution of carbonate bands (integrated IR intensity) around 1600 and 1300 cm^{-1}.

poisoning“ from excess oxygen. On the other hand, when 1.3 kPa water is added to the idealized reformate, the rate becomes surprisingly stable (only -19%; white circles).

We think, that a thorough investigation of these differences in the long-term deactivation (*i. e.*, stabilizing effects by water and hydrogen (and / or *in-situ* produced water)) provides an important key to the understanding of the deactivation process itself. Consequently, in the next step we follow the time-evolution of surface species during reaction in idealized reformate (figure III-58a; 1 kPa CO, $\lambda = 2$; 80°C) and during CO oxidation in pure nitrogen (not shown here for brevity) by *in-situ* DRIFTS. During time on-stream we notice an enormous growth of IR-bands in the region below 1700 cm^{-1} (bands at 1300, 1360, 1480-1530, 1550-1625 and 1635-1720 cm^{-1}), which are attributed to either carbonate (CO_3^{2-}) or carboxylate (CO_2^-) species [71, 136, 250, 305]. As for the formate species, which were recognized during selective CO oxidation over Pt/γ-Al$_2$O$_3$ (see chapter III-1.2.2), the amount of by-products (evaluated by a TPD in pure nitrogen conducted after several hours of reaction; not shown here) exceeds several times the number of surface metal atoms, which is a indication for the location of these carbonates / carboxylates on the support.

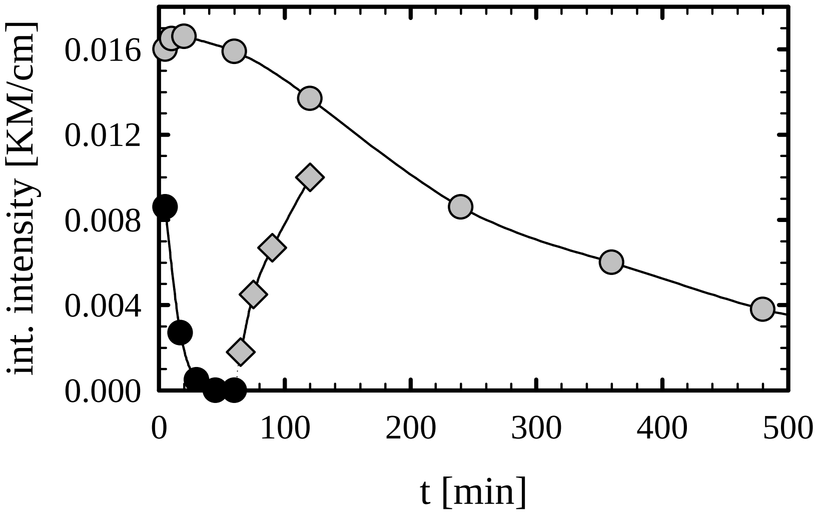

Figure III-59: Time-evolution of the CO$_{ad}$-band during selective CO oxidation in idealized reformate (○), during CO oxidation in a pure nitrogen background (●) and after switching back to idealized reformate (◇; 1 kPa CO, λ = 2; 80°C)

In window b of figure III-58, the time evolution for the build-up of these by-products (evaluated *via* integration of the bands at 1250-1400 and 1550-1700, resp.) is illustrated. After a few minutes of reaction the surface is almost saturated and the following increase is only very slow with proceeding time. This fast saturation, which is on a completely different time-scale as the activity decrease, seems to vote against a „carbonate poisoning“ model as an explanation, at least on first sight.

The time-evolution of DRIFTS spectra in a hydrogen-free reaction mixture (1 kPa CO, λ = 2, rest N_2; 80°C) seemed practically identical (and is therefore not shown explicitely here), with one small exception. The small band at ~1450 cm^{-1} (see arrow in figure III-58), which emerged slowly in idealized reformate, was completely absent during CO oxidation in a pure N_2 background. As will be rationalized in the following context, we assign this band to bicarbonate species (HCO_3^-), which are formed by a proton transfer from water (or OH^--groups) to carbonates:

$$CO_3^{2-} + H_2O \leftrightarrow HCO_3^- + OH^- \qquad \text{(III-3.3).}$$

Additionally to the evolution of by-products, we also monitored the IR band for CO adsorbed on the gold surface during CO oxidation in idealized reformate and in a pure N_2 background, respectively, which is indicated by a band around 2113 cm^{-1} (after subtracting the gas-phase CO contributions). From figure III-59 it is evident that the signal decreases slowly during reaction in idealized reformate (grey circles), which would resemble the time-scale of

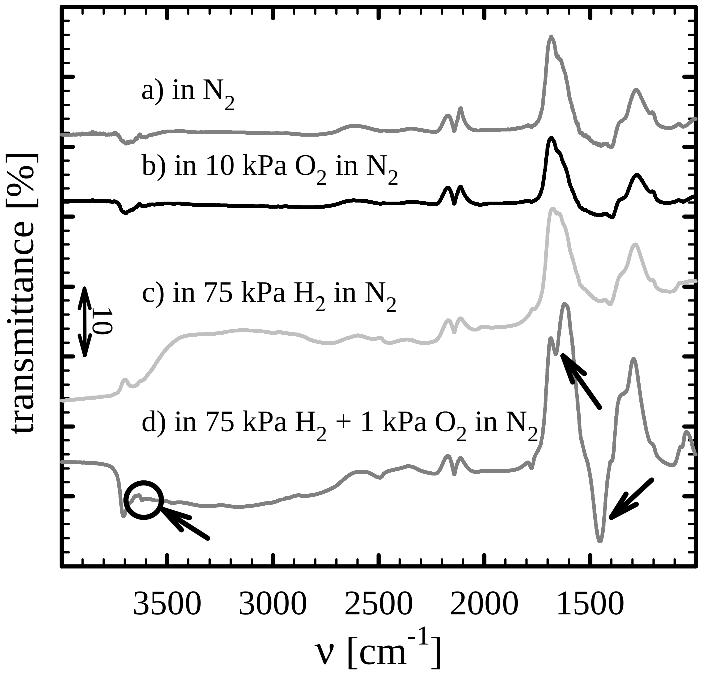

Figure III-60: Difference of DRIFTS-spectra after 1 h CO oxidation (1 kPa CO, λ = 2; 80°C) and after purging for 30 min. in different gas mixtures - Upward bands indicate a loss, downward bands an increase.

deactivation more closely. Likewise, the CO_{ad} band decreases much more rapidly in the hydrogen-free mixture (black circles), again consistently with the activity trend, and is hardly to recognize after 40 min.. Since the band position of the CO remains unchanged at 2113 cm^{-1} in both experiments, we feel that not only θ_{CO} but also the oxygen coverage must have been reduced proportionally, since a change in the CO_{ad}:O_{ad} ratio would influence the CO_{ad}-band position markedly ([248]; see also chapter 3.3.2).

When 75 kPa hydrogen are added after the CO signal has disappeared during CO oxidation in a pure N_2 background, the corresponding IR band grows again (grey squares), indicating, that hydrogen, or, more likely, the *in-situ* produced water (from the H_2 + O_2 reaction, which is now possible in a hydrogen-rich atmosphere), exhibits a stabilizing effect on the CO_{ad} coverage.

Since the water (or hydrogen) seems to play an important role in the deactivation process, we decided to take a closer look on possible interactions with the carbonate / carboxylate species formed during reaction. After accumulating these by-products during one hour of CO oxidation in a pure nitrogen background (1 kPa CO, λ = 2; 80°C), we exposed the Au/α-Fe_2O_3 catalyst to different gases at 80°C and recorded the decomposition behaviour by DRIFTS. In figure III-60 difference spectra are presented, where the spectrum obtained at the end of the CO oxidation reaction was divided by a spectrum recorded after 30 min. exposure

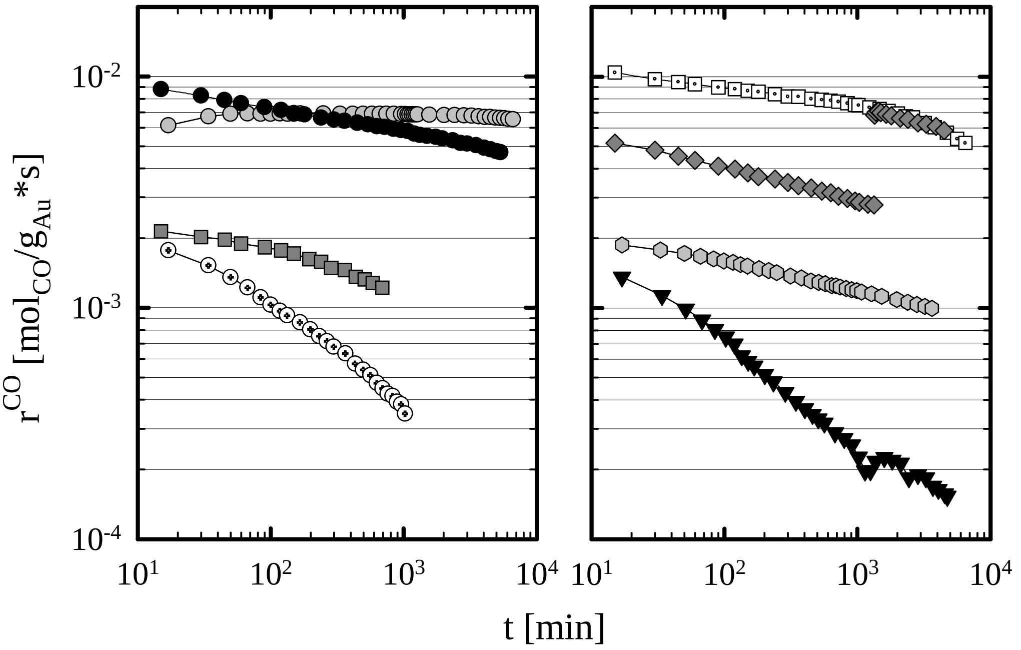

Figure III-61: Deactivation behaviour of Au/α-Fe_2O_3 (no. 061197) during CO oxidation (1 kPa CO, λ = 2; 80°C): ●idealized reformate (differential flow); ○idealized reformate (total conversion); ■more realistic reformate with 25 kPa CO_2 $^{(*)}$; ⊙CO oxidation in a pure N_2 background $^{(*)}$; ⊡idealized reformate with 1.3 kPa H_2O; ◆idealized reformate with switch to 1.3 kPa H_2O $^{(*)}$. - For comparison: ⬡Pt/γ-Al_2O_3 (200°C) and ▼Au/α-Fe_2O_3 (no. 201196) in idealized reformate. - *: "aged" catalyst

to the „purging gas“. Upward pointing bands indicate a reduction of the corresponding surface species during „purging“, the growth of species is characterized by downward bands. In the first three gas mixtures (pure nitrogen, mixed with 10 kPa O_2 and with 75 kPa H_2) the carbonate / carboxylate bands decrease somewhat, which indicates the relative lability of these species, but the degree of decomposition (indicated identical band intensities) is similar in all three atmospheres. In contrast, a mixtures, which contains 75 kPa hydrogen and 1 kPa oxygen (similar to idealized reformate), enabling now the *in-situ* water production, enhances clearly the decomposition of the by-products. Moreover, new bands arise at 1450, 1650 and 3615 cm^{-1} (indicated by arrows), which are associated with bicarbonate species (HCO_3^-) [137, 138, 248, 253]. Hence these rather labile bicarbonate species [306] appear to be the intermediates of a water induced decomposition process of carbonates:

$$H_2O\ (\text{or } OH^-) + CO_3^{2-} \leftrightarrow HCO_3^- + OH^-\ (O^{2-}) \qquad \text{(III-3.4)}$$

$$HCO_3^- \leftrightarrow CO_2\uparrow + OH^- \qquad \text{(III-3.5)}$$

We also investigated the decomposition in an atmosphere of 1.3 kPa water in nitrogen, but this experiment was recorded on a different spectrometer and in a different DRIFTS cell, so that a simple comparison of absolute intensities may be misleading. Consequently, this difference spectrum was omitted in figure III-60. Nevertheless, we noticed an extremely fast decomposition of carbonates in the water containing mixture, similar to the H_2 + O_2 mixture, along with the evolution of bicarbonate bands, as would be expected from the preceeding experiments. In a first conclusion, we may record, that the presence of water, which stabilizes the rate, promotes the decomposition of the support-bound by-products and (as a consequence, as will be specified below) mitigates the reduction of the surface CO (and also O) coverage during the PROX reaction.

b) Reversible deactivation on amorphous samples

Figure III-61 shows the deactivation over the Au/α-Fe_2O_3 sample no. 061197 in different reaction atmospheres (all 1 kPa CO, λ = 2; 80°C), which was prepared by deposition-precipitation and featured a much more amorphous iron oxide structure after calcination, as was confirmed by XRD measurments. The time-evolution of the activity on Pt/γ-Al_2O_3 (grey hexagons; at 200°C) and the Au/α-Fe_2O_3 sample no. 201196 (black triangles), which was discussed above, in idealized reformate are added for comparison. The stability of the 061197 sample in idealized reformate under differential flow conditions, where the decrease is only 34% (similar to the 37% of Pt/γ-Al_2O_3), is clearly superior compared to the 83% on the sample no. 201196. Surprisingly we detected that the degree of deactivation is strongly dependent upon the absolute conversion (in $\%_{CO}$). When the degree of conversion was increased – by either reducing the flow rate or decreasing the portion of inert α-Al_2O_3 in the reactor, which was required as a dilutent in order to guarantee differential flow conditions for our conversion measurements [26] – the rate became definitely more stable (not shown here for brevity). Finally, at total conversion, we could not even recognize any loss of activity for a period of almost six days (grey circles). We attribute the difference between the differential and integral measurements to the larger absolute water concentration (produced *in-situ*) in the latter case. This is underlined by a similar positive effect of water on the deactivation behaviour of the sample no. 061197, when it is additionally admitted (1.3 kPa) to the idealized reformate. On the freshly prepared catalyst the response was small (white dotted squares; deactivation 28% instead of 34%). But in measurements conducted one year later on the „aged“ catalyst, the effect was more pronounced with the initial deactivation being 44% for the dry reaction mixture (diamond symbols), whereas the activity behaviour resembled the „old“ measurement (on the freshly prepared catalyst) after switching to the wet mixture.

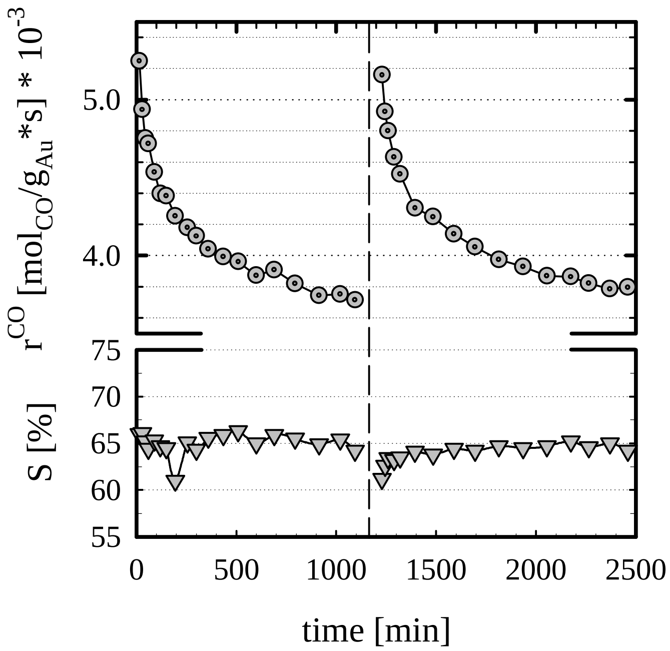

Figure III-62: Activity (upper window) and selectivity (bottom) of Au/α-Fe_2O_3 (061197) at 80°C in idealized reformate (1 kPa CO, $\lambda = 2$) - intermediate purging with 135 Nml/min pure N_2 at 80°C for 60 min. after approximately 1200 min. of reaction (dashed line).

Similar to what was noticed for the other sample in the preceeding section, in a hydrogen-free mixture the deactivation is markedly stronger, this time running up to 80%. In a more realistic reformate, containing 25 kPa CO_2, the deactivation is also slightly enhanced (47%), as would be expected from the enhanced by-product accumulation on the support in such an atmosphere.

In principle both gold catalyst samples show the same trend, but the deactivation is much more distinct on the samples which were prepared by coprecipitation at > 60°C. This leads to a change in the reversibility of the activity loss. Whereas the severely deactivated sample no. 201196 (after several hours of CO oxidation in a pure nitrogen background) showed no recovery upon purging with pure nitrogen for 30 min. and only a small effect after purging with a mixture containing 75% H_2 and 1% O_2 for 30 min. at reaction temperature, the 061197 sample regained more than 80% of its initial activity (idealized reformate; 1 kPa CO, $\lambda = 2$; 80°C) after purging the reactor for just 15 min. with pure nitrogen. After prolonged purging for one hour, almost the complete initial activity is recovered (see figure III-62).

If we compare the formation of by-products during time on-stream, we notice again such a gradual difference in the DRIFTS spectra (figure III-63). The spectra match each other very close in shape, but even though the dilution (with α-Al_2O_3) was 2.5 times higher for the sample no. 061197, which, in the worst case, may cause a signal decrease of the same

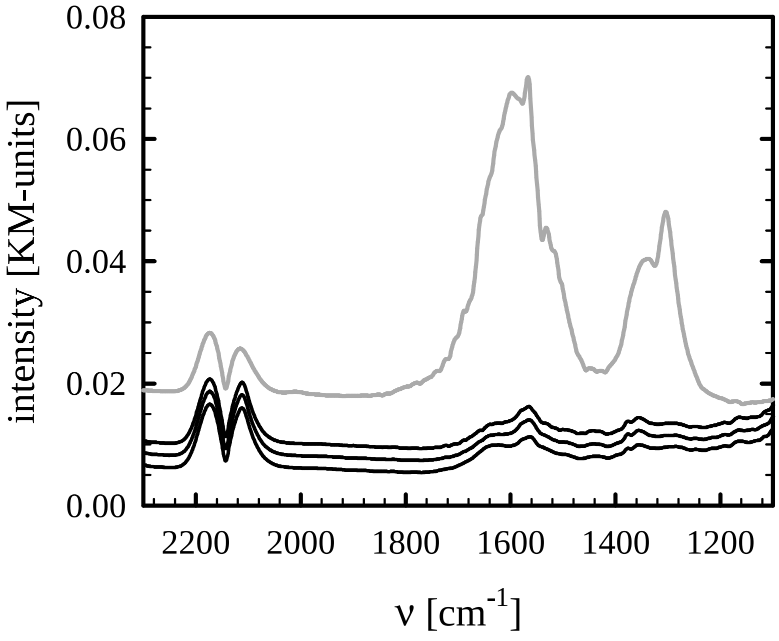

Figure III-63: Time-evolution of DRIFTS-spectra in idealized reformate (1 kPa CO; λ = 2; 80°C) over Au/α-Fe_2O_3 (no. 061197); spectra taken after 5, 20 and 60 min., resp. (arranged ascendingly) - For comparison: DRIFTS-spectrum of Au/α-Fe_2O_3 (no. 201196) after 1 h CO oxidation (grey line; 1 kPa CO; λ = 2; 80°C)

magnitude (but probably much less, since the penetration depth of the infrared beam increases simultaneously due to the enhanced reflectance), and if we take into consideration that there might be slight differences in the spectroscopic properties of the two Au/α-Fe_2O_3 samples, there is more than one order of magnitude difference in the band intensity for the carbonate / carboxylate bands. This may serve as a well explanation for the reduced deactivation of the recent sample. Other than on the sample no. 201196, the intensity of the CO_{ad}-band is not reduced during reaction (within a measurement tolerance of 5-10%).

c) Deactivation model

The reversible nature of the deactivation clearly argues against models, where the gold crystallites or the support are slowly restructured into a thermodynamic more stable conformation. Furthermore, deactivation is only observed for those substrates, which also form stable bulk carbonates (such as Fe_2O_3, $Mg(OH)_2$); but, *e. g.*, not for a Au/γ-Al_2O_3 catalyst (see chapter III-3.7).

Since the time-scale of the carbonate / carboxylate formation does not match the deactivation behaviour, but the activity loss is clearly dependent upon the water content, which decomposes the by-products, we propose the following model:

* During the (selective) CO oxidation carbonates and carboxylates are produced on the support, which blocks active sites for the CO oxidation(*e. g.*, at the Au-Fe_2O_3 interface) or the oxygen supply from the support phase. On the sample no. 201196 the by-products (or CO_{2ad}, which is rather stable on gold; see next chapter) are accumulated to such a large amount, that the CO_{ad} is even sterically blocked. An alternative explanation for the pronounced intentsity decrease of the IR CO_{ad}-band on this sample would also be the slow formation of bulk iron carbonate. The original Au-Fe_2O_3 interface (metal-semiconductor) induces a negative charge at the perimeter atoms of the gold clusters by the Schottky-junction effect [262], which may influence the adsorption strength of CO [307]. With the destruction of that interface, adsorption on these sites may become less favourable, resulting in a decreased surface coverage. Of course we cannot exclude an additional alteration of the IR cross section by such charge transfer effects, which may over-emphasize this effect.

* The presence of OH-groups (or water), which are continously replaced (at least partly) in the immediate surrounding of the gold particles during the PROX reaction by the parallely occuring hydrogen oxidation, enhances the decomposition of the carbonates and prevents the fast poisoning of the reaction. Consequently, this would lead to a zone which is relatively free of carbonates / carboxylates around the gold clusters (see figure III-64). When the replacement is not fast enough (dry reformate at differential conversion) or completely missing (CO oxidation in a pure nitrogen background) this carbonate-free zone melts slowly, which causes the observed permanent loss in reactivity (*i. e.*, the catalyst surface slowly dries off). When the OH-groups are replaced at a rate which is fast enough, the deactivation is reduced, or even completely stopped.

* The less deactivating Au/α-Fe_2O_3 (*e. g.*, 061197) samples feature a much more amorphous support structure after calcination, which probably contains more OH-groups from the beginning. We may speculate that in addition the formation of by-products is more difficult on an amorphous Fe_2O_3 support, which would explain the somewhat more pronounced deactivation of the „aged“ catalyst in figure III-56.

In summary we have shown that the degree of deactivation during reaction over Au/α-Fe_2O_3 catalysts depends on a subtle balance between the hydration degree of the support and its ability to form poisoning carbonate / carboxylate species. The highly reversible nature (at least

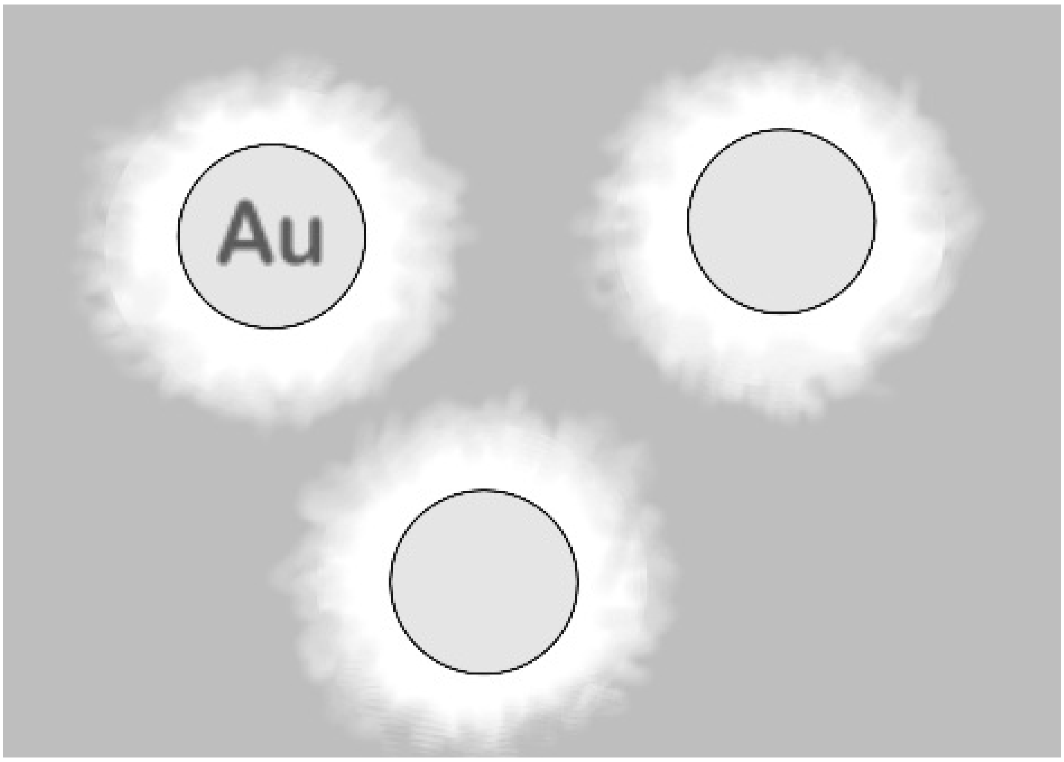

Figure III-64: Surface model for the by-product distribution during reaction – *grey*: carbonates / carboxylates; *white*: water / OH^--rich decomposition zone.

on the samples with an amorphous support structure) of the deactivation compared to other catalysts (see, *e. g.*, section III-2.2.1) is a further aspect, which makes Au/α-Fe_2O_3 a very promising candidate for industrial applications, *e. g.*, in vehicles for the purification of hydrogen produced from the steam-reformation of methanol, which is used as a feed gas for PEM fuel cells [14, 16].

3.5 Effects of CO_2 and H_2O on the activity / selectivity

Since the CO has a rather moderate adsorption energy on the Au surface, causing a low steady-state coverage during reaction (see chapter III-3.2), in principle a lot of free metal surface remains for the coadsorption of other molecules. Therefore, especially for gold catalysts it is important to take a look at possible effects on the activity or selectivity when changing from idealized to more realistic reformates, containing water and / or CO_2.

As for Pt/γ-Al_2O_3 (see chapter 1.3) we will first take a short look at the influence of water on the PROX reaction at 80°C and subsequently investigate CO_2-containing mixtures by combined DRIFTS and GC measurements.

3.5.1. Selectivity enhancement by water

There exists a vast number of studies, where the influence of coadded water on the CO oxidation over supported gold catalysts has been investigated. But the results differ extremely – even on equally prepared catalysts and using the same type of support. From the Haruta group predominantly positive effects are reported over a large variety of support materials, *e. g.*, the activity of a Au/α-Fe_2O_3 catalyst (1 kPa CO in air; 30°C) increased from 95% to total conversion upon addition of water (0.6-4 kPa) [234]. This was different from pure support oxides, which were deactivated seriously by moisture [240]. Positive effects were also claimed among others for Au/TiO_2, Au/Co_3O_4 or Au/NiO [71, 240, 243, 248]. Sakurai *et al.* demonstrated, that this observed reactivity enhancement cannot be the result of the water-gas shift equilibrium (eq. III-1.7), since the shift activity over Au/TiO_2 was negligible at such low temperatures [308]. Likewise, Park *et al.* noticed a very slight but positive effect of 0.7 kPa for their Au catalyst calcinated at 400°C, supported on TiO_2, Fe_2O_3 or Al_2O_3 (1 kPa CO, λ = 10 or 20; T = 40 - 80°C). In contrast, Bollinger and Vannice claim an irreversible decrease of activity by a factor three for Au/TiO_2 after the addition 0.6 kPa H_2O (4.8 kPa CO, λ = 2; 40°C) [253]. Similar observations were made by Grunwaldt *et al.*, who noted a reduced activity over Au/TiO_2 (0.25 kPa CO, λ = 2; 30°C) with only 0.1 kPa H_2O present in the reaction atmosphere, but in their study the effect was easily reverted by simply switching back to a dry mixture [268]. As far as the H_2 oxidation reaction is concerned, which has to be regarded for the PROX process, no relevant data could be found.

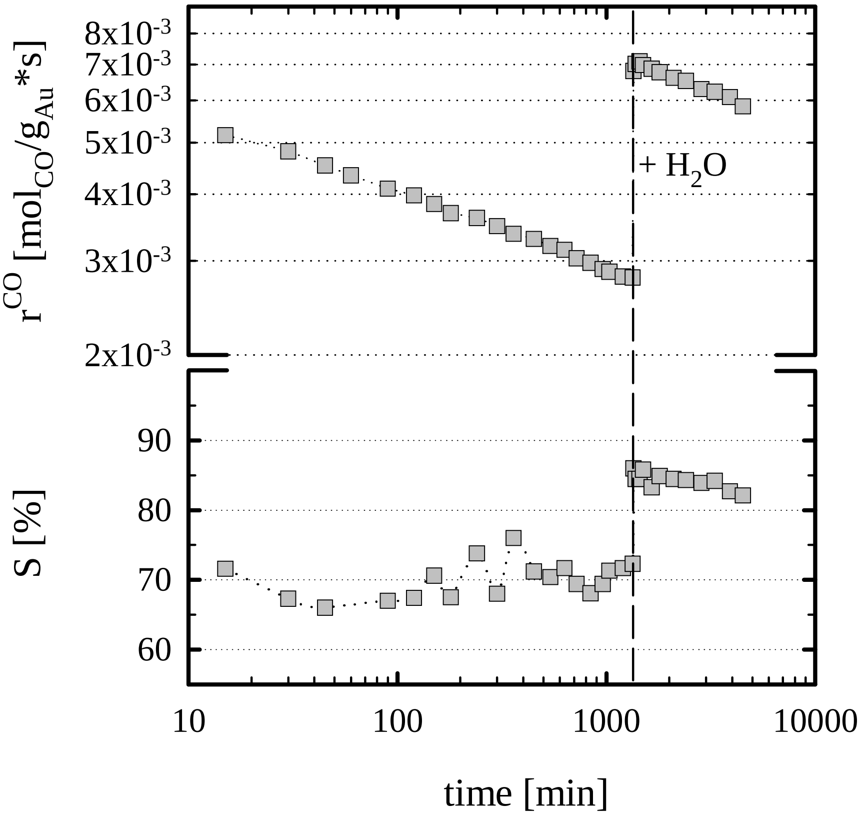

Figure 65: Activity (upper window) and selectivity (lower window) during a switch-experiment over Au/α-Fe_2O_3 at 80°C in idealized reformate (1 kPa CO, $\lambda = 2$) - first dry mixture and after 1300 min. 1.3 kPa H_2O added.

In our own measurements we tested the influence of water (1.3 kPa) on the selective CO oxidation at the envisaged operation temperature of 80°C in idealized reformate (1 kPa CO, $\lambda = 2$) for several Au/α-Fe_2O_3 catalysts. Surprisingly no uniform effect is observed on the different samples. Whereas, *e. g.*, on the freshly conditioned sample no. 061197 (See table III-10) virtually no influence upon the activity was seen after switching to a wet reaction mixture, the aged (several month after preparation) catalyst shows a slight increase of the reaction rate (+35% compared to the initial rate; see figure III-65) along with a clearly stabilizing effect, which was already discussed in the preceeding chapter. In contrast, on the sample no. 280598N even a slightly negative influence of water (rate -35% after admission of 1.3 kPa water to the reaction mixture) was seen. As a comprehensive conclusion for our catalysts, it may be claimed, that no matter if one sample reacts somewhat positive and another slightly negative upon the addition of water, the absolute effect on the CO oxidation is generally rather moderate (max. ±35%). Since for the sample no. 061197 we observed even a different water influence on the freshly prepared and aged catalyst (which differ mainly in the crystallinity of the support material; see section III-3.4.1), we can conjecture that smallest differences in the microstructure of our catalysts, which are not obvious from table III-10, may already cause the observed differences in behaviour.

But whereas the effect on the CO oxidation activity is quite small and not uniform, it is striking that the admission of water to idealized reformate produces an increase in selectivity of 15-20%, which is similar for all Au/α-Fe_2O_3 samples. As a consequence the calculated H_2 oxidation rate must have been reduced by a factor 2-3 in the presence of water.

We also tried to repeat the experiment in figure III-65 in our DRIFTS cell. But upon the admission of 1.3 kPa water to idealized reformate (1 kPa CO, $\lambda = 2$; 80°C) the CO_{ad} band dissolves in a very broad diffuse band at around 2100 cm^{-1} (FWHM ~120 cm^{-1}; not shown here for brevity), which is very difficult to analyse. Therefore we cannot make any precise statements on the CO coverage or band shifts in the presence of water. Boccuzzi *et al.* observed a similar effect (increase of absorbance around 2000 cm^{-1}, but here with an FWHM of the same magnitude) after addition of 0.2 kPa water to 0.5 kPa CO over Au/ZnO and speculated about an electronic effect arising from the icreased production of V_0^+ (monovalent oxygen vacancy) levels on the oxide support [248]. A possible reaction pathway is, *e. g.*:

$$CO + H_2O + O^{2-} \rightarrow HCO_3^- + H + V_0^{2+} \rightarrow HCO_3^- + V_0^+ + H^+ \quad \text{(III-3.6)}$$

In the DRIFTS spectra indeed a strong intensity increase of the bands assigned to bicarbonates in the presence of water is observed, as was shown in the preceeding section for the sample no. 201196 (which applies also to the other Au/α-Fe_2O_3 samples). This would be consistent with this hypothesis.

During our activity screenings we also tested the influence of water on the performane of a Au/TiO_2 sample (no. 170899; for characterization see tables III-10). It is interesting to note, that it fully paralleled the above described behaviour of the Au/α-Fe_2O_3 samples upon addition of 1.3 kPa water to idealized reformate (1 kPa CO, $\lambda = 2$; 80°C) and showed an increased selectivity by about 15% (not shown here for brevity).

There is much space left for speculation on the exact nature of the water effect, but it can be definitely concluded that H_2O exhibits a strong negative influence on the H_2 oxidation reaction, which leads to the observed selectivity enhancement on Au/α-Fe_2O_3 (and also on Au/TiO_2). The extremely one-sided nature of the effect (affecting only the H_2 oxidation) implies furthermore either a different reaction scheme for the CO and H_2 oxidation or a

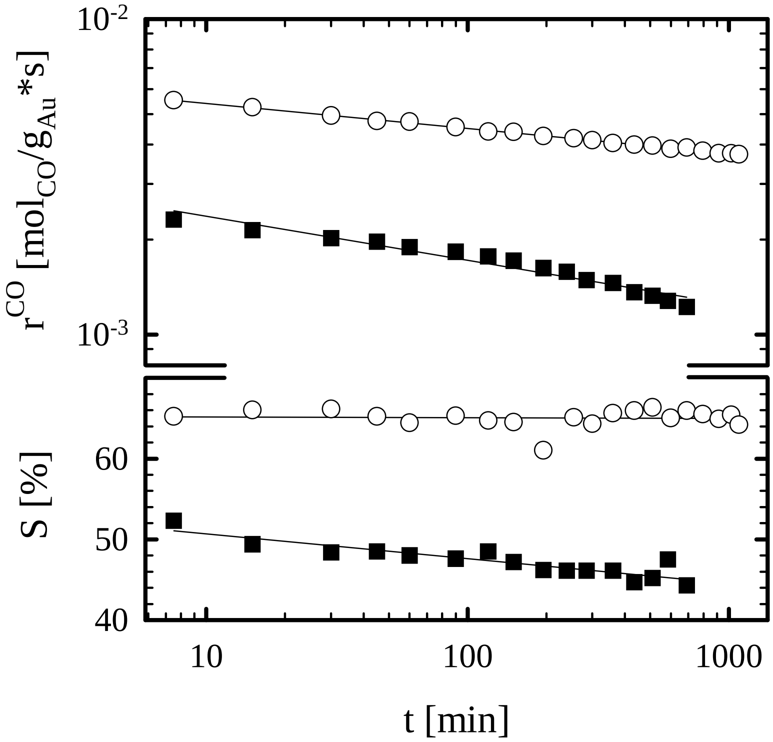

Figure 66: Long-term evolution of activity (upper window) and selectivity (lower window) over Au/α-Fe_2O_3 in idealized reformate (○; 1 kPa CO, $\lambda = 2$) and with 25% CO_2 (■) at 80°C.

reaction on different surface sites. But due to the lack of reference studies on model systems, which could provide a more basic insight into the H_2 oxidation reaction over supported gold catalysts, we cannot draw any further conclusions here.

3.5.2 Performance in CO_2-containing mixtures

Before we investigate the temperature dependence we will first take a look at changes in the long-term behaviour at our standard reaction conditions (1 kPa CO, $\lambda = 2$; 80°C) when replacing the nitrogen of the idealized reformate by CO_2.

In figure III-66 the activity (upper window) and selectivity (lower window) for the sample no. 061197, recorded over several hours under constant conditions, are compared. Quite clearly the reactivity for the CO oxidation is reduced by a factor 2.5 in the presence of 25 kPa carbon dioxide. A similar behaviour applies to all other Au/α-Fe_2O_3 catalysts, which were tested for CO_2-containing gases - in most cases the activity decrease is even stronger (*e. g.*, factor 4 for the 280598 sample). Consistently, Hoflund and coworkers noticed a reduced reactivity on their Au/MnO_x catalyst by a factor of two in the presence of 16 kPa CO_2 (1 kPa CO, $\lambda = 1$; 55°C), but they did not give any explanations [230]. The deactivation during time on-stream is

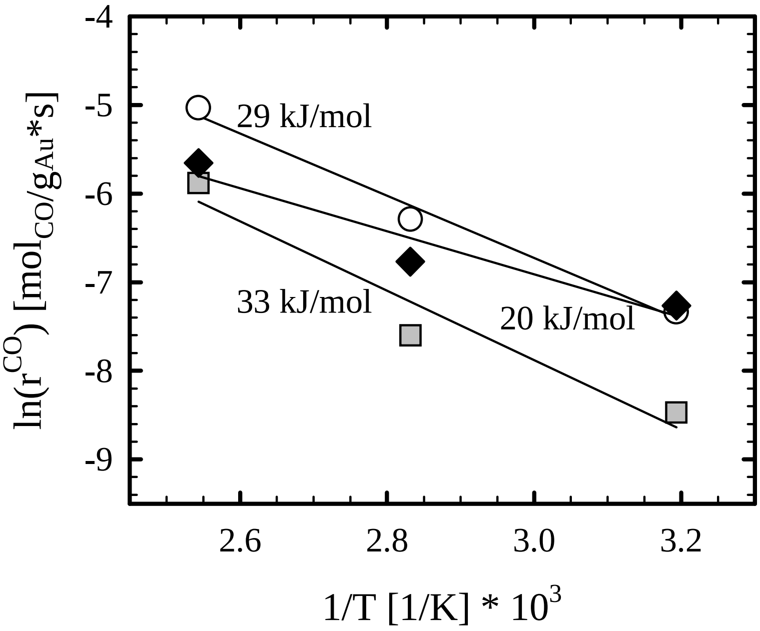

Figure III-67: Arrhenius diagram for the turnover frequency of CO oxidation over Au/α-Fe_2O_3 in idealized reformate (○; 1 kPa CO, λ = 2), a mixture containing 25 kPa CO_2 (▨), and in a realistic reformate (◆; 25 kPa CO_2; 1.3 kPa H_2O).

also more pronounced in the CO_2-rich mixture (-50% compared to -20% in the idealized reformate; measured at similar absolute CO conversion values). With respect to chapter III-3.4 this may well be attributed to an enhanced by-product formation (carbonates / carboxylates) on the support, which was assumed to severely inhibit the CO oxidation reaction.

A very striking effect is the change in selectivity, which decreases absolutely by 15-20% in the presence of CO_2 and even keeps a slightly negative tendency during time on-stream. Other than in the preceeding section, where the water blocked almost exclusively the H_2 oxidation, now predominantly the CO oxidation rate is affected, whereas the conversion of hydrogen, calculated *via* selectivity, is about equal in both gas mixtures (only -20% in the presence of CO_2). Hence the effect of CO_2 on the selective CO oxidation over Au/α-Fe_2O_3 seems to be just the opposite of the water effect described in the preceeding section.

In figure III-67 the temperature dependence (40 - 120°C) of the CO oxidation rate over Au/α-Fe_2O_3 (no. 280598) in different gas mixtures is compared in the form of an Arrhenius diagram. In idealized reformate (1 kPa CO, λ = 2) an activation energy of 29 ± 5 kJ/mol is obtained, which correlates quite well to the 31 kJ/mol determined by Kahlich *et al.* under identical conditions on our sample no. 201196 [26] or to the 35 kJ/mol given by Haruta *et al.* for the CO oxidation without hydrogen over a coprecipitated Au/α-Fe_2O_3 catalyst (0.2 - 6 kPa CO; 1 - 20 kPa O_2) [71].

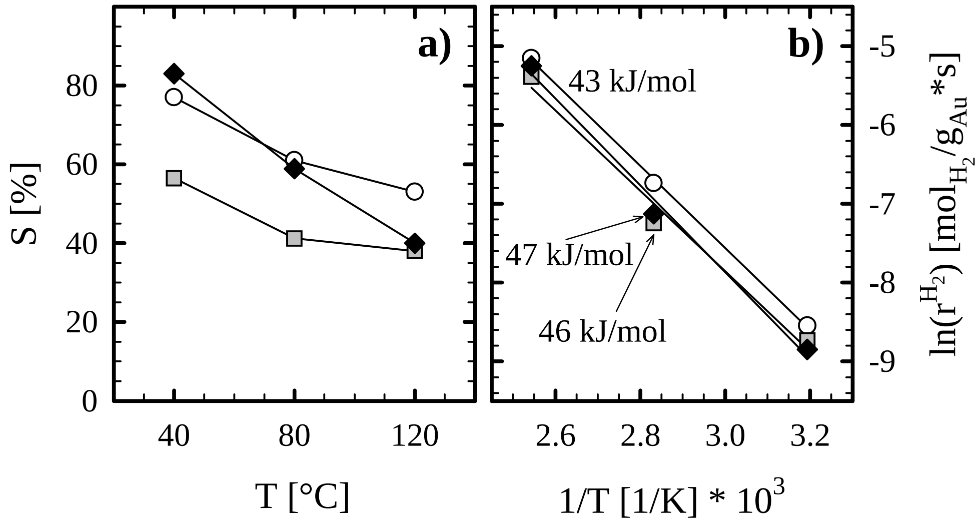

Figure III-68: (a) Selectivity and (b) Arrhenius diagram for the calculated turnover frequency of H_2 oxidation over Au/α-Fe_2O_3 in idealized reformate (○ ; 1 kPa CO, λ = 2), a mixture containing 25% CO_2 (▨), and in a realistic reformate (◆ ; 25 kPa CO_2; 1.3 kPa H_2O).

Upon replacing the nitrogen of the idealized reformate by CO_2 (25 kPa), the reactivity is decreased by a factor 3-4, but the activation energy remains almost constant (33 ± 5 kJ/mol). When 1.3 kPa water is added to the CO_2-containing mixture, the activity is partially restored, an effect, which is more pronounced at lower temperatures. As a consequence the activation energy is reduced to a lower value around 20 kJ/mol (± 5 kJ).

The selectivity (figure III-68a) parallels this behaviour: With 25 kPa CO_2 the selectivity is reduced by about 20% as a consequence of the reduced CO oxidation rate, but the temperature-dependence found for idealized reformate is completely retained. Upon additional admission of water to the reaction mixture, the selectivity behaviour changes and S decreases now linearly with higher temperatures at a very steep slope. In window b (figure III-68) the H_2 oxidation rates, calculated *via* selectivity, are displayed. Quite clearly, the changes are much smaller than for the CO oxidation reaction. In the presence of 25 kPa CO_2, the rate decreases by only 20-40%. And, what is very surprising in view of the preceeding section, in the additional presence of water, the H_2 oxidation rate remains unchanged, hence the influence of water in CO_2-rich mixtures is to restore the CO oxidation reaction and not to suppress the competing H_2 + O_2 reaction as was found for idealized reformate. As a consequence of the minor changes for the rates of the H_2 oxidation the resulting activation energy remains constant at around 45 kJ (± 7 kJ).

To get a better insight into the mechanisms leading to the CO_2-induced poisoning of the CO oxidation over Au/α-Fe_2O_3, we gradually increased the CO_2 content in an idealized reformate

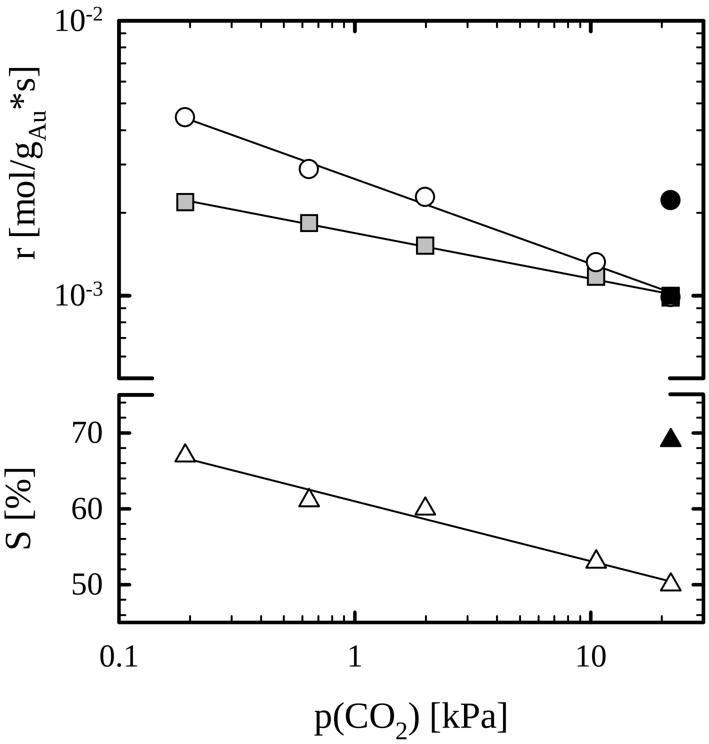

Figure III-69: CO$_2$ dependence of the CO (○) and H$_2$ oxidation activity (▨; upper window) and of the selectivity (△;lower window) over Au/α-Fe$_2$O$_3$ in CO$_2$-containing reformate (1 kPa CO, λ = 2) at 80°C. *black symbols*: after addition of 1.3 kPa H$_2$O.

(1 kPa CO, λ = 2, 9 kPa N$_2$, up to 22 kPa CO$_2$, balance H$_2$) at 80°C (sample no. 280798). This experiment was conducted in a newly designed DRIFTS cell (see appendix A), which allows for a synchronous analysis of IR-bands and conversion data (GC) within very small tolerances.

In figure III-69 the rates for CO and H$_2$ oxidation (upper window) and the corresponding selectivities (lower window) at increasing CO$_2$-contents are displayed (each data point acquired after 30 min.). The selectivity decreases strongly with increasing CO$_2$ content as a direct consequence of the more pronounced reduction of the CO oxidation rate (factor 4-5) compared to the H$_2$ oxidation (only factor 2), ending up at only 50% for a CO$_2$ content similar to real reformates. Upon addition of 1.3 kPa water to this reaction mixture (black symbols) again exclusively the CO oxidation rate is almost restored to its initial value, wheras the competing reaction remains totally unaffected, which leads to a strongly enhanced selectivity of ~70%.

In the IR data obtained simultaneously, shown in figure III-70, a significant blue-shift of the linearly bound CO$_{ad}$-band (from 2110.5 cm^{-1} to 2114.1 cm^{-1}) at higher CO$_2$-contents is seen, accompanied by an increase in the integrated intensity of 25% (Therefore the shift cannot just

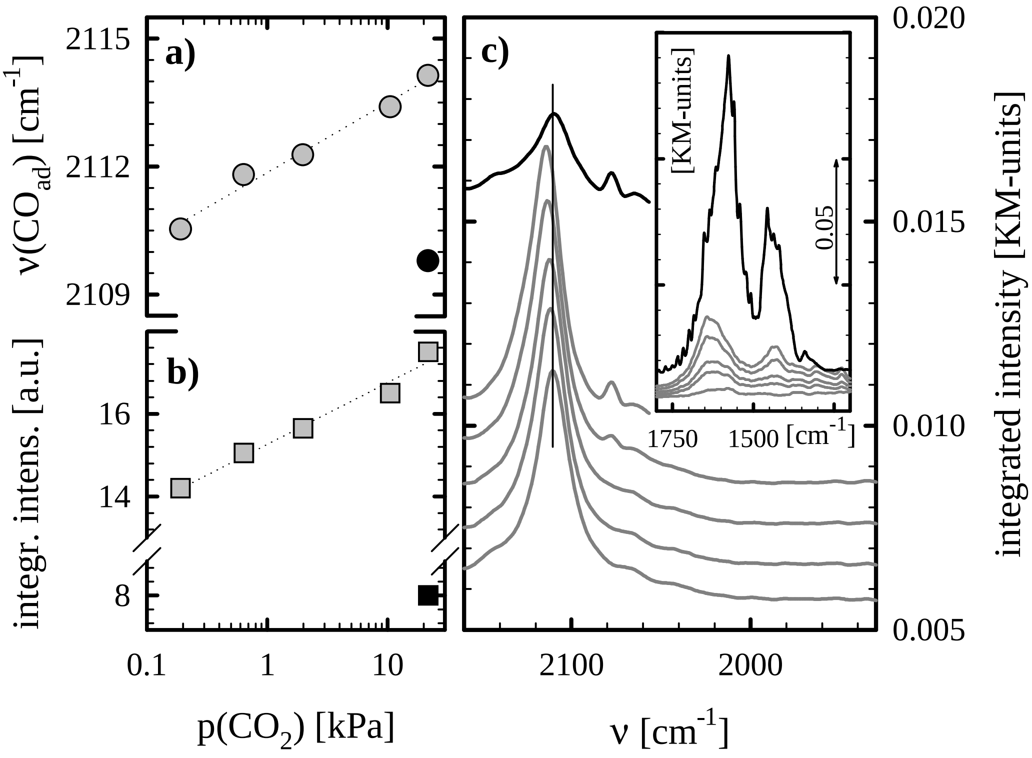

Figure III-70: CO_2 dependence of the DRIFTS CO_{ad}-signal on Au/α-Fe_2O_3 in CO_2-containing reformate: *a)* band position (○), *b)* integrated IR intensitiy (□); *c)* DRIFTS spectra of the CO_{ad}-region (CO_2 content increases upward); *inset*: by-products seen in the DRIFTS spectra; *black symbols / line*: after addition of 1.3 kPa H_2O.

be the result of a reduced CO_{ad} coverage). These effects strongly suggest the coadsorption of CO_2 on the gold particles. CO_2 acts as an electron acceptor, reducing the electron density in the nearby Au-atoms, which should induce such a blue-shift (similar effects for band position and intensity were also observed upon admission of oxygen to a CO / N_2 mixture; see chapter 3.3.2). This coadsorbed CO_2 may either directly block the sites for CO oxidation or alter the reactivity by its electronic influence, characterized by the blue-shift for the CO_{ad}-band. At higher partial pressures of CO_2 a second band evolves in the spectral region for linearly bound CO_{ad} at around 2067 cm^{-1}. It had been neither observed in our own measurements without CO_2 nor reported in any literature study dealing with IR spectroscopy during CO oxidation in CO_2-free mixtures over Au catalysts, therefore it is clearly bound to the presence of coadsorbed CO_2. But the exact nature of this new linearly bound CO_{ad} species is still unknown.

The coadsorption of CO_2 on Au was already suggested in a study from Bollinger and Vannice on a Au/TiO_2 catalyst, where they noticed shoulders at 2320 and 2378 cm^{-1} for a central band at 2342 cm^{-1} (correlated with adsorbed CO_2 on TiO_2), which they assigned to adsorbed CO_2

on the gold particles [253]. They also mention that the CO_2 inhibits the CO oxidation activity and that this effect is reversible, which fits excellently to the mechanistic picture, developed in this section. This model, including coadsorption of CO_2, is also likely in view of studies by the Christmann group on Au(110), where an activation energy for desorption of ~27 kJ/mol was evaluated for the oxygen-precovered surface, which is not too far away from the E_d^* of CO (40 kJ/mol) [302]. Therefore, at such high partial pressures indeed a significant surface coverage is expected.

It is interesting to note, that Schwank reported a reduced activity for the reaction

$$^*CO + CO_2 \leftrightarrow {}^*CO_2 + CO \qquad \text{(III-3.7)}$$

over supported Au catalysts with an increased $p(CO_2)/p(CO)$ ratio, which equally underlines, that CO_2 acts as a poison for the CO adsorption / oxidation [221].

An additional negative contribution for the performance may arise from the adsorption of CO_2 on the support, especially at $Au\text{-}Fe_2O_3$-interface sites, possibly as CO_2^--species, which would inhibit the oxygen supply from the support, as was proposed by Fukushima *et al.*, who observed a negative influence of CO_2 on the CO oxidation over a Au/MgO catalyst ([260]; see also preceeding chapter). But such an effect would be expected to affect both, the CO and H_2 oxidation rate, in the same way.

Upon the addition of 1.3 kPa water the CO_{ad}-band shifts back to the orignal position (figure III-70), but the integrated intensity is strongly decreased and the band becomes somewhat broader. A possible explanation for the reverted band shift is, that adsorbed CO_2 is removed from the Au surface in the presence of water. Indeed in the inset window in figure III-70, which shows the spectral region below 1700 cm^{-1}, a strong increase of bands, assigned to by-products on the support, is noted. Especially the bands at ~1600 and 1450 cm^{-1}, which could be attributed to bicarbonate species, grow strongly (see also section 3.4.2). A possible reaction pathway on a hydrated surface would be:

$$CO_{2ad} + OH^- \rightarrow HCO_3^- \qquad \text{(III-3.8)}$$

Other than in the CO_2-free mixture (idealized reformate), this time the H_2 oxidation is absolutely not affected by the presence of water. But on the one hand, the rate has already been reduced somewhat by the presence of CO_2. Moreover it may be speculated, if an effect which creates oxygen vacancies on the support, as was proposed by Boccuzzi *et al.* for the presence of water ([257]; eq. III-3.6) could be inhibited or compensated in the presence of CO_2.

As a short summary of this chapter it can be recorded, that water and CO_2 exhibit opposite effects on the CO oxidation. H_2O blocks the $H_2 + O_2$ reaction (in a CO_2-free mixture), CO_2 predominatly reduces the CO oxidation activity. Due to the DRIFTS results the latter is attributed to the coadsorption of CO_2 on the gold particles. Additional adsorption on the support may inhibit the oxygen supply and further contribute to the reduced performance. The presence of water in a CO_2-containing mixture releases the inhibition of the CO oxidation. Both effects seem to be more or less additive and, as a consequence, compensate each other. The one-sided nature of the water- and CO_2-effects on either the CO or H_2 oxidation strongly suggest different reaction sites and / or mechanisms for both reactions over Au/α-Fe_2O_3.

3.6 Reverse water-gas shift over Au/α-Fe_2O_3

Since supported gold catalysts are not only active for the low-temperature CO oxidation, but also for a vast variety of other catalytic reactions, *e. g.*, partial oxidation of hydrocarbons, hydrogenation of CO and unsaturated hydrocarbons or reduction of nitrogen oxides [239, 240], recently some groups examined the water-gas shift reaction over such systems and reported an outstanding activity, almost similar to the commercially employed Cu/ZnO catalyst [70, 308, 309].

In this section we will study the reverse water-gas shift reaction

$$CO_2 + H_2 \rightarrow CO + H_2O \qquad \text{(III-3.9)}$$

analogous to the investigations on the above described catalyst systems (see chapters III-1.3.2 and III-2.2.3). Measurements were performed on the sample no. 061197 (for characterization see tables III-10), which turned out to be our most active gold catalyst for CO oxidation. The sample was diluted with α-Al_2O_3, similar to the PROX measurements. The reactant gas mixture contained ~74 kPa, 1.3 kPa H_2O and ~25 kPa CO_2. Data points were taken after 30 min. of reaction before increasing the temperature to the next setpoint.

In figure III-71 the reverse water-gas shift activity (Arrhenius diagram) of Au/α-Fe_2O_3 is compared to that of Pt/γ-Al_2O_3. Obviously both catalysts exhibit approximately the same activity in the temperature interval investigated between 150 and 250°C. The TOF for Au/α-Fe_2O_3 at 150°C is $8.3*10^{-4}$ s^{-1} (corresponding to a rate of $2.1*10^{-6}$ $mol_{CO}/g_{Au}*s$), which is in excellent agreement with the activity of ca. $1*10^{-3}$ s^{-1} ($2*10^{-6}$ $mol_{CO}/g_{Au}*s$) reported by Sakurai *et al.* for Au/Fe_2O_3 in a mixture of 67 kPa H_2, 23 kPa CO_2, balance Ar [308]. When extrapolated to the envisaged temperature level for the selective CO oxdiation of 80°C, a TOF of $1.2*10^{-5}$ s^{-1} ($2.9*10^{-8}$ $mol_{CO}/g_{Au}*s$) is calculated. In earlier measurements by Kahlich *et al.* a similar order of magnitude for the reverse water-gas shift ($< 3*10^{-8}$ $mol_{CO}/g_{Au}*s$) was estimated for the sample no. 201196 at 80°C, but the absolute conversion was too small, to determine more precise values [26]. Since the activity for the selective CO oxidation at 80°C is comparable to that of Pt/γ-Al_2O_3 at 200°C, but the rate for the WGS is significantly lower on the gold catalyst due to the reduced temperature level, the resulting turndown ratio for the load following behaviour in a PROX stage is theoretically improved by almost three orders of magnitude. Hence the Au catalyst should be a suitable catalyst for a final PROX stage in the two stage concept proposed by Kahlich *et al.* [12]. The activation energy for the reverse water-gas shift is 76 kJ/mol, somewhat higher than on the platinum catalysts.

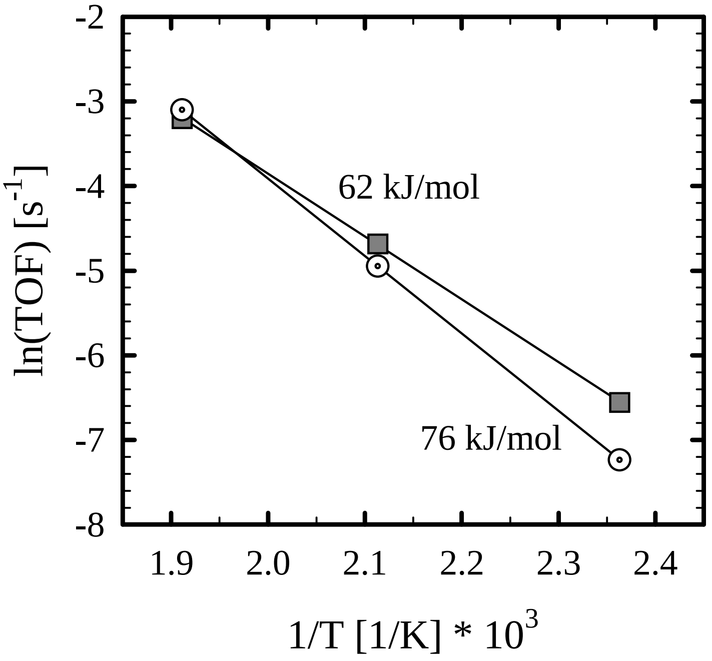

Figure III-71: Arrhenius diagram for the turnover frequency of the reverse water-gas shift reaction on Au/α-Fe_2O_3 (⊙) and Pt/γ-Al_2O_3 (■) in a mixture of 74 kPa H_2, 1.3 kPa H_2O, rest CO_2.

It should be noted that at temperatures above 250°C the measured rates were lower as would be expected from a simple extrapolation in the Arrhenius presentation. This is obviously caused by a progressing reduction of the support to Fe^0 [310] as was also confirmed in subsequent *post-mortem* XPS-measurements.

catalyst	**no.**	**prep.** ($^{T\,[°C]}/_{pH}$) 1)	**Au:Me [at-%]**	**calcination at**	**BET** 2) **[m^2/g]**
Au/α-Fe_2O_3	-	DP ($^{80+60}/_{7.8-8.1+8-8.4}$)	ca. 1	400°C - 30 min.	54 3)
Au/NiO_x	190499	CP ($^{60}/_{8.5}$)	1.7	400°C - 30 min.	67
Au/TiO_2	170899	IMP ($^{60}/_{5-5.5}$)	1.7	400°C - 30 min.	56
Au/CeO_x	130897	CP ($^{80}/_{6.5-7.2}$)	2.5	250°C - 30 min.	91
Au/CeO_x*VO_x	170699	CP ($^{60}/_{5.7}$)	3.7 4)	400°C - 30 min.	
Au/MnO_x	200298	DP ($^{60}/_{7.0+4.5-5}$) 5)	1.0	400°C - 30 min.	
Au/SnO_x	160699D4	DP ($^{60}/_{5-5.3}$)	2.1	400°C - 30 min.	82
Au/$Mg(OH)_2$	200499	CP ($^{60}/_{8.5}$)	1.3	300°C - 30 min.	74
Au/MgO	200499	CP ($^{60}/_{8.5}$)	1.3	400°C - 30 min.	105
Au/γ-Al_2O_3	180799	IMP ($^{60}/_{7.5-8}$)	1.7	400°C - 30 min.	107

1) DP = deposition-precipitation, CP = coprecipitation, IMP = impregnation 2) after calcination
3) statistical average of DP-catalysts in table III-10 4) wt-% 5) from $NaMnO_4$

Table III-12-A: Au catalysts prepared with different support materials (prepared at the ZSW Ulm): preparation & conditioning.

3.7 Other support materials

In chapter III-3.1 we have seen, that the reactivity of gold clusters is significantly enhanced when they are supported on a metal oxide, which is able to supply large amounts of oxygen for the CO oxidation reaction, such as Fe_2O_3. In order to evaluate, whether they are equally suitable, we have tested several other support materials, which have been reported to yield highly active gold catalysts, namely $Mg(OH)_2$ [269, 303], MnO_x [31, 224, 311], NiO_x [234, 265] and TiO_2 [237, 240, 253, 258, 312]. Moreover, we have prepared gold catalysts on metal oxides, which are well known for exhibiting such oxygen storage / adsorption properties when they are combined with platinum metals, *e. g.*, SnO_2 [176-178] or CeO_2 [313-315]. The tested catalysts are listed in table III-12-A (preparation / conditioning methods, Au loading & BET surface).

Figure III-72 provides a graphical illustration for the activity / selectivity tests of the various samples for selective CO oxidation in idealized reformate under our standard conditions (1 kPa CO, $\lambda = 2$; 80°C). Additionally, the activity and selectivity as well as the calculated turnover frequencies are listed in table III-12-B. Quite clearly, the Au/α-Fe_2O_3 samples (grey circles – no. 061197, which was the most active, and no. 280598, an average sample, are displayed; see table III-10-B) show a superior activity and a rather high selectivity, when compared to the other support materials. Only Au/TiO_2 (white diamonds) comes close,

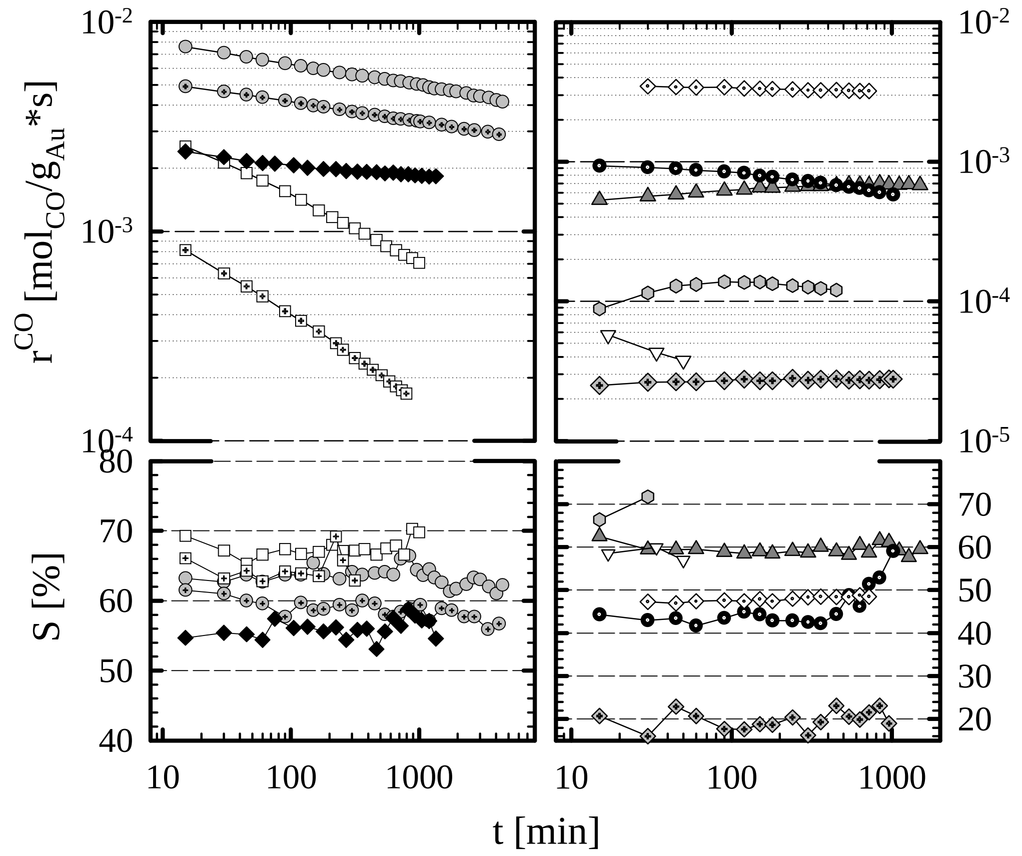

Figure III-72: Activity (*upper window*) and selectivity (*lower window*) of several Au catalysts in idealized reformate (1 kPa CO, $\lambda = 2$; 80°C): ● $Au/\alpha\text{-}Fe_2O_3$ (no. 061197), ⊕ $Au/\alpha\text{-}Fe_2O_3$ (no. 280598), ◆ Au/NiO_x, □ $Au/Mg(OH)_2$, ⊞ Au/MgO, ◇ Au/TiO_2, ▲ $Au/\gamma\text{-}Al_2O_3$, ⊙ Au/SnO_2, ◈ $Au/CeO_x{*}VO_x$, ⬡ Au/MnO_x, ▽ Au/CeO_2.

especially after a few hours on stream, due to its superior long-term stability (only -10% within 1000 min.), but its selectivity is somewhat lower, probably due to the active participation of the titania in the $H_2 + O_2$ reaction *via*

$$2\,Ti^{4+} + H_2 \leftrightarrow 2\,Ti^{3+} + 2\,H^+ \qquad \text{(III-3.10)}$$

$$2\,Ti^{3+} + \tfrac{1}{2}\,O_2 \leftrightarrow 2\,Ti^{4+} + O^{2-} \qquad \text{(III-3.11),}$$

similar to what has been observed for Pt/TiO_2 (see chapter III-1.3.1). A similar redox mechanism probably happens on the vanadium oxide component of the $Au/CeO_x{*}VO_x$, but due to its low activity it is not of interest, anyway. NiO_x also seems to be an interesting support material, increasing the reactivity of Au, when compared, *e. g.*, to Al_2O_3, which is not known to exhibit any oxygen storage properties, but is not as effective as Fe_2O_3 or TiO_2. The enhanced activity of gold supported on these three metal oxides (Fe_2O_3, TiO_2 and NiO_x) as

catalyst	preparation 1)	Au : Me [at-%]	d_{Au} [nm]	p(CO) [kPa]	$p(O_2)$ [kPa]	r (*10^4) [mol_{CO}/g_{Au}*s]	TOF 2) [s^{-1}]	S [%]	E_a [$^{kJ}/_{mol}$]	ref.
Au/FeO_x	DP	2.0	3.6	0.2 - 6 3)	1 - 20 3)	13	0.7	-	35	[71]
	IMP 4)	1.7	2.9	1	20	11 5)	0.5	-	15	[294]
Au/NiO_x	CP	2.0		0.5	10	0.4 - 1.2 5,6)		-		[265]
Au/TiO_x	IMP7)	0.4	33	4.9	4.9	8.1	4.5 8)	-	29	[253]
	DP	1.3	2.9	1	20	33	1.3	-	27	[233]
	IMP 4)	1.8	3	1	20	20 5,9)	0.8			[258, 266]
	IMP 4)	1.2	30	1	20	2.0	0.7	-	12	[258, 267]
	IMP 10)	0.8		1	0.6	0.87		-	32	[316]
Au/MnO_x	CP	2.0	2.8	1	1	0.34 5)	0.02 8)	> 45 11)		[31]
	CP	10		1	0.5	0.09 - 0.13 5,12)		-		[224, 311]
Au/$Mg(OH)_2$	DP	1.5	0.6 - 1.2	1	20	> 51 13)	> 1.2	-		[269]
Au/Al_2O_3	DP	0.2	2.4	1	20	13	0.5	-	32	[270]

1) DP = deposition-precipitation, CP = coprecipitation, IMP = impregnation, CVD = chemical vapor deposition 2) spherical particles assumed for calculation
3) reported reaction orders were zero 4) with phosphine-stabilized Au complex 5) measured at high conversion
6) extrapolated from r =$1.5*10^{-5}$ mol/g_{Au}*s at 20°C with 15 < Ea < 30 kJ/mol 7) pre-reduced at 200°C in H_2 after calcination
8) ca. 2.3 s^{-1}, when calculated for 1 kPa CO and $\lambda = 2$ with the reported reaction orders of 0.5 (CO) and 0.08 (O_2) at 30°C
9) extrapolated from r = $9.6*10^{-3}$ mol/g_{Au}*s at 28°C with E_a = 12 kJ/mol 10) pre-reduced at 500°C 11) reaction mixture contains 98 kPa H_2
12) extrapolated from r = $6*10^{-6}$ mol/g_{Au}*s at 55°C with 15 < E_a < 30 kJ/mol 13) extrapolated from r = $1.2*10^{-4}$ mol/g_{Au}*s at -70°C with E_a > 15

Table III-13: Kinetic data calculated from previous studies (extrapolated to our standard temperature of 80°C) for gold catalysts supported on different support materials.

catalyst	$d_{Support}$ 1) [nm]	d_{Au} 1) [nm]	r *10^4 2) [mol/g_{Au}*s]	TOF 3) [s^{-1}]	S [%]	other
Au/α-Fe_2O_3	16 - 17	2.6 - 7	39	1.3 - 3	65 4)	see tables III-10
Au/NiO_x	9.6	4.3	20	1.2	56	XPS: Ni^{III} after conditioning
Au/TiO_2	21 5)	4.6	33	2.0	48	TiO_2: Degussa P25
Au/CeO_x	4.0 6)	11.0 6)	0.4 7)	0.02	~60	
Au/CeO_x-VO_x			0.28			
Au/MnO_x	amorphous	< 4	1.4 8)	0.04 - 0.09	~70	Mn_2O_3 after conditioning
Au/SnO_x	9.0 8)	14.8 8)	8.2	0.25 - 0.5	43	
Au/$Mg(OH)_2$	13 - 21	< 4	14	0.5 - 0.9	67	
Au/MgO	5.3	6.0	3.8	0.3	64	
Au/γ-Al_2O_3	5 - 11	4.4	6.3	0.35	59	γ-Al_2O_3: Degussa no. 213

1) after calcination (XRD or TEM) 2) after 2 h 3) spherical particles assumed for calculation
4) statistical average of DP-catalysts in table III-10 5) 92% anatase
6) after calcination at 300°C (2 h) 6) after 50 min. 7) after 30 min. 8) after calcination at 800°

Table III-12-B: Au catalysts prepared with different support materials (ZSW Ulm): characterization, activity & selectivity.

well as the measured turnover frequencies are in excellent agreement, when compared to the results of several previous studies – in most cases for the CO oxidation in a pure nitrogen background – , which are summarized in table III-13. Moreover, Au/NiO_x exhibits also a satisfying long-term stability (-23% within 1000 min.) and a selectivity similar to Au/α-Fe_2O_3.

With $Mg(OH)_2$ and γ-Al_2O_3, which should be „inert“ support materials (especially the latter), nevertheless quite active catalysts are produced, exhibiting turnover frequencies only one order of magnitude lower than with the reducible metal oxides. But in contrast, their activity strongly depends on the size of the gold clusters and is only high for very small particles, which probably causes the lower TOFs on our samples when compared to the literature values in table III-13. A similar trend was recognized by Okumura *et al.*, who showed that even for Au/SiO_2 high turnover frequencies are obtained, if only the gold clusters are prepared small enough, which was achieved by a CVD method [270]. As was already discussed in chapter III-3.1.2 the dissociative oxygen adsorption proceeds probably directly on the Au clusters for these systems and decreases rapidly with increasing particle size, which in turn causes a reduced activity. Consequently „Au/MgO“, *i. e.*, the Au/$Mg(OH)_2$ catalysts conditioned at higher temperatures, shows an even lower rate and TOF, which is caused by the enhanced sintering of the gold clusters during calcination. A major drawback to the Au/magnesia catalysts is their very rapid deactivation (-80-90% within 1000 min.), probably a consequence of the fast formation of a closed $MgCO_3$ surface layer (monitored by TGA), which blocks the adsorption of further reactants and was also observed in XRD after 3 days in reformate feed gas [274].

For Au/MnO_x, which was proposed for the selective CO oxdiation by Torres Sanches *et al.* [31], a rather low reactivity was noticed, but the absolute values are again in good agreement with the literature values. A possible explanation for the poor performance could be the strong tendency for the formation of bulk $MnCO_3$, which would occur from the produced CO_2.

The catalyst samples, supported on CeO_2, SnO_2 and on a mixed oxide CeO_2*VO_2, yielded dissappointingly low TOFs, although a small enhancing effect for the SnO_2 is visible, when it is compared to Au/γ-Al_2O_3. But if we consider the support particle diameters obtained by XRD, it is obvious, that the gold particles are considerably larger than the metal oxide particles, which counteracts the formation of a large and reactive metal-support interface. Moreover, the selectivity of Au/SnO_2 is quite low with only 44%, which is also more similar to unsupported gold [234] and therefore underlines the very imperfect interface formation on this sample.

In summary we may conclude, that Fe_2O_3 and TiO_2 supports yield the most active catalysts due to their oxygen adsorption properties. Au/α-Fe_2O_3 owns the better selectivity, nevertheless Au/TiO_2 is interesting, since it exhibits a better long-term stability and, seen from the engineeric point of view, may allow for a much more simple preparation of formed catalysts (*e. g.*, pellets). Gold catalysts on non-reducible oxides (*e. g.*, $Mg(OH)_2$, Al_2O_3) are only active, when the Au is in a highly dispersed state, but none of our samples could match the superior activity of the Au/α-Fe_2O_3 or Au/TiO_2 samples. Au/CeO_2 or Au/SnO_x may be promising new candidates, but the preparation procedure needs to be improved, so that larger support particles are obtained after conditioning (*e. g.*, by an impregnation method). These samples are currently produced, and the results will be published later.

3.8. Summary on gold catalysts

On the molecular level of the CO oxidation on supported gold catalyst we have seen that the reaction proceeds between CO_{ad} and O_{ad} adsorbed on the metal component. Whereas CO adsorbs directly on the gold, on active support materials (FeO_x, NiO_x, TiO_2) the oxygen is supplied *via* the support, where it adsorbs in the form of molecular species and dissociates subsequently at the Au-MeO_x interface. This mechanism explains the observed independence of the turnover frequency from the gold particle size for Au/α-Fe_2O_3, but involves also a strong dependence on the interface structure. In general, those samples, which were prepared predominantly from a ferrihydrite precursor, yield the smallest Au particles after conditioning. The best activity is achieved after calcination at 300-400°C, when the gold is present as Au^0. Na-residuals from the preparation step seem to have only a small direct influence on the turnover frequency, but induce sintering of the gold particles during calcination.

The CO coverage at our reaction conditions in idealized reformate (up to 1 kPa CO, $\lambda = 2$; 20 - 120°C) is far from saturation. Based on a comparison of our DRIFTS results with published values it is estimated to be ≤ 0.2 ML. The low surface coverage explains the strong dependence of θ_{CO} upon the partial CO pressure, corresponding to the middle, steep regime of a Langmuir adsorption isotherme, as well as the observed decoupling of the H_2 and CO oxidation reaction. As a consequence, this leads to the observed decrease of selectivity with decreasing p_{CO}. It also rationalizes the temperature dependence for the CO reaction order, which was noticed in our kinetic investigations.

The Au/α-Fe_2O_3 catalysts slowly loose activity during storage („off-line deactivation“), caused by a slow, irreversible crystallization process of the initially amorphous support, and during the PROX reaction („on-line deactivation“). The latter shows large gradual differences on the various samples, being less severe and rather reversible on those catalysts with a very amorphous support structure. The accumulation of carbonates / carboxylates during time on-stream on the support and at the interface is believed to be responsible for the slow decrease of reactivity. The deactivation is mitigated in the presence of water, which decomposes the poisonous by-products *via* formation of less stable bicarbonate species, resulting in a reduced decrease of conversion rates at integral flow conditions.

When proceeding to more realistic reformates, we note, that the presence of water strongly enhances the selectivity in idealized reformate (+ 15-20% at 1.3 kPa H_2O) by suppressing the H_2 oxidation reaction, but the exact nature of this effect could not be elucidated. CO_2 exhibits the opposite effect, a strong poisoning of the CO oxidation, leading to a reduced selectivity by ~20% (at 25 kPa CO_2), which is suspected to be caused by the coadsorption of CO_2 on the gold or at interfacial sites. As a result of the enhanced carbonate / carboxylate formation in the presence of CO_2, also the „on-line“ deactivation intensifies. Fortunately, the presence of H_2O compensates the negative effects arising from the presence of CO_2, which in the end should results in an excellent performance of Au/α-Fe_2O_3 catalysts in real mixtures from steam reformed methanol.

The low operation temperature level (ca. 80°C) along with a slightly larger activation energy for the reverse water-gas shift reaction leads to a drastically improved turndown ratio for the load following behaviour of the PROX stage in mobile applications, when compared to that of standard platinum metal catalysts.

When comparing different gold / metal oxide systems, the activity of Au/TiO_2 comes close to the performance of our Au/α-Fe_2O_3 catalyst. The slectivity is slightly lower, but the long-term stability is superior. Other combinations, like, *e. g.*, Au/SnO_2, may also be active, but the preparation still needs to be improved, in order to optimized the metal-support interface.

In summary, Au/α-Fe_2O_3 catalysts should be excellently suitable for the envisaged PROX application due to their high reactivity, relative „inertness“ towards mixtures containing water and CO_2 and their large PROX / shift ratio at the envisaged operation temperature level of around 80°C.

We believe, that the performance of todays „simple“ supported gold system is near the maximum achievable level, since the gold particle size is already close to the lower limit with ~2.5 nm. With other support material (*e. g.*, TiO_2) the industrial production of formed catalyst samples may be facilitated, but in the end these oxides will barely exceed the enhancing properties of the iron oxide, since diffusion of oxygen is not the rate limiting step on these catalysts. Improved catalysts may be gained from modifying the metal component by alloying with other metals, which would increase the adsorption energy and therefore also the resulting CO_{ad} coverage and hence lead to a better selectivity and perhaps also higher reactivity (at least at low CO concentrations). An interesting candidate, *e. g.*, could be gold-copper alloys, since the second component is quite cheap and the alloy formation probably would decrease the nobility of the gold but increase it for the copper.

IV. SUMMARY & FUTURE PERSPECTIVES

In the previous chapters we have studied three different catalyst systems for the selective CO oxidation in H_2-rich gas: pure Pt catalysts (especially Pt/γ-Al_2O_3), a platinum catalyst modified by alloy formation with another metal (Pt_3Sn/Vulcan) and gold catalysts (in particular Au/Fe_2O_3). Compared to standard Pt catalysts which require higher temperatures above 150°C to operate at reasonable rates, the latter low temperature PROX catalysts are characterized by a combination of facile oxygen adsorption and largely inhibited hydrogen adsorption under reaction conditions. This can be achieved either by an active material that is inert for both, hydrogen and oxygen adsorption, but allows for CO adsorption, and where oxygen adsorption proceeds on the support material (*i. e.*, Au/Fe_2O_3), or by a material that would be active for adsorption of all reaction partners, but which is blocked for hydrogen and consequently also for oxygen adsorption by a CO adlayer. In the latter case oxygen adsorption, but not hydrogen adsorption, must be possible on the support material or on oxidic islands on the metal particles themselves (Pt_3Sn/Vulcan). In all of these cases the oxidation reactions will take part at the interface between the different areas, or *via* a spill-over process. In all of these cases the reaction is not limited by CO desorption, which is the limiting factor for the PROX reaction on Pt catalysts at temperatures below 150°C.

For all three catalyst systems, the selectivity is a function of the steady-state CO coverage under operation conditions. On Pt/γ-Al_2O_3 the saturation coverage, which is maintained over a large range of operation conditions, leads to a rather constant selectivity by the blocking of the hydrogen adsorption. On the low-temperature catalysts the selectivity is also very high due to the high activation barrier for dissociative hydrogen adsorption. However, on the latter it decreases very fast at decreasing CO partial pressures or increasing temperatures as a result of the reduced CO surface coverage.

All investigated systems show a more or less severe tendency for deactivation during time on-stream, but the reasons and therefore the degree of reversibility are very different. The CO self-poisoning on Pt as well as the blocking by surface carbonate / carboxylate species on the recently prepared Au/Fe_2O_3 catalysts are easily relieved, whereas the irreversible deactivation on Pt_3Sn/Vulcan, which is probably the result of a slow segregation effect, constitutes a major drawback for its technical application.

Upon changing the reaction atmosphere from a simplified composition without CO_2 and H_2O, which was used in most of our kinetic experiments (*e. g.*, [7, 12, 26]), to more realistic simulations of a real methanol reformer gas, we found that the platinum-based systems suffer especially from large H_2O-contents, which decrease the selectivity significantly. Au/α-Fe_2O_3 is more sensitive to CO_2, but this effect is almost outweighted by the presence of water, therefore this catalyst seems to be the best suited system for an application in real reformate. Nevertheless, the effects of H_2O and CO_2 are of such a moderate extent, that the approach *via* idealized reformate indeed seems to provide a reasonable basis for quite accurate reactor calculations.

Within this work we have introduced two low-temperature alternatives for the PROX reaction, which should be both capable of removing completely the CO impurities from a methanol reformer feed gas stream. We have explained their high activity as well as the selectivity behaviour. On basis of this mechanistic understanding new future catalyst systems may be designed, which are even more effective. One may think of platinum alloys containing other elements (*e. g.*, Co, Fe, Ni or Ti), which may lead to the formation of more stable bimetallic particles or of alloyed gold catalysts (*e. g.*, Au-Ti or Au-Cu), where the extremely noble character of the gold is mitigated, which would increase the steady-state CO coverage.

V. REFERENCES

[1] T. Engel and G. Ertl, *Adv. Catal.,* **28** (1979) 1

[2] J. A. Rodriguez and D. W. Goodman, *Surf. Sci. Rep.,* **14** (1991) 1

[3] B. E. Nieuwenhuys in „*Elementary Reaction Steps in Heterogeneous Catalysis*“, R. W. Joyner, R. A. van Santen, eds., Kluwer Academic Publishers, Dodrecht (1993) 155

[4] S. H. Oh and R. M. Sinkevitch, *J. Catal.,* **142** (1993) 254

[5] J. R. Stetter and K. F. Blurton, *Ind. Eng. Chem. Prod. Res. Dev.,* **19** (1980) 214

[6] M. Watanabe, H. Uchida, H. Igarashi, and M. Suzuki, *Chem. Lett*, (1995) 21

[7] M. J. Kahlich, H. A. Gasteiger, and R. J. Behm, *J. Catal.,* **171** (1997) 93

[8] E. Riedel, „*Anorganische Chemie*“, 2nd edition, de Gruyter, Berlin (1990)

[9] M. J. Kahlich, *Diploma thesis,* University of Ulm (1996)

[10] E. G. Pow, M. Talaba, L. McNeilly, D. S. Watkins, and D. A. Lines, US Patent, 5,316,747 (issued 9. 10. 1994)

[11] R. F. Buswell, R. Cohen, L. McNeilly, and D. S. Watkins, US Patent, 5,750,076 (issued 12. 5. 1999)

[12] M. J. Kahlich, H. A. Gasteiger, and R. J. Behm, *J. New Mat. Electrochem. Systems,* **1** (1998) 39

[13] Daimler Benz AG, Brochure „*Necar II - Fahren ohne Emissionen*“ (1996)

[14] R. A. Lemons, *J. Power Sources,* **29** (1990) 251

[15] J. Schulz, *Spektrum der Wissenschaft,* **April** (1993)

[16] S. Kawatsu, *J. Power Sources,* **71** (1998) 150

[17] D. P. Wilkinson and D. Thompsett in "*New Materials for Fuel Cell and Modern Battery Systems II*", 6.-10.07.97, Montreal, Savadogo, O. and Roberge, P. R., Eds., Ecole Polytechnique de Montreal, (1997) 266

[18] J. C. Amphlett, R. F. Mann, and B. A. Pappley, *Int. J. Hydrogen Energy,* **21** (1996) 673

[19] „*CRC Handbook of Chemistry and Physics*“, 66th edition, Weast, R. C., ed., CRC Press, Boca Raton (1985)

[20] S. Gottesfeld, US Patent, 4,910,099 (issued 20. 3. 1990)

[21] G. J. K. Acres, J. C. Frost, G. A. Hards, R. J. Potter, T. R. Ralph, D. Thompsett, G. T. Burstein, and G. J. Hutchings, *Catal. Today,* **38** (1997) 393

[22] K. Sekizawa, S.-I. Yano, K. Eguchi, and H. Arai, *Appl. Catal. A: General*, **169** (1998) 291

[23] T. R. Ralph, *Plat. Met. Rev.*, **41** (1997) 102

[24] G. Colsman, *Berichte des FZ Jülich,* **3127** (1995)

[25] M. J. Kahlich, *Dissertation*, University of Ulm (2000)

[26] M. J. Kahlich, H. A. Gasteiger, and R. J. Behm, *J. Catal.*, **182** (1999) 430

[27] M. L. Brown, A. W. Green, G. Cohn, and H. C. Andersen, *Ind. Eng. Chem.,* **52** (1960) 841

[28] C. Plog, W. Maunz, T. Stengel, and R. Andorf, EU Patent, 0,650,923 A1 (issued 3. 5. 1995)

[29] T. Hara, K. Kato, and N. Takada, US Patent, 5,648,182 (issued 15. 7. 1997)

[30] M. Sato and K. Shiraishi, US Patent, 5,658,681 (issued 19. 8. 1997)

[31] R. M. Torres Sanchez, A. Ueda, K. Tanaka, and M. Haruta, *J. Catal.*, **168** (1996) 125

[32] M. M. Schubert, *Diploma thesis*, University of Ulm (1996)

[33] O. Levenspiel, „*Chemical Reaction Engineering*“, John Wiley & Sons, New York (1972)

[34] M. J. Kappers and J. H. van der Maas, *Catal. Lett.*, **10** (1991) 365

[35] R. Queau, D. Labroue, and R. Poilblanc, *J. Catal.*, **69** (1981) 249

[36] G. Blyholder, *J. Phys. Chem,* **68** (1964) 2772

[37] R. M. Hammaker, S. A. Francis, and R. R. Risches, *Spectrochim. Acta,* **21** (1965) 1295

[38] A. Crossley and D. A. King, *Surf. Sci.,* **68** (1977) 528

[39] M. Primet, *J. Catal.,* **88** (1984) 273

[40] M. J. Kappers, *Dissertation*, University of Utrecht (1993)

[41] A. Drochner, M. Fehlings, K. Krauß, and H. Vogel, *GIT Labor-Fachzeitschrift,* **5/99** (1999) 476

[42] J. J. Benitez, I. Carrizosa, and J. A. Odriozola, *Appl. Spec.,* **47** (1993) 1761

[43] J.-D. Grunwaldt, M. Maciejewski, O. S. Becker, P. Fabrizioli, and A. Baiker, *J. Catal.,* **186** (1999) 458

[44] J. J. Benitez, I. Carrizosa, and J. A. Odriozola, *Appl. Surf. Sci.,* **84** (1995) 391

[45] R. S. S. Murthy, J. P. Blitz, and D. E. Leyden, *Anal. Chem.,* **58** (1986) 3167

[46] B. M. Weckhuysen and R. A. Schoonheydt, *Catal. Today,* **49** (1999) 441

[47] H. G. Hecht, *Appl. Spec.,* **37** (1983) 348

[48] P. Kubelka and F. Munk, *Z. Tech. Phys.,* **11** (1931) 593

[49] M. P. Fuller and P. R. Griffiths, *Anal. Chem.,* **50** (1978) 1906

[50] P. R. Griffiths and J. A. de Haseth, „*Fourier Transform Infrared Spectroscopy*“, John Wiley & Sons, New York (1986)

[51] B. C. Smith, „*Fundamentals of Fourier Transform Infrared Spectrometry*“, CRC Press, Boca Raton (1996)

[52] I. M. Hamadeh, D. King, and P. R. Griffiths, *J. Catal.,* **88** (1984) 264

[53] D. J. J. Fraser and P. R. Griffiths, *Appl. Spec.,* **44** (1990) 193

[54] Harrick Scientific Corporation, Pamphlet „*Diffuse Reflection Attachment*“ (1994)

[55] T. Hattori, K. Shirai, M. Niwa, and Y. Murakami, *Bull. Chem. Soc. Jpn.,* **54** (1981) 1964

[56] K. van Every and P. R. Griffiths, *Appl. Spec.,* **45** (1991) 347

[57] P. J. Brimmer and P. R. Griffiths, *Appl. Spec.,* **42** (1988) 242

[58] Harrick Scientific Corporation, Pamphlet „*Reaction Chamber for the Praying Mantis Diffuse Reflectance Attachment*“ (1993)

[59] R. L. White, *Appl. Spec.,* **46** (1992) 1509

[60] R. Barth, R. Pitchai, R. L. Anderson, and X. E. Verykios, *J. Catal.,* **116** (1989) 61

[61] S. A. Yeboah, S.-H. Wang, and P. R. Griffiths, *Appl. Spec.,* **2** (1984) 259

[62] D. A. Shirley, *Phys. Rev. B,* **5** (1972) 4709

[63] G. Feldmeyer, *Dissertation*, University of Ulm (2000)

[64] H. Schubert, U. Guntow, K. Hofmann, and R. Schlögl, *Fresenius J. Anal. Chem.,* **356** (1996) 127

[65] S. Hackenberg, *Diploma thesis*, University of Ulm (1996)

[66] S. Hackenberg, *Dissertation*, University of Ulm (2000)

[67] J. T. Gleaves, J. R. Ebner, and T. C. Kuechler, *Catal. Rev. Sci. Eng.,* **30** (1988) 49

[68] J. W. Niemantsverdriet, „Spectroscopy in Catalysis“, VCH, Weinheim (1995)

[69] D. Andreeva, V. Idakiev, T. Tabakova, and A. Andreev, *J. Catal.,* **158** (1996) 354

[70] D. Andreeva, T. Tabakova, V. Idakiev, P. Christov, and R. Giovanoli, *Appl. Catal. A: General,* **169** (1998) 9

[71] M. Haruta, S. Tsubota, T. Kobayashi, H. Kageyama, M. J. Genet, and B. Delmon, *J. Catal.,* **144** (1993) 175

[72] S. Lin and M. A. Vannice, *Catal. Lett.,* **10** (1991) 47

[73] O. Heudorfer, *Diploma Thesis*, FH Ravensburg-Weingarten (1996)

[74] N. W. Cant, P. C. Hicks, and B. S. Lennon, *J. Catal.,* **54** (1978) 372

[75] J. Sarkany and R. D. Gonzalez, *Appl. Catal.,* **5** (1983) 85

[76] Y.-E. Li, D. Boecker, and R. D. Gonzalez, *J. Catal.,* **110** (1988) 319

[77] Y. J. Mergler, A. van Aalst, J. van Delft, and B. E. Nieuwenhuys, *Appl. Catal. B: Environmental,* **10** (1996) 245

[78] J. G. E. Cohn, US Patent, 3,216,782 (issued 9. 11. 1965)

[79] J. C. Bonacci, T. G. Otchy, and T. Ackerman, US Patent, 4,238,468 (issued 21. 12. 1980)

[80] J. H. Kolts, P. A. Tooley, and S. H. Brown, US Patent, 5,017,357 (issued 1991)

[81] N. E. Vanderborgh, T. V. Nguyen, and J. Guante, US Patent, 5,271,916 (issued 1993)

[82] H. K. Straschil and W. Egbert, German Patent, 1,567,492 C3 (issued 22. 11. 1999)

[83] M. J. Kahlich, M. M. Schubert, M. Hüttner, M. Noeske, H. A. Gasteiger, and R. J. Behm in "*New Materials for Fuel Cells and Modern Battery Systems II*", July 06.-10., Montreal, Savadogo, O. and Roberge, P. R., Eds., Ecole Polytechnique de Montreal, (1997) 642

[84] H. Muraki, S.-I. Matunaga, H. Shinjoh, M. S. Wainwright, and D. L. Trimm, *J. Chem. Tech. Biotechnol.,* **52** (1991) 415

[85] D. W. Dabill, S. J. Gentry, H. B. Holland, and A. Jones, *J. Catal.,* **53** (1978) 164

[86] N. D. Hoyle, P. Kumarasamy, V. A. Self, P. A. Sermon, and M. S. W. Vong, *Catal. Today,* **47** (1999) 45

[87] R. Dümpelmann, N. W. Cant, and D. L. Trimm, *Catal. Lett.,* **32** (1995) 357

[88] P. J. Berlowitz, C. H. F. Peden, and D. W. Goodman, *J. Chem. Phys.,* **92** (1988) 5213

[89] T. A. Nijhuis, M. Makkee, A. D. van Langenveld, and J. A. Moulijn, *Appl. Catal. A: General,* **164** (1997) 237

[90] L. K. Verheij, M. B. Hugenschmidt, L. Cölln, B. Poelsema, and G. Comsa, *Chem. Phys. Lett.,* **166** (1990) 523

[91] S. Ljungström, B. Kasemo, A. Rosen, T. Wahnström, and E. Fridell, *Surf. Sci.,* **216** (1989) 63

[92] B. E. Hayden, K. Kretzschmar, A. M. Bradshaw, and R. G. Greenler, *Surf. Sci.,* **149** (1985) 394

[93] R. G. Greenler, K. D. Burch, K. Kretzschmar, R. Klauser, A. M. Bradshaw, and B. E. Hayden, *Surf. Sci.,* **152/153** (1985) 338

[94] B. E. Hayden and A. M. Bradshaw, *Surf. Sci.,* **125** (1983) 787

[95] G. Ertl, M. Neumann, and K. M. Streit, *Surf. Sci.,* **64** (1977) 393

[96] J. S. Luo, R. G. Tobin, D. K. Lambert, G. B. Fisher, and C. L. DiMaggio, *Surf. Sci.,* **274** (1992) 53

[97] M. R. McClellan, J. L. Gland, and F. R. McFeeley, *Surf. Sci.,* **112** (1981) 63

[98] R. A. Shigeishi and D. A. King, *Surf. Sci.,* **58** (1976) 379

[99] B. N. J. Persson, F. M. Hoffmann, and R. Ryberg, *Phys. Rev. B,* **34** (1986) 2266

[100] Y. Y. Yeo, L. Vattuone, and D. A. King, *J. Chem. Phys.,* **106** (1997) 392

[101] C. T. Campbell, G. Ertl, H. Kuipers, and J. Segner, *Surf. Sci.,* **107** (1981) 207

[102] J. L. Gland and E. B. Kollin, *J. Chem. Phys.,* **78(2)** (1983) 963

[103] E. G. Seebauer, A. C. F. Kong, and L. D. Schmidt, *Surf. Sci.,* **176** (1986) 134

[104] D. M. Collins and W. E. Spicer, *Surf. Sci.,* **69** (1977) 85

[105] T. H. Lin and G. A. Somorjai, *Surf. Sci.,* **107** (1981) 573

[106] R. W. McCabe and L. D. Schmidt, *Surf. Sci.,* **66** (1977) 101

[107] J. T. Yates, *J. Vac. Sci. Technol. A,* **13(3)** (1995) 1359

[108] T. E. Jackman, J. A. Davies, D. P. Jackson, W. N. Unertl, and P. R. Norton, *Surf. Sci.,* **120** (1982) 389

[109] J. Fair and R. J. Madix, *J. Chem. Phys.,* **73(7)** (1980) 3480

[110] P. Hollins, *Surf. Sci. Rep.,* **16** (1992) 51

[111] S. L. Bernasek, K. Lenz, B. Poelsema, and G. Comsa, *Surf. Sci.,* **183** (1987) L319-L324

[112] D. H. Parker, D. A. Fischer, J. Colbert, B. E. Koel, and J. L. Gland, *Surf. Sci.,* **258** (1991) 75

[113] P. R. Norton, J. A. Davies, and T. E. Jackman, *Surf. Sci.,* **121** (1982) 103

[114] B. Poelsema, G. Mechtersheimer, and G. Comsa, *Surf. Sci.,* **111** (1981) 519

[115] B. Klötzer and E. Bechthold, *Surf. Sci.,* **295** (1993) 374

[116] C. S. Shern, *Surf. Sci.,* **264** (1992) 171

[117] K. Christmann and G. Ertl, *Surf. Sci.,* **60** (1976) 365

[118] E. Hahn, A. Fricke, H. Röder, and K. Kern, *Surf. Sci.,* **297** (1993) 19

[119] D. Hoge, M. Tüshaus, and A. M. Bradshaw, *Surf. Sci.,* **207** (1988) L935-L942

[120] D. H. Parker, D. A. Fischer, J. Colbert, B. E. Koel, and J. L. Gland, *Surf. Sci. Lett.,* **236** (1990) L372-L376

[121] M. A. Henderson and J. T. Yates, *Surf. Sci.,* **268** (1992) 189

[122] H. Wang, R. G. Tobin, D. K. Lambert, G. B. Fisher, and C. L. DiMaggio, *Surf. Sci.,* **330** (1995) 173

[123] H. Wang, R. G. Tobin, and D. K. Lambert, *J. Chem. Phys.,* **101** (1994) 4277

[124] C. S. Kim, C. Korzeniewski, and W. J. Tornquist, *J. Chem. Phys.,* **100** (1994) 628

[125] M. M. Schubert, M. J. Kahlich, G. Feldmeyer, M. Hüttner, S. Hackenberg, H. A. Gasteiger, and R. J. Behm, *J. Catal.,* in preparation

[126] N. W. Cant, *J. Catal.,* **62** (1980) 173

[127] R. H. Nibbelke, M. A. J. Campman, J. H. B. J. Hoebink, and G. B. Marin, *J. Catal.,* **171** (1997) 358

[128] N. W. Cant and D. E. Angove, *J. Catal.,* **97** (1986) 36

[129] F. Zaera, J. Liu, and M. Xu, *J. Chem. Phys.,* **106** (1997) 4204

[130] J. A. Anderson, *J. Chem. Soc. Faraday Trans.,* **88** (1992) 1197

[131] D. M. Haaland and F. L. Williams, *J. Catal.,* **76** (1982) 450

[132] M. J. Kahlich, H. A. Gasteiger, and R. J. Behm, *poster contribution at „XXXII. Jahrestreffen deutscher Katalytiker*", 17.-19.3, Friedrichroda, Germany (1999)

[133] M. M. Schubert, H. A. Gasteiger, and R. J. Behm, *J. Catal.,* **172** (1997) 256

[134] Y. Fu, L. Kraus, and H. Knözinger, *J. Molec. Catal.,* **52** (1989) 113

[135] A. T. Bell, *J. Molec. Catal. A,* **100** (1995) 1

[136] A. A. Davydov, *„Infrared Spectroscopy of Adsorbed Species on the Surface of Transition Metal Oxides*", C. H. Rochester, ed., John Wiley & Sons, Chichester (1990)

[137] J. L. Robbins and E. Marucchi-Soos, *J. Phys. Chem,* **93** (1989) 2885

[138] Y. Fu, L. Kraus, M. I. Zaki, C. Kappenstein, B. Tesche, and H. Knözinger, *J. Molec. Catal.,* **44** (1988) 295

[139] J. A. Anderson and C. H. Rochester, *Catal. Today,* **10** (1991) 275

[140] J. J. Benitez, R. Alvero, M. J. Capitan, I. Carrizosa, and J. A. Odriozola, *Appl. Catal.,* **71** (1991) 219

[141] J. J. Benitez, R. Alvero, I. Carrizosa, and J. A. Odriozola, *Catal. Today,* **9** (1991) 53

[142] P. Mars, J. J. F. Scholten, and P. Zwietering, *Adv. Catal.,* **14** (1963) 35

[143] M. R. Columbia, A. M. Crabtree, and P. A. Thiel, *J. Am. Chem. Soc.,* **114** (1992) 1231

[144] J. J. Benitez, I. Carrizosa, and J. A. Odriozola, *J. Chem. Soc. Faraday Trans.,* **89** (1993) 3307

[145] M. M. Schubert, M. J. Kahlich, M. Hüttner, S. Hackenberg, H. A. Gasteiger, and R. J. Behm, *poster contribution at „Catalysis: Fundamentals and Practice*" 14.-18.09, York (1997)

[146] J. Sarkany, M. Bartok, and R. D. Gonzalez, *J. Catal.,* **81** (1983) 347

[147] F. Solymosi, *J. Molec. Catal.,* **65** (1999) 337

[148] D. Wolf, M. Barre-Chassonnery, M. Höhenberger, A. van Veen, and M. Baerns, *Catal. Today,* **40** (1998) 147

[149] S. Akhter and J. M. White, *Surf. Sci.,* **171** (1986) 527

[150] B. L. Mojet, J. T. Miller, and D. C. Koningsberger, *J. Phys. Chem. B,* **103** (1999) 2724

[151] A. Szabo, M. A. Henderson, and J. T. Yates, *J. Chem. Phys.,* **96** (1992) 6191

[152] S. Fuchs, T. Hahn, and H.-G. Lintz, *Chem. Engin. Proc.,* **33** (1994) 363

[153] N. W. Cant, *J. Catal.,* **74** (1982) 411

[154] C. Hardacre, R. M. Ormerod, and R. M. Lambert, *Chem. Phys. Lett.,* **206** (1993) 171

[155] K. Eberle, B. Rohland, J. Scholta, and R. Stroebel, German Patent, 19,615,562 C1 (issued 9. 10. 1997)

[156] J. C. Trocciola, C. R. Schroll, and R. R. Lesieur, US Patent, 5,330,727 (issued 19. 7. 1994)

[157] M. S. Spencer, *Catal. Lett.,* **32** (1995) 9

[158] Y. Amenomiya and G. Pleizier, *J. Catal.,* **76** (1982) 345

[159] A. Basinska, L. Kepinski, and F. Domka, *Appl. Catal. A: General,* **183** (1999) 143

[160] A. Erdöhelyi, K. Fodor, and G. Suru, *Appl. Catal. A: General,* **139** (1996) 131

[161] G. C. Chinchen and M. S. Spencer, *J. Catal.,* **112** (1988) 325

[162] D. C. Grenoble, M. M. Estadt, and D. F. Ollis, *J. Catal.,* **67** (1981) 90

[163] K. Kochloefl in „*Handbook of Heterogeneous Catalysis*“, G. Ertl, H. Knözinger, and J. Weitkamp, eds., VCH, Weinheim (1997) 1831

[164] M. R. Columbia and P. A. Thiel, *J. Electroanal. Chem.,* **369** (1994) 1

[165] R. F. Buswell, R. Cohen, L. McNeilly, and D. S. Watkins, US Patent, 5,518,705 (issued 21. 5. 1999)

[166] P. C. H. Mitchell, P. Wolohan, D. Thompsett, and S. J. Cooper, *J. Molec. Catal. A: Chemical,* **119** (1997) 223

[167] D. P. Wilkinson, EU Patent, 96302406.1 (issued 1996)

[168] D. P. Wilkinson, H. V. Voss, J. Dudley, G. J. Lamont, and V. Basura, US Patent, 5,482,680 (issued 1996)

[169] H. A. Gasteiger, N. M. Markovic, and P. N. Ross in "*4. Ulmer Elektrochemische Tage - Elektrochemie für Energie und Umwelt*, Ulm, Garche, J., Ed., Universitätsverlag Ulm GmbH, (1997) 193

[170] T. J. Schmidt, H. A. Gasteiger, and R. J. Behm, *J. New Mat. Electrochem. Systems,* **2** (1999) 27

[171] J. Arana, P. Ramirez de la Piscina, J. Llorca, J. Sales, N. Homs, and J.-L. G. Fierro, *Chem. Mater.,* **10** (1998) 1333

[172] M. Shibata and N. Furuya, *J. Electroanal. Chem.,* **269** (1989) 217

[173] D. R. Schryer, B. T. Upchurch, J. D. van Norman, K. G. Brown, and J. Schryer, *J. Catal.,* **122** (1990) 197

[174] P. A. Sermon, V. A. Self, and E. P. S. Barrett, *J. Molec. Catal.,* **65** (1991) 377

[175] A. Boulahouache, G. Kons, H.-G. Lintz, and P. Schulz, *Appl. Catal. A: General,* **91** (1992) 115

[176] G. B. Hoflund, B. T. Upchurch, E. J. Kielin, and D. R. Schryer, *Catal. Lett.,* **31** (1995) 133

[177] K. Grass and H.-G. Lintz, *J. Catal.,* **172** (1997) 446

[178] L. S. Sun, S. Y. Li, and B. L. Li, *React. Kinet. Catal. Lett.,* **62** (1997) 151

[179] J. A. Rodriguez, *Surf. Sci. Rep.,* **24** (1996) 223

[180] R. J. Behm, *Acta Phys. Polon.,* in press

[181] C. T. Campbell in „*Handbook of Heterogeneous Catalysis*“, G. Ertl, H. Knözinger and J. Weitkamp, eds., VCH, Weinheim (1997) 814

[182] B. Hammer and J. K. Norskov in „Theory of Adsorption and Surface Reaction“, R. M. Lambert and G. Pacchioni, eds., Kluwer Academic Publishers, Dodrecht (1997) 285

[183] P. N. Ross, *J. Vac. Sci. Technol. A,* **10(4)** (1992) 2546

[184] A. H. Haner, P. N. Ross, U. Bardi, and A. Atrei, *J. Vac. Sci. Technol. A,* **10(4)** (1992) 2718

[185] M. T. Paffett, S. C. Gebhard, R. G. Windham, and B. E. Koel, *J. Phys. Chem.,* **94** (1990) 6831

[186] M. M. Schubert, M. J. Kahlich, H. A. Gasteiger, and R. J. Behm, *J. Pow. Sources,* **84** (1999) 175

[187] Y. Li and B. E. Koel, *Surf. Sci.,* **330** (1995) 193

[188] R. Bouwman, L. H. Toneman, and A. A. Holscher, *Surf. Sci.,* **35** (1973) 8

[189] G. B. Hoflund, D. A. Asbury, P. Kirszensztejn, and H. A. Laitinen, *Surf. Interface Anal.,* **9** (1986) 169

[190] D. A. Asbury and G. B. Hoflund, *Surf. Sci.,* **199** (1988) 552

[191] J. A. Anderson, *Catal. Lett.,* **13** (1992) 363

[192] A. G. T. M. Bastein, F. J. C. M. Toolenaar, and V. Ponec, *J. Catal.,* **90** (1984) 88

[193] K. Balakrishnan and J. Schwank, *J. Catal.,* **138** (1992) 491

[194] S. de Miguel, A. Castro, O. Scelza, J.-L. G. Fierro, and J. Soria, *Catal. Lett.,* **36** (1996) 201

[195] L.-C. de Menorval, A. Chaqroune, B. Coq, and F. Figueras, *J. Chem. Soc. Faraday Trans.,* **93** (1997) 3715

[196] T. T. P. Cheung, *Surf. Sci.,* **177** (1986) L887-L895

[197] A. F. Lee, C. J. Baddelely, M. S. Tikhof, and R. M. Lambert, *Surf. Sci.,* **373** (1997) 195

[198] D. A. Asbury and G. B. Hoflund, *J. Vac. Sci. Technol. A,* **5(4)** (1987) 1132

[199] B. A. Sexton, A. E. Hughes, and K. Foger, *J. Catal.,* **88** (1984) 466

[200] A. F. Lee and R. M. Lambert, *Phys. Rev. B,* **58** (1998) 4156

[201] G. Meitzner, G. H. Via, F. W. Lytle, S. C. Fung, and J. H. Sinfelt, *J. Phys. Chem.,* **92** (1988) 2925

[202] M. T. Paffett, A. D. Logan, R. J. Simonson, and B. E. Koel, *Surf. Sci.,* **250** (1991) 123

[203] S. D. Gardner, G. B. Hoflund, and D. R. Schryer, *J. Catal.,* **119** (1989) 179

[204] Y.-X. Li, J. M. Stencel, and B. H. Davis, *Appl. Catal.,* **64** (1990) 71

[205] G. B. Hoflund and D. A. Asbury, *Langmuir,* **2** (1986) 695

[206] J. Llorca, P. Ramirez de la Piscina, J.-L. G. Fierro, J. Sales, and N. Homs, *J. Molec. Catal. A: Chemical,* **118** (1997) 101

[207] S. R. de Miguel, M. C. Roman-Martinez, E. L. Jablonski, J.-L. G. Fierro, D. Cazorla-Amoros, and O. A. Scelza, *J. Catal.,* **184** (1999) 514

[208] R. Srinivasan, R. J. de Angelis, and B. H. Davis, *J. Catal.,* **106** (1987) 449

[209] R. Srinivasan, R. J. de Angelis, and B. H. Davis, *Catal. Lett.,* **4** (1990) 303

[210] Y.-X. Li, K. J. Klabunde, and B. H. Davis, *J. Catal.*, **128** (1991) 1

[211] L. D. Sharma, M. Kumar, A. K. Saxena, D. S. Rawat, and T. S. R. Prasada Rao, *Appl. Catal. A: General,* **168** (1998) 251

[212] H. H. C. M. Pinxt, B. F. M. Kuster, D. C. Koningsberger, and G. B. Marin, *Catal. Today,* **39** (1998) 351

[213] J. F. Moulder, W. F. Stickle, P. E. Sobol, and K. D. Bomben, „*Handbook of X-Ray Photoelectron Spectroscopy*“, J. Chastain, ed., Perkin Elmer Corp., Eden Prairie (1992)

[214] E. Janin, M. Björkqvist, T. M. Grehk, M. Göthelid, C.-M. Pradier, U. O. Karlsson, and A. Rosengren, *Appl. Surf. Sci.,* **99** (1996) 371

[215] A. D. Logan and M. T. Paffett, *J. Catal.,* **133** (1992) 179

[216] C. T. Campbell, G. Ertl, H. Kuipers, and J. Segner, *J. Chem. Phys.,* **73** (1980) 5862

[217] M. R. Voss, H. Busse, and B. E. Koel, *Surf. Sci.,* **414** (199) 330

[218] P. Samson, A. Nesbitt, B. E. Koel, and A. Hodgson, *J. Chem. Phys.,* **109** (1998) 3255

[219] A. G. Sault, R. J. Madix, and C. T. Campbell, *Surf. Sci.,* **169** (1986) 347

[220] D. A. Outka and R. J. Madix, *Surf. Sci.,* **179** (1987) 351

[221] J. Schwank, *Gold Bull.,* **16** (1983) 103

[222] L. Stobinski and R. Dus, *Czech. J. Phys.,* **43** (1993) 1035

[223] B. Hammer and J. K. Noerskov, *Nature,* **376** (1995) 238

[224] S. D. Gardner, G. B. Hoflund, B. T. Upchurch, D. R. Schryer, and E. J. Kielin, *J. Catal.,* **129** (1991) 114

[225] G. Croft and M. J. Fuller, *Nature*, **269** (1977) 585

[226] W. M. H. Sachtler and R. A. van Santen, *Appl. Surf. Sci.,* **3** (1979) 121

[227] H. Verbeek and W. M. H. Sachtler, *J. Catal.,* **42** (1976) 257

[228] C. Xu and B. E. Koel, *Surf. Sci. Lett.,* **304** (1994) L505-L511

[229] J. Llorca, N. Homs, J. Arana, J. Sales, and P. Ramirez de la Piscina, *Appl. Surf. Sci.,* **134** (1998) 217

[230] G. B. Hoflund, S. D. Gardner, D. R. Schryer, B. T. Upchurch, and E. J. Kielin, *Langmuir,* **11** (1995) 3431

[231] D. R. Schryer, B. T. Upchurch, B. D. Sidney, K. G. Brown, G. B. Hoflund, and R. K. Herz, *J. Catal.,* **130** (1991) 314

[232] G. C. Bond, *Gold Bull.,* **5** (1972) 11

[233] M. Haruta, *Catal. Today,* **36** (1997) 153

[234] M. Haruta, H. Kageyama, N. Kamijo, T. Kobayashi, and F. Delannay, (1988) 33

[235] W. S. Epling, G. B. Hoflund, J. F. Weaver, S. Tsubota, and M. Haruta, *J. Phys. Chem.,* **100** (1996) 9929

[236] A. Knell, P. Barnickel, A. Baiker, and A. Wokaun, *J. Catal.,* **137** (1992) 306

[237] S. D. Lin, M. A. Bollinger, and M. A. Vannice, *Catal. Lett.,* **17** (1993) 245

[238] S. K. Tanielyan and R. L. Augustine, *Appl. Catal. A: General,* **85** (1992) 73

[239] C. Mohr, H. Hofmeister, M. Lucas, and P. Claus, *Chem. Ing. Tech.,* **71** (1999) 869

[240] M. Haruta, *Catal. Surv. Jap.,* **1** (1997) 61

[241] D. Thompson, *Gold Bull.,* **32** (1999) 12

[242] D. Thompson, *Gold Bull.,* **31** (1998) 111

[243] M. Haruta, T. Kobayashi, H. Sano, and N. Yamada, *Chem. Lett.,* (1987) 405

[244] A. Grigorova, A. Palazov, J. Mellor, J. A. J. Tumilty, and A. H. Gavin, US Patent, 5,759,949 (issued 2. 6. 1998)

[245] S. Aoyama, EU Patent, 0,743,694 A1 (issued 20. 11. 1996)

[246] N. D. S. Canning, D. A. Outka, and R. J. Madix, *Surf. Sci.,* **141** (1984) 240

[247] J. France and P. Hollins, *J. Electr. Spectr. Rel. Phenom.,* **64/65** (1993) 251

[248] F. Boccuzzi, A. Chiorino, S. Tsubota, and M. Haruta, *J. Phys. Chem.,* **100** (1996) 3625

[249] J.-D. Grunwaldt and A. Baiker, *J. Phys. Chem.*, **103** (1999) 1002

[250] H. Liu, A. I. Kozlov, A. P. Kozlova, T. Shido, K. Asakura, and Y. Iwasawa, *J. Catal.*, **185** (1999) 252

[251] S. Minico, S. Scire, A. M. Crisafulli, and S. Galvagno, *Catal. Lett.*, **47** (1997) 273

[252] D. R. Rainer, C. Xu, P. M. Holmblad, and D. W. Goodman, *J. Vac. Sci. Technol. A*, **15(3)** (1997) 1653

[253] M. A. Bollinger and M. A. Vannice, *Appl. Catal. B: Environmental*, **8** (1996) 417

[254] D. H. Parker and B. E. Koel, *J. Vac. Sci. Technol. A*, **8(3)** (1990) 2585

[255] J. M. Gottfried, K. J. Schmidt, K. Christmann, and S. L. M. Schroeder, *Surf. Sci.*, in preparation

[256] J.-D. Grunwaldt, *Dissertation*, ETH Zürich (1998)

[257] F. Boccuzzi, A. Chiorino, S. Tsubota, and M. Haruta, *Catal. Lett.*, **29** (1994) 225

[258] A. I. Kozlov, A. P. Kozlova, H. Liu, and Y. Iwasawa, *Appl. Catal. A: General*, **182** (1999) 9

[259] K. Fukushima, G. H. Takaoka, J. Matsuo, and I. Yamada, *Jpn. J. Appl. Phys.*, **36** (1997) 813

[260] T. Fukushima, T. Kikuta, K. Shindo, and T. Hattori in "*Proceedings of the First Tokyo Conference on Advanced Catalytic Science and Technology*", 1.-5. July 1990, Tokyo, Yoshida, S., Takezawa, N., and Ono, T., Eds., Kodansh Ltd. and VCH, (1990) 493

[261] J. T. Richardson, „*Principles of Catalyst Development*“, 2nd edition, Plenum Press, New York (1992)

[262] J. C. Frost, *Nature*, **18** (1988) 577

[263] M. Valden, D. Lai, and D. W. Goodman, *Science*, **281** (1998) 1647

[264] M. Valden, S. Pak, X. Lai, and D. W. Goodman, *Catal. Lett.*, **56** (1998) 7

[265] W.-X. Zhang, Y.-G. Tao, M.-J. Jia, T.-H. Wu, and X.-M. Li, *Chem. J. Chin. Univers.*, **19** (1998) 1317

[266] Y. Yuan, K. Asakura, A. P. Kozlova, H. Wan, K. Tsai, and Y. Iwasawa, *Catal. Today*, **44** (1998) 333

[267] Y. Yuan, K. Asakura, H. Wan, K. Tsai, and Y. Iwasawa, *Catal. Lett.*, **42** (1996) 15

[268] J.-D. Grunwaldt, C. Kiener, C. Wögerbauer, and A. Baiker, *J. Catal.,* **181** (1999) 223

[269] D. A. H. Cunningham, W. Vogel, H. Kageyama, S. Tsubota, and M. Haruta, *J. Catal.,* **177** (1998) 1

[270] M. Okumura, S. Nakamura, S. Tsubota, T. Nakamura, M. Azuma, and M. Haruta, *Catal. Lett.,* **51** (1999) 53

[271] N. W. Cant and P. W. Frederickson, *J. Catal.,* **37** (1975) 531

[272] S. Tsubota, T. Nakamura, K. Tanaka, and M. Haruta, *Catal. Lett.,* **56** (1998) 131

[273] G. Feldmeyer, M. M. Schubert, S. Mössmer, M. Möller, and R. J. Behm, *J. Catal.,* in preparation

[274] V. Plzak, B. Rohland, and L. Jörissen, *poster contribution at "50. Annual Meeting of the International Society of Electrochemistry* , Pavia, Italy (1999)

[275] J. Shen, B. Guang, M. Tu, and Y. Chen, *Catal. Today,* **30** (1996) 77

[276] A. Olowe, *Adv. X-Ray Anal.,* **38** (1995) 749

[277] J. Lauterbach, K. Asakura, and H.-H. Rotermund, *Surf. Sci.,* **313** (1994) 52

[278] A. P. Kozlova, A. I. Kozlov, S. Sugiyama, Y. Matsui, K. Asakura, and Y. Iwasawa, *J. Catal.,* **181** (1999) 37

[279] J. M. Gottfried, K. J. Schmidt, K. Christmann, and S. L. M. Schroeder, *Catal. Lett.,* in preparation

[280] Y.-M. Kang and B.-Z. Wan, *Catal. Today,* **26** (1995) 59

[281] U. Heiz, Lecture „*Chemie kleiner Metallcluster auf Oxiden: Jedes Atom zählt*“, University of Ulm (16.04.1999)

[282] K. Blick, T. D. Mitrelias, J. S. J. Hargreaves, G. J. Hutchings, R. W. Joyner, C. J. Kiely, and F. E. Wagner, *Catal. Lett.,* **50** (1998) 211

[283] D. A. H. Cunningham, W. Vogel, R. M. Torres Sanches, K. Tanaka, and M. Haruta, *J. Catal.,* **183** (1999) 24

[284] A. P. Kozlova, S. Sugiyama, A. I. Kozlov, K. Asakura, and Y. Iwasawa, *J. Catal.,* **176** (1998) 426

[285] F. E. Wagner, S. Galvagno, C. Milone, A. M. Visco, L. Stievano, and S. Calogero, *J. Chem. Soc. Farady Trans.,* **93** (1997) 3403

[286] M. Haruta, N. Yamada, T. Kobayashi, and S. Iijima, *J. Catal.,* **115** (1989) 301

[287] Z. M. Liu and M. A. Vannice, *Catal. Lett.,* **43** (1997) 51

[288] C. Sze, E. Gulari, and B. G. Demczyk, *Mat. Res. Soc. Symp. Proc.,* **286** (1993) 143

[289] E. D. Park and J. S. Lee, *J. Catal.,* **186** (1999) 1

[290] A. M. Visco, A. Donato, C. Milone, and S. Galvagno, *React. Kinet. Catal. Lett.,* **61** (1997) 219

[291] M. A. P. Dekkers, M. J. Lippits, and B. E. Nieuwenhuys, *Catal. Lett.,* **56** (1998) 195

[292] F. Boccuzzi, G. Cerrato, F. Pinna, and G. Strukul, *J. Phys. Chem. B,* **102** (1998) 5733

[293] C.-K. Chang, Y.-J. Chen, and C.-T. Yeh, *Appl. Catal. A: General,* **174** (1998) 13

[294] Y. Yuan, A. P. Kozlova, K. Asakura, H. Wan, K. Tsai, and Y. Iwasawa, *J. Catal.,* **170** (1997) 191

[295] Y.-M. Kang and B.-Z. Wan, *Appl. Catal. A: General,* **128** (199) 53

[296] C. Ruggiero and P. Hollins, *Chem. Soc. Faraday Trans.,* **92** (1996) 4829

[297] Y. Iizuka, H. Fujiki, N. Yamauchi, T. Chijiiwa, S. Arai, S. Tsubota, and M. Haruta, *Catal. Today,* **36** (1997) 115

[298] P. Dumas, R. G. Tobin, and P. L. Richards, *Surf. Sci.,* **171** (1986) 579

[299] D. J. C. Yates, *J. Colloid Interface Sci.,* **29** (1969) 194

[300] G. McElhiney and J. Pritchard, *Surf. Sci.,* **60** (1976) 397

[301] M. L. Kottke, R. G. Greenler, and H. G. Tompkins, *Surf. Sci.,* **32** (1972) 231

[302] J. M. Gottfried, K. J. Schmidt, K. Christmann, and S. L. M. Schroeder, Poster contribution at "*18th European Conference on Surface Science*", 21.9., Vienna, Austria, (1999)

[303] W. Vogel, D. A. H. Cunningham, K. Tanaka, and M. Haruta, *Catal. Lett.,* **40** (1996) 175

[304] Y.-M. Kang and B.-Z. Wan, *Catal. Today,* **35** (1997) 379

[305] K. Tanaka and J. M. White, *J. Phys. Chem.,* **86** (1982) 4708

[306] Y. Fu, L. Kraus, and H. Knözinger, *Chin. J. Chem. Phys,* **2** (1989) 125

[307] D. M. Cox, R. O. Brickman, K. Creegan, and A. Kaldor, *Mat. Res. Soc. Symp. Proc.*, **206** (1991) 43

[308] H. Sakurai, A. Ueda, T. Kobayashi, and M. Haruta, *Chem. Commun.* (1998) 271

[309] D. Andreeva, V. Idakiev, T. Tabakova, A. Andreev, and R. Giovanoli, *Appl. Catal. A: General*, **134** (1996) 275

[310] O. J. Wimmer, P. Arnoldy, and J. A. Moulijn, *J. Phys. Chem.*, **90** (1986) 1331

[311] G. B. Hoflund, S. D. Gardner, D. R. Schryer, B. T. Upchurch, and E. J. Kielin, *Appl. Catal. B: Environmental*, **6** (1995) 117

[312] S. Tsubota, D. A. H. Cunningham, Y. Bando, and M. Haruta in „Preparation of Catalysts IV“, G. Poncelet, ed., Elsevier Science B. V., Elsevier (1995) 227

[313] C. Serre, F. Garin, G. Belot, and G. Maire, *J. Catal.*, **141** (1993) 1

[314] C. Serre, F. Garin, G. Belot, and G. Maire, *J. Catal.*, **141** (1993) 9

[315] C. Hardacre, R. M. Ormerod, and R. M. Lambert, *J. Phys. Chem.*, **98** (1994) 10901

[316] N. W. Cant and N. J. Ossipoff, *Catal. Today*, **36** (1997) 125

VI. ACKNOWLEDGEMENT

I want to thank all those numerous people, who have contributed to my work within the last three years. Especially, I want to acknowledge:

- **Prof. R. J. Behm** and **H. A. Gasteiger** for the supervision of my thesis work.
- **Prof. J. Garche** (ZSW Ulm) for his moral and financial support over the last few months.
- **B. Heise** (Department of Experimental Physics) for his engaged support within the Graduiertenkolleg.
- **V. Plzak** (ZSW Ulm), who prepared the gold catalysts, characterized them by XRD and TGA and revised the corresponding parts of this thesis.
- **M. Kahlich**, who performed the largest part of the kinetic measurements within the PROX project.
- **S. Hackenberg** for managing the CO titration experiments and the TPDs.
- **G. Feldmeyer** and **M. Hüttner** for their XPS measurements and some additional conversion experiments.
- **A. C. van Veen** and **Prof. M. Muhler** (Department of Technical Chemistry, Ruhr-University Bochum) for the TAP isotope studies.
- **S. L. M. Schroeder** (Institute of Physical and Theoretical Chemistry, FU Berlin) for supplementing XAFS and in-situ XRD measurements.
- **J.-D. Grunwaldt** (Haldor Topsøe) for a revision of the chapters III-3.1 and III-3.2.
- **Venugopal** (IICT, Hyderabad, India) for his help with the CO_2- / H_2O-measurements.
- **H. H. C. M. Pinxt** (DSM group) for providing XAFS reference spectra.
- **G. Mestl** (Institute of inorganic chemistry, FHI Berlin) for making the TEM photographs on the platinum catalysts.
- **M. Adelt** (Institute of chemical physics, FHI Berlin) for his help with the coverage calculation algorithm.
- **E. Auer** (Degussa) and **J. Giallombardo** (E-TEK) for providing the catalyst samples.
- **T. Häring** and **G. Bräth** for their engaged technical help with my setup.

Financial support for this work came from the '**Stiftung Energieforschung**' (project no. A 0000 8295) and via a fellowship by the Deutsche Forschungsgemeinschaft, within the **Graduiertenkolleg** 'Molekulare Organisation und Dynamik an Grenz- und Oberflächen'.

But most of all, I have to thank **my parents** for their incredible support during the last years.

APPENDIX

A. Improved DRIFTS-cell design

As was explicitely shown in the first chapters, DRIFTS is a quite simple, but nevertheless powerful method for surveying surface species *in-situ* on disperse catalysts under realistic reaction conditions (see, *e. g.*, [41, 46, 51, 56]). But many commercially available DRIFTS cells are predominantly designed for the identification of organic compounds (*e. g.*, in quality control) and not optimized for *in-situ* applications in heterogenous catalysis.

In the preceeding chapters, we presented IR measurements during the selective CO oxdiation in H_2-rich gases over supported noble metal catalysts. Most of the data were obtained in a commercially available DRIFTS cell by Harricks (HV-DR2) and in a very closely related copy, produced by our university workshop, respectively (See chapter II-1.2.2). But these cells have both many disatvantages, which limit the range of applicable reaction conditions and the reliability of results:

a) An unfavourable geometry of the catalyst bed (ID 6.3 mm, but height only 3.1 mm), which may lead to flow irregularities in some parts of the catalyst bed, sometimes even to channeling effects. With exothermic reactions (as is, *e. g.*, the case for the CO or H_2 oxidation reaction) large temperature gradients may occur from the center of the catalyst bed to the outside, especially at irregular flow rates. The existence of flow rate and temperature gradients may cause artifacts in the resulting spectra, leading to a false interpretation of the acquired data. Another, more practical problem is the loss of material by the erosion of the catalyst bed as a consequence of channeling along the wall, which additionally produces a more rough surface, decreasing the absolute signal during the measurement.

b) A large background reactivity of the cell itself (stainless steel) for some reactions, impairing measurements at high temperatures or low reactant concentrations. Schubert demonstrated in his diploma thesis, that, *e. g.*, for the selective CO oxidation of 1 kPa CO ($\lambda = 2$; atmospheric pressure: 75 kPa H_2, balance N_2) measurements at more than 200°C are impossible with the commercial Harricks DRIFTS cell, since the oxygen and CO conversion exceed 10% (at a flow rate of 120 Nml/min) in the empty cell [32]. At a reduced CO content of 0.1 kPa ($\lambda = 2$; similar conditions), even 150°C, which represents already the lower limit of the interesting temperature range for, *e. g.*, our Pt/γ-Al_2O_3

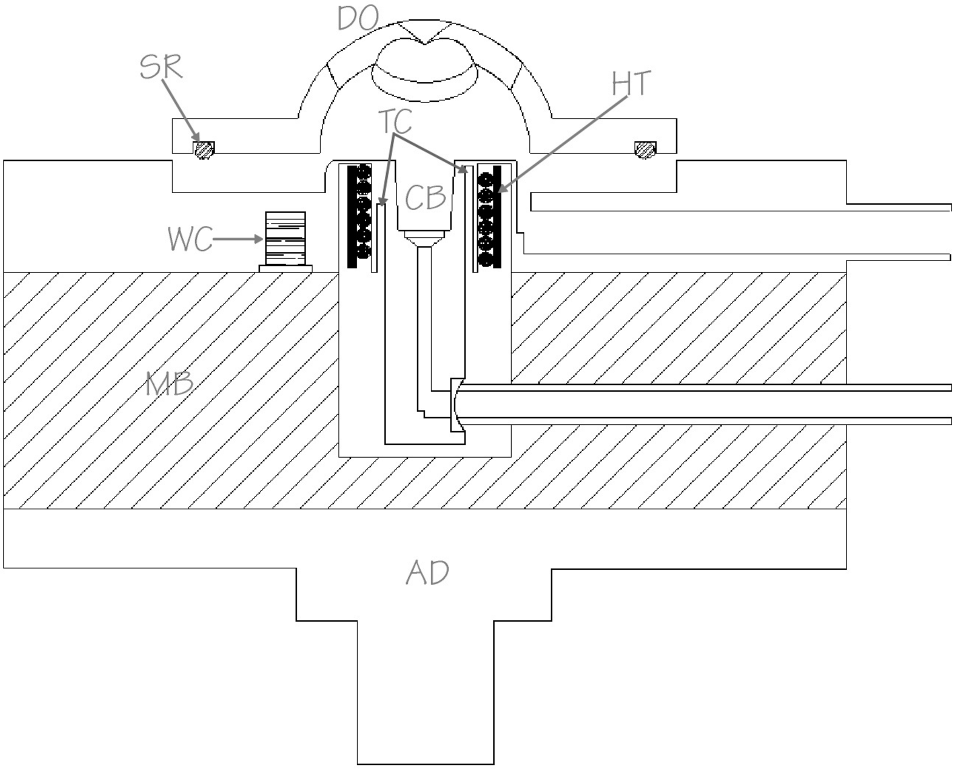

Fig A-1: Drawing of the new DRIFTS cell.

catalyst, is a problem. These large background contributions are predominantly a consequence of the oversized heating rod, which warms up not only the catalyst bed but also extended wall surfaces of the cell interior.

c) A large gas volume of the cell (esitmated to be >10 ml), which causes long response times after changing the reaction atmosphere. Finally, the large surface area of the cell interior additionally contributes to the above mentioned high background reactivity.

d) Leaking, caused by the outlet gas channel, which is stuck only loosely into a whole at the bottom of the catalyst bed. Hence, depending on the pressure drop over the catalyst material, a large fraction of the gas is not passing through the powder, but going directly to the outlet - sometimes more than 50% of the overall gas flow (estimated by GC analysis of conversion data). Thus any simultaneously collected conversion data shows large tolerances (see, *e. g.*, chapter III-1.3.3) and there is always the danger of producing artifacts in the DRIFTS spectra due to mass transport effects, if for example one reactant component is completely used up during reaction in the reduced flow rate over the catalyst bed.

Hence we developed a new DRIFTS cell, compatible for the use with the original „praying mantis“ mirror compartment by Harricks (PM-DRA-2-XXX). The basic concepts of course can be easily adapted for other products. The major intention was the implementation of a

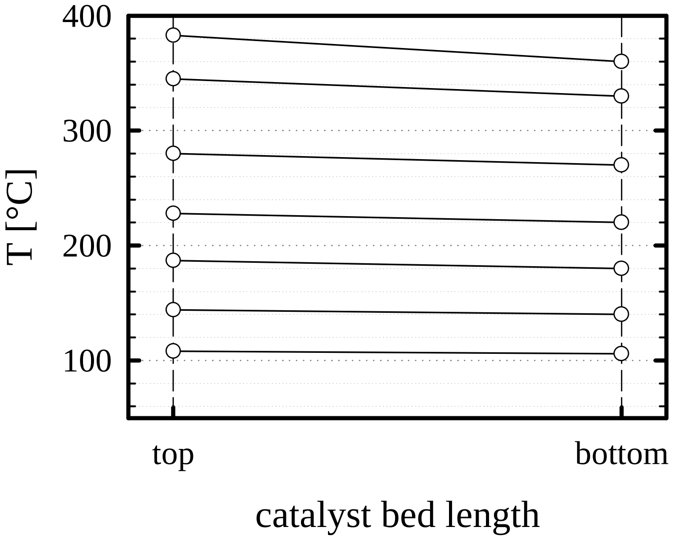

Figure A-2: Temperature-profile at the inner wall of the catalyst bed.

better catalyst bed into the cell (with a geometry similar to common microreactors), containing about 80-120 mg of catalyst, which allows for an accurate on-line analysis of conversion data during a DRIFTS experiment. Important prerequisites were the prevention of gas leaking and the reduction of the background activity to acceptable values. After introducing the construction, we will present very detailed examinations on the properties necessary for the envisaged applications, which will demonstrate, that the new cell design is well suitable for a simultaneos acquisition of correct kinetic data during a DRIFTS measurement series.

Figure A-1 provides an overview over the whole construction: The catalyst is situated on a circular steel net, which rests on the small edge at the bottom of the catalyst bed (CB). The temperature is regulated by a heater (HT) of hollow cylinder shape which surrounds the outer wall of the catalyst bed. The latter consists of a ceramic ring with a resistant wire (CrNi; 0.2 mm) mounted on the inner side. Good contact to the catalyst bed walls is established by a ceramic paste of high thermal conductivity (Polytech 944). On the outside the heater it is thermally isolated by a small gap. The temperature is regulated by a conventional low voltage power supply. A K-type thermocouple (TC; Ø 0.1 mm; Watlow) can be inserted into small holes (two possible positions) inside the catalyst bed walls in order to control the actual temperature level. Below the catalyst bed an outlet gas tube is attached *via* a thread (sealed by a small Viton ring). Tubes for gas supply (as well as for the cooling water) are connected *via* VCO fittings to the cell (Swagelok). From above the cell is closed by a dome (DO), with an identical geometry as in the original HV-DR2 cell. It contains two ZnSe-windows (∅ 13 mm) and a glass window on the back-side for surveying the experiment. Below the dome a

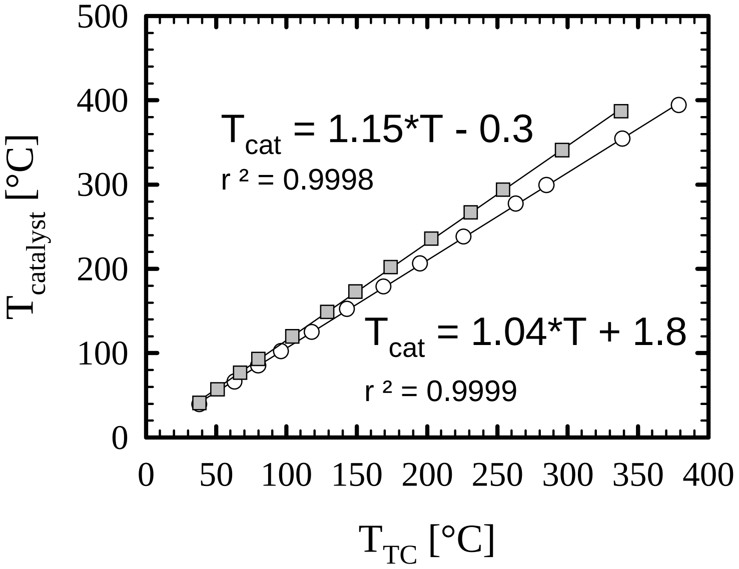

Figure A-3: Calibration of the temperature in the catalyst bed as a function of the measured temperature at the thermocouples - white circles: in 20 Nml/min N_2; grey squares: in 100 Nml/min of 75% H_2, rest N_2

horseshoe-shaped water cooling (WC) is implemented into the cell body to prevent an overheating of the sealing ring (SR; Kalrez). The top part of the cell is made from stainless steel, wheras the middle block (MB) consists of copper for providing a good thermal conductivity. On the bottom an adapter part (AD) is attached in order to mount the cell on the original basis of the HV-DR2 cell.

The changed geometry (catalyst bed ID only 4 mm (top), compared to 6.3 mm for the commercial Harricks cell, leading to a much smaller probing area) of course causes a corresponding loss in the absolute signal intensity of roughly 50%. Therefore, the scanning time now theoretically requires a four-fold increase, in order to obtain spectra of equal quality (*i. e.*, similar SNR) [50].

Two very important preconditions for measurements on a „real“ microkinetic catalyst bed are a constant temperature level over the whole bed lenght, which is quite difficult to arrange with such a small heater, and a correct temperature calibration. In figure A-2, the temperature profiles for different temperatures up to 400°C are displayed. The difference between the top and the bottom of the catalyst bed is constant at 5% for all temperatures, a deviation, which is quite satisfying. It should be mentioned, that the commercial Harricks DRIFTS cell, which we use here for comparison, has an excellent temperature profile as well.

The recorded temperature calibration (the temperature inside an α-Al_2O_3 filled catalyst bed *vs* the output of the thermocouple) is shown in figure A-3. For the maximum level of 400°C a power output of approximately 90W is required. The temperature dependence is linearly, which allows an easy calculation of the temperature in the catalyst bed from the aquired equations in fig. A-3. Unfortunately, the calibration revealed a slight dependence upon the composition of the gas mixture flowing through the cell. When 75% hydrogen are added (grey squares), the top surface of the cell, and as a consequence also the thermocouple inside the wall, are cooled down due to the increased thermal conductivity of the gas phase, leading to larger temperature difference (+ 10%) between the catalyst bed and the thermocouple when compared to a flow of pure nitrogen (white circles). Hence, for the new DRIFTS cell design a correction at the temperature controlling device would be necessery, when the composition of the gas phase changes drastically, *e. g.*, in a „switch experiment“. The dependence upon the absolute flow rate was much smaller, showing a difference of approximately ± 2°C for 150 and 20 Nml/min at 200°C, respectively. Due to the small dependence of the T-calibration on the gas phas composition, for most „simple“ experiments, the commercial DRIFTS cell is preferred, showing virtually no difference between the calibrations in the two different gas mixtures, at least as long as no synchronous kinetic data is required.

After demonstrating the general suitability of the new design for DRIFTS experiments on a powder catalyst bed, we checked the background conversion of the new cell in a typical gas mixture, required for our PROX experiments (1 kPa CO, λ = 2 in 75 kPa H_2, rest N_2; 40 Nml/min). The CO and oxygen conversion of the α-Al_2O_3 filled DRIFTS cell, recorded in an ascending temperature row by on-line analysis with a GC, are displayed in figure A-4. Only at temperatures as high as 300°C, a noticeable consumption of oxygen is observed (white circles), but even the loss of 11% oxygen at 400°C would in principle still be tolerable for rough conversion measurements at high concentrations (*i. e.*, partial pressures of 1 kPa and more). The background CO conversion performance is excellent as well with a maximum of only 2% at 400°C (white squares), and absolutely no methanation activity is observed.

In comparison to the background activity of the commercial Harricks cell obtained under identical conditions (grey symbols), where, *e. g.*, at 250°C already a conversion level of 20% for both, CO and O_2, is reached, the new DRIFTS cell design is clearly superior, which now enables measurements at low reactant concentrations or elevated temperature levels.

Finally, the cell was tested in a real experiment, *i. e.*, the oxidation of CO in an idealized reformate over Au/α-Fe_2O_3 (1 kPa CO, λ = 2 in 9 kPa N_2, up to 22 kPa CO_2, balance H_2; 80°C), where the position of the linearly bound CO_{ad} species and the by-product formation as

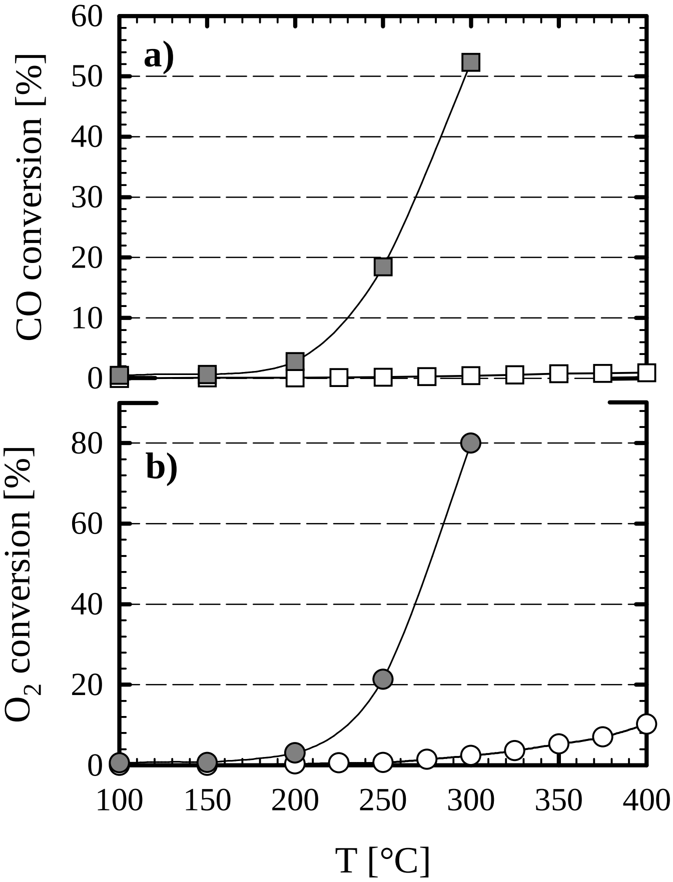

Figure A-4: Activity of the DRIFTS cells (filled with α-Al_2O_3) in simulated reformate (1 kPa CO; $\lambda = 2$): *a)* CO conversion and *b)* oxygen conversion at a flow rate of 40 Nml/min - empty symbols: newly designed cell; filled symbols: original Harricks HV-DR2 cell.

well as the activity and selectivity were recorded as a function of a slowly increasing CO_2 partial pressure. The correspondig data along with an interpretation was already presented in section III-3.4.2. The measured activity in the DRIFTS cell at the lowest CO_2-content (*i. e.*, without addition) is in excellent agreement with the rate obtained in idealized reformate (1 kPa CO, $\lambda = 2$; 75 kPa H_2, rest N_2) in our microkinetic measurements in the quartz reactor ($4.45 \cdot 10^{-3}$ compared to $4.38 \cdot 10^{-3}$ $mol_{CO}/g_{Au} \cdot s$; data taken after 30 min.) as well as the selectivity (67% *vs* 64%), which demonstrates, that very accurate kinetic data may be obtained with the new cell design.

In summary we have seen, that our new cell is generally suitable for the observation of heterogeneous catalyst under reaction conditions. The excellently low background activity along with the new geometry of the catalyst bed allows for the simultaneous recording of very accurate kinetic data.

B. Addititonal figures

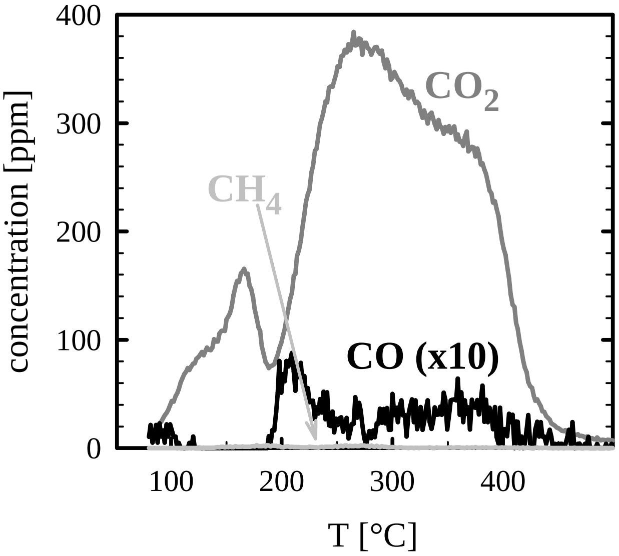

Figure B-1: Temperature programmed desorption of formate species from Pt/γ-Al_2O_3 (accumulated during 6 h of selective CO oxidation at 165°C with 1 kPa CO and $\lambda = 2$) in 12 Nml/min N_2 at 5 K/min (residual CO was removed previously with 10 kPa O_2 in N_2 at 80°C)

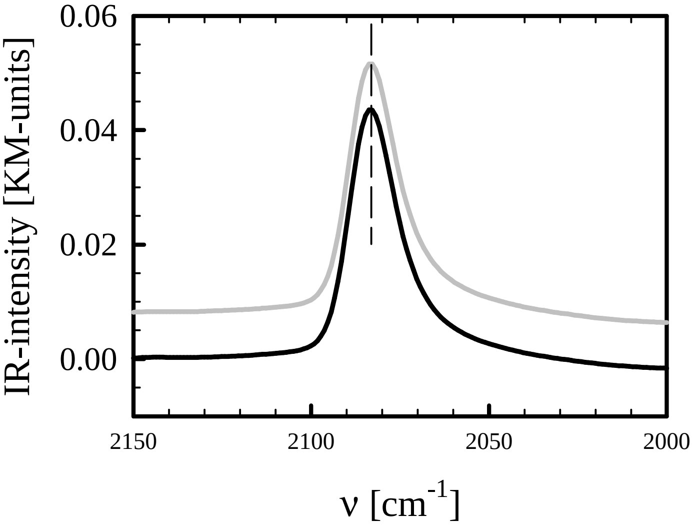

Fig. B-2: DRIFTS-spectra for region of linearly bound CO_{ad} on Pt/SiO_2: ━━ during selective CO oxidation oin idealized reformate with 1 kPa CO and $\lambda = 2$ at 150°C and ── after switching to a mixture containig 1.3 kPa water additionally (both spectra taken after 30 min. in the corresponding atmosphere).

C. English abstract

The selective CO oxidation in H_2-rich gases is investigated over three different catalyst systems - supported platinum (especially Pt/γ-Al_2O_3), a supported bimetallic catalyst (Pt_3Sn/Vulcan) and supported gold (especially Au/α-Fe_2O_3). Compared to standard Pt catalysts which require higher temperatures above 150°C to operate at reasonable rates, the latter low temperature PROX catalysts are characterized by a combination of facile oxygen adsorption and largely inhibited hydrogen adsorption under reaction conditions. This can be achieved either by an active material that is inert for both, hydrogen and oxygen adsorption, but allows CO adsorption, and where oxygen adsorption proceeds on the support material (*i. e.*, Au/Fe_2O_3), or by a material that would be active for adsorption of all reaction partners, but which is blocked for hydrogen and consequently also for oxygen adsorption by a CO adlayer. In all of these cases the oxidation reactions will take part at the interface between the different areas, or *via* a spill-over process and the reaction is not limited by CO desorption, which is the limiting factor for the PROX reaction on Pt catalysts at temperatures below 150°C.

For all catalysts the selectivity is generally a function of the steady-state CO coverage under operation conditions. On Pt/γ-$Al_2O_3$the saturation coverage, which is maintained over a large range operation conditions, leads to a rather constant selectivity. For the low-temperature catalysts the selectivity is also very high due to the high activation barrier for the dissociative adsorption of hydrogen. On the latter systems the selectivity decreases very fast at decreasing CO partial pressures or increasing temperatures as a result of the reduced CO surface coverage.

All investigated systems show a more or less severe tendency for deactivation during time on-stream, but the reasons and also the degree of reversibility are very different.

Upon changing the reaction atmosphere from a simplified composition without CO_2 and H_2O, which was used for our kinetic experiments, to more realistic simulations of a real methanol reformer gas, it is found that especially the platinum-based systems suffer from a large H_2O-content, which decreases the selectivity significantly, wheras Au/α-Fe_2O_3 is more sensitive to CO_2. Nevertheless, the effects of H_2O and CO_2 are of such a moderate extent, that the approach *via* idealized reformate (without CO_2 and H_2O) indeed seems to provide a reasonable basis for future reactor calculations.

For Pt and Au a large variety of support materials is tested, but none of them appears to be significantly superior to the originally employed Pt/γ-Al_2O_3 or Au/α-Fe_2O_3 catalysts.

D. Deutsche Zusammenfassung (german abstract)

Im Rahmen dieser Arbeit werden Mechanismen der selektiven CO Oxidation werden auf unterschiedlichen geträgerten Edelmetallen untersucht – Platin (v. a. $Pt/\gamma\text{-}Al_2O_3$), ein bimetallischer Katalysator (Pt_3Sn/Vulcan) sowie Gold (v. a. $Au/\alpha\text{-}Fe_2O_3$). Im Vergleich zu reinen Platinsystemen, die Reaktionstemperaturen von mindestens 150°C erfordern, werden auf letzteren Systemen durch ein Zusammenspiel vereinfachter Sauerstoffadsorption sowie großteils blockierter Wasserstoffadsorption enstprechend hohe Aktivitäten schon bei wesentlich niedrigeren Temperaturen erreicht. Voraussetzung ist ein Metall auf dem lediglich CO, nicht aber O_2 und H_2, adsorbiert ($Au/\alpha\text{-}Fe_2O_3$) oder auf dem die Adsorption letzterer Moleküle durch eine gesättigte CO Schicht blockiert wird. Der notwendige Sauerstoff wird jeweils räumlich getrennt über eine weitere Katalysatorkomponente (FeO_x bzw. Sn/SnO_x) aufgenommen. Die anschließenden Oxidationsreaktionen finden an der Grenzfläche oder nach einem „Spill-over“-Prozess eines der Reaktanden statt. In jedem Fall wird die CO Oxidation, anders als bei reinen Platin-Katalysatoren, nicht durch die CO Desorption limitiert.

Weiterhin ist für alle untersuchten System die gemessene Selektivität direkt von der CO-Bedeckung unter Reaktionsbedingungen abhängt. Auf $Pt/\gamma\text{-}Al_2O_3$führt die Sättungsbedeckung, die für einen breiten Bereich von Reaktionsbedingungen festgestellt wird, zu einer relativ konstanten Selektivität. Die ebenfalls sehr hohen Selektivitätswerte der „Niedertemperatur-Katalysatoren“ erklären sich aus einer hohen Aktivierungsbarriere für die dissoziative Wasserstoffadsorption. Bei diesen Systemen fällt jedoch die Selektivität stark mit fallendem CO Partialdruck oder steigender Temperatur als Folge der reduzierten CO Bedeckung.

In Langzeitexperimenten werden für alle untersuchte Systeme Desaktivierungstendenzen festgestellt. Die genauen Ursachen sowie die Reversibilität der Desaktivierung sind jeweils individuelle Eigenschaften jedes untersuchten Katalysatorsystems.

Beim Übergang von einer vereinfachten Gaszusammensetzung ohne CO_2 und H_2O, die für die Mehrzahl der kinetischen Experimente benutzt wurde, zu realistischeren Simulationen von Methanol-Reformat wird festgestellt, daß auf Pt basierende Systeme vor allem durch Wasser beeinträchtigt werden (führt zu niedrigerer Selektivität), während $Au/\alpha\text{-}Fe_2O_3$ durch CO_2 negativ beeinflußt wird. Die Effekte sind allerding in jedem Fall relativ gering, so daß die Messungen in der vereinfachten Gasatmosphäre in der Tat eine gute Basis für zukünftige Reaktorrechnungen darstellen.

Ausserdem wurden für Pt und Au noch zahlreiche weitere Trägermaterialien getestet, von denen jedoch bei keinem eine entscheidende Verbesserung im Vergleich zu den zunächst verwendeten Pt/γ-Al_2O_3 und Au/α-Fe_2O_3-Systemen festzustellen war.

E. List of publications

- M. J. Kahlich, M. M. Schubert, M. Hüttner, M. Noeske, H. A. Gasteiger, R. J. Behm; Kinetics of the Selective CO Oxidation in H_2-Rich Gas on Supported Noble Metal Catalysts“; *Conf. Proc. „New Materials for Fuel Cell and Modern Battery Systems II“*, O. Savadogo and P. R. Roberge, Eds.; Ecole Polytechnique de Montreal, Montreal; 642 (1997)

- M. M. Schubert, H. A. Gasteiger, R. J. Behm; „Surface Formates as Side Products in the Selective CO Oxidation on Pt/γ-Al_2O_3“; *J. Catal.***172**, 256 (1997); Research Note

- M. M. Schubert, M. J. Kahlich, H. A. Gasteiger, R. J. Behm; „Correlation between CO Surface Coverage and Selectivity/Kinetics for the Preferential CO Oxidation over Pt/γ-Al_2O_3 and Au/α-Fe_2O_3: An in-situ DRIFTS Study“; *J. Pow. Sources* **84**, 175 (1999)

- M. M. Schubert, M. J. Kahlich, M. Hüttner, S. Hackenberg, G. Feldmeyer, H. A. Gasteiger, R. J. Behm; „Bimetallic PtSn Catalyst for Selective CO Oxidation in H_2-Rich Gases at Low Temperatures“; *J. Catal*., in preparation

- M. M. Schubert, S. Hackenberg, A. C. van Veen, M. Muhler, V. Plzak, R. J. Behm; „CO Oxidation over Supported Gold Catalysts - ‘Inactive’ and ‘Active’ Supports and their Role in the Reaction Process“; *J. Catal.*, submitted

- G. Feldmeyer, M. M. Schubert, C. Hartmann, M. Möller, R. J. Behm; „Au/TiO_2 Catalysts for the Selective CO Oxidation in H_2-rich gas Prepared from Diblockcopolymer Micelles“; in preparation

- M. M. Schubert, M. J. Kahlich, H. A. Gasteiger, R. J. Behm; „Selective CO Oxidation in H_2-Rich Gas over Pt/γ-Al_2O_3: Effects from the Coadsorption of CO and Hydrogen and Dependence of the Selectivity on the CO Coverage“; *J. Phys. Chem. B*, in preparation

- M. M. Schubert, T. Häring, H. A. Gasteiger, R. J. Behm; „New DRIFTS-cell Design for the Simultaneous Acquisiton of Spectroscopic and Kinetic Data“; in preparation

- M. M. Schubert, V. Plzak, J. Garche, R. J. Behm; „Activity, Selectivity and Long-Term Stability of Different Supported Gold Catalysts for the Preferential CO Oxidation in H_2-Rich Gas“; *Catal. Lett.*, in preparation

F. Lebenslauf (curriculum vitae)

Markus Matthias Schubert

Persönliche Daten:

Geboren: 28. August 1971

Geburtsort: München

Eltern: Felix Schubert, geb. 26.03.42, Oberstudienrat, 83313 Siegsdorf, Sportfeldstr. 8
Elisabeth Schubert (geb. Maß), geb. 3.11.44, Studienrätin, 83313 Siegsdorf, Sportfeldstr. 8

Ausbildung:

09.77 bis 07.81	Grundschule Siegsdorf
09.81 bis 06.90	Chiemgau-Gymnasium Traunstein
06.90	Abitur
10.91 bis 09.96	Studiengang „Diplom Chemie“ and der Universität Ulm
11.93	Vordiplom Chemie
09.96	Abschluß Diplom Chemie im 10. Semester *Betreuer*: Prof. Dr. R. Jürgen Behm *Titel*: „*In-Situ* DRIFTS (diffuse reflectance infrared Fourier transform spectrometry) Messungen zur Charakterisierung der selektiven CO-Oxidation in H_2-reichem Gas“
seit 10.96	Promotion an der Universität Ulm

Wehrdienst von 07.90 bis 03.91,
anschließend als Zeitsoldat (W 15) übernommen bis 09.91

Anstellungen:

Studentische Hilfskraft im Praktikum für physikalische Chemie, Universität Ulm:

10.95 bis 02.96	„Fortgeschrittenenpraktikum“
04.96 bis 07.96	„Grundpraktikum“

Wissenschaftliche Hilfskraft im Praktikum für physikalische Chemie, Universität Ulm:

04.97 bis 07.97	„Fortgeschrittenenpraktikum“

Stipendium:

08.97 bis 10.99 Mitglied im Graduiertenkolleg „*Struktur und Dynamik an Grenz- und Oberflächen*“ der Universität Ulm